Republic of Iraq
Ministry of Higher Education and Scientific Research
University of Babylon
College of Engineering
Civil Engineering Department

Structural Behavior of High Strength Reinforced Concrete Beams with Out of Plane Part

A Dissertation
Submitted to the College of Engineering of the University of Babylon
in Partial Fulfillment of the Requirements for the Degree of Doctor of Philosophy in Engineering / Civil Engineering / Structures

By

Murtada Sadah Mohsin Salim

Supervised by

Prof. Dr. Nameer A. Alwash

Prof. Dr. Mohammed M. Kadhum

وَالرَّاسِخُونَ فِي الْعِلْمِ يَقُولُونَ

آمَنَّا بِهِ كُلٌّ مِنْ عِنْدِ رَبِّنَا

صدق الله العلي العظيم

سورة آل عمران (الآية ٧)

Certificate

We certify that the thesis titled ***"Structural Behavior of High Strength Reinforced Concrete Beams with Out of Plane Part"***, was prepared by ***"Murtada Sadah Mohsin"***, under our supervision at University of Babylon as a fulfillment of the partial requirements for the degree of Doctor of Philosophy in Civil Engineering (Structural Engineering).

Signature:

Name: Prof. Dr. Nameer A. Alwash

Date: / / 2022

Signature:

Name: Prof. Dr. Mohammed M. Kadhum

Date: / / 2022

Certificate of the Examining Committee

We certify that as an examining committee that we have read this dissertation entitled "**Structural Behavior of High Strength Reinforced Concrete Beams with Out of Plane Part**", and examined the student "**Murtada Sadah Mohsin**", in its content and what related to it, and found it meets the standard of dissertation for the degree of Doctor of Philosophy in the Civil Engineering (Structure Engineering).

Signature:

Name: **Prof. Dr. Ammar Yaser Ali**

(Chairman)

Signature:

Name: **Prof. Dr. Khattab Saleem Abdul-Razzaq**

(Member)

Signature:

Name: **Prof. Dr. Thaar S.Al-Gasham**

(Member)

Signature:

Name: **Asst. Prof. Dr. Saad Jabbar Abbas AL-Wazni**

(Member)

Signature:

Name: **Asst. Prof. Dr. Muhammed Jawad Kadhim**

(Member)

Signature:

Name: **Prof. Dr. Nameer A. Alwash**

(Member and Supervisor)

Signature:

Name: **Prof. Dr. Mohammed M. Kadhum**

(Member and Supervisor)

Approved by the Head of the Civil Engineering Department

Signature:

Name: **Prof. Dr. Thair J. Mizhir**

Date: / /

Approved by the Acting Dean of the College of Engineering

Signature:

Name: **Prof. Dr. Hatem H. Obeid**

Date: / /

To my parents, Sadah and Ibtisam

Thank you for your prayers, support and guiding me to the way of the science and knowledge. You have the great credit for what I have achieved now.

To my lovely wife, Rafa

For your infinite love and support

Many Thanks for permanently being there for me

To my brothers and sisters

To other family and friends

Great Thanks for always giving me your love and support

ACKNOWLEDGEMENTS

First of all, I would like to express my deepest thanks and gratitude to the Almighty God for giving me the power to carry out this research.

I want to express my sincere gratitude to my supervisors Prof. Dr. Nameer A. Alwash and Prof. Dr. Mohammed M. Kadhum, for their continued knowledgeable advising, contributing to my learning experience, and encouraging me throughout this research.

Thanks to all other faculty members and staff of the Department of Civil Engineering for their contributions and encouragement during my years of study in the University of Babylon.

Many thanks to Wasit University / College of Engineering / Civil Engineering Department for their assistance and advices in completing the experimental work of this research.

ABSTRACT

This research includes experimental investigations and finite element analyses (FEA) for the structural behavior of the fixed ended reinforced concrete beams with out of plane parts that are made of high strength concrete (HSC) and normal strength concrete (NSC) subjected to static load.

The experimental program consists of testing fourteen beam models. Two of these beams are straight and one is made with normal strength concrete and the other with high strength concrete and all the others were non-straight and made with out of plane parts. All the models have the same cross section dimensions of 150 mm width and 200 mm depth with a total span of 2000 mm and clear span of 1500 mm.

The main variables that considered in the experimental study are: the number of the out of plane parts (one, two, and three), type of concrete (normal strength concrete (NSC) and high strength concrete (HSC)), adding torsional reinforcement in conjunction of using high strength concrete (HSC), and increasing the length of the out of plane parts of normal strength concrete (NSC) beam models. In addition, another parameter was evaluated using FEA that includes the increasing number of the out of plane parts more than those studied experimentally.

The results showed that the increasing the number of the out of plane parts leads to decrease their load capacity. However, the beams with an even number of the out of plane parts were better than the beams with an odd number of the out of plane parts (e.g. the beam with two out of plane parts is better than the beams with one number of the out of plane parts). Such reduction in ultimate load capacity reached about 70% in some cases in the present study. Using HSC led to a little enhancement of the ultimate load capacity and the reduction in ultimate load capacity reaches about 60% in

compared with NSC straight beam. The use of torsional steel reinforcement in conjunction of using high strength concrete leads to a noticeable improvement in the load bearing capacity of the beams with out of plane parts but remained lower than NSC straight beam by about 20% to 50%. It has been found that increasing length of the out of plane parts have a little effect on the beams capacity but led to decrease their deflection by by about 5% to 32%.

Generally, the deflection of all the beams with out of plane parts is higher than NSC straight beam and these deflections decreased with the increasing number and length of the out of plane parts. In addition, the ductility of the beams with one and two out of plane parts is lower than that of the straight beam but the beam with three out of plane parts have the highest ductility and it has been observed that ductility increased gradually with the increasing number of the out of plane parts.

Furthermore, it is not possible to design and reinforce the beams with out of plane parts considering it likes a straight beam because it has different values of shear force, bending moment, and torsion. However, it is possible to adobe the procedure of design the straight beam with lower strength reduction factor.

Finally, three-dimensional (3D) nonlinear finite element analysis has been carried out to conduct the numerical investigation of the general behavior of the beam models by using ABAQUS software in this work. The comparison between numerical analysis and experimental results have shown a reasonable validity of the numerical analysis where the average difference ratio based on the ultimate loading capacity of about 4% and 19% for the central deflection for all the analyzed models.

TABLE OF CONTENTS

LIST OF TABLES

LIST OF FIGURES

LIST OF PLATES

NOTATION

The major symbols used in this dissertation are listed below:

Symbol	Descriptions
A	Specimen cross-sectional area, (mm^2)
A_1	The area under the ascending part of load-deflection curve, (mm^2)
A_2	The area under the descending part of load-deflection curve, (mm^2)
As	Area of steel reinforcement
C3D8R	An 8-node linear brick with reduced integration and hourglass control
E	Energy absorption
E_0	Initial modulus of elasticity
E_c	Modulus of elasticity of concrete, (GPa)
E_{el}	Elastic energy absorption
E_{pl}	Plastic energy absorption
G_f	Fracture energy
E_u	Energy absorption at ultimate load
L	Length of the specimen, (mm)
L_r	Roof load
P	Peak load, (kN)

P_{cr}	First cracking load, (KN)
P_L	Passing ability ratio
P_u	Ultimate loading capacity, (MPa)
R	Rain load
S	Snow load
S_1	Stress corresponding to a longitudinal strain equal to 0.00005
S_2	Stress corresponding to 40% ultimate load
SP	Superplasticizer, (L)
$T3D2$	A 2-node linear 3-D truss
W/C	Water to cement ratio
a	Average distance between point load and the nearest support, (mm)
b	Average width, (mm)
d	The diameter of the cylinder, (mm)
d_c	Compression damage parameter of concrete
d_t	Tension damage parameter of concrete
f_{b0}/f_{c0}	Ratio between the initial equibiaxial compressive yield stress and the initial uniaxial compressive yield stress
f_c'	Concrete compressive strength, (MPa)
f_{co}	Uniaxial compression stress, (MPa)

f_{cr}	Cracking strength of concrete, (MPa)
f_{ct}	Tensile strength of concrete, (MPa)
f_{cu}	Cube compressive strength, (MPa)
f_r	Modulus of rupture of concrete, (MPa)
f_t	Splitting tensile strength, (MPa)
ℓ	Clear span of beam, (mm)
w_s	Width of maximum crack at the service load, (mm)
w_u	Width of maximum crack at the ultimate load, (mm)
ϵ	Flow potential eccentricity
ε_1	Longitudinal strain produced by stress S_1
ε_2	Longitudinal strain produced by stress S_2
ε_c	Concrete compressive strain at the compressive stress σc
ε_{co}	Strain corresponding to fc'
$\tilde{\varepsilon}_c^{in}$	Inelastic compressive strain of concrete
ε_t	Concrete tensile strain
εt_1	Transverse strain produced by stress at mid-height of the specimen corresponding to S_1
εt_2	Transverse strain produced by stress at mid-height of the specimen corresponding to S_2
θ_U	Angle of twist at ultimate load , (degree)

θ_y	Angle of twist at yield load , (degree)
μ	Ductility index
μ_E	Energy ductility index
μ_s	Shear ductility index
μ_θ	Torsion ductility index
ρ'	The ratio of main compression reinforcement
ρ_b	The balance ratio of main reinforcement
ψ	Dilation angle, (degree)
ε_{0t}^{el}	Elastic tensile strain corresponding to the undamaged concrete material
ε_c^{el}	Elastic compressive strain of concrete
$\tilde{\varepsilon}_c^{pl}$	Equivalent compressive plastic strain of concrete
ε_y	Rebar yield strain
ε_{cr}	Cracking strain of concrete
ε_s	Tensile strain of steel reinforcement
ε_s^{el}	Elastic tensile strain of steel reinforcement
ε_s^{pl}	Plastic tensile strain of steel reinforcement
ε_t^{ck}	Cracking tensile strain of concrete
$\tilde{\varepsilon}_t^{pl}$	Equivalent tensile plastic strains of concrete

ν	Poisson's ratio
ρ	The ratio of main reinforcement
σ_s	Tensile stress of steel reinforcement
$\sigma b0$	Initial equibiaxial compressive yield stress
σc	Concrete compression stress
$\sigma c0$	Initial uniaxial compressive yield stress
$\bar{\hat{\sigma}}_{max}$	Maximum principal effective stress, (MPa)
Δ_U	The deflection at ultimate load , (mm)
Δ_y	Mid-span deflection corresponding to the first yielding of the reinforcement, (mm)
$\emptyset$	Nominal Bar size, (mm)

ABBREVIATIONS

The major abbreviations used in this dissertation are listed below:

Abbreviation	Description
ABAQUS	Finite Element Analysis Software
ACI	American Concrete Institute
ASTM	American Society For Testing And Materials
B.M.D	Bending Moment Diagram
BS	British Standard
BSI	British Standard Institute
CDP	Concrete Damage Plasticity
CFRP	Carbon Fiber Reinforced Polymer
Exp.	Experimental
FEA	Finite element analysis
FEM	Finite Element Method
FRC	Fiber Reinforced Concrete
g	gram
GGBFS	Ground Granulated Blast Furnace Slag
GPa	Giga Pascal (equal to $1000 \times n/mm^2$ (mpa))
HPFRC	High-Performance Fiber Reinforced Concrete

HRWRA	High Range Water Reducing Admixture
HSC	High Strength Concrete
Hz	Hertz
IQS	Iraqi Quality Standardization
kg	Kilogram
LVDT	Linear Variable Differential Transformer
LWA	Lightweight Aggregate
MPa	Mega Pascal (mn/m^2)
NSC	Normal Strength Concrete
PFA	Pulverised Fuel Ash Admixture
S.F.D	Shear Force Diagram
SCC	Self-Compacted Concrete
SF	Silica Fume
SPs	Superplasticizers
SSD	Saturated Surface Dry
T.M.D	Torsional Moment Diagrame
VMAs	Viscosity Modifying Agents
Vol.	Volume

Chapter One: Introduction

1-1 General

Reinforced concrete structure frequently allows the designer to combine the architectural and structural functions, accordingly, for this purpose, the axis of concrete beams is required in special cases to change in non-straight forms without using supports at the change points. This change in the axis of the beam may lead to a change in its structural behavior in terms of its strength including bending, shear, torsion, and lateral-torsional buckling as compared with the straight members.

There are many factors that affect the structural behavior of reinforced concrete beam under loading, which include member geometry, reinforcement strength, the ratio of longitudinal and transverse reinforcement, and the concrete compressive strength **(Arafah, 2000)**[(1)]. Beam with high strength concrete gives a safe prediction, due to a rising factor of safety with increasing compressive strength. This is considered useful, since the number of available HSC tests in torsion is limited, compared to normal strength concrete **(Khalel, 2013)** [(2)].

The use of HSC leads to a reduction in the number of supports, as well provide longer spans and fewer beams that capable to support the same magnitude of loading. Furthermore, using HSC leads to reduce axial shortening for the members under compression effect **(Jagana, and Vinodh, 2017)**[(3)]. With the increase of the concrete strength, the beam ductility increases as well with an invariable amount of reinforcement, but up to a value of $f_c' = 105$ MPa. Any increase in concrete strength above this value will lead to a reduction in ductility **(Rashid and Mansur, 2005)** [(4)].

The beams with out of plane part that is studied in this research has been exposed to the combined loading of bending moment, torsional moment, and shear forces, so there was made of high strength concrete to improve the structural behavior of the beams under these types of loading based on the results of previous studies that will be mentioned in chapter two.

1-2 Applications of Concrete Beams With Out of Plane Part

The main purposes of using this type of beams are in corner beams, balcony beams, grid beams system, beams with winged loading arms, zig-zag balanced concrete beams, and other architectural application requirements. Several of the beams with out of plane part have been used in different locations of the world in the ancient and recent years as listed below:

1- Iztapalapa Children Museum, Ciudad de México. 2015 which was designed by *Mendoza Partida Architectural Studio* by using zigzag reinforced concrete beams supported concrete columns and walls and carry V-shaped roof shown in Figure (1-1).

Figure (1-1): Iztapalapa Children Museum, Ciudad de México (Studio, M. P. A., 2015).

2- Complex grid beams layout in buildings due to regular or irregular column placement of large commercial Chinese reinforced concrete buildings as shopping centers or the lower floors of office buildings as shown in Figure (1-2).

Figure (1-2): Complex structural layout, China (Herr, and Fischer, 2013).

3- Modern concrete building structure under construction by (**Anon, 2020)**[(7)].

Figure (1-3): Modern concrete buildings with cantilever corner balcony beams (Anon, 2020).

4- Cross-bracing reinforced concrete beams used in *Cavernous Budapest Metro Stations* to reduce the need for columns, enabling the platform areas to become open and uninterrupted spaces by **(Griffiths, 2014)**[(8)].

Figure (1-4): Cross-bracing concrete beams in Budapest metro stations (Griffiths, 2014).

5- Concrete beams for staircase and balconies at the National Theatre, London (**Ahsmann, 2011**) [(9)].

Figure (1-5): Concrete balconies at the National Theatre, London (Ahsmann, 2011).

6- Applications of concrete beams with out of plane part in Iraq

Al Dala hotel, (Iraq/ Karbala)

Um Abeha hotel, (Iraq/ Najaf)

Commercial buildings under construction, (Iraq/ Wasit)

Figure (1-6): Applications of concrete beams with out of plane part in Iraq.

1.3 High Strength Concrete Beams

1.3.1 Historical Development of High Strength Concrete

Concrete had been gradually developed over many years in compressive strength property to became high-strength concrete. Concrete compressive strength of (34 MPa) was supposed as high-strength in the 1950's. It was commercially used in the early 1960's with compressive

strengths (41 and 52 MPa) where one of its applications in *Chicago's Water Tower Place*. In the early 1970s, (62 MPa) concrete was being produced. Recently, HSC had been used in cast-in-place structures with compressive strengths approaching (138 MPa).

For a long time, concrete with compressive strength of more than (41 MPa) was accessible in just a couple of areas. However, the applications of high-strength concrete had increased, and high-strength concrete today utilized in numerous pieces of the world. The development has been conceivable because of late improvements in innovation and demand for a higher-strength concrete increase, **(Russell et al., 1977)** [10].

1.3.2 Advantages of High-Strength Concrete

High strength concrete used in the construction of sustainable buildings for structural behavior improvement, safety, and economic considerations as listed below:

1- Provides long-term durability and reduces the required rehabilitation and avoid demolition in the future which significantly affects project costs.

2- High-strength concrete had increased the building safety because it did not burn and less toxic fumes when exposed to fire, and higher resistance to freezing, thawing, and chemical attack. **(Elbasha, 2013)** [11].

3- Higher strength, better performance, and greater stiffness due to higher modulus of elasticity with high compressive and flexural strengths.

4- The use of high strength concrete provides longer spans of beams that lead to a decrease in the number of supporting elements, an increase in the usable space, and decrease in the permanent action of structure self–weight

which causes a reduction in the size of the foundation. **(Kovačević and Džidić, 2018)** [12].

1.3.3 Disadvantages of High-Strength Concrete

1- Increased quality control is needed in order to maintain the special properties desired. High-strength concrete must meet high-performance standards consistently in order for it to be effective.

2- Careful materials selection is necessary. High quality materials must be used. These materials may cost more than materials of lower quality.

3- Allowable stress design discourages the use of high-strength concrete. One solution is to use load factor and resistance design when using high-strength concrete.

4- Minimum cover over reinforcement or minimum thickness of members may restrict the realization of maximum benefits.

5- Available prestress force in a member may be inadequate to achieve maximum strength. Sixth, low water to cementitious materials ratios require special curing requirements.

6- Since serviceability conditions such as deflection can control design, increased capacity may not be fully utilized (Peterman). **(Kovačević and Džidić, 2018)** [12].

1.3.4 Applications of High-Strength Concrete

The use of high strength concrete gives remarkable benefits. Due to these benefits, high strength concrete is now being used in lots of applications, together with buildings, offshore structures, bridge members, overlays, and pavements.

In tall buildings, high-strength concrete presents scopes for reduced column sizes, resulting in slender buildings and large reductions in dead loads (Perenchio, 1973). In parking structures, high-strength concrete is additionally used to minimize chloride penetration. Although the cost per unit volume of high-strength concrete is likely to be greater than that of normal-strength concrete, given the mechanical advantages of high strength concrete, the total initial cost of building an engineered structure incorporating high-strength concrete can be less. An examples of high strength concrete building applications and their development throughout the world are listed in Table (1-1) **(ACI Committee 363. 2010)** [(13)].

Table (1-1):- Buildings with high-strength concrete. (ACI Committee 363. 2010). (Continued).

Building	**City**	**Year***	**Total stories**	**Maximum design concrete strength**
				MPa
Trump Tower	New York	—	68	55
Collins Place	Melbourne	—	44	55
Helmsley Palace Hotel	New York	1978	53	55
Larimer Place Condominiums	Denver	1980	31	55
City Center Project	Minneapolis	1981	52	55
NCNB Corporate Center	Charlotte	1990	60	55
499 Park Avenue	New York	—	27	59
The Seine Johuku	Nagoya	—	45	60
Rialto Tower	Melbourne	1985	60	60

Table (2-1):- (Continued).

Building	**City**	**Year***	**Total stories**	**Maximum design concrete strength**
				MPa
Bank of China Tower	Hong Kong	1989	70	60†
New Century Hotel	Beijing	1990	31	60†
Central Plaza	Hong Kong	1992	78	60†
Jin Mao	Shanghai	1997	88	60†
SEG Plaza	Shenzhen	1998	75	60†
Royal Bank Plaza	Toronto	1975	43	61
Richmond-Adelaide Center	Toronto	1978	33	61
Midcontinental Plaza	Chicago	1972	50	62
Frontier Towers	Chicago	1973	55	62
Water Tower Place	Chicago	1975	79	62
River Plaza	Chicago	1976	56	62
Chicago Mercantile Exchange	Chicago	1982	40	62
Grande Arche de la Defense	Paris	1988	—	65
Columbia Center	Seattle	1983	76	66
Interfirst Plaza	Dallas	1983	72	69
Scotia Plaza	Toronto	1988	68	69
Platinum Tower	Panama	1993	56	70
Governor Phillip Tower	Sydney	1993	54	70
Eugene Terrace	Chicago	1987	44	76
Telecom Corporate	Melbourne	1992	47	80

Table (3-1):- (Continued).

Building D 3	Brussels	—	24	80†
Petronas Twin Towers	Kuala Lumpur	1995	85	80†
Baiyoke Tower	Bangkok	1996	90	80
e-Tower	São Paulo	2002	42	80
311 S. Wacker Drive	Chicago	1988	70	83
One Peachtree Center	Atlanta	1990	62	83
Society Tower	Cleveland	1990	63	83
Trump World Tower	New York	2000	90	83
505 5th Avenue	New York	2004	30	83
BfG Building	Frankfurt	1990	47	85†
Bay Adelaide Center	Toronto	1991	57	85
Dain Bosworth/ Nieman Marcus	Minneapolis	—	39	97
900 N. Michigan Ave.	Chicago	1986	15	97
Pacific First Center	Seattle	1987	45	97
Two Union Square	Seattle	1987	62	97
225 W. Wacker Drive	Chicago	1988	30	97
111 George Street	Brisbane	1993	27	100
De Geno Leasing House	Eschborn	1995	—	105†
Herriot's	Frankfurt	2002	18	125
Brillia Tower	Tokyo	2004	45	130

*Year in which high-strength concrete was cast.

†Cube strength

1.4 Objectives and Study Aims

The purpose of this study is to conduct a laboratory test and numerical analysis by finite element method on high strength reinforced concrete beams with out of plane part under the influence of vertical static load with utilizing different compressive strength of the concrete and variable amount of longitudinal and transverse reinforcement. This aim will be established through the achievement of the following objectives:

1. Comparing of the structural behavior of reinforced concrete beams that are made with out of plane part with other straight reinforced concrete beams.

2. Studying the effects of increasing number of the out of plane parts on the reinforced concrete beams behavior.

3. Studying the effects of the change in the spans of out of plane parts on the behavior of reinforced concrete beams.

4. Studying the effects of the concrete compressive strength on the structural behavior of the beams.

5. Investigating the behavior of the beams under the effect of changing the amount of longitudinal and transverse reinforcement.

6. An enhanced ABAQUS software, for the finite element analysis of the structural behavior of beams, in relation to the load-carrying capacity, torsional capacity, failure modes, cracks and deflection. This finite element models will be validated by the current research experimental results. Furthermore, studying another parameters that affect on the behavior of the beams that will not be consider in experimental work.

1-5 Research Significance

The significance of this research is concluded as follows:

1- The structural behavior of the beams with out of plate parts as compared with the straight beam is not available yet, so this research explained the differences between them by using of NSC and HSC in the fabrications of reinforced concrete beams to show its effect concrete strength on the structural behavior of the beams.

2- In addition to study the effects of the presence of the out of plate parts on the structural behavior, the effects of increasing their length was also studded in this research.

3- The effects of torsion reinforcement in conjunction with using of HSC in the fabrications of reinforced concrete beams is limited, but it was studded in this research to show its effect on the structural behavior of the beams with out of plate parts as compared with the NSC and HSC straight beams.

4- The load bearing capacity and failure modes of the beams with out of plate parts as compared with the straight beams was explained.

A large part of the research interest have focused on the structural behavior of reinforced concrete straight beams with or without side loading arms under pure torsion or combined loading of shear and bending plus torsion, but it is too limited available researches about reinforced concrete beam with out of plane parts.

This research provides a detailed study by experimental and numerical analysis on the behavior of different cases of the beams with out of plane parts with different types of concretes and patterns of reinforcement.

1.6 Layouts of the Thesis

This thesis contains sevens chapters. The current chapter followed by chapter two which presents a review of the previous researches on the structural behavior of HSC beams under combined loading of the bending moment, shear, and torsion. Also it refers to the previous works on the structural behavior of reinforced concrete beams with out of plane part under combined loading. Chapter three explains methodology of the experimental program carried out in this research which consists of the properties of materials that used, mix proportions, test procedure, specimens' geometry, reinforcement details, and the used molds.

Chapter four presents the experimental results and the discussion of them. The results of the tested beams have been illustrated and detailed through the crack propagation, failure modes, load capacity, twisting angles, mid-span load-deflection relation, flexural ductility, as well as curvatures at the mid-span of beams.

Chapter five illustrates the numerical modeling by using the finite element method which employs a commercial package of ABAQUS in FE models preparation. It also explains the types of elements that are used in idealization, in addition to nonlinear solution techniques related to (ABAQUS/CAE) analyzer software. At last, the numerical results that obtained from ABAQUS finite element analyzer, the comparisons, and verifications with the experimental test results of beams were displayed in this chapter.

Finally, the conclusions of the present work and the recommendations for future work are pointed out in chapter seven.

Chapter Two: Review of Literatures

2.1 Introduction

This chapter presents the experimental results of the work, theoretical and analytical solutions of the previous researches that are related to the subject of this research and provided an overview about the parameters that affect on the structural behavior of non-straight beams and conclusions of the effects of such parameters and the solutions which improved the structural behavior.

This chapter is organized as the following: ductile and flexural behavior of HSC beams, shear behavior of HSC beams, torsional behavior of HSC beams, and previous researches on the structural behavior of the reinforced concrete beams with out of plane part. Finally, concluding remarks are presented.

2.2 Previous Research on Structural Behavior of HSC Beams

2.2.1 Flexural Behavior and Ductility of HSC Beams

Ashour, 2000 [14] analyzed nine high-strength rectangular reinforced concrete beams to study the effect of change concrete compressive strength among 48, 78, and 102 MPa and increase of flexural tensile reinforcement ratio among 1.18, 1.77, and 2.37% on load-deflection behavior and displacement ductility.

Beams dimensions were 200 × 250 mm with span length 3400 mm were simply supported and were subjected to two-point loads at the distance between the two loading points 500 mm. The experimental test results exhibited that as concrete compressive strength increases for the same

longitudinal reinforcement ratio, all of the cracking moment, flexural rigidity, and the displacement ductility increased up to some limits and thereafter decreases as f′c increased.

Pam et al, 2001 [15] carried out a group of tests on 20 rectangular singly reinforced concrete beams with dimensions 200 mm ×300 mm, and 3000 mm length. Normal and high-strength concrete with compressive strength from 35 to 100 MPa was used to cast the beams. The research aims to study the flexural behavior and to compare the flexural ductility of normal and high-strength concrete beams with different reinforcement ratios. All of the beams that were tested are simply supported at a span of 2600 mm under applied two-point loads near the mid-span.

The authors concluded that the increase of the concrete strength beyond the level of f′c = 80 MPa offered little advantage when both strength and ductility considered, thus when f′c > 80 MPa is used in beam structures, its ductility needs to be significantly improved. The effect of the tension steel to balance steel ratio was explained as at similar ratios ρ/ρ_b, the ductility is generally lower at higher concrete strengths and vice versa. Furthermore, at a given concrete strength, the ductility was higher when the ρ/ρ_b ratio was small and it is lower when increasing the ρ/ρ_b ratio.

Ho et al, 2003 [16] used analytical method to study the post-peak moment-curvature behavior of singly reinforced concrete beam with in situ concrete compressive strength ranging from 30 to 100 MPa and used the sections actual stress-strain curves of the materials and took into account the stress path dependence of the reinforcement stress.

The flexural ductility was dependent on both the concrete compressive strength and the tension steel ratio. At a given concrete compressive strength, the ductility decreased as the tension steel ratio increased. On the other hand, at a given tension reinforcement ratio, the ductility increased slightly as the concrete compressive strength increased, albeit a higher strength concrete should be less ductile.

Rashid and Mansur, 2005 [17] studied the flexural response of 16 high strength reinforced beams with concrete compressive strengths ranging from 40 to 130 MPa and change the ratios of tensile and compressive reinforcement (ρ and ρ', respectively) and spacing s of lateral ties as the main parameters under a four-point loading system over a span of 3400 mm.

The study reported that maximum crack width was not significantly affected by the tensile reinforcement ratio at service load, but it increased as concrete strength was increased. When fixing the amount of single reinforcement, the ductility of a beam had been found to increase with an increase of concrete strength f′c, but up to a value of f′c= 105 MPa and reduction in ductility at any increase in concrete strength above this value.

Compression steel reinforcement together with transverse ties confined the concrete in the compression zone enhanced the beam's ability to deform without a significant strength loss before the final collapse, also the confinement increased the strain capacity of the concrete before it disintegrates, thus enhancing the ductility of a beam.

Arslan and Gihanli, 2010 [18] carried out numerical analysis to evaluate the effects of various compressive strengths of concrete (f′c) from 50 to 110 MPa at increments of 5 MPa and tensile reinforcement ratio (ρ)

from 0.0059 to 0.0708 at increments of 0.0059 on the curvature ductility of reinforced HSC beam of singly reinforced beam section 200 mm× 250 mm.

The results of numerical analyses indicated that the curvature ductility decreases for f′c≥ 50 MPa while ρ/ρ_b increases, but when increasing the concrete compressive strength up to a certain limit and decreasing ρ/ρ_b ratio curvature ductility increased as compared the result to the ACI code.

Muhaisin, 2012 [19] evaluated the experimental results of many other researchers and the results of his proposed formula to study the long-term deflection for reinforced concrete beams taking into account the effect of increasing compressive strength of concrete from 20 MPa to 100 MPa and the compression to tension reinforcement ratio (ρ'/ρ) from 0.25 to 1.

Based on the test results and the results of the proposed formula, the long-term deflection was highly reduced when increasing the compressive strength of concrete with the reduced compressive reinforcement ratio, but when high strength concrete is used, the compressive reinforcement became less significant in reducing the long term deflection.

Al-Kamal, 2019 [20] studied the nominal flexural strength of high-strength concrete beams by using the proposed stress block which was verified using an experimental database of 52 tested singly under-reinforced HSC beams with a compressive strength greater than 55 MPa, and the proposed models are compared with models of various design codes and proposals of other researchers.

Based on the experimental result and the developed proposed triangular stress block in this work, the author concluded that the proposed stress block was simplest and conservative for a wide range of concrete

strengths as compared with many models proposed by codes and proposals. The difference of stress block was less effect on the nominal flexural strength for HSC beams as expressions in the ACI 318 equivalent stress block. Therefore, the ACI 318 equivalent stress block could be used to calculate the flexural strength of HSC beams.

2.2.2 Shear Behavior and Ductility of HSC Beams

Cladera and Mari, 2005 [21] conducted an experimental program on eighteen reinforced concrete beams using high strength concrete that were 200 mm wide × 400 mm deep with a shear span of 1080 mm by applied tow point load to study the influence of the concrete compressive strength on the shear strength of beams with and without shear reinforcement.

The results showed that the splitting strength of the concrete with compressive strength 60 MPa was lower than that of 75 MPa and 100 MPa. The brittle behavior was observed in the beams without web reinforcement and it was brisker their failure at higher concrete compressive strength. For beams with the same amount of transverse reinforcement, the stirrups became more effective when concrete compressive strength increased.

Abd-Alla et al, 2007 [22] experimentally investigated and theoretically analyzed the behavior of thirty-six simply supported beams with rectangular cross-sections of width (b=100 mm) and effective depth (d=200 mm) which made of three types of concrete grade (normal, medium and high strength reinforced concrete) was the concrete compressive strength ($f'c$ = 25, 60 and 90 MPa) to study the effect of the concrete compressive strength, the web reinforcement and the main steel ratio (ρ) on the shear strength and the ductility of the beams.

Based on the experimental results and the discussions reported in this study, results showed that the higher concrete compressive strength leads to the higher initial crack load, and the number of cracks and their widths decreased, and this was attributed to the increase in tensile strength. As the increases of longitudinal steel reinforcement ratio (ρ), the penetration of the flexural crack decreased and the beams become more ductile. With the increase of web reinforcement in conjunction with an increase of concrete compressive strength, the longitudinal strain values at the shear span decreased.

Yi and Lv, 2009 [23] showed an experimental study of 19 beams were 2600 mm span, 200 mm wide, and 400 mm depth to investigate the effects of concrete compressive strength, stirrups rebar strength, inclined stirrup angle, and the amount of longitudinal reinforcement on failure mode, shear ductility index and shear capacity of the beams.

The test demonstrated that the increase of concrete strength leads to increase shear capacity, also exhibited a more ductile response, and the shear ductility index of HSC beams with high-strength stirrups was twice when used as compared with the use of normal strength concrete and stirrups. The shear ductility index represented the ratio of the area of the load-deflection response up to $0.75P_{Max}$ in the descending portion, to the area up to P_{Max} as shown in Figure (2-1) and explained as:

$$\mu_s = \frac{A_1 + A_2}{A_1}$$

Where; μ_s is the shear ductility index, A_1 is the area under load- deflection curve at deflection Δ_U that corresponding to the ultimate load (P_{Max}), A_2 is the area under load- deflection curve at deflection $3\Delta_U$.

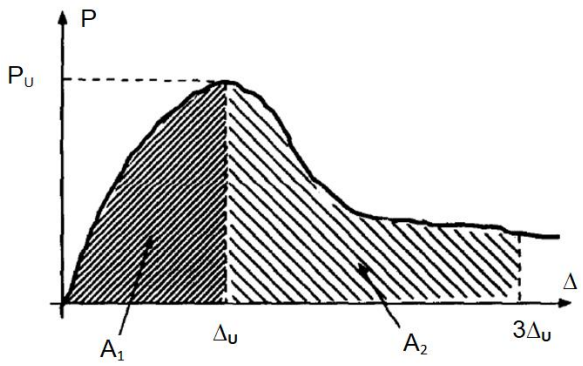

Figure (2-1): Schematic diagram for definition of shear ductility ratio (μ_s). (Ahmad, S. H, 1995).

Hamrat et al, 2012 [25] tested twenty-six reinforced concrete beams experimentally to investigate the effects of transverse reinforcement on the crack patterns, the ultimate carrying capacity, and the ductility of beams made of high strength concrete and normal strength concrete. The concrete beams were divided into three series according to the different compressive strengths of concrete (44 MPa, 65 MPa, and 86 MPa).

Investigation results showed that the bond between steel and concrete increased which led to improve the ductility and indicate a better restraint of cracking when concrete compressive strengths increased. After concrete cracking, transverse reinforcement controlled better the crack opening with less open of diagonal crack widths for high strength concrete as compared with normal strength concrete. The shear strength of high-strength concrete beams were improved by the presence of transverse reinforcement and the failure mode was changed from shear to flexure.

Ismail, 2016 [26] experimentally examined 24 reinforced concrete deep beams to investigate the effect of concrete strength, shear span to depth ratio, shear reinforcement, and member depth on the shear behavior of the

beams, then performed the finite element analysis by ABAQUS software to represent the concrete behavior in a more confident way and validated against experimental results on the beams.

The experimental and numerical results showed that the concrete strength and shear span to depth ratio were the most important parameters that affected on the behavior of the reinforced concrete deep beams. The minimum amount of shear reinforcement increased the shear capacity by around 20% but further increases in shear reinforcement did not provide significant additional load capacity, as failure was ruled by concrete crushing. Also, it was shown from the results that shear capacity increased with increasing concrete compressive strength and this increase was clearer for beams with smaller shear span to depth ratios.

Tahenni et al, 2019 [27] experimentally and theoretically studied the shear behavior of six high-strength reinforced concrete beams to investigate the effects of the concrete strength and the transverse reinforcement on the shear behavior of the beams. The beams dimensions were 100 mm width and 150 mm depth with an effective span of 900 mm.

The experimental results compared with the theoretical values were predicted by the different design codes and it was concluded that HSC beams without stirrups exhibit a relatively brittle behavior and lower ductility, but when the stirrups were added the HSC beams became more ductile and the ultimate shear resistance increased.

2.2.3 Torsional Behavior and Ductility of HSC Beams

Hossain et al, 2006 [28] evaluated reinforced concrete beams by theoretical models to study the effect of concrete compressive strength on

the torsional behavior of beams. Experimental results carried out by previous research of solid rectangular reinforced beams made of normal and high-strength concrete types used to compare with the theoretical models.

Based on the results of the theoretical models and experimental results could be concluded that the torsional strength and the cracking load of HSC were higher than NSC for beams that had the same amount of reinforcement. Also, it was seen that increasing concrete compressive strength from 35 to 78 MPa result in an increase of the ultimate torsional strength of HSC beams by approximately 1.2 occasions than that of NSC beams.

Chiu et al, 2007 [29] experimentally investigated torsional strength, torsional ductility, and the crack patterns of thirteen HSC and NSC full-size beams with low amounts of torsional reinforcement. The parameters of the study were the effect of the volumetric ratio of torsional reinforcements, the concrete compressive strength, and the aspect ratio of the beams on the behavior. The torsional cracking strength and torsional resistance of structural concrete beams for design purposes were calculated according to ACI 318-05 Code. The torsional ductility index, based on the angular deformation per unit meter (twist), is defined as follows:

$$\mu_\theta = \frac{\theta_u}{\theta_y}$$

where; θ_u is the ultimate twist (corresponding to the ultimate torque); and θ_y is the yielding twist (corresponding to the yielding torque).

The test results showed that the HSC specimens designed with lower ratios of transverse to longitudinal torsional reinforcement behaved as a brittle failure mode, but when this ratio was increased, both of HSC and NSC beams behaved with a ductile failure mode.

Rahal, 2013 [30] calculated the ultimate torsional moment of normal and high-strength concrete beams by proposed a simple non-iterative model and its adequacy was evaluated by comparing the results of torsional strength with the experimental results from the 152 test specimens reported in the literature of the research. ACI and CSA building standard conditions and those of two developed iterative analytical models used to compare with experimental results.

The results showed that the ultimate torsional strength was increased as concrete compressive strength. The codes equations showed that ultimate crushing torsional stress of high-strength concrete was un-conservative and did not give a satisfactory result against over- reinforced sections. Subsequently, the under-reinforced sections equation calculation was commonly conservative, more so in HSC.

Hafez and Hassan, 2015 [31] used the nonlinear finite element analysis method to study the behavior of high-strength reinforced concrete sections subjected to pure torsion that was based on the experimental results from previous investigated models. The investigated parametric was a reduction of steel reinforcement ratio, effect the reduction of concrete cross-section, increasing of concrete compressive strength from 45 to 90 MPa.

Test results showed that the increase of concrete compressive strength was improved each of ductility, cracking torque, and ultimate torque for the same cross-section. The failure torque was increased by 40% when the compressive strength increased by 30%. The reduction of the steel reinforcement led to a decrease in the ultimate failure torque and increasing the angle of twist at cracking and failure torque. Also, the reduction of

concrete cross-section had a large effect on the overall behavior of sections, increasing cracking and decreasing failure torque.

Praksh et al., 2016 [32] analyzed experimentally nine normal strength concrete and nine high strength concrete beams with constant width (100 mm), and depth (100 mm) with an effective span of 800 mm to study the torsional behavior of these beams when changing the concrete grade from 50 MPa to 80 MPa and more than 100 MPa grade with varying longitudinal and transverse reinforcement ratios. The aims of this investigation were ductility behavior, cracking torsional strength, ultimate torsional strength, failure pattern, torque-rotation behavior, torsional stiffness, and strains.

The results of the investigation concluded that with the increase of concrete compressive strength, the torsional strength of beam also increased for beams designed with the same amount of reinforcement. It has been observed that increasing transverse reinforcement spacing lead to decreasing the torsional strength for NSC beams, but the effect of transverse reinforcement was not clear in HSC beams. The failure of HSC beams was bursting type at the ultimate torsional moments and the longitudinal reinforcement effect was not much as compared with the transverse reinforcement. However, the ultimate torsional shear stress of all the beams was increased as the longitudinal reinforcement ratio increased.

Waryosh et al., 2018 [33] investigated the deformation responses of reinforced concrete beams under pure torsion by testing twelve simply supported concrete beams classified into three types according to their compressive strength (NSC, HSC, and SCC). The objectives of the research were to study the effect of concrete type and its compressive strength on the torsional behavior of beams. Concrete strengths were (20 and 40MPa) for

NSC, (60 and 75MPa) for HSC, and (40 and 60MPa) for SCC. Beams dimensions were 100 mm width, 200 mm depth, and 2000 mm span.

Based on the data from the experimental results reported in the study, the researchers concluded that the HSC type of beams was the strongest type and had the most stiffness followed by the SCC type, depending on their ultimate carrying load. Also showed that increasing of the compressive strength of section produce increased the stiffness of the beams, and each of the angles of twist and longitudinal strain was decreased.

Prabaghar and Kumaran, 2019 [34] tested eight reinforced concrete beams that were made of two grades of concrete strength 20 MPa and 30 MPa with two ratios of longitudinal reinforcements 0.56% and 0.85% as well as transverse reinforcements spacing as 50 mm and 75 mm to study the effects of these parameters on the torsional behavior of the beams. Schematic and experimental test setup of the beams showed in Figure (2-2).

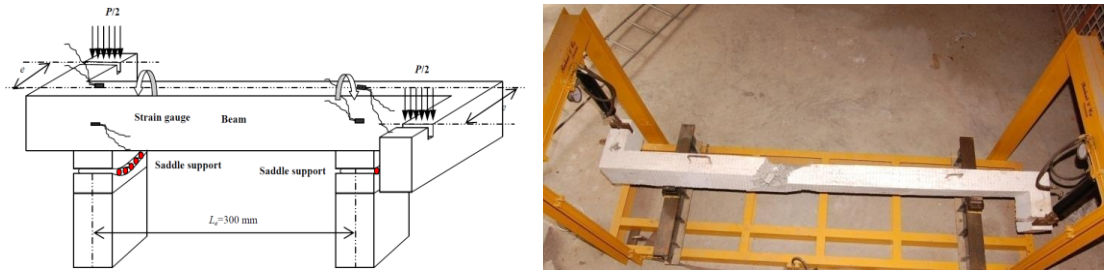

Figure (2-2): (a) Schematic diagram of beam supported on saddle support; (b) Experimental setup and failure mode (Prabaghar and Kumaran, 2019).

From the experimental test results, the study concluded that the increasing each of concrete compressive strength and longitudinal steel ratio result in increase in the maximum angle of twist and torsional strength. In addition, the specimens with stirrups spacing of 50 mm showed identical

values of torque and twist value at the ultimate load in spite of the concrete grade and the reinforcement ratios.

2.3 Previous Researches on Structural Behavior of Reinforced Concrete with Out of Plane Part

Owainati, 1973 [35] studied experimentally the behavior of thirty-eight rectangular reinforced concrete beams tested under different combinations of torsion, bending, and shear loadings with the change each of torsion to shear ratio, transverse reinforcement ratio, and longitudinal reinforcement ratio. Beams geometry and experimental test setup showed in Figure (2-3).

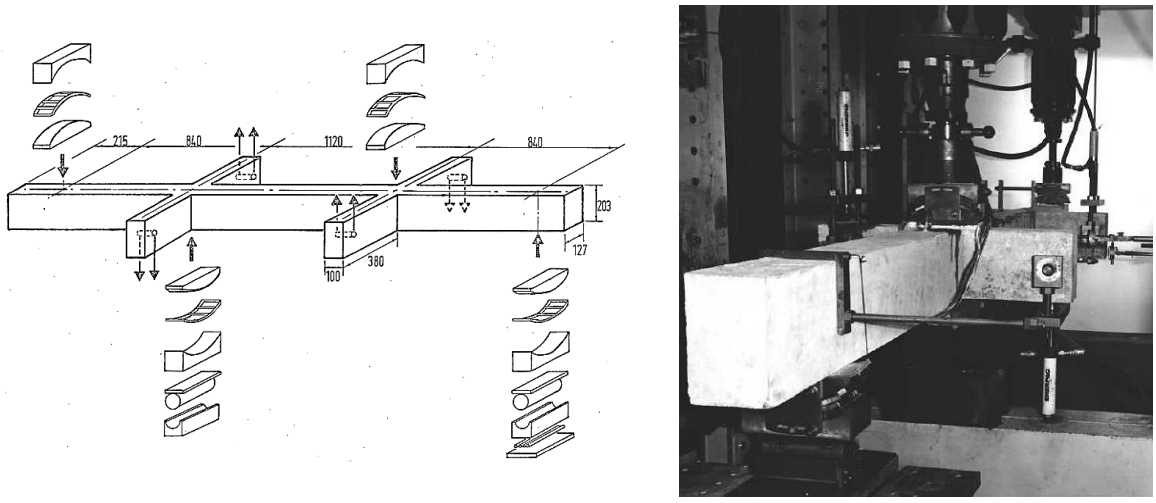

(a) (b)

Figure (2-3): (a) Beams geometry and supports details; (b) Experimental test setup (Owainati, S.A.R., 1973).

Test results were classified into three categories according to the loading system (pure torsion, torsion plus bending, and torsion plus bending and shear) and concluded that the failure occurred by torsion plus bending was governed. When the beam was under pure torsion the cracks shapes were inclined on the top face and perpendicular to those on the opposite

face. If applied low torsion to shear ratio, the cracks were parallel of the two sets. At medium torsion to shear ratios, inclined cracks were vanished from the subtractive face. The increase of longitudinal and transverse reinforcement led to improve each of the cracking and ultimate load, but the transverse reinforcement is more effective in increasing the cracking torque.

Ali and Anis, 1983 [36] analyzed reinforced concrete floor to spandrel beam assembly by experimental work and analytical solution to investigate the effects of loading arrangement, the amounts of longitudinal and transverse reinforcement in the spandrel beams, and the concrete compressive strength on the structural behavior like flexural strength, torsional capacity, and deformations. The structural model is loaded by two types of loading, first one by applying concentrated load at mid-span of the floor beam (Group GR1) and the second one by applying concentrated load at the joint of floor beam to spandrel beam in addition to first loading (Group GR2) as shown in Figure (2-4) and Table (2-1).

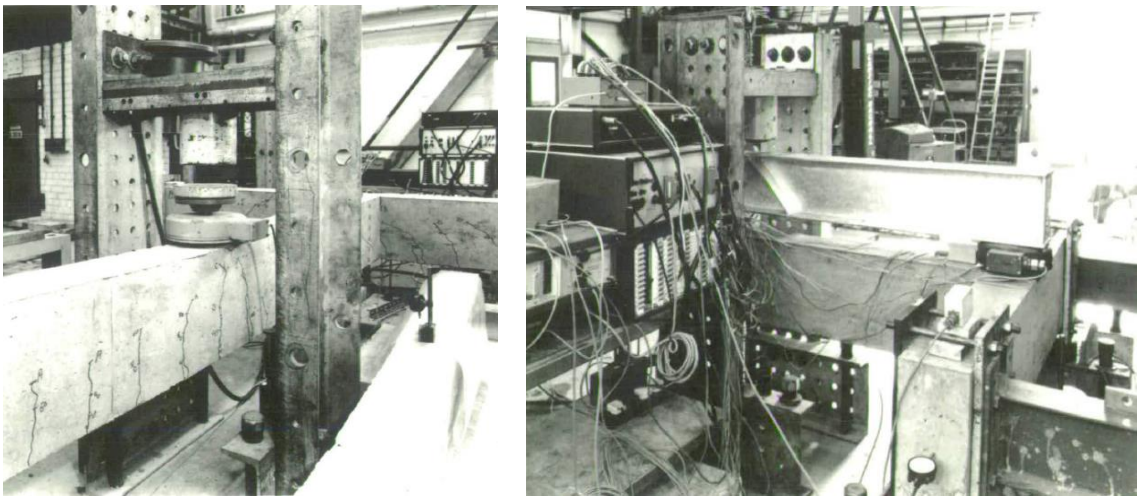

Loading at the floor beam Loading at the floor beam and joint

Figure (2-4): Experimental loading setup (Ali and Anis, 1983).

Table (2-1):- Details of test models by (Ali and Anis, 1983)

Group No.	No. of Specimens	Details
GR1	4 B1 B2 B3 B4	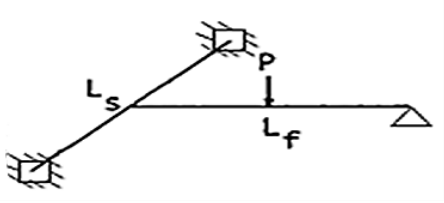 *L_f = Ls =2700 mm **h_f = h_S =300 mm d_f = d_S =280 mm b_f = b_S =150 mm • No longitudinal steel for torsion was provided in the spandrel beams. • Floor beams were equally reinforced.
GR2	4 B5 B6 B7 B8	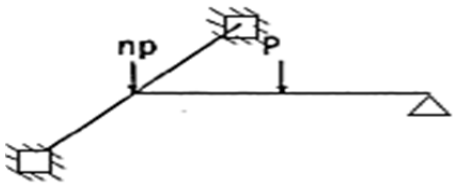 n = 0.5 *L_f = Ls =2700 mm **h_f = h_S =300 mm d_f = d_S =280 mm b_f = b_S =150 mm • No longitudinal steel due to torsion was provided in the spandrel beams. • Floor beams were equally reinforced identical to GR1-floor beams.

* s and f are referred to the spandrel and floor beams respectively.

According to loading setup case two, the spandrel beams represent the member subjected to combined loading of bending, shear plus torsion. Test

results showed that the model ductility decreased when exposed to this type of loading according to the load-deflection curve and increase the angle of twist at the ultimate load because of the increase in the length of the floor beam as shown in Figure (2-5). The longitudinal reinforcement did not consider to resist pure torsional load but it was used to contribute in resisting stresses by dowel action under the effect of torsion and shear loads. Transverse reinforcement in members exposed to torsion was not reached to their yielding strength at failure, but was reached to their yielding point and controlled the crack propagation at the members exposed to combined loading. The cracking and ultimate torque increased by increasing concrete strength for the beams under combined bending and torsion moment.

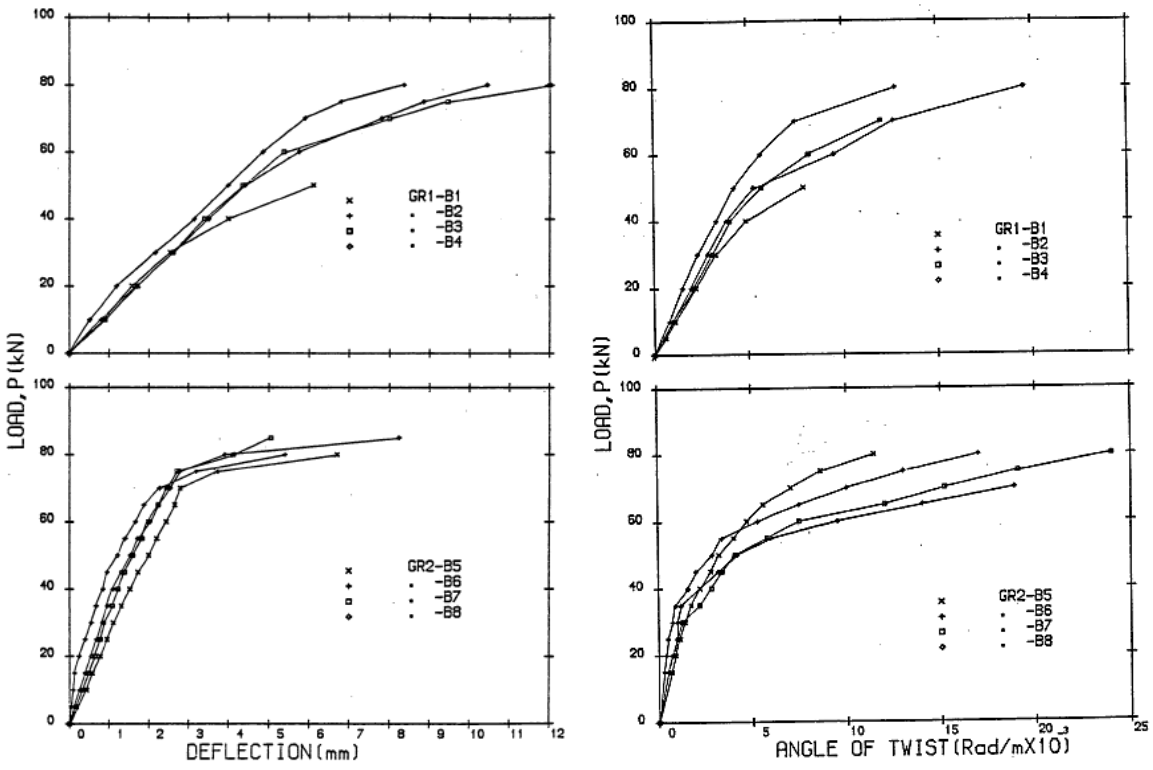

Figure (2-5): Load-deflection and load- angle of twist curves by (Ali and Anis, 1983).

Rahal and Collins, 2003 [37] experimentally evaluated ACI and AASHTO-LRFD design provisions for the rectangular reinforced concrete beams under combined loading of shear and torsion made with changing the compressive strength to compute the required amounts of transverse reinforcement for torsion used different compression diagonals inclined angles θ of space truss analogy model. Angles there were 30^0 as a lower and value 45^0 as an upper value for the ACI provision and 36^0 for the AASHTO-LRFD provision. Beams geometry, reinforcement, and test setup are shown in Figure (2-6).

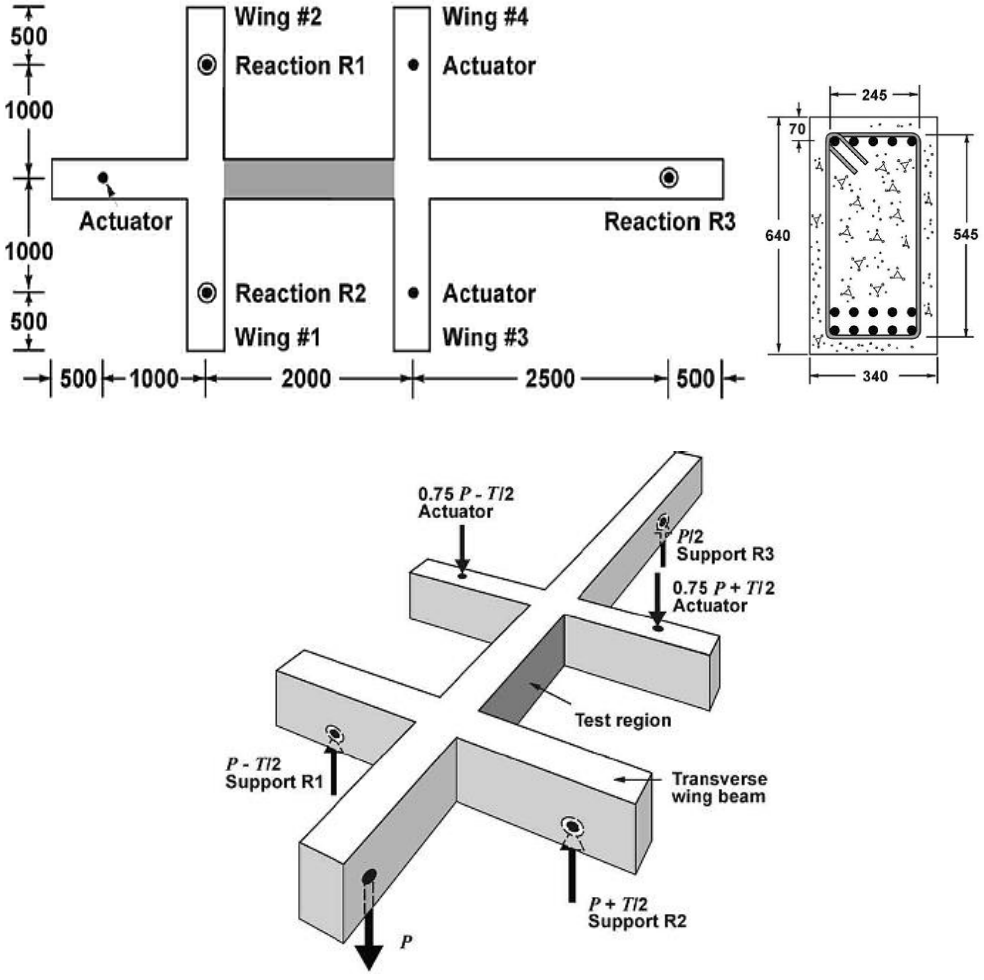

Figure (2-6): Beams geometry, reinforcement, and test setup (Rahal and Collins, 2003).

It was discovered that the ACI arrangements gave moderate outcomes if the suggested estimation of 45^0 is utilized for the inclination of the compression diagonals, but the utilization of reduced θ allowed by the ACI which is 30^0, gave less reliable outcomes, with disappointment loads being over-assessed for high torsion to shear proportions. The use of AASHTO-LRFD with θ of about 36^0 gave reliable and sensibly precise evaluations of the failure loads and was in acceptable concurrence with the watched crack patterns. It is recommended that in utilizing the ACI torsion arrangements, more economical and more consistent designs would be gotten if a θ estimation of 36^0 was utilized for non-prestressed areas instead of the proposed estimation of 45 degrees. Shear to torsion relations and comparison of calculated θ and observed angle of cracks are shown in Figure (2-7).

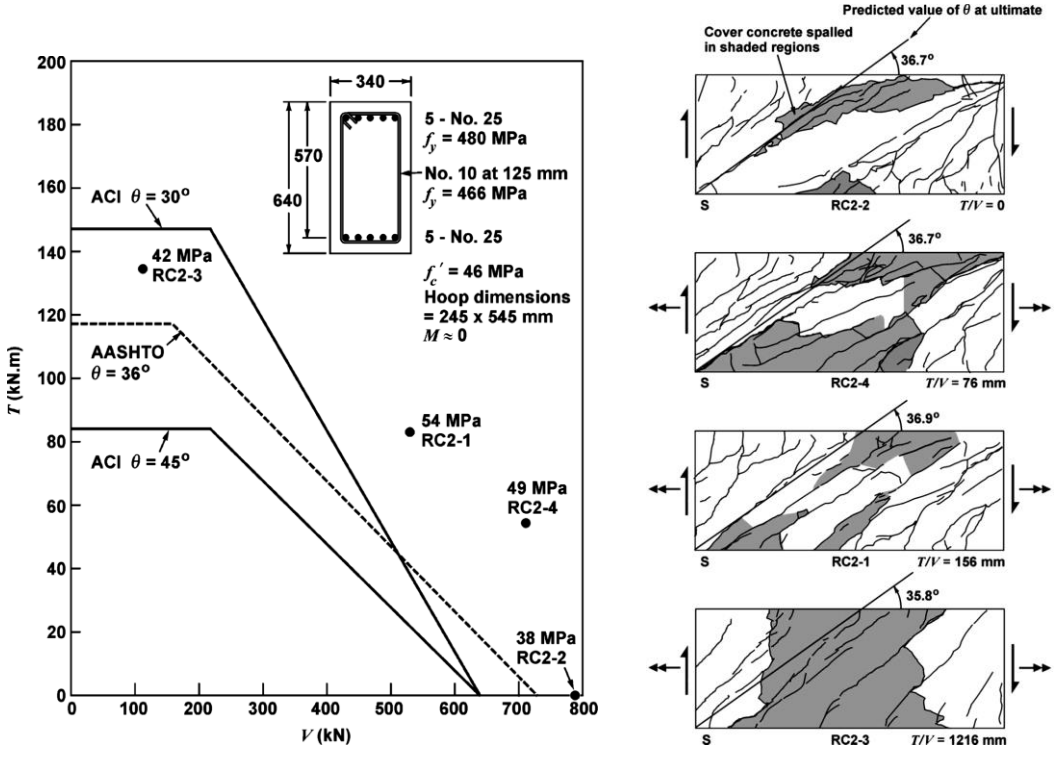

(a) (b)

Figure (2-7): (a) Shear-torsion interaction diagrams; (b) Comparison of calculated θ and observed angle of cracks (Rahal and Collins, 2003).

Kamiński and Pawlak, 2011 [38] presented experimental, numerical analyses and theoretical analyses results of reinforced concrete beams made of angular inverted L-shape and rectangular cross-sections. The beams were loaded under two categories of loading to study the load capacity and stiffness of these angular beams. The first type of loading was a solely torsional moment and the second type was a combined load of a torsional moment, a shearing force, and bending moment. The beams geometry, reinforcement, change of sections, and experimental setup showed in Figure (2-8).

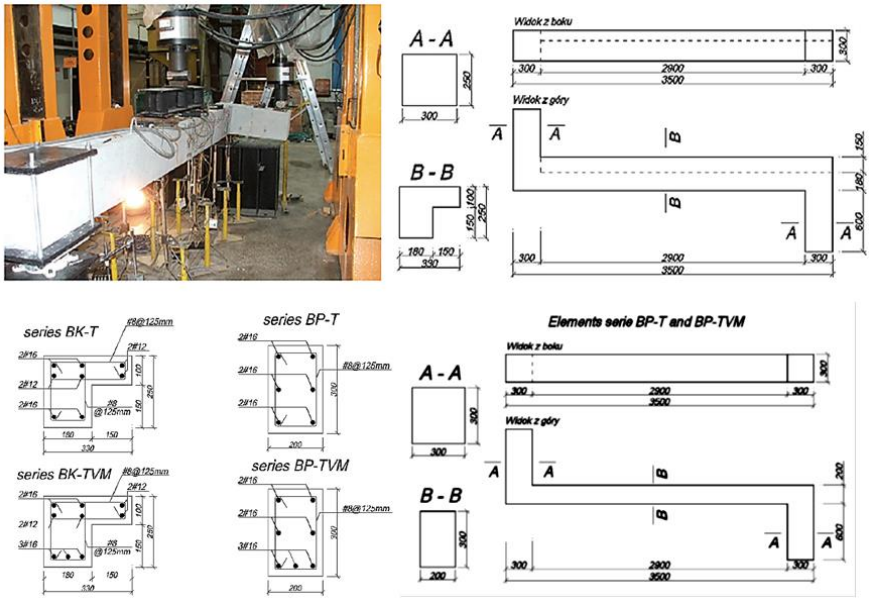

Figure (2-8): Geometry and experimental setup of tested beams (Kamiński and Pawlak, 2011).

Based on the experimental, numerical and theoretical analyses results, the study concluded that the load capacity and stiffness were decreased for the beams under both a torsional moment and a bending moment as compared with the beams loaded with solely a torsional moment.

ACI 445.1R-12, 2013 [39] explained the behavior of solid and hollow reinforced rectangular concrete beams under three types of loading pure torsion, bending plus torsion, and shear plus torsion based on the theoretical and experimental results of many previous researches in these fields. The loading of bending plus torsion without shearing forces for the test region (mid span) as shown in Figure (2-9) was a better case of loading because it was easier when applied constant torsional moment with applying bending moment on the central part of tested beams along time. In these studies, the torsional moment to bending moment ratio was controlled by distances e and a.

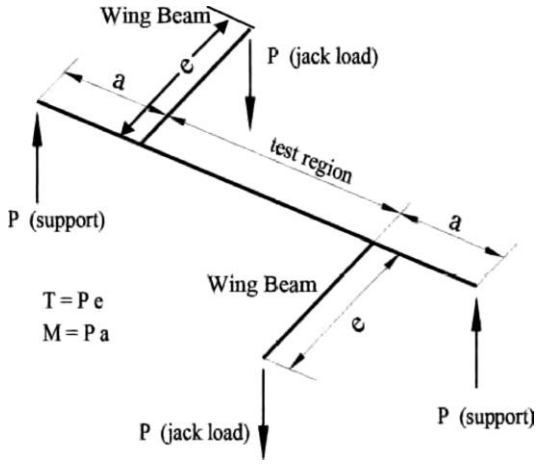

Figure (2-9): Test setup for a beam under torsion and flexure loading (ACI 445.1R-12, 2013) .

Results of the researches showed that the presence of a bending moment reduced the torsional ductility of the beams, as shown in Figure (2-10). The torsion to bending moment ratio affected on the diagonal angle of the crack patterns, in the case of pure torsion, the crack was diagonal on the bottom face, and in the case of pure bending, the cracks angle became normal to the longitudinal axis of the beam.

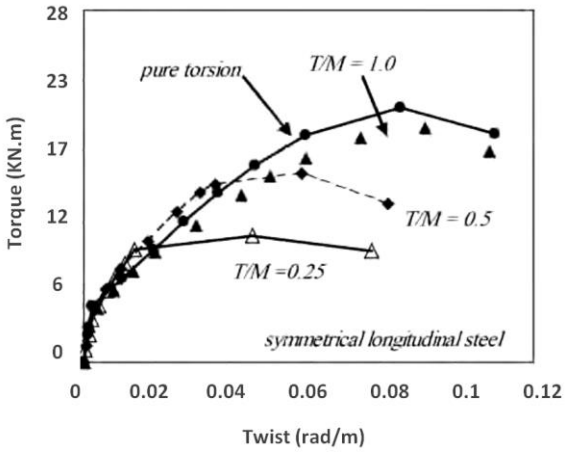

Figure (2-10): Torque and twist relationships at various Torsion/Moment ratios (ACI 445.1R-12, 2013).

The case of torsion with shear loading was relatively limited mainly because shear force cannot be assumed without causing a bending moment along the beam's test region. Therefore, the torsion to shear condition was achieved only at the point of inflection. Otherwise, an experimentally observed torsion to shear interaction curve was a part of the torsion-shear-bending moment curve on the torsion to shear coordinate plane. Additionally, the pure shear strength of a beam could not be determined experimentally. Torsional moment reduced the shear strength of the beam, especially if the applied torsion is more than 25% of pure torsional strength.

At last, in all the loading cases the post-cracking strength and ductility were significantly affected by the longitudinal and transverse reinforcement directions as compared with beams reinforced in the longitudinal direction only. Also, the behaviors of these members were dependent on the distribution and amount of longitudinal reinforcement.

Qian and Li, 2013 [40] tested reinforced concrete frames subjected to the loss of a ground corner which represents corner panels. Seven one-third-

scale RC frames were tested to investigate their performance. The parameters of the study of the tested specimens were the change of beam transverse reinforcement ratios, type of design detailing (nonseismic or seismic), and beam span aspect ratios. Frame test setup, geometry, and its reinforcement showed in Figure (2-11).

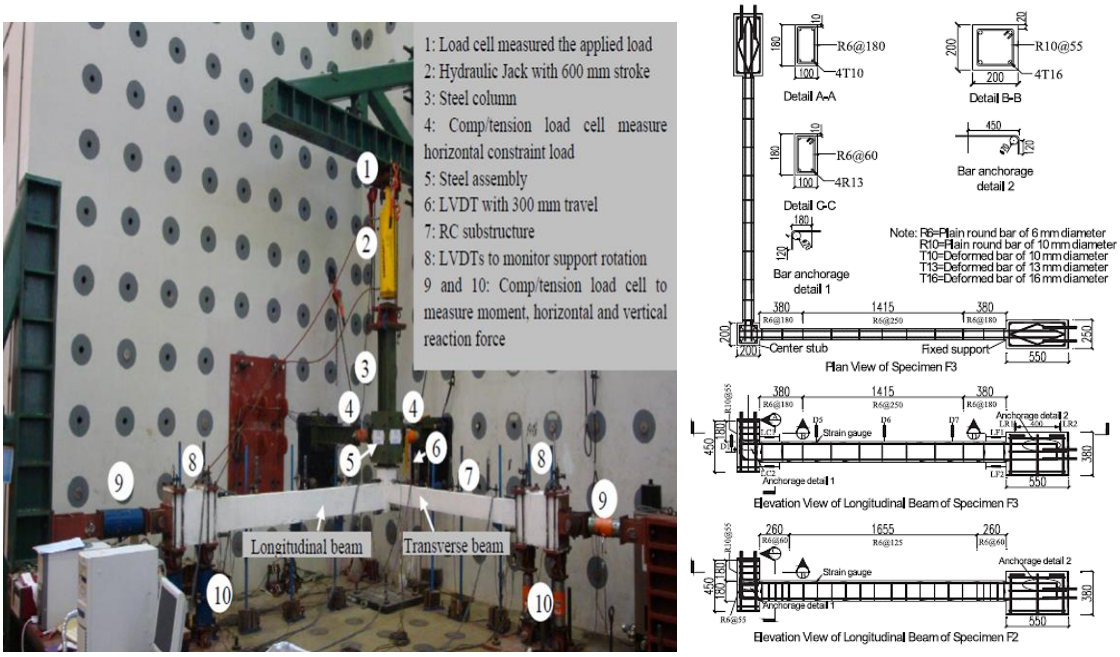

(a) **(b)**

Figure (2-11): a- frame test setup; b- Frame geometry and its reinforcement (Qian et. Al., 2013).

From experimental and analytical results, it was concluded that the loss of corner column caused the progressive collapse of the frame and the flexural capacity of the beams increased when the longitudinal beam reinforcement increased led to improve of the frame behavior, and plastic hinge developed at the beam end near to the corner joint when placed a moderate amount of transverse reinforcement in the corner joint region. Test results also specified that there are two methods to improve the behavior of

RC frames to resist progressive collapse caused by missing a corner column. The first method was by increasing the flexural capacity of the beam by increasing the longitudinal reinforcement ratio. The second method was by improving the shear strength of the corner joint by adding more transverse reinforcement at the joint to confine the corner joint.

Elsayed et al, 2015 [41] studied experimentally the structural behavior of reinforced concrete beams with inclined cantilevers to explore the effect of increasing the angle of cantilever inclination from zero to 90 degrees and the reinforcement ratio on the beams' structural behavior. Ten beams with dimensions of 120 mm width ×300 mm depth and constant 1000 mm simply supported span with different cantilever span were tested. The specimen's geometry, reinforcement ratios, and change of cantilevers inclination showed in Figure (2-12).

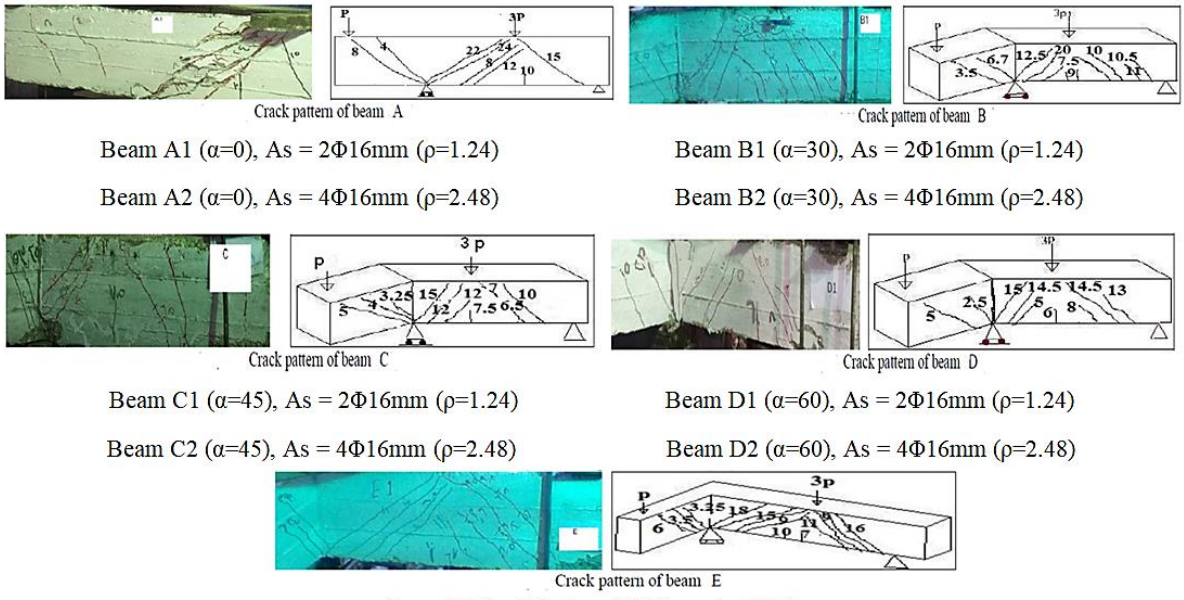

Figure (2-12): Details of beams (Elsayed et al, 2015).

From the experimental results, they concluded that decreasing of cracking loads and ultimate loads were slightly affected by increasing the angle of inclination, but the maximum deflection, maximum strain, and the overall stiffness of beams were highly affected and all beams failure modes were diagonal tension cracks. The increasing of main longitudinal reinforcement ratios led to the increase of all the diagonal cracking load, ultimate load, and flexural cracking load respectively.

Karim et al, 2016 [42] experimentally tested four reinforced fibrous high strength concrete beams that were designed according to ACI318-14 with a constant of clear span to depth ratio and the height to width ratio to study the effect of additional reinforcements in the concrete idealized core zone under pure torsional loading and check the effects of secondary shear flow zone on the torsional capacity. Space truss analogy theory assumed that the solid concrete section behaves as a thin-walled tube. The thin-walled tube could be defined as the idealized shear flow zone, while the area inside of the tube was considered as idealized core zone. The longitudinal and transverse reinforcement ratios were constant at the main shear flow zone but increased the percentage of the area in the idealized core zone at the additional reinforcement zone. Beams reinforcement and experimental test setup is shown in Figure (2-13).

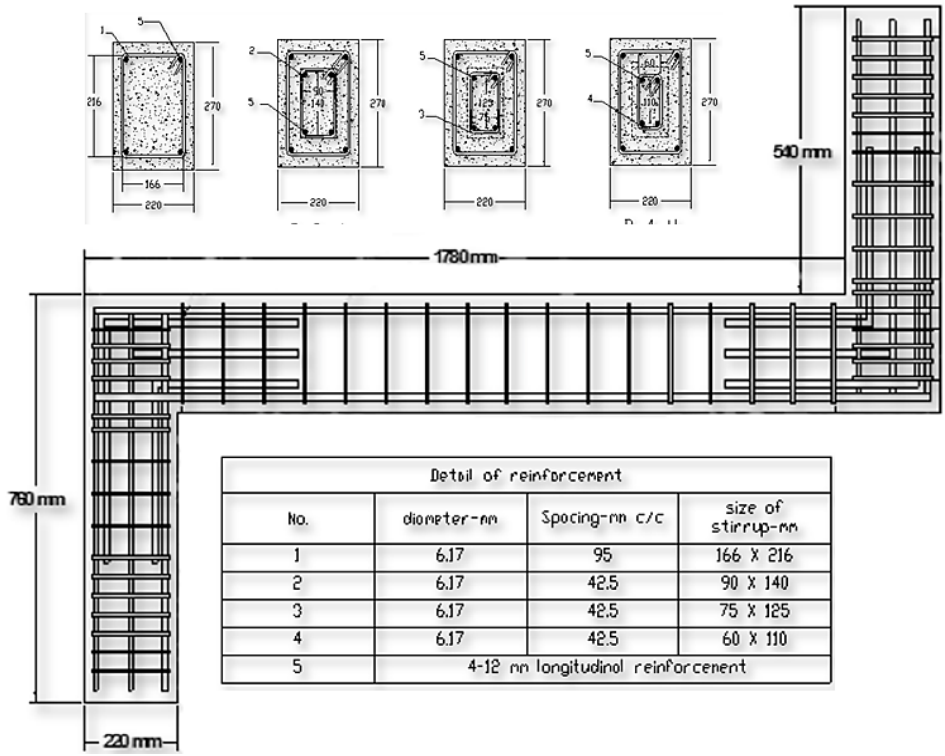

Detail of reinforcement			
No.	diameter-mm	Spacing-mm c/c	size of stirrup-mm
1	6.17	95	166 X 216
2	6.17	42.5	90 X 140
3	6.17	42.5	75 X 125
4	6.17	42.5	60 X 110
5	4-12 mm longitudinal reinforcement		

(a) Reinforcement details

(b) Test setup

Figure (2-13): (a) Beams reinforcement; (b) Experimental test setup (Karim et al, 2016).

The research conclusions included that the additional transverse and longitudinal reinforcements in the idealized core zone were increased the torsional capacity at the ultimate load and improved the twisting angle and shear strain at the ultimate load, but the cracking torsional moment was not improved because it was influenced proportionally by the compressive strength of concrete. Result of beams behavior is shown in Figure (2-14).

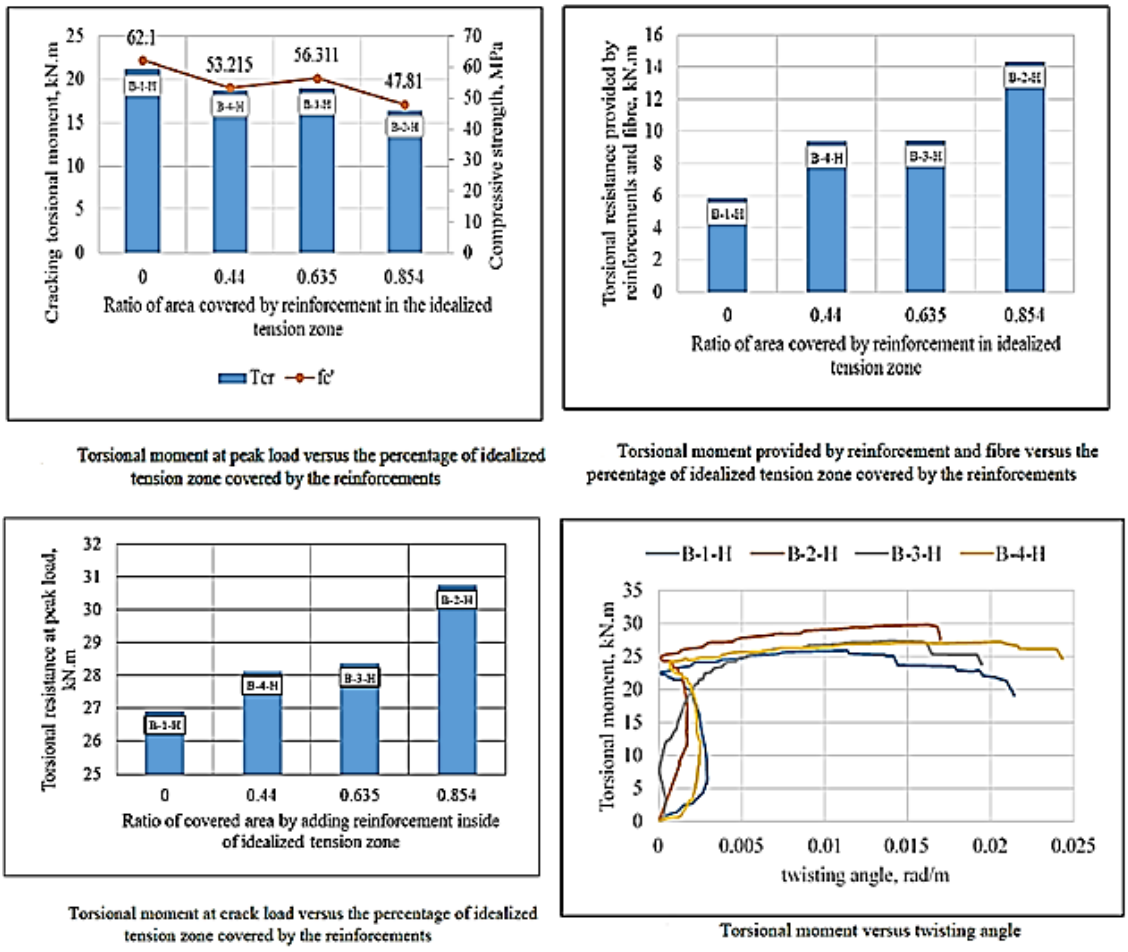

Figure (2-14): Results of beams behavior (Karim et al, 2016).

Nagendra and Naresh, 2017 [43] tested a cantilever reinforced concrete L-section beams under torsional loading by experimental work and finite element analysis by ANSYS software to study the effects of longitudinal and transverse reinforcement reductions on the beams behaviors

under torsional loading conditions. The control beam was designed as a cantilever beam to resist the design bending moment, and then the second beam with a reduced longitudinal reinforcement ratio by 30% and the third beam with reduced 30% of transverse reinforcement. Beams reinforcement and test setup showed in Figure (2-15).

(a) Control beam Second beam Third beam

(b)

Figure (2-15): (a) Beams reinforcement; (b) Experimental test setup (Nagendra and Naresh, 2017).

As result, the experimental and finite element analysis results provided that the ultimate torsion was decreased by 25.71% when decreasing the longitudinal reinforcement and 28.57% when decreasing the transverse reinforcement as compared with reference beam. In addition, the beam with

reducing longitudinal reinforcement failed earlier than beam with reducing of transverse reinforcement because it had bending crack in addition to torsional cracks which made it weaker.

Buda-Ożóg, 2017 [44] analyzed six cantilevers reinforced concrete beams made in a full scale with cross-section 300mm x 300mm that were loaded by torsional moment, bending moment, and a shear force to investigate torsional capacities, stiffness, the influence of reinforcement type on deformation, and cracking patterns then the experimental results compared with the calculated results from equations based on the previous theories. Beams were classified into three groups in the experimental tests, each group consist of two beams with reinforcement obtained based on the first strut, and tie models with the concrete compression diagonal strut were inclined to the axis of the chord at the angle of 45 °, 37 °, 26.6^{o} respectively. Geometry and reinforcement of beams and experimental test setup is shown in Figure (2-16).

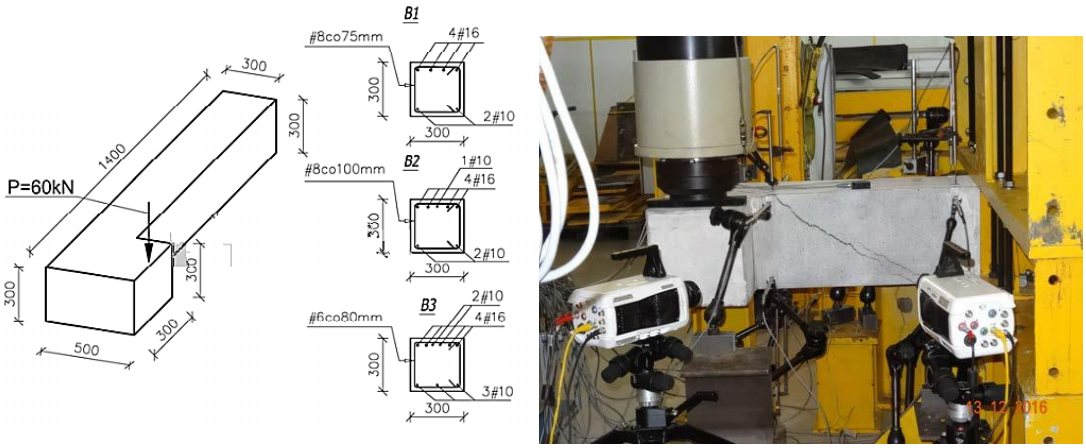

(a) (b)

Figure (2-16): (a) Geometry and reinforcement of beams; (b) Experimental test setup (Buda-Ożóg, 2017).

From experimental tests and theoretical results of the research, it was concluded that load-bearing capacity of the strut and tie models were highly lower than the capacity calculated from equations based on the previous theories and experimental tests. Also, the beams with diagonal strut inclined at the angle of 45^0 that based on strut and tie models when reinforcement prepared were generally higher stiffness and load-bearing capacities than other beams as shown in Figure (2-17). The concrete compression diagonal struts is inclined to the axis of the chords at angle of 45° separated by cracks on each side of the vertical elements of truss that were represented by stirrups reinforcement and horizontal element that were represented by the top and bottom chords of the truss that represents tension reinforcement and compressed accordingly. This indicated that transverse reinforcement was more effective in the transmission of torsion moment than longitudinal reinforcement.

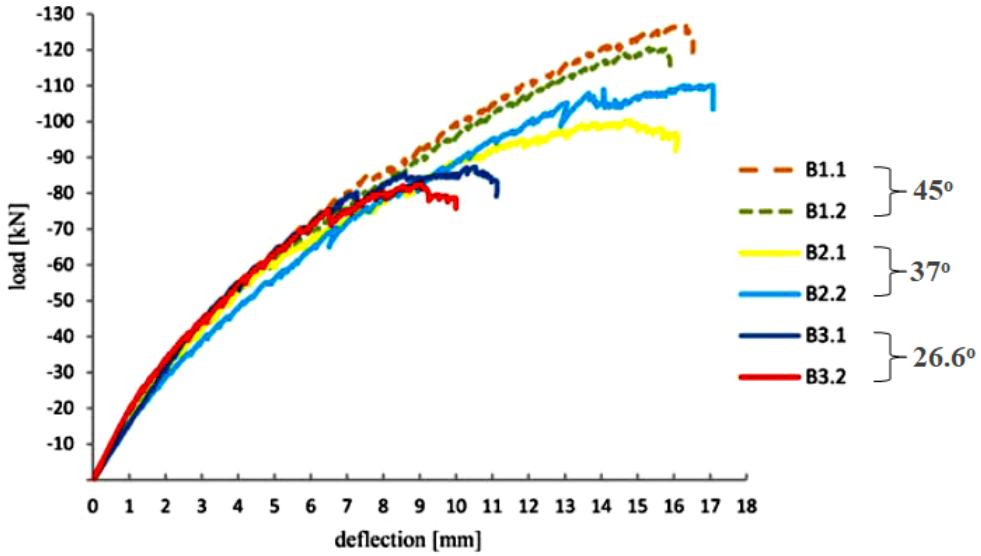

Figure (2-17): The load and deflection relationship (Buda-Ożóg, 2017).

The term "diagonal compression" that was used in the space truss analogy or strut and tie method and mentioned in the previous research

above was explained in the ACI-code as shown in Figure (2-18). Furthermore, the forces that acting on the section under torsion are explained in Figure (2-19).

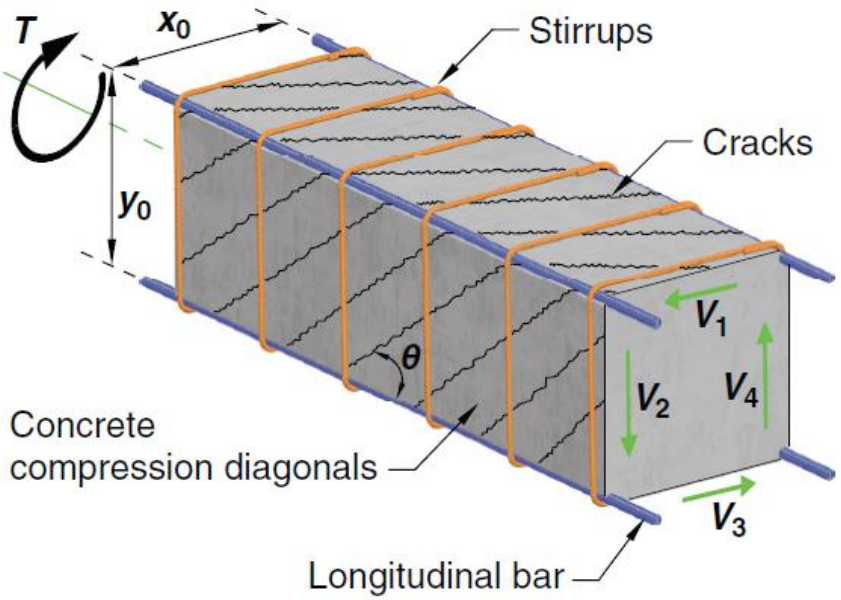

Figure (2-18): space truss analogy (ACI-Code, 2019).

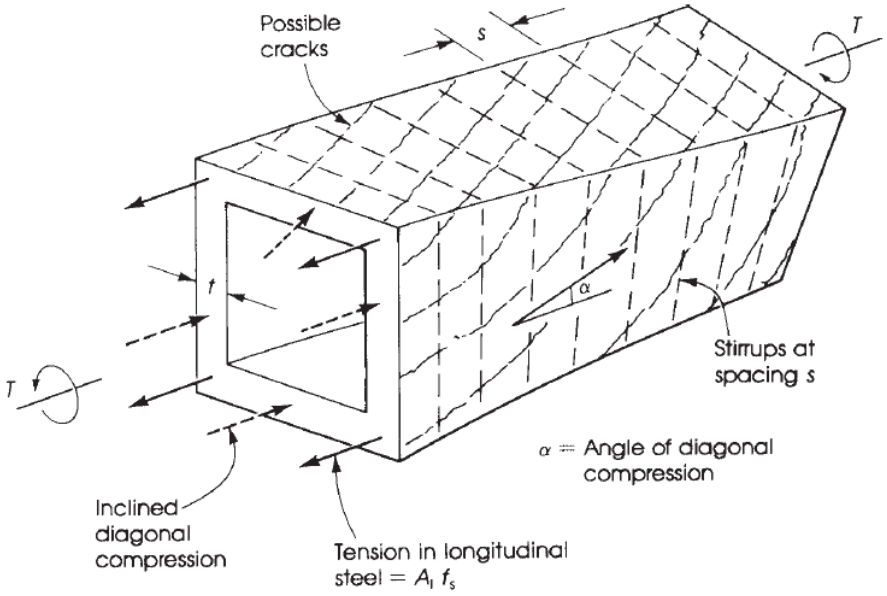

Figure (2-19): Forces on section under torsion (space truss analogy) (Hassoun and Al-Manaseer, 2020).

2.4 Concluding Remarks

From the previous researches that were presented in this chapter, several remarks were concluded regarding the structural behavior of the reinforced concrete beams flexural with the out of plane part:

1- Most researches over the past years focused on the investigation of the structural behavior of concrete beams under the effect of the combined loads that were applied on the beams by cast in place or loading steel side arms in pure torsion or combined of shear force, bending moment, and torsion moment, but it was too limited or in the otherwise is not available researches about reinforced concrete beam with out of plane parts.

2- Researches in the literature review showed that increasing concrete compressive strength led to improve ductility of the straight concrete beam up to about 80-100 MPa and thereafter decreased as compressive strength was increased. In this study, the ductility of the straight beam and the beams with out of plane part was studied by using concrete with a maximum compressive strength 78 MPa to prove this fact for the straight beam and to investigate if it is possible to explore this fact for the beams with out of plane part.

3- Most researches studied the structural behavior of the concrete beam focused on one mid span part supported by two ends with a rotatable supports or fixed ends, but more than one part between the supports has not studied yet, so in this current study the beams with more than one part was studied.

4- The previous researches studied the structural behavior of the concrete beams under the effect of some parameters like loading type, concrete grad, and reinforcement ratios and compared the results of the tested

beams with reinforced beam have same their geometry but the comparison with the straight beam is too limited. In this current study, all the results of the tested beams were compared with the results of the tested straight beam.

5- The studies concluded that the increasing concrete compressive strength led to increase all of the shear force, bending moment, and torsional moment capacities and the increasing longitudinal and transverse reinforcement ratios caused increasing of these capacities of the straight beams. In the current study the effect of concrete compressive strength and reinforcement ratios on capacities of the straight and non-straight beams were studied.

6- Most researches studied the structural behavior of the concrete beams under pure bending, pure shear, and pure torsion then compared their behaviors with the beams under combined of these loads and concluded that the beams under combined loads has capacities lower than the beams under pure load. In the current study, the straight beams loaded with pure load while the beams with the out of plane part were loaded by the same loading protocol but they are exposed to combined loads according to their geometries.

Chapter Three: Experimental Work

3.1 Introduction

The main purpose of the experimental work of this research is to study the structural behavior of high strength reinforced concrete beams with *Out of Plane Part* that can be achieved by using fourteen models with different arms of out of plane part and different ratios of reinforcement. The details of the experimental program are presented in this chapter.

This chapter contains details of the materials that have been used in this study and, it consists of a series of standard tests according to the Iraqi and American standards (IQS) and (ASTM); respectively. Material properties of cement, coarse aggregate, fine aggregate, mineral admixture (Silica fume), and chemical admixture (SP) used in this study are reported.

Thereafter, the mix proportion of NSC and HSC according to the trial mixes, the final mix design, and specimens' preparation are presented. Also, mixing procedures are presented in addition to the casting and curing process. Then, the fresh concrete tests which have been carried out for NSC and HSC mixes during its fresh state are all described. In hardened state, various testing procedures for the mechanical properties of steel reinforcement and concrete at 28 days are presented according to the specifications which consist of density, compressive strength, tensile strength (flexural and splitting), and elastic modulus.

This chapter also includes detailed information about beam formwork and reinforcement preparation procedure. Finally, the measurements and testing setup are explained. Through beam model tests, vertical deflection, and rotation were measured at the points of change in the span axis. Also,

crack width, cracks propagation and distribution in tension and compression faces for all reinforced concrete beam models are performed.

3.2 Material Properties

3.2.1 Cement

Ordinary Portland cement (CEM I-R 42.5) manufactured in Iraq city/ Al-Sulaymaniyah with the trade mark of (Mass) had been used throughout this investigation for casting all the specimens. **Appendix-A** listed the chemical and physical properties of this cement in Tables (A-1) and (A-2); respectively. The test results showed that the cement adapts to the provisions of **Iraq specification No. (5)-1984** [45]. These tests were carried out in the National Center for Construction Laboratories / Laboratory Baghdad.

3.2.2 Fine Aggregate

Badra natural sand was used in this work. It was tested to determine grading and other physical properties. The grading of this sand within zone 2 and conformed to **Iraqi specification No.45 / 1984** [46] as shown in Table (A-3), Table (A-4) and Plate (3-1), see **Appendix-A**.

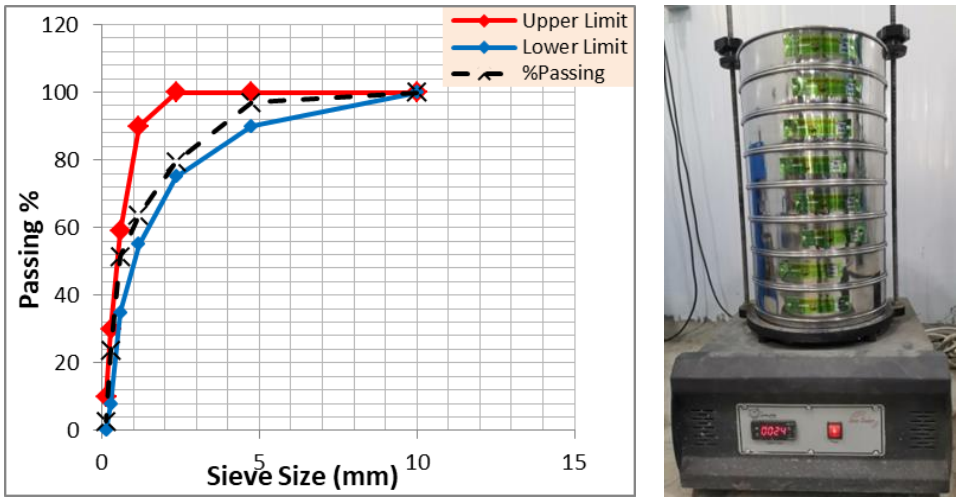

Plate (3-1): Sieve analysis and grading curve of fine aggregate.

3.2.3 Coarse Aggregate

In this study, the coarse aggregate with a maximum size of 12.5 mm used for manufacturing concrete beams. It was cleaned and crushed gravel from (Gallate) region. All the used coarse aggregate with separated at sieve size (12.5mm) to isolate the aggregate with particles size more than 12.5 mm which after that was washed until removal of all dust and fine material and dried in the air then to fulfill the requirement of saturated surface dry condition, after that, it was ready for use, see Plate (3-2). The grading and other physical properties of the used coarse aggregates are conformed to the limits of Iraqi specification **No.45 / 1984** [46] and presented in Plate (3-3) and in the Tables (A-5) and (A-6) of Appendix A.

Plate (3-2): Preparing coarse aggregate (gravel).

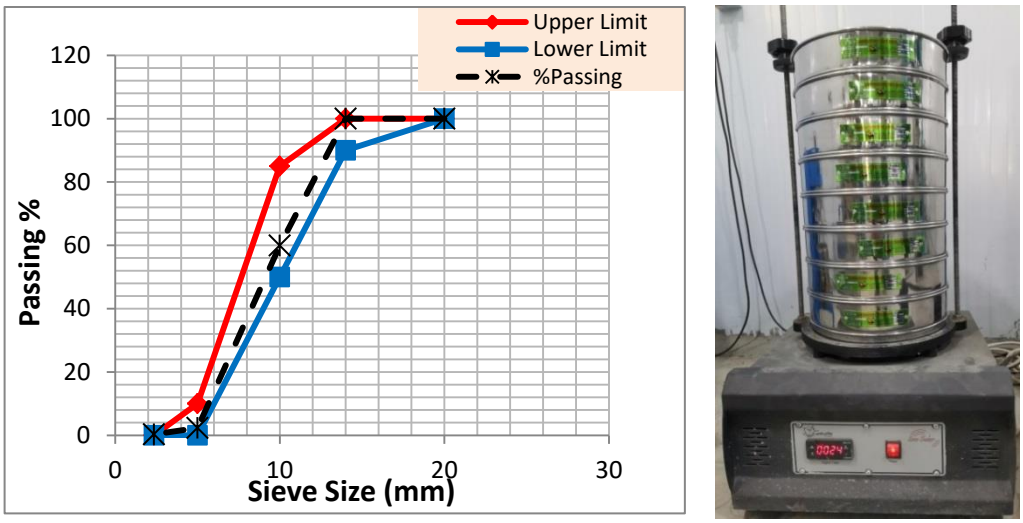

Plate (3-3): Sieve analysis and grading curve of coarse aggregate.

3.2.4 Silica Fume

Micro Silica Fume had been used as a mineral admixture added to the mixture as a partial replacement of the cement in the production of HSC. In this study, silica fume used was U.A.E production which is commercially known as Mega MS (D) bought from local markets.

The physical properties and chemical composition of the SF which be used in this study are shown in Table (A-7) and Table (A-8) respectively, see Appendix-A which were got from the manufacture data sheet which conforms the requirements of **ASTM C1240-05** [47].

3.2.5 Superplasticizer (HRWRA)

A high range water reducer as a chemical admixture was used with mineral admixture silica fume to produce HSC. High Performance Superplasticizer Concrete Admixture with commercial name (Sika ViscoCrete -5930L) complies with **ASTM C494** [48] Type G and F and BS EN 934 part 2: 2001. It is suitable for use with all types of Portland cement and cement replacement materials such as PFA, GGBFS, and microsilica.

The optimum dosage between 0.2-2% liters by weight of cement can be used for high strength concrete. Appendix A-6 shows the typical properties of Sika ViscoCrete -5930L.

3.2.6 Water

Ordinary tap water was used for concrete mixing and curing in present work.

3.2.7 Steel Bars and Stirrups Reinforcement

The Ukrainian steel bars with nominal diameter (12 mm) were used as longitudinal reinforcing for flexural and torsional reinforcement, while (8 mm) diameter was used in transverse reinforcement. All of the steel rebars were tested by a computerized tensile test machine in order to find out their behavior and mechanical properties. Tensile tests were conducted according to **ASTM A496-02** [49] requirements. See Appendix-A Table (A-9) and Plate (3-4).

Plate (3-4): Testing the mechanical properties of steel bars.

3.3 Mix Proportion

3.3.1 Normal Strength Concrete Mix Design

The normal strength concrete (NSC) was designed according to the American method of mix proportions selection (**ACI Committee 211.1-91**) [(50)]. The target concrete strength (fc′) was 35 MPa at 28 days for test specimens as mentioned in Table (3-3) of Models Identification (section 3.8.3).

The mix proportions of the designed normal strength concrete (NSC) are shown in Table (3-1).

Table (3-1):- The mix proportions of normal strength concrete.

Parameter	Quantity
Cement (Kg/m^3)	400
Sand (Kg/m^3)	818.16
Coarse Aggregate (Kg/m^3)	946
Water (Kg/m^3)	214.6
W/C Ratio	0.54
Slump mm	60
Fresh Density (Kg/m^3)	2604
Air Dry Density (Kg/m^3)	2404
*fc′ (28 days) MPa	35

* f'_c is the average of three cylinders 150X300 mm

3.3.2 High Strength Concrete Mix Design

The high strength concrete (HSC) was designed by depending on the data of some HSC mixtures used previously which had given in **(ACI Committee 363.2R-11)** [51]. The design of mix ratio was adjusted to achieve strength requirement with laboratory trial mixes and the local materials would supersede these tables for the specific project. The target concrete strength (fc′) for all test specimens was 75 MPa at 28 days. The information of HSC trail mixes is shown in Table (3-2).

Table (3-2):- Trail mixes proportion of high strength concrete.

No. of Mix / **Parameter**	**1**	**2 selected**	**3**
Cement (Kg/m^3)	425	487	513
Sand (Kg/m^3)	810	676	685
Coarse Aggregate (Kg/m^3)	1110	1070	1080
SF% Wt. of Cement	9.57	8.8	7.73
Water (Kg/m^3)	128	155	130
SP% Wt. of Cement	3.62	2.53	3.37
W/C Ratio	0.3	0.29	0.25
Slump mm	180	220	210
Fresh Density (Kg/m3)	2708	2624	2604
Air Dry Density (Kg/m3)	2500.26	2485	2548.37
*fc′ (28 days) MPa	83.22	75.69	56.22

* f'_c is the average of three cylinders 150X300 mm

3.4 Mixing Procedures

All the trial batches of concrete mix design and beams concrete mixing was carried out by using a laboratory drum mixer with a capacity of 0.1 m^3 as shown in Plate (3-5). The mixer was kept clean, moist, and free of water before the beginning of the mixing process. This mixer was utilized for the mixing of NSC and HSC.

Plate (3-5): Laboratory Drum Mixer.

3.4.1 NSC Mixing Procedure

NSC was mixed according to **(ASTM C 192/C 192M-15)** [52]. Coarse aggregate was added to the mixer and about 25% of the mixing water was used and mixed for three minutes. Then fine aggregate was added and about 25% of the mixing water and mixed for three minutes. At last, the cement

and the remaining water were added and the mixer was operated for two minutes.

3.4.2 HSC Mixing Procedure

HSC was mixed according to (**ACI 363R-10)** [53] with altered steps of adding water and Superplasticizer until to get the workability and consistency of the mixture. The HSC mixing procedure was stated as below:

1- Mix silica fume and cement in dry condition.

2- Mix Superplasticizer with water for 5 minutes out of the mixer.

3- Place half quantity of coarse and fine aggregate in the mixer.

4- Add all the (Portland cement + silica fume).

5- Add the remaining of coarse and fine.

6- Add all the (water + Superplasticizer) in the mixer and mix 3 minutes.

3.5 Molding, Casting, and Curing Process

The molds that used to cast the beams were made of plywood. The internal surfaces of the cubes, cylinders, prisms molds were well cleaned and oiled to avoid adhesion with concrete after hardening. After that, the reinforcement was placed in the true position for all the beam molds by using concrete spacers at the bottom and side faces to achieve the thickness of the concrete cover.

All beam molds were firmed by a steel frame and placed on the vibrator table. Then, carefully the mixed concrete was poured. As recommended in **ASTM C192/C192M−15** [54], a vibrator table (frequency 3600 vibrations per minute -60 Hz) was used to compact each one of the concrete models. The vibration process was stopped when the air bubbles stop to appear and the concrete surface became smooth.

The upper concrete surface was finished to smooth the face after the casting process by using a steel trowel. Then, a plastic sheet was placed on each mold with an average temperature of 25°C to avoid plastic shrinkage.

The molds were removed from the specimens after 24 hours, and then all of them were placed in the water to achieve ponding curing type as recommended in the **ACI 363R-10** [(53)] and **ASTM C192/C192M−15** [(54)].

After the end of the curing period, the beams models were painted by white emulsion to ensure the monitoring of cracks propagation during testing. After that, the beams models were sketched to specify the location of testing points as described in Plate (3-6).

(A) Molds and placement of reinforcement.

Plate (3-6): Preparing concrete beams and symbols. (Continowed)






(B) Casting, finishing and plastic sheet covering process.


(C) Curing and paint process.

Plate (3-6): (Continued).

3.6 Tests of Fresh Concrete Properties

Fresh properties of NSC and HSC were measured by using the following tests:-

3.6.1 Slump Flow Test

The slump flow test of NSC and HSC was performed in accordance with **ASTM C 143/C 143M-05a** [55] as shown in Plate (3-7).

Plate (3-7): Slump flow test.

3.6.2 Fresh Density Test

The fresh density test of NSC and HSC was conducted according to **ASTM C138 / C138M - 17a** [56] by taking the average result of two cylinders 150×300 mm.

Plate (3-8): Fresh density test.

3.7 Tests of Hardened Concrete

3.7.1 Hardened Density Test

A hardened density test of NSC and HSC was carried out by taking the average result of two cylinders 150×300 mm. This test was done according to **ASTM C642 - 13** [(57)].

3.7.2 Cylinder Compressive Strength

The compressive strength test of NSC and HSC was done according to **ASTM C39/C39M-05** [(58)]. The result of compressive strength was obtained by taking the average value of the two cylinders (150×300 mm) tested at 7, 28, 56, and 90 days by using a hydraulic compression test machine with 2000 kN capability, as shown in Plate (3-9).

Plate (3-9): Cylinder compressive strength test.

3.7.3 Cube Compressive Strength Test

According to **BS1881- part 116:2000** [(59)], the compressive strength of concrete was tested by using a cube of 150 mm for NSC and HSC and

compressed under uniaxial load perpendicular to the face of the cube, as shown in Plate (3-10).

Plate (3-10): Cube compressive strength test.

The average of three cubes was adopted from NSC and HSC and the cubes were tested at 28 and 90 days.

3.7.4 Static-Elastic Modulus and Poisson′s Ratio Test

The elastic modulus (E) and Poisson's ratio were tested according to **ASTM C469 /C469M-14** [(60)], as shown in Plate (3-11). The readings values of electrical strain gages that fixed horizontally and vertically on the face of cylinders (150×300 mm) were recorded and the results were the average of readings for two specimens.

Plate (3-11): Stress-strain relationship and static-elastic modulus tests.

The modulus of elasticity was measured by test devices as shown in Plate (3-11) according to the formula of Ec based on 40% of the stress-strain curve as follow:

$$E_c = \frac{S_2 - S_1}{\epsilon_2 - \epsilon_1} \qquad (3.3)$$

Where:

E_c = Elastic modulus, GPa.

S_2 = Stress conforming to 40 % of maximum load, GPa.

S_1 = Stress conforming to the longitudinal strain of 50 millionths, GPa.

ϵ_2 = Longitudinal strain produced by stress, S_2.

ϵ_1 = Longitudinal strain produced by stress, S_1.

The Poisson's ratio was measured according to the formula of (ν) based on 40% of the stress-strain curve as follow:

$$\nu = \frac{\epsilon_{t2} - \epsilon_{t1}}{\epsilon_2 - \epsilon_1} \qquad (3.4)$$

where:

ν = Poisson’s ratio.

ϵ_{t2} = Transverse strain at midheight of the specimen produced by stress S_2.

ϵ_{t1} = Transverse strain at midheight of the specimen produced by stress S_1.

ϵ_2 = Longitudinal strain produced by stress S_2.

ϵ_1 = Longitudinal strain produced by stress S_1.

3.7.5 Test of Splitting Tensile Strength

In NSC and HSC, the splitting tensile strength was tested according to **ASTM C496 / C496M - 17** [61] by using two concrete cylinders of (100 mm diameter ×200 mm length) were tested at 28,56 and 90 days. The plywood strips with 3.0 mm thick, 25 mm wide, and 200 mm length were located at the top and bottom of the cylinder specimen as shown in Plate (3-12), it is achieved by applying diametrical compressive force with a capacity of 2000 kN along the specimen length until failure of the cylinder into two halves by longitudinal crack breaks.

Plate (3-12): Splitting tensile strength test.

The average result of two cylinders taken to evaluate the tensile strength as:

$$f_t = \frac{2P}{\pi L d} \qquad (3.5)$$

Where:

f_t = splitting tensile strength (MPa),

P = maximum applied load indicated by the testing machine (N),

L = length (mm), and

d = diameter (mm).

3.7.6 Flexural Tensile Strength Test (Modulus of Rupture)

The test was carried out according to **ASTM C78 / C78M−18** [(62)] procedure by using two concrete prisms of dimensions (100×100×400) mm as shown in Figure (3-1) and Plate (3-13).

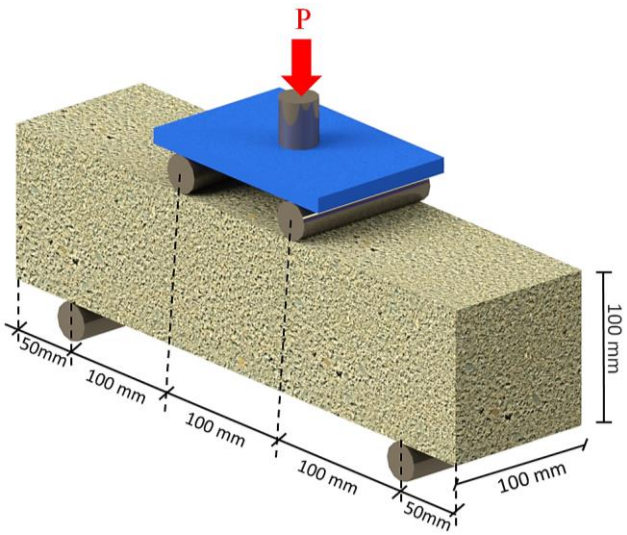

Figure (3-1): Schematic of flexural strength test

Plate (3-13): Two-point load flexural strength test.

The specimens were tested at 28, 56, and 90 days, and the average of two specimen's results was used to evaluate each test. Flexural strength expressed as the modulus of rupture was determined using the results obtained from a simple beam using third-points loading with a clear span of 300 mm, as shown in Plate (3-13). The flexural strength of concrete prisms was determined by using the following formula:

$$f_r = \frac{P.L}{bd^2} \qquad (3.6)$$

Where:

f_r = rupture modulus (MPa),

P = the ultimate applied load (N),

L = the length of the span c/c(mm),

b = average width of prism (mm), and d is average depth of prism (mm).

3.8 Beam Models Identification

The beams were classified according to their compressive strength, geometry, and reinforcement as explained in Table (3-3) and in order to identify the experimental and numerical analysis for the research parameters.

Table (3-3):- Symbols of tested out of plane part beam models.

Symbols	Refer to
NSC-S	Normal Strength Concrete Straight Beam
NSC-1OP	Normal Strength Concrete Beam with One Out of Plane Part
NSC-2OP	Normal Strength Concrete Beam with Two Out of Plane Parts
NSC-3OP	Normal Strength Concrete Beam with Three Out of Plane Parts
HSC-S	High Strength Concrete Straight Beam
HSC-1OP	High Strength Concrete Beam with One Out of Plane Part
HSC-2OP	High Strength Concrete Beam with Two Out of Plane Parts
HSC-3OP	High Strength Concrete Beam with Three Out of Plane Parts
HSC-1OPT	High Strength Concrete Beam with One Out of Plane Part and added Torsional Reinforcement
HSC-2OPT	High Strength Concrete Beam with Two Out of Plane Parts and added Torsional Reinforcement
HSC-3OPT	High Strength Concrete Beam with Three Out of Plane Parts and added Torsional Reinforcement
NSC-I-1OP	Normal Strength Concrete Beam with Increase length of One Out of Plane Part
NSC-I-2OP	Normal Strength Concrete Beam with Increase length of Two Out of Plane Parts
NSC-I-3OP	Normal Strength Concrete Beam with Increase length of Three Out of Plane Parts

The geometry and reinforcement details of the tested beams are shown in Figure (3-2) to (3-11).

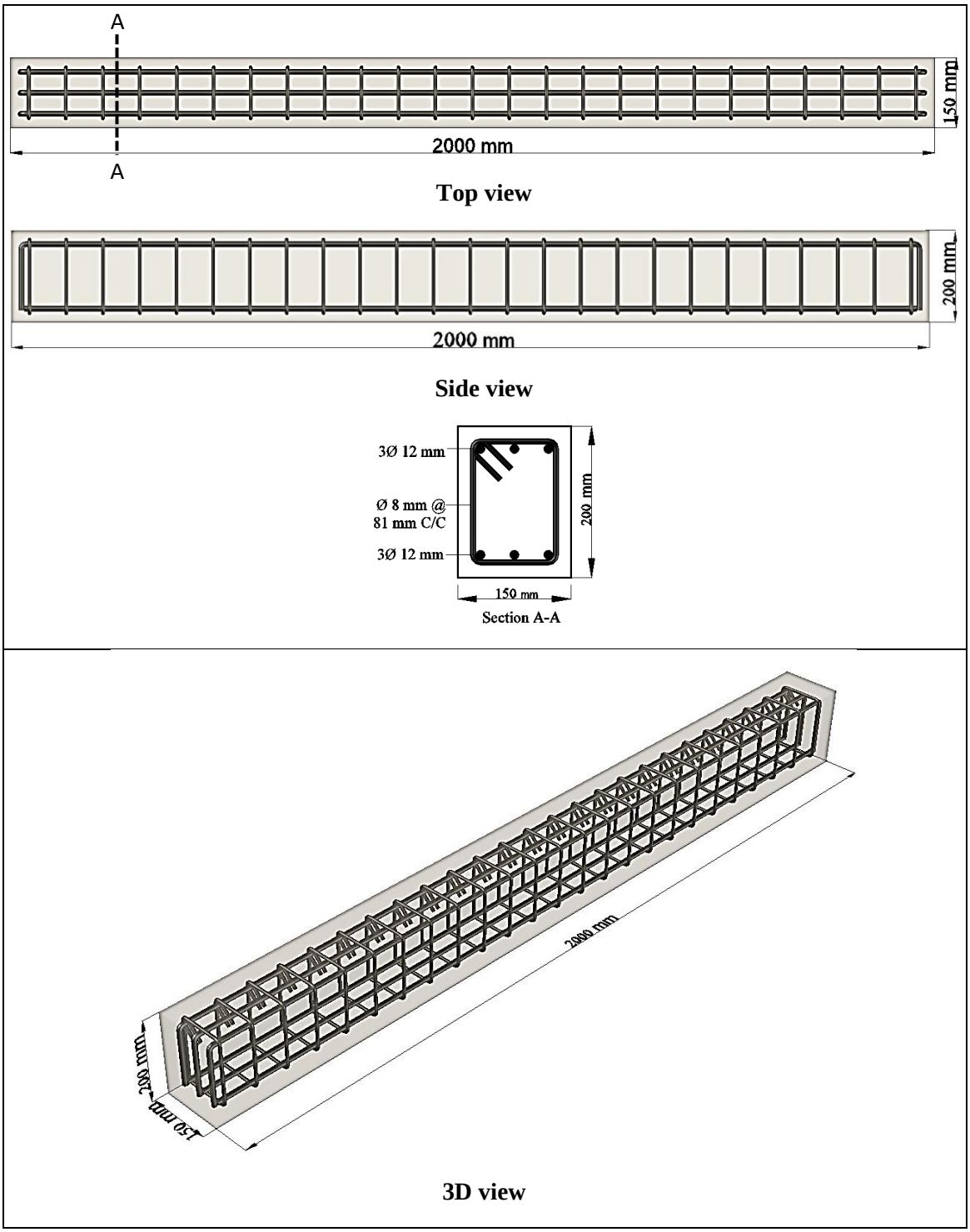

Figure (3-2): Geometry and reinforcement details of beam models (NSC-S and HSC-S).

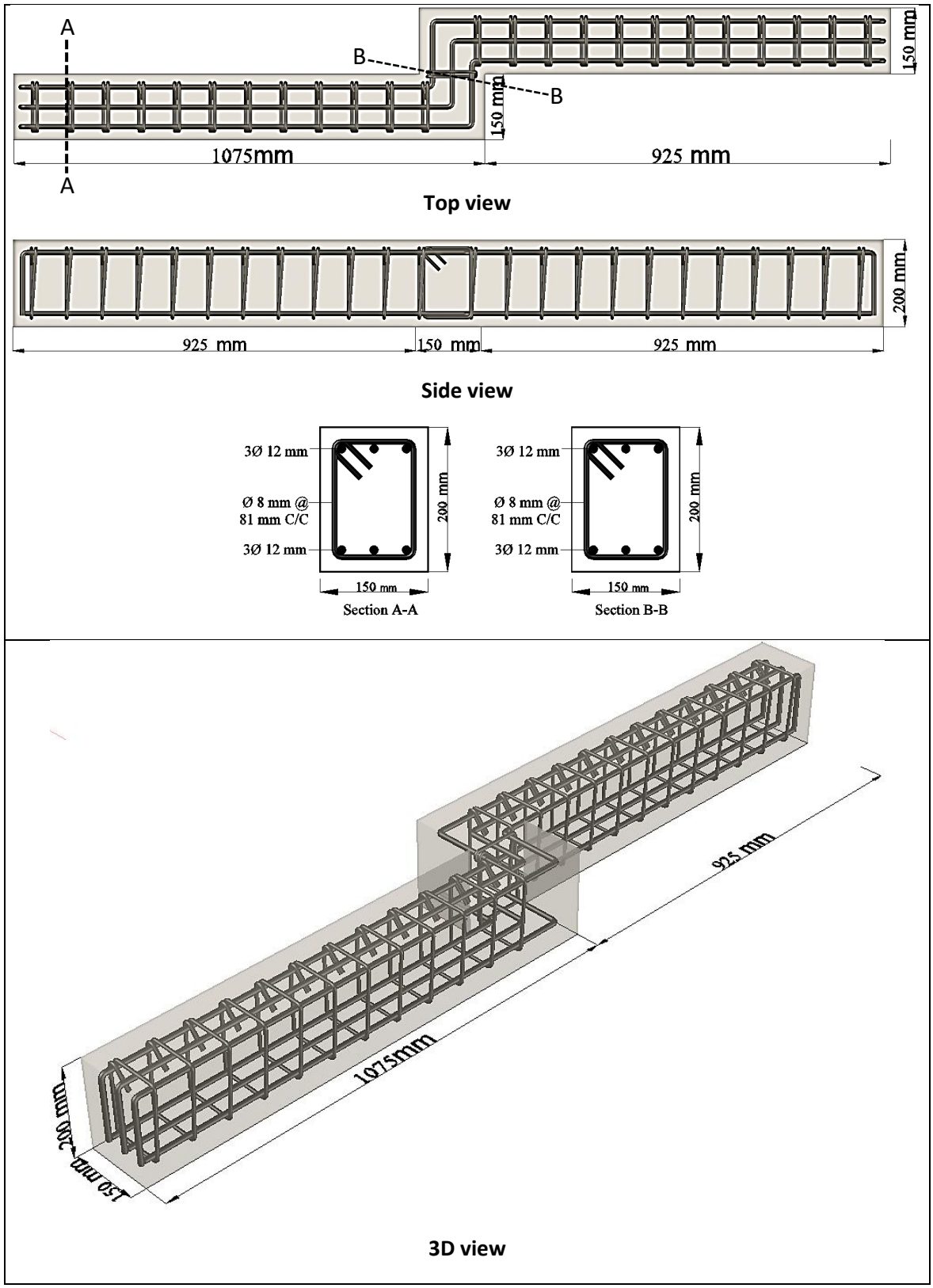

Figure (3-3): Geometry and reinforcement details of beam models (NSC-1OP and HSC-1OP).

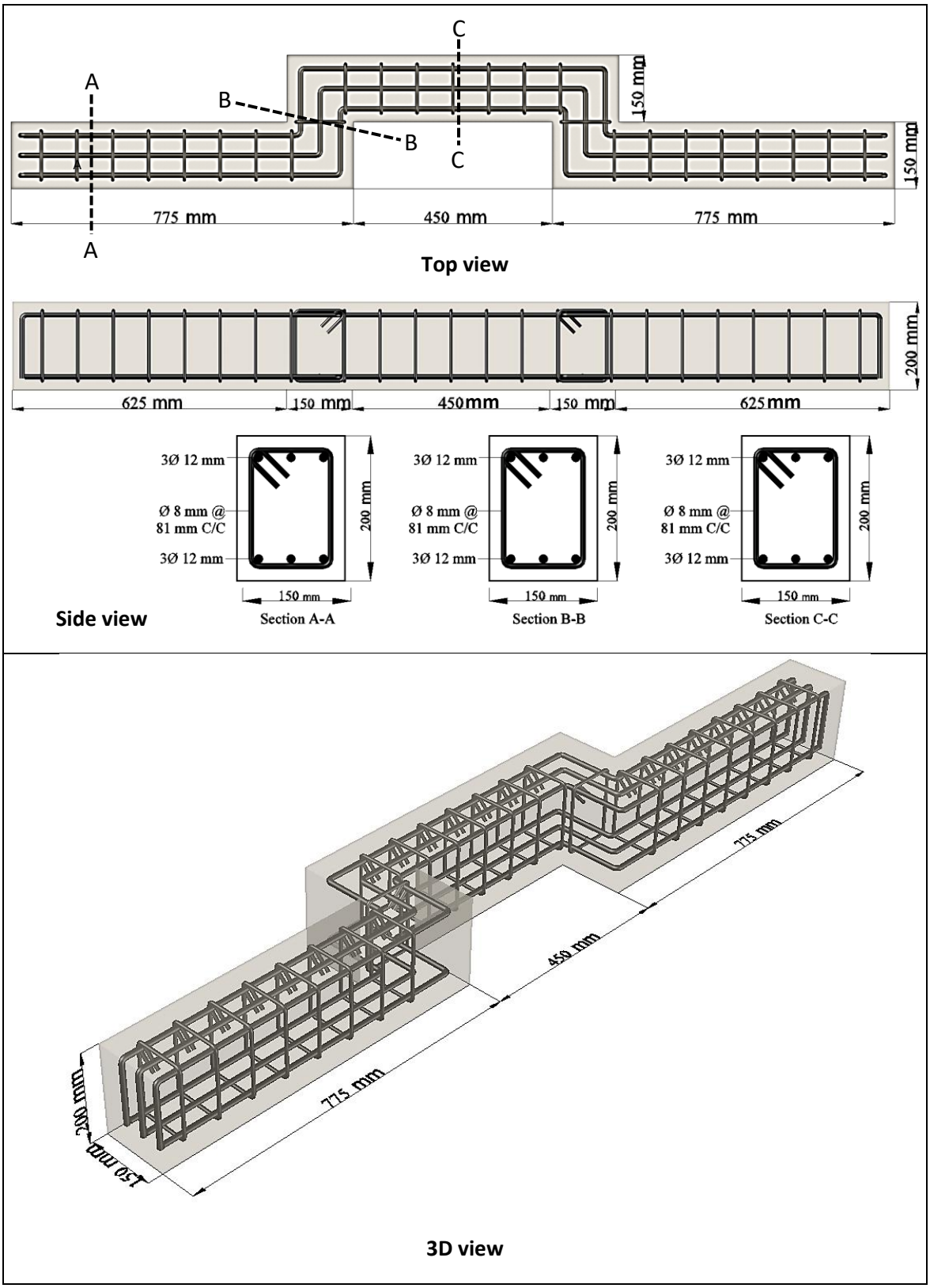

Figure (3-4): Geometry and reinforcement details of beam models (NSC-2OP and HSC-2OP).

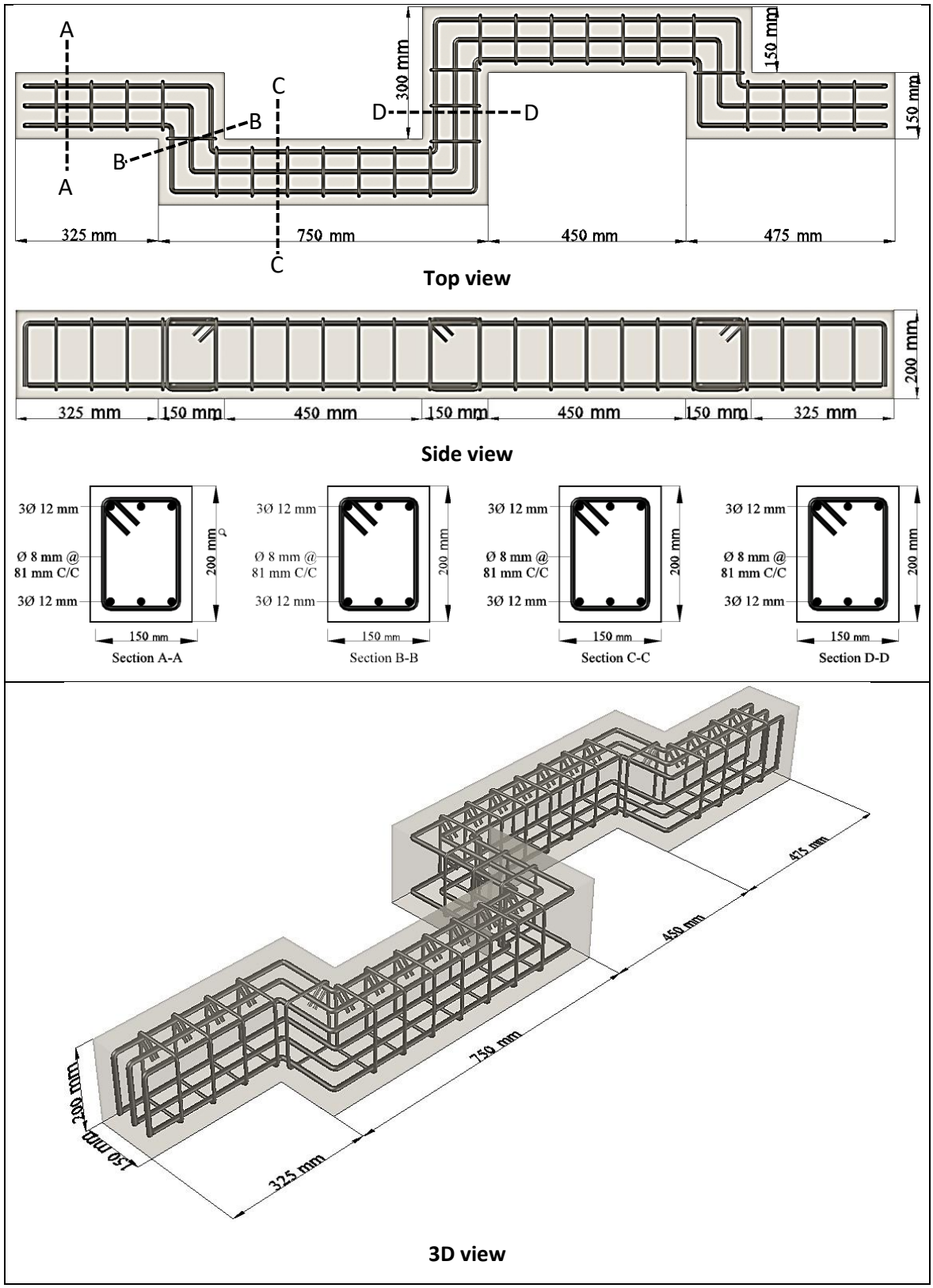

Figure (3-5): Geometry and reinforcement details of beam models (NSC-3OP and HSC-3OP).

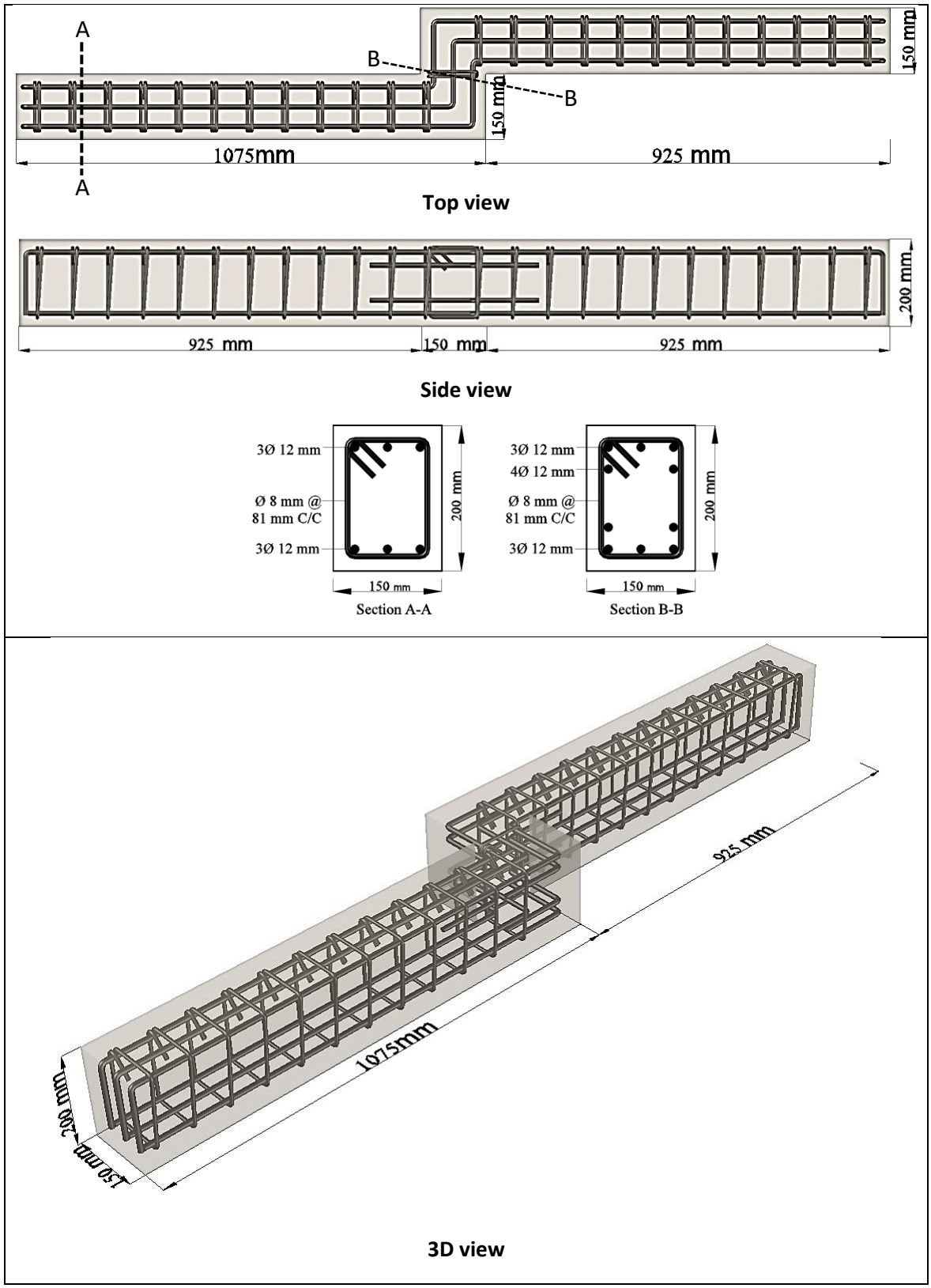

Figure (3-6): Geometry and reinforcement details of beam models (HSC-1OPT).

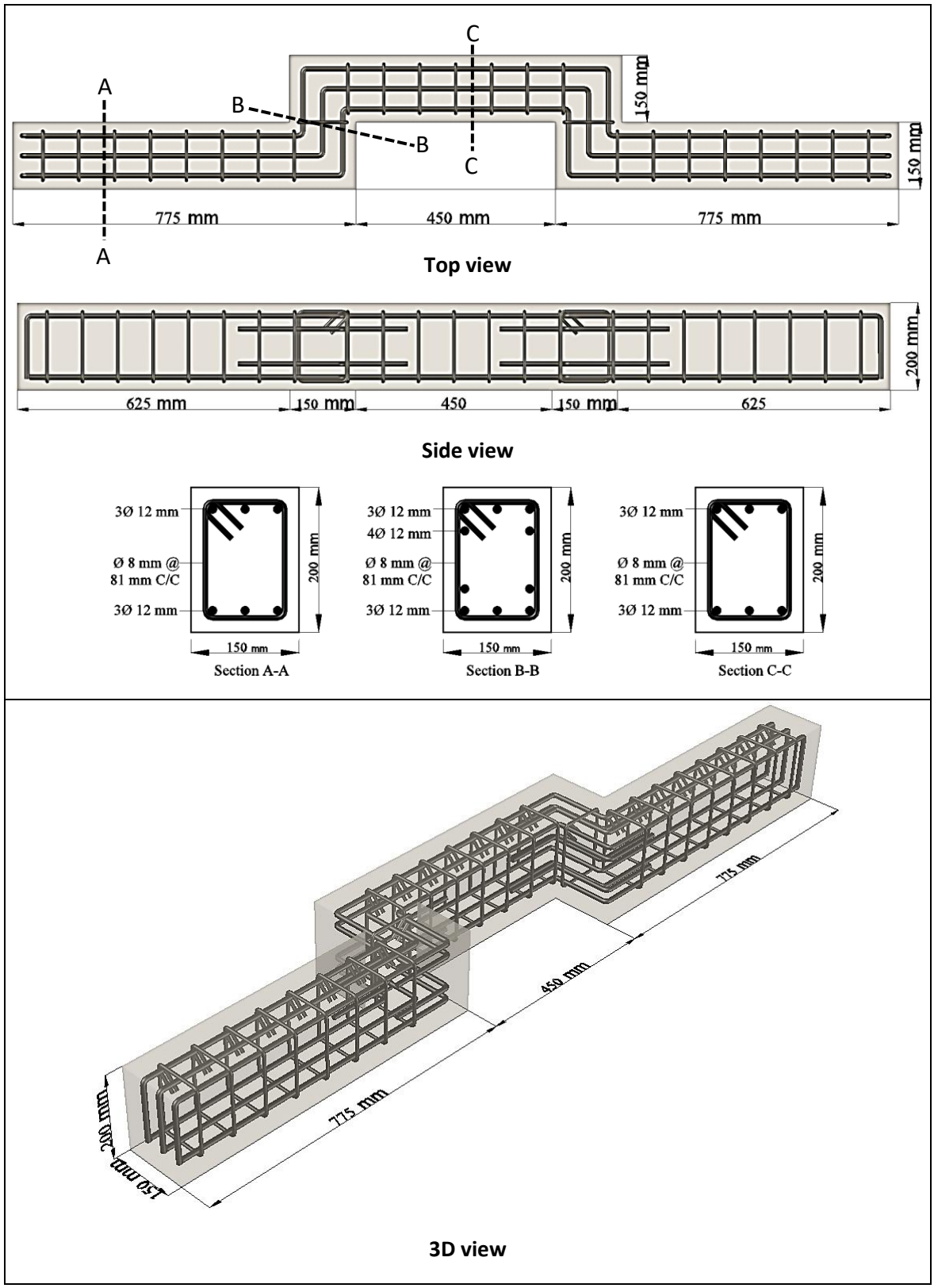

Figure (3-7): Geometry and reinforcement details of beam models (HSC-2OPT).

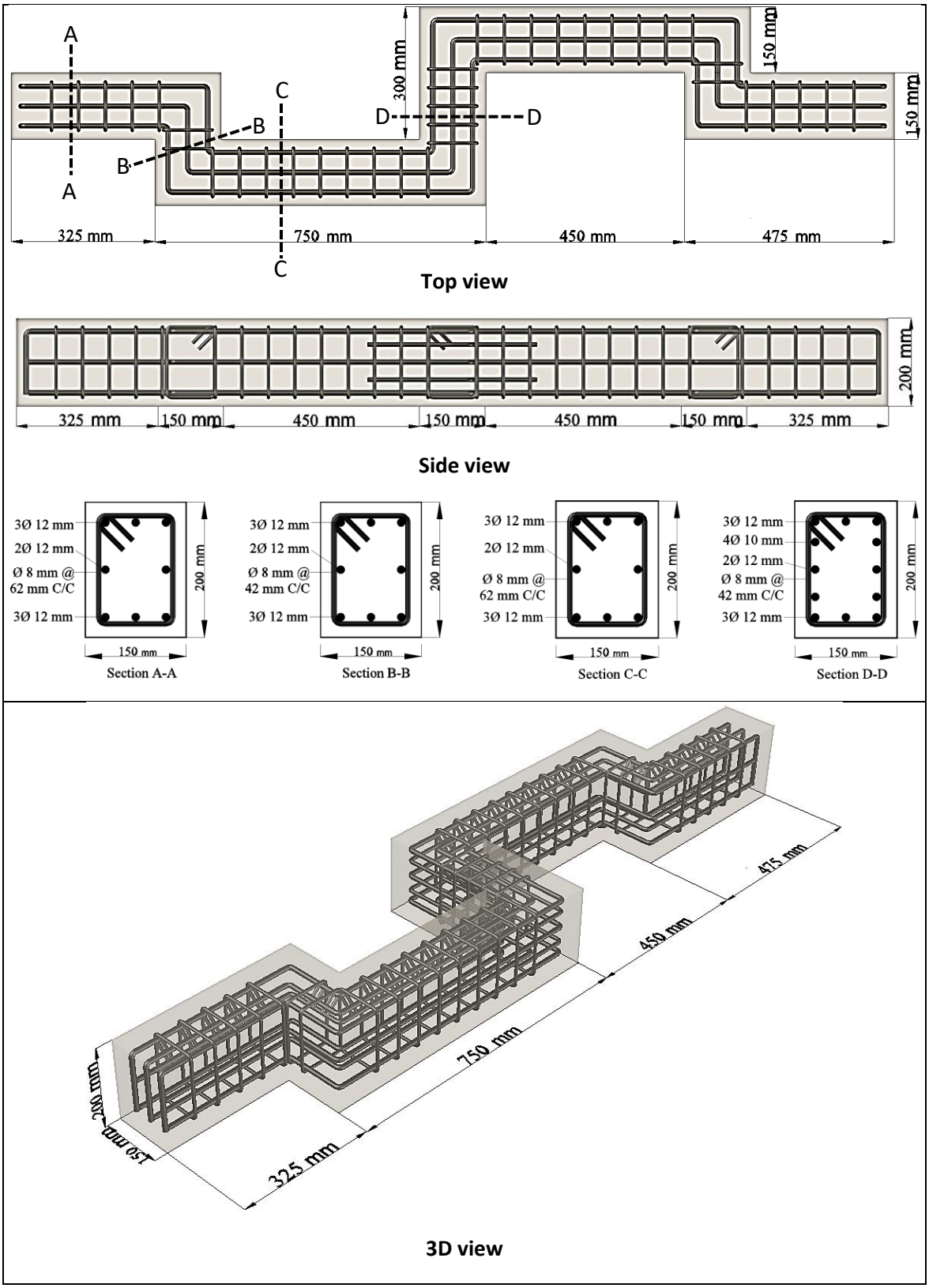

Figure (3-8): Geometry and reinforcement details of beam models (HSC-3OPT).

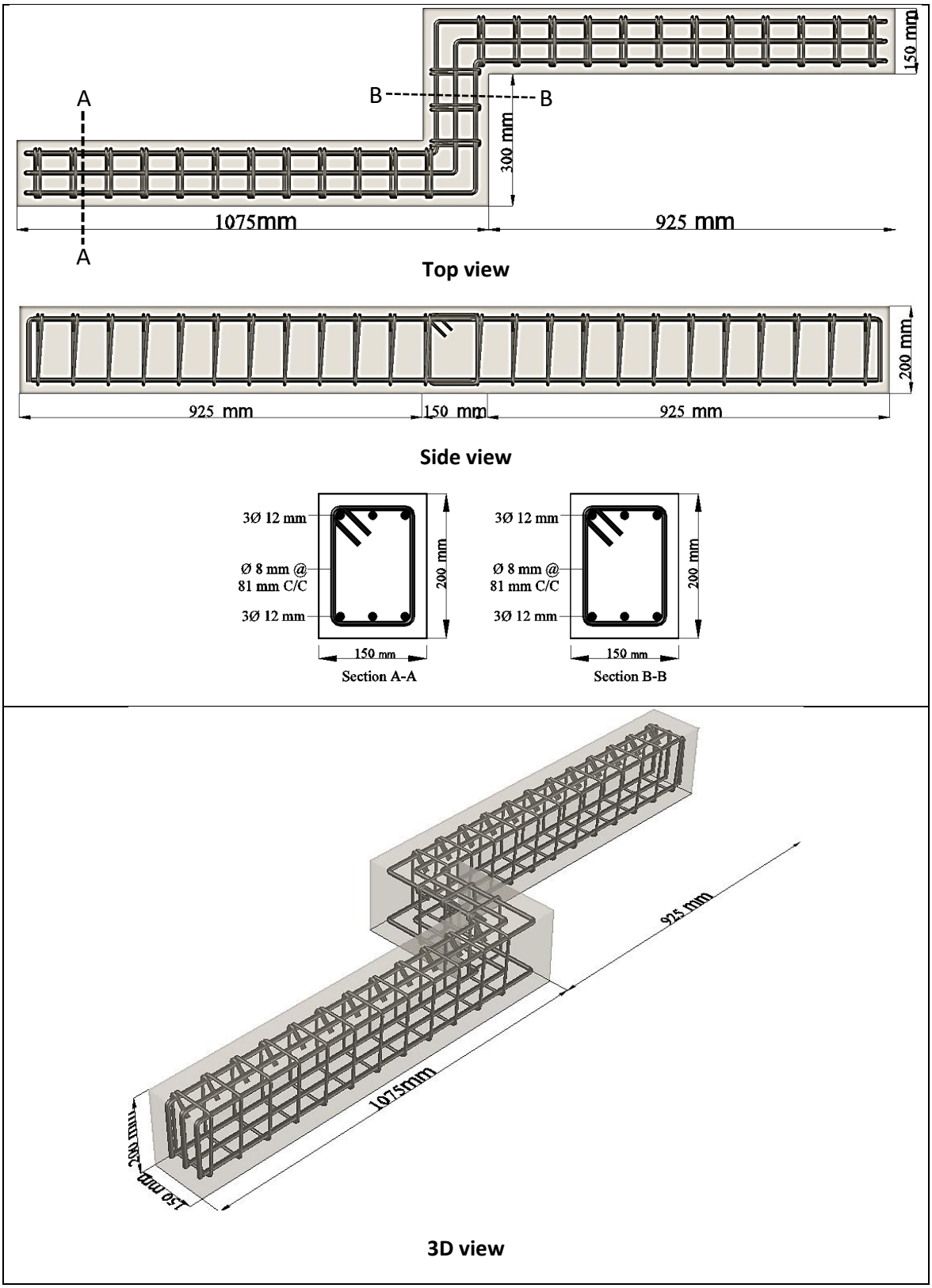

Figure (3-9): Geometry and reinforcement details of beam models (NSC-I-1OP).

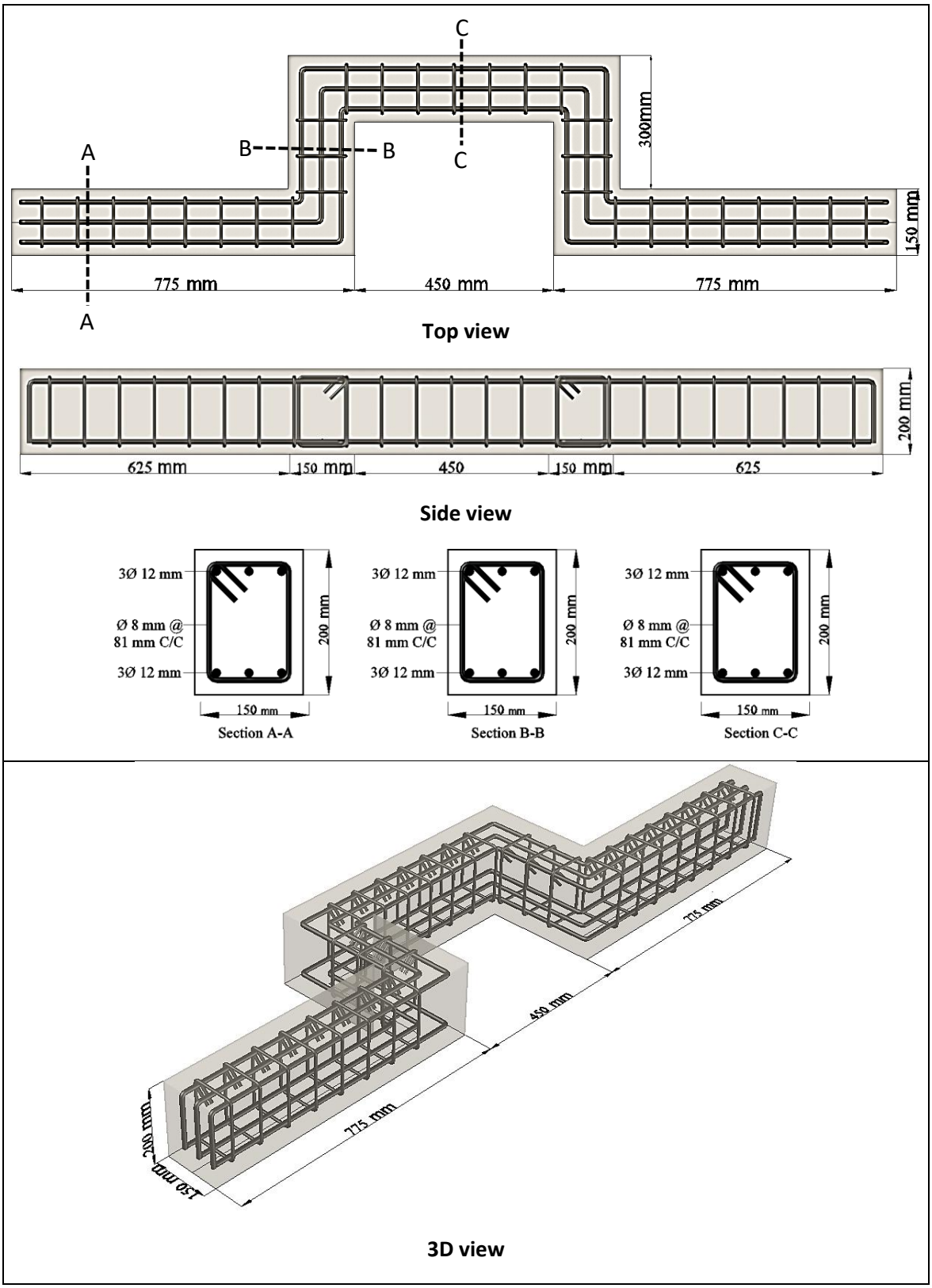

Figure (3-10): Geometry and reinforcement details of beam models (NSC-I-2OP).

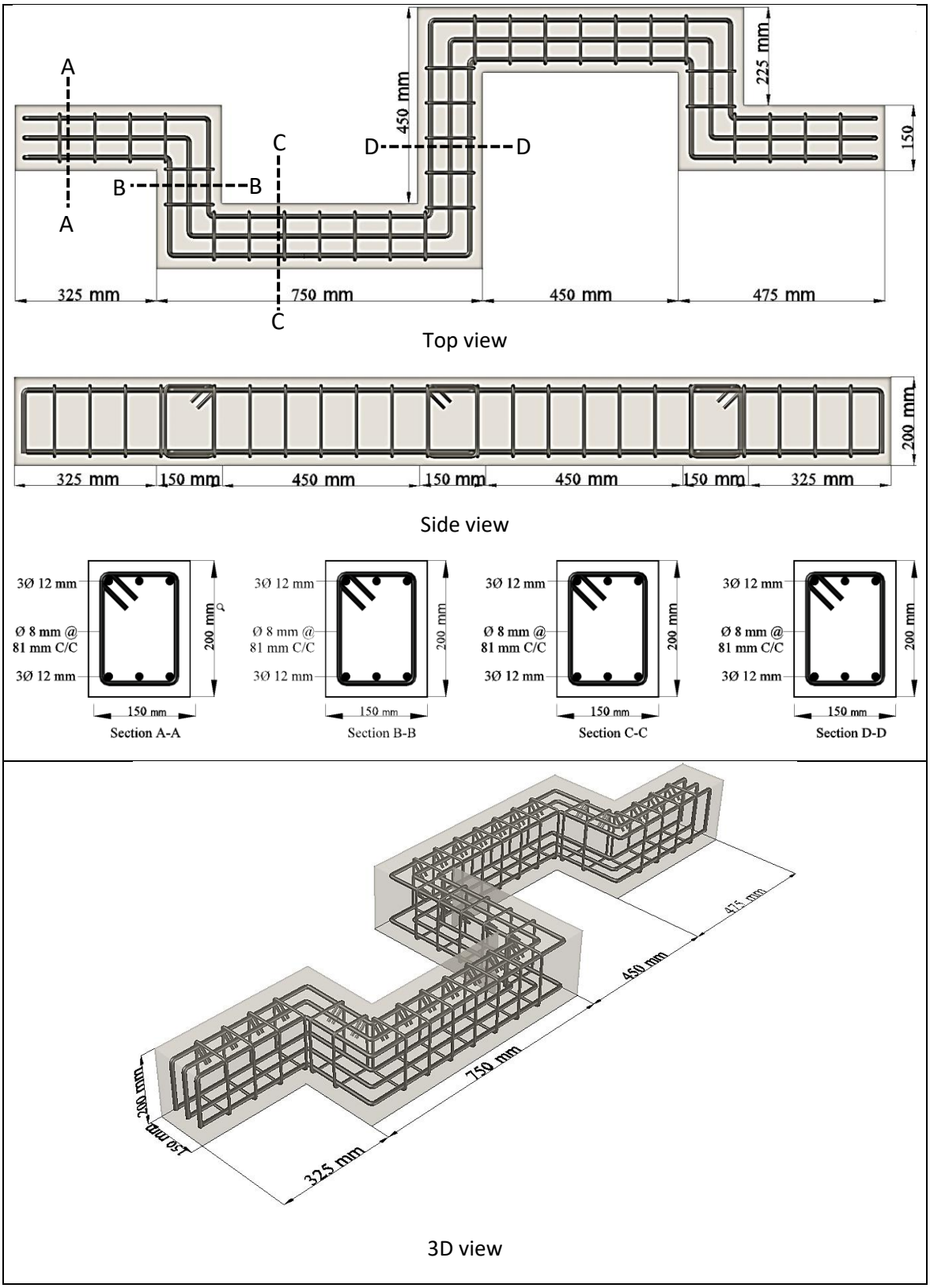

Figure (3-11): Geometry and reinforcement details of beam models (NSC-I-3OP).

3.8.1 Case Study No.1

This study investigated the effect of number and location of out of plane parts of normal strength concrete (NSC) beams on their structural behavior as compared with the normal strength concrete straight beam. This study included NSC-S, NSC-1OP, NSC-2OP, and NSC-3OP beam models.

Model NSC-S was used as a control beam that had been made with NSC and designed according to ACI code 318-2019 as shown in appendix B. This model was tested under static load until failure.

3.8.2 Case Study No.2

This study investigated the effect of replacement of normal strength concrete (NSC) by high strength concrete (HSC). This study included HSC-S, HSC-1OP, HSC-2OP, and HSC-3OP beam models.

Model HSC-S was used as a second control beam which is used as a reference beam for the beams that are made with HSC. This model was made with HSC and it was reinforced similarly to the NSC-S beam.

3.8.3 Case Study No.3

This study investigated the effect of adding torsional reinforcement at each part of the beams with the out of plane parts in conjunction with the replacement of normal strength concrete (NSC) by high strength concrete (HSC). This study included HSC-1OPT, HSC-2OPT, and HSC-3OPT beam models.

3.8.4 Case Study No.4

This study investigated the effect of increasing the length out of plane parts of normal strength concrete (NSC) beams on the structural behavior as compared with the NSC-S and the other NSC beams that made with out of

plane parts. This study included NSC-I-1OP, NSC-I-2OP, and NSC-I-3OP beam models.

The reinforcement of all the beams that were mentioned in the above cases were explained in schematic Figure (3-2) to (3-11) and Plate (3-14).

Straight beams

Beam with one out of plane part

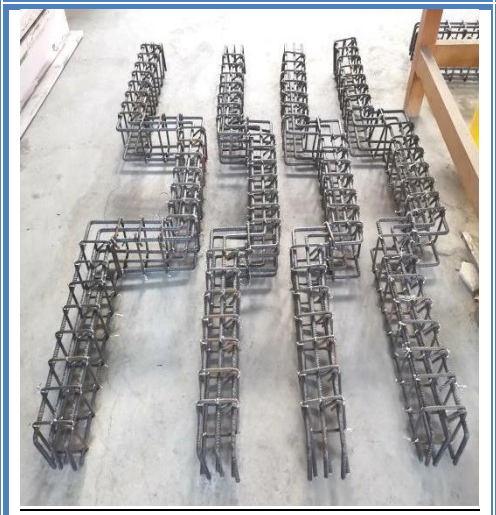

Beam with two out of plane parts

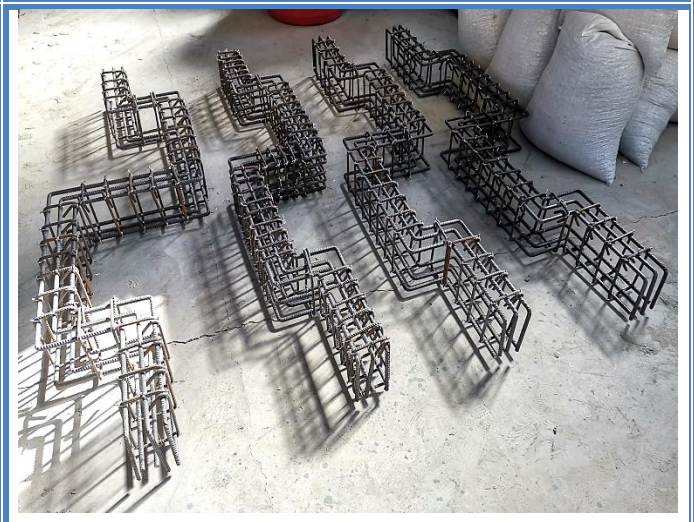

Beam with three out of plane parts

Plate (3-14): Reinforcement details of all the beam models.

3.9 Instruments and Testing Procedure of Beam Models

To achieve the main objective of the laboratory test, the basic step was to prepare the required boundary conditions as follows:

3.9.1 Supports Condition and Loading

Special clamping rigid steel frame of (150 X 150 mm) HP-sections and channel-sections was designed according to **AISC** [63] code by using Autodesk Robot Structural Analysis and Autodesk Advance steel software as shown in Figure (3-12) and its details are explained in **Appendix-D**. This support used to test all beam models, which were clamped to ends of beams. Eight steel columns were connected to each other's by steel beams at the sides, top, and bottom by weld and bolted connections to give a fixed supported condition to a rectangular beam section with an effective span of 1500 mm. The load applied on the tested beams by a double HP-section spreader beam, and the supported part of the beam was 150 mm, while the 100 mm of the beam span was remained out of the support that had been used as a continuous part in order to get the fixity of the supports. According to **ACI 445R-99** [64] that recommended (if the shear span-to-depth ratio (a/d) decreases below about 2.5, members become deep and it will fail under shear, so the load was applied with a shear span (a) that located from support points to the loading point, with a length of 450 mm to achieve (a/d) ratio equal to 2.65 which satisfy the flexural failure. The interior flexural span between the loading points was 600 mm in length; see Figure (3-12) to (3-14) and Plate (3-15).

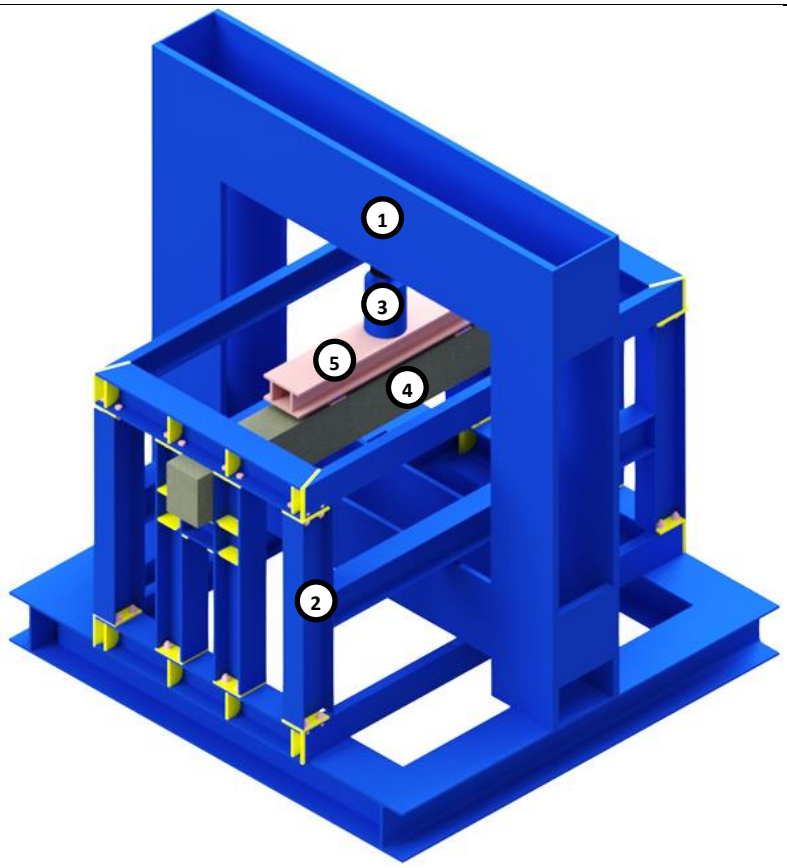

1- Testing Machin

2- Steel Support

3- Load Cell

4- Concrete Beam

5-Spreader Beam

(a) 3-Dimensions view

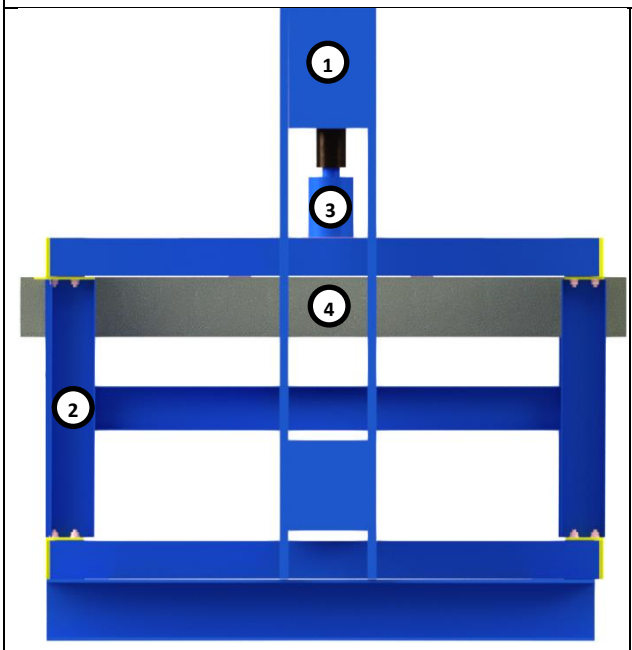

(b) Side view

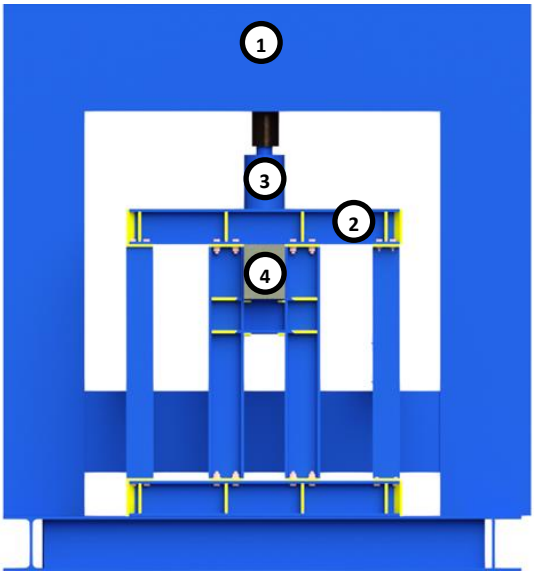

(c) Front view

Figure (3-12): Scheme of Steel Supporting Frame.

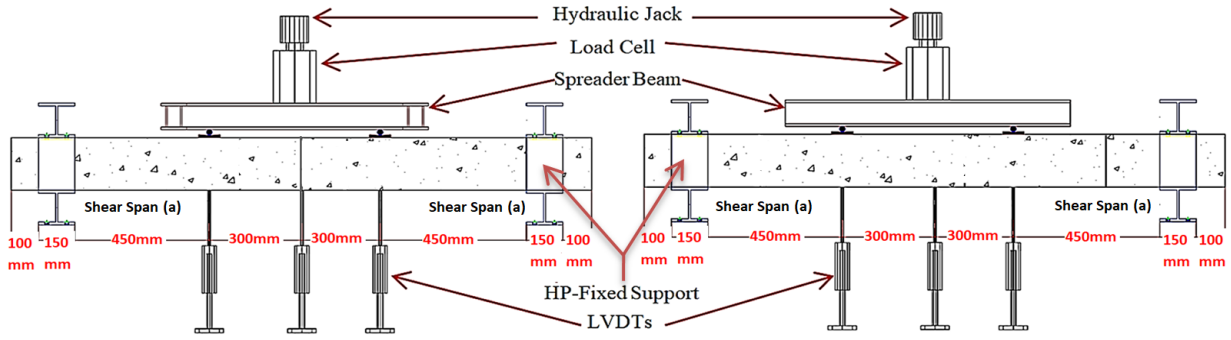

Beam with one out of plane part **Straight beam**

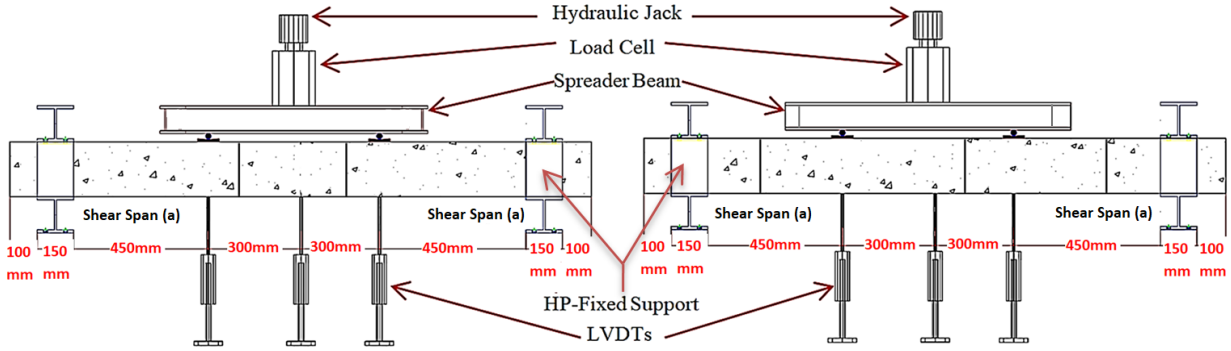

Beam with two out of plane parts **Beam with three out of plane parts**

Figure (3-13): Scheme of 2D test set up.

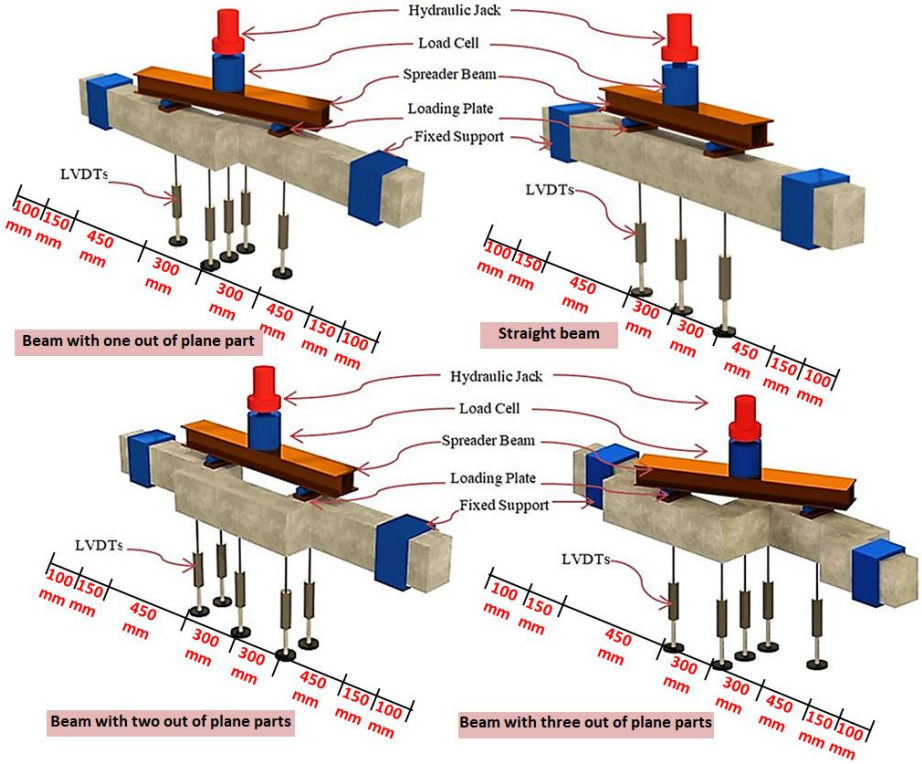

Figure (3-14): Scheme of test set up.

Plate (3-15): Steel support preparation and experimental test set up.

3.9.2 The Test Setup and Equipment

3.9.2.1 Universal Testing Machine

All the beam models were tested by a universal testing machine with a capacity of 1000 kN under monotonic up to ultimate load. The universal machine used existed in the laboratory of structural in the Department of Civil Engineering at Wasit University. The load readings were measured by a load cell that was installed between the jack and a spreader stiff beam as shown in Figure (3-13), Figure (3-14), and plate (3-15).

3.9.2.2 Deflections and Mid Span Rotations of The Beams

The deflections and mid span rotations were measured by a Linear Variable Differential Transducers (LVDT).

Five vertical LVDTs were positioned under the tested beam models at the center point, the loading points, and the out plane parts to record the deflection at mid span and under the loading points to get the deflection shape and the angle of twist. The angle of twist was measured by taking the difference between readings of back and front LVDTs divided by the distance between them. Figure (3-13), Figure (3-14), and plate (3.15) show the schematic and experimental test set up.

All the test instrumentations were connected to a data logger that was computerized to readings and saving the data per second during the experiment time. Plate (3-16) shows the instrumentations that were used.

(a) LVDTs

(b) Data logger

(c) Computer control

Plate (3-16): Five LVDTs, data logger, and computer were used for deflection and rotation reading.

3.9.2.3 Crack width

An optical micrometer with an accuracy of 0.005 mm was used to measure cracks width for all beam models.

All the beams were painted with white color to make it easy to monitor the cracks propagation and measure their width, the cracks were detected and drawn on the front and back faces in addition to the top face of the tested beams as shown in Plate (3-17). This investigation aimed to

measure crack location and width at the first cracking load and ultimate load, also to draw cracks pattern in order to identify failure mode of beams.

Plate (3-17): Monitoring crack width by using a photic micrometer.

3.9.3 Testing Procedure

All the beams were tested by applied concentrated two-point loads and supported by clamped fixed supports at the two ends.

The steel frame was designed and prepared to be able to support the beams and considered as a partial fixity which intended to be fixed at the ends to provide sufficient lateral stability for torsion. The frame was divided into several frames, the side, front, back, top, and bottom frame, and the

parts of each frame were connected by welding, and then the frames were connected to each other by bolted connection. The steel members at each end of the supports were clamped to the beam firmly by the bolts with a ¾" diameter, and they could be removed once the test was done. Inner faces of the supports were shimmed with 1/4" steel plates to provide additional room for dimensional tolerances and ensure uniform contact along the supports and to avoid the slippage between the beam and support.

Rubber plates (8 mm thickness) were provided on the top face of the concrete beam and located under the loading steel plate to avoid non-uniform stress distribution.

In this study, the loading was monotonic. The load was applied gradually up to failure. Test started with the application of 5 kN to set and check LVDT. At zero loading, initial reading of load cell and LVDTs were obtained. The first cracking load and its location were recorded. Then the load was applied of 10 kN and at each load increment, observations of cracks development on the beams were traced by pencil. Also, for each model, maximum crack width and its location were measured. The deflections and rotations were measured for each step and were recorded at each second of testing time. The loading was continued until the ultimate load.

The failure mode of the beam models were stated when no further increase of the loading readings were recorded with a noticeable large deflection in addition to large flexure, shear, and torsional cracking. The beam was removed carefully from the test rig after the test completion.

Chapter Four: Experimental Results and Discussion

4.1 Introduction

This chapter presents and discusses the test results of the experimental program that had been described in chapter three in a tabulated and a graphical forms.

The experimental test results of (NSC) and (HSC) hardened properties are explained and discussed first, and then the second part of this chapter describes the experimental results of fourteen beam models.

4.2 Mechanical Properties of Concrete

The hardened properties from control specimens for NCC and HSC beam models were tested at 7, 28, 56, and 90 days age and listed in Table (4-1).

A common compressive strength test age for NSC is 28 days produced good results, especially when it is not required early strength or early evaluation, whereas HSC may gain considerable strength at later ages (56 or 90 days) when construction requirements allow the concrete more time to develop strength before loads are imposed. **(ACI 363R-10)** [53].

Table (4-1):- Mechanical properties of concrete test results of control specimens for all beam models.

Mechanical Properties	NSC				HSC			
	7 days	28 days	56 days	90 days	7 days	28 days	56 days	90 days
Hardened Density (kN/m^3)	-	24.04	-	24.21	-	24.85	-	25.38
Cylinder Compressive Strength (MPa)	21.19	34.77	36.19	37.62	71.26	75.69	76.07	79.38
Poisson′s Ratio	-	0.22	-		-	0.24	-	
Cube Compressive Strength (MPa)	25.34	37.96	38.46	38.595	81.87	85.75	85.81	85.83
Splitting Tensile Strength (MPa)	-	2.25	-	2.56	-	4.39	-	4.52
Modulus of Rupture (MPa)	-	4.81	-	6.23	-	7.72	-	10.06
Modulus of Elasticity (GPa)	-	22.01	-	27.60	-	34.39	-	40.98

4.2.1 Fresh Properties of Concrete

The fresh properties of concrete were examined through workability slump flow test and fresh density. The slump was 60 mm for NSC and 215 for HSC, while the fresh density for NSC and HSC were 26.04 and 26.24 KN/m^3 respectively.

4.2.2 Hardened Density of Concrete

The air dry (hardened) density for NSC and HSC were measured at 28 days and at the day of the test beams (90 days) and presented in Table (4-1). Results showed that the air-dry density of HSC was somewhat higher than NSC that was prepared with the same raw materials.

4.2.3 Cylinders and Cubes Compressive Strength

The average compressive strength was evaluated at 7, 28, 56, and 90 days and it was (21.19, 34.77, 36.19, and 37.62 MPa) for NSC cylinders (fc') and (25.34, 37.96, 38.46, and 38.59 MPa) for cubes (f_{cu}), whereas the average compressive strength of HSC cylinders and cubes were (71.26, 75.69, 76.07 and 79.38 MPa) and (81.87, 85.81, 85.81 and 85.83 MPa) respectively, as shown in Table (4-1).

From Table (4-1), the ratio of the average cube to cylinder compressive strength (*fcu / fc'*) for NSC at 7, 28, 56, and 90 days were (1.196, 1.092 and 1.062, and 1.025) respectively. While, the ratio of the average cube to cylinder compressive strength (*fcu / fc'*) for HSC at 7, 28, and 56 days were (1.149, 1.138, 1.128, and 1.081), respectively. It can be seen that the ratio of the cube to cylinder compressive strength for NSC and HSC decreased with time. The cylinder compressive strength gained with age for both types of concrete are shown in Figure (4-1)

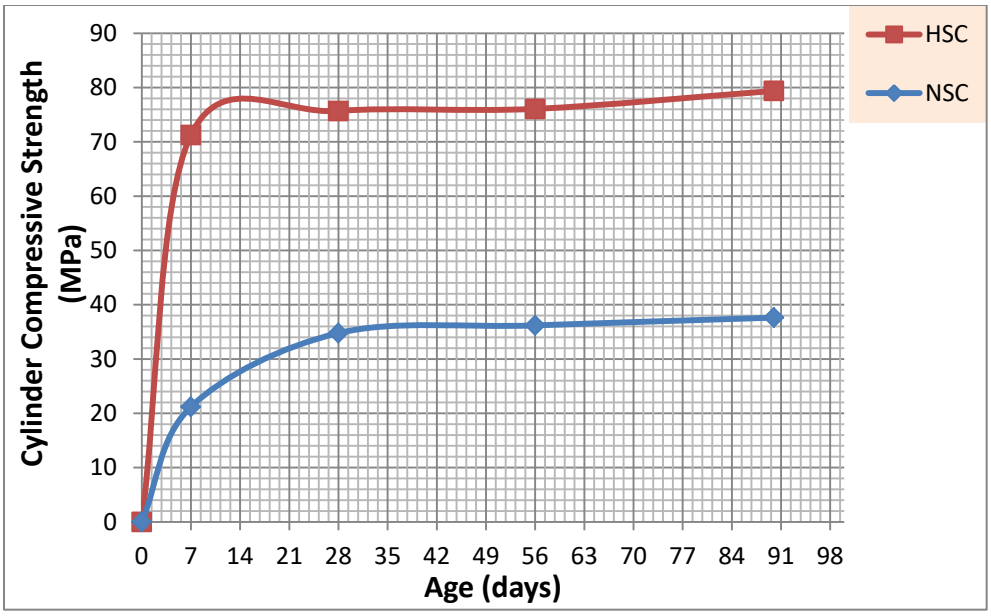

Figure (4-1): Strength gain with age for HSC and NSC.

4.2.4 Splitting Tensile Strength

The splitting tensile strength (f_{sp}) results of NSC and HSC beam models were estimated at 28, and 90 days and explained in Table (4-1). It was (2.25, and 2.56 MPa) for NSC and (4.39, and 4.52 MPa) for HSC. The percentage ratio of the splitting tensile strength to the compressive strength (f_{sp} / fc') of NSC at 28, and 90 days was (6.47%, 6.80%), while in HSC was (10.19%, 12.67%).

4.2.5 Flexural Tensile Strength (*fr*)

The flexural tensile strength of NSC and HSC were estimated at 28 and 90 days and its results are shown in Table (4-1). This property also expressed as the modulus of rupture (f_r) and its relationship with the compressive strength at 28 days is (f_r=0.62$\sqrt{fc'}$) for NSC, but in HSC is (f_r=0.94$\sqrt{fc'}$) as recommended in the **ACI 363R-10** [53].

4.2.6 Poisson's Ratio

Poisson′s Ratio for NSC and HSC at 28 days are 0.22 and 0.24 respectively. Primarily based on the experimental results, Poisson’s ratio reduced whilst water/cement ratio increased.

In addition, Poisson’s ratio of HSC at the elastic limit appeared corresponding to the probable limit of values for NSC.

4.2.7 Modulus of Elasticity

The slope of the chord for the uniaxial stress-strain curve between the point corresponding to 40 percent of the maximum stress and the point corresponding to a strain of 0.00005 represents the secant modulus of elasticity. The modulus of elasticity of concrete Ec is related to its density and compressive strength.

The average modulus of elasticity at 28 and 90 days are 22.01 and 27.60 GPa for the NSC and 34.39 and 40.98 GPa for HSC as shown in Table (4-1).

From the results, it could be concluded that the NSC had a modulus of elasticity at 28 and 90 days lower than HSC modulus of elasticity by about 35.99% and 30.96%, respectively.

4.2.8 Stress-Strain Behavior in Uniaxial Compression

The axial compressive stress-strain curves of NSC and HSC at 28 days are shown in Figure (4-2).

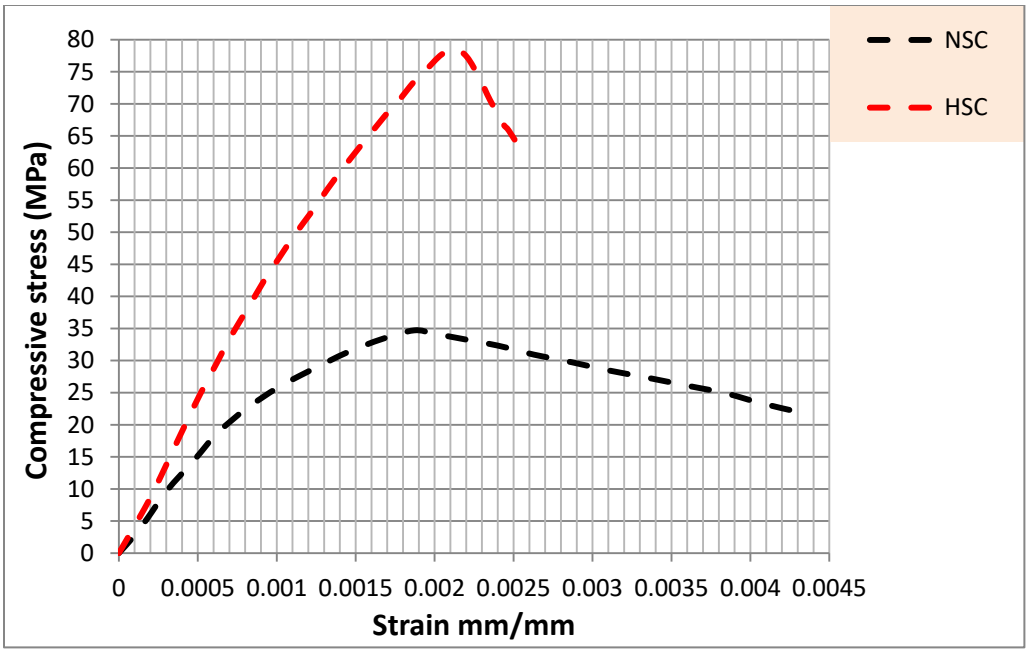

Figure (4-2): compressive stress-strain curves of NSC and HSC.

The shape of the ascending part of the stress-strain curve was more linear and sharper for HSC, and its strain at the maximum stress was somewhat higher than NSC. High strength concrete showed fewer internal micro cracking than normal strength concrete for a given axial strain.

4.3 Experimental Results of Beam Models

The results were based on fourteen beam models tested in Wasit University Structure Laboratory. All the beam models were tested under static load.

The discussion of the test results was based on several variables that have been examined to show their influence on the structural behavior of the tested beam models. These studies were used to investigate the effects of four parameters and each parametric study contains several beam models as mentioned in chapter three.

The results of the tests were discussed considering the first cracking load, ultimate load, the load- deflection curve, deflected shape, the load-rotation curve, cracking behavior, and failure mode. Most of the test results data had been transferred to graphical form for ease of interpretation.

4.3.1 Ultimate Load and Deflection

Five LVDTs were used to measure the deflection and rotation. One at the center to measure the mid span deflection, two below the point load to measure the deflection and draw deflected shape, and two in front and back at mid span to measure the mid span rotation. The recorded ultimate load and deflection are presented in Table (4-2) for beam models.

Table (4-2):- Deflection and rotation at ultimate load for each beam model. (Continued).

Beam models symbol	**Ultimate load Pu (kN)**	**Mid-span deflection (mm) at ultimate load**	**Mid-Span angle of twist (degree) at ultimate load**
NSC-S	576.76	26.79	0^0
NSC-1OP	369.36	61.21	2.58^0
NSC-2OP	392.30	45.92	3.55^0
NSC-3OP	176.14	31.09	1.44^0
HSC-S	757.57	40.85	0^0
HSC-1OP	384.51	51.21	2.44^0
HSC-2OP	404.88	35.68	1.95^0

Table (4-2):- (Continued).

HSC-3OP	241.57	32.42	1.41^0
HSC-1OPT	460.48	49.67	2.65^0
HSC-2OPT	467.96	34.52	2.99^0
HSC-3OPT	289.30	31.47	1.92^0
NSC-I-1OP	369.29	48.70	0.56^0
NSC-I-2OP	387.24	31.26	0.65^0
NSC-I-3OP	176.45	29.54	0.56^0

4.3.1.1 Load-Deflection Curve

The beam models under loading were shown in three stages of behavior, first stage is the elastic stage that can be described by a nearly linear shape between the load and the deflection. In this stage, the concrete section was uncracked and reinforcement was not yielded yet and both the concrete and reinforcement behaved essentially elastic.

The second stage was elastic-plastic behavior when the relation of the load and deflection changed to a nonlinear behavior with distinctive changes in slope by increasing deflections. This stage occurred when the stiffness of the beams decreased and the primary cracking of the concrete section was started to appear.

The third stage was the plastic behavior and the load-deflection relation was also nonlinear and in which, as a load slightly increased lead to

a larger deflection. In this stage, the slope of the load-deflection curve was decreased as a result of reinforcement post-yielding and reached to the yield strain. In general, a nonlinear behavior was observed after concrete cracking and continued up to failure.

Case Study No.1:- Investigated the effect of number and location of out of plane parts of NSC beams on their load-deflection response as compared with the NSC straight beam. The NSC-1OP, NSC-2OP, and NSC-3OP beam showed ultimate load lower than the NSC-S beam by about 35.96%, 33.33%, and 69.46% respectively and their mid span deflection was higher than NSC-S beam by 56.23%, 41.66%, and 13.83% at the ultimate load and 181.05%, 143.17%, and 3.94% at the service load. Figure (4-3) shows the load versus central deflection of these beam models.

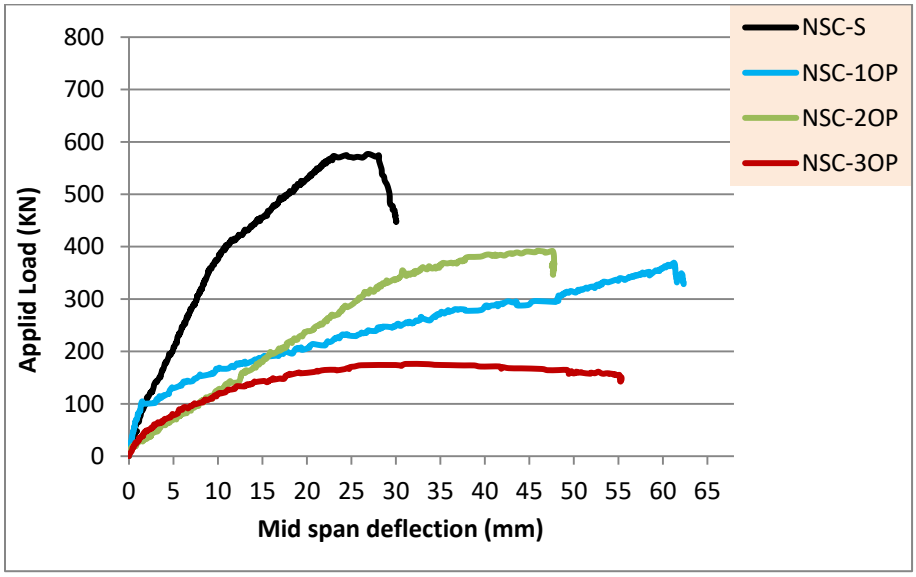

Figure (4-3): Effect of number and location of out of plane part on load-central deflection response beam models.

The effect of the location of the out of plane part relative to the mid span of the beam on the behavior was detected by the test result showed that

the NSC-2OP beam had ultimate load higher than the NSC-1OP and NSC-3OP beams by (5.84%) and (55.10%). This behavior is due to the axis of the mid span part of NSC-2OP beam was parallel to the beam axis and decreased the applied torsional moment at this part which led to increasing the load-carrying capacity, while the NSC-1OP and NSC-3OP have mid-span part perpendicular to the beam axis and increase torsional moment at these parts which led to decrease the load-carrying capacity. In addition, the load-deflection responses at each stage of the behavior (elastic, elastic-plastic, and plastic) were affected by the number and location of out of plane parts. In general, the beams with even number of the out of plane parts had load bearing capacity higher than the beams with odd number of the out of plane parts.

Case Study No.2:- Investigated the effect of increasing compressive strength of concrete on the load-deflection response of HSC beams with the out of plane parts as compared with the NSC and HSC straight beams. The HSC beam models showed higher ultimate load when compared with the NSC beam models that modeled with same geometry and reinforcement, but their capacity remained smaller than NSC-S by about 33.33%, 29.80%, and 58.11% respectively and their deflections at the ultimate load were somewhat higher than NSC-S by 47.68%, 24.91%, and 17.36% and at the service load were 137.14%, 76.87%, and 60.39% respectively. Figure (4-4) shows the load versus central deflection of these beam models.

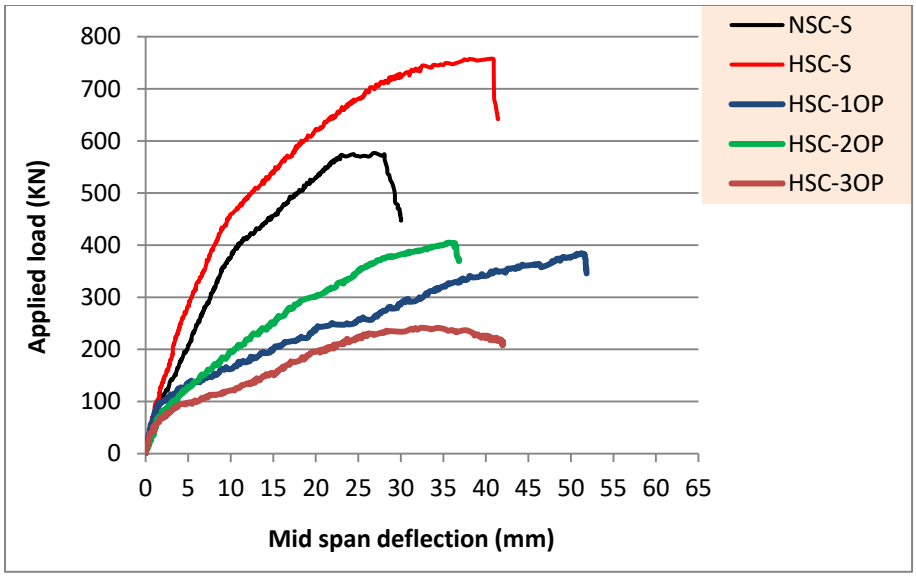

Figure (4-4): Effect of replacement NSC by HSC on the load-central deflection for beam models

The behavior of HSC beams with the out of plain parts as compared with the HSC-S showed that the HSC-1OP, HSC-2OP, and HSC-3OP beam models showed ultimate load lower than HSC-S by about 49.24%, 46.55%, and 68.11%, while the capacity of NSC-S was 23.86% lower than HSC-S.

This means that using HSC in beams with out of plane part was of limited enhancement on its strength.

Case Study No.3:- Investigating the influence of adding torsion reinforcement at each part of the beams with the out of plane parts on load-bearing capacity and load-deflection behavior. The reinforcement was added to each part of the beam according to its own torsion.

The torsion reinforcement has a noticeable effect on increasing load-bearing capacity and a clear effect on increasing measured deflections as shown in Figure (4-5).

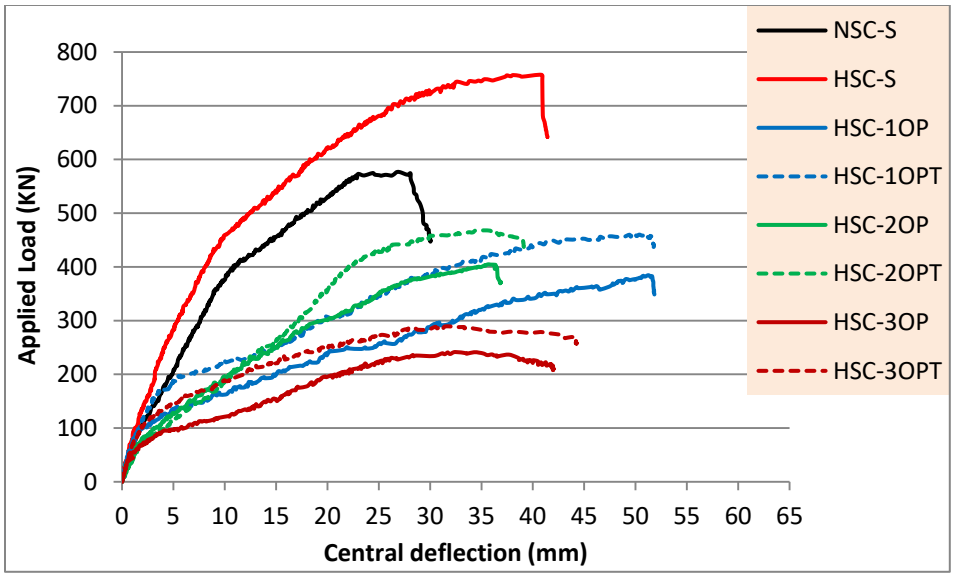

Figure (4-5): Effect of using torsion reinforcement on load-central deflection for HSC beam models as compared with HSC-S and NSC-S beam.

The HSC beam models with torsion reinforcement (HSC-1OPT, HSC-2OPT, and HSC-3OPT) showed higher ultimate load, but it was remained lower than the NSC-S beam by 20.16%, 18.86% and 49.84% and their deflections were higher than NSC-S beam 46.06%, 22.39%, and 14.87% at the ultimate load and 116.97%, 97.66%, and 21.89% at the service load.

The behavior of HSC beams with torsion reinforcement as compared with the HSC-S showed that the HSC-1OPT, HSC-2OPT, and HSC-3OPT beam models had ultimate load lower than HSC-S by about 39.15%, 38.22%, and 61.82%.

Furthermore, the adding torsion reinforcement enhanced the load bearings capacity of the HSC-1OPT, HSC-2OPT, and HSC-3OPT beam models by about 19.75%, 15.58%, and 19.76% as compared with the HSC beams without using torsion reinforcement.

Case Study No.4:- Evaluating the beams behavior by increasing the length of out of plane parts. The length increased by 150 mm in NSC-I-1OP and NSC-I-2OP, but for NSC-I-3OP it was increased by 150 mm for mid span part and 75 mm for the first and last out of plane parts. The behavior of each beam with its similar beam whose out of plane parts length were not increased and the control NSC-S beam model were shown in Figure (4-6) to Figure (4-8).

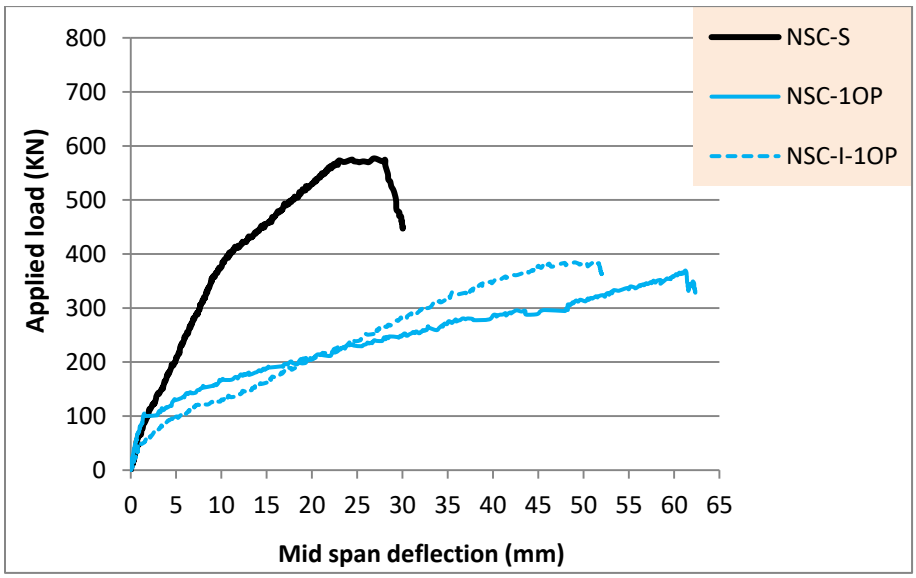

Figure (4-6): Effect of increasing length of out of plane part on load-central deflection for NSC-I-1OP beam models as compared with NSC-1OP and NSC-S beam.

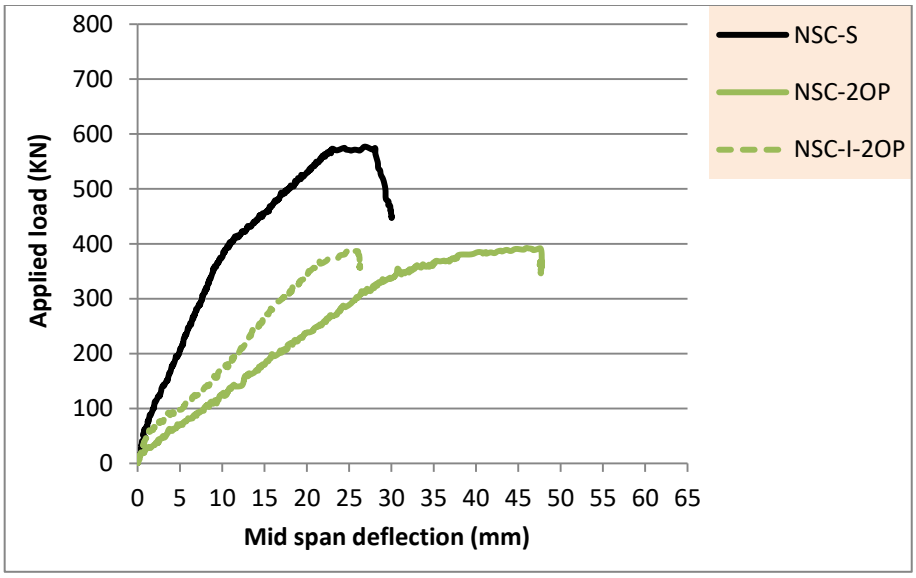

Figure (4-7): Effect of increasing length of out of plane part on load-central deflection for NSC-I-2OP beam models as compared with NSC-2OP and NSC-S beam.

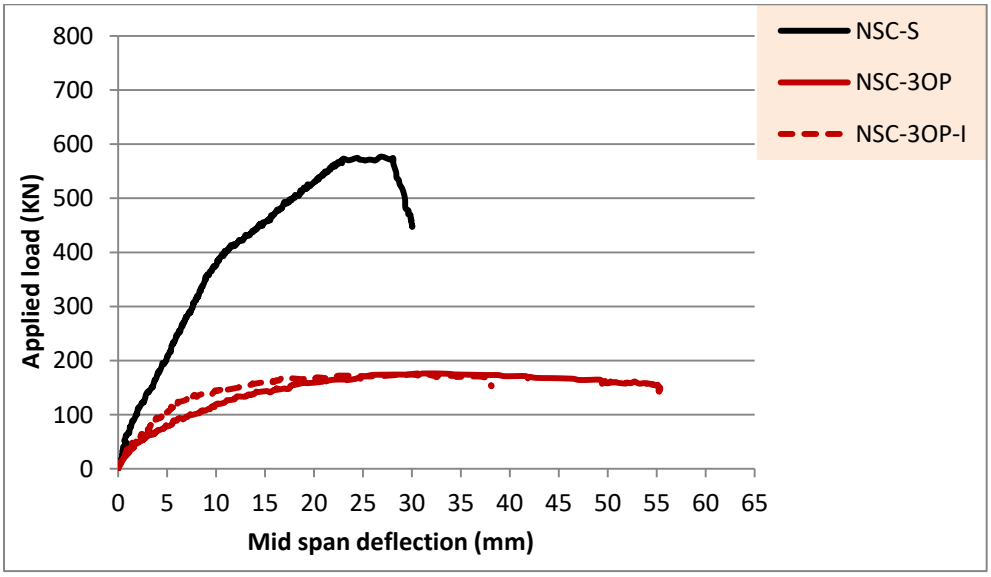

Figure (4-8): Effect of increasing length of out of plane part on load-central deflection for NSC-I-3OP beam models as compared with NSC-3OP and NSC-S beam.

The NSC-I-1OP model showed ultimate load lower than NSC-S and NSC-1OP by about 35.97% and 0.02%, and for deflections was 44.98% higher NSC-S but 20.43% lower than NSC-1OP.

On the other hand, the NSC-I-2OP model showed ultimate load lower than NSC-S beam and NSC-2OP beam by 32.85% and 1.28%, while their deflections was 14.30% higher NSC-S beam but 31.92% lower than NSC-2OP beam.

The last one, NSC-I-3OP model was also showed ultimate load lower than NSC-S beam by 69.40% but higher than NSC-3OP beam by 0.176%, while their deflections was 9.30% higher NSC-S beam and 4.98% lower than NSC-3OP beam.

From the figures and Table (4-2), it can be seen that the increase length of out of plane parts had a little effect on its capacity but the deflection highly affected.

In addition to the load-deflection results, the ultimate load of each beam was calculated relative to the ultimate load of NSC-S control beam, and the results were shown in Figure (4-9).

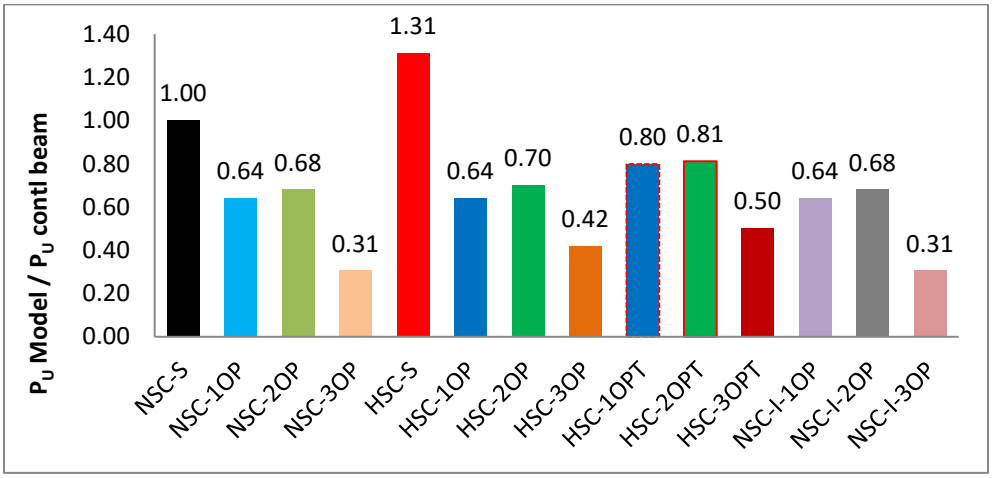

Figure (4-9): Ultimate load of each beam relative to the ultimate load of the NSC-S beam.

The Committee **(ACI 318M-19)** [65] proposed strength reduction factor in the design procedure of the structural members to take precautions about variations in material strengths and member dimensions, inaccuracies in the design equations, to reflect the available ductility of the member under considered load, and to reflect the member importance in the structure. The reduction factors that proposed for the bending moment, shear, and torsion were 0.90, 0.75, and 0.75 respectively. These factors were used in the design of straight control beam (NSC-S beam) in the current study.

It is worth to mention again that the NSC and HSC beams with out of plane parts were reinforced by the reinforcement of the straight beam but they were showed lower bearing capacity. Therefore, it is not possible to design and reinforcing the beams with out of plane part by using the same reduction factors of the straight beam, and that it is not reliable to be loaded with the same loading.

It is possible to suggest a new strength reduction factors for the design of the beams with out of plane parts based on the strength reduction factors of the straight beam but modified them according to the ratios of the ultimate load of the beams with out of plane parts to the ultimate load of the straight beams from the present study as:

$$\phi_{out} = \phi_S \times \frac{P_U\ Out}{P_U\ S} \qquad (4.1)$$

Where; ϕ_{out} is strength reduction factor of the beams with out of plane part, ϕ_S is the strength reduction factor of the straight beam (according to ACI 318-19), P_U Out is the ultimate load of the beams with out of plane part, and P_U S is the ultimate load of the straight beam.

The new proposed strength reduction factors of the NSC beams with out of plane part are shown in Table (4-3).

Table (4-3):- Proposed strength reduction factors of the NSC beams with out of plane part

BEAM	$\frac{P_{U\ out}}{P_{U\ S}}$	Strength reduction factors		
		Shear	Bending	Torsion
NSC-S	-	0.75	0.9	0.75
NSC-1OP	0.64	0.50	0.60	0.50
NSC-2OP	0.68	0.50	0.60	0.50
NSC-3OP	0.31	0.25	0.30	0.25

4.3.1.2 Deflected Shape

The deflected shape of all the tested beam models has been drawn depending on the deflection readings at the mid span and under the load points that was monitored by the LVDTs at these points that explained in Figure (3-16).

The lowest ultimate load of the tested beams was considered as the loading level to draw the deflected shapes of the tested beams. The ultimate load (176.14 kN) of the NSC-3OP beam was the lowest one and the corresponding deflection of all the beams at this loading level was selected for drawing the deflected shapes.

Case Study No.1:- The effect of the number and location of out of plane parts of NSC beams on their deflected shape as compared with the NSC straight beam at the load (176.14 kN) are shown in Figure (4-10).

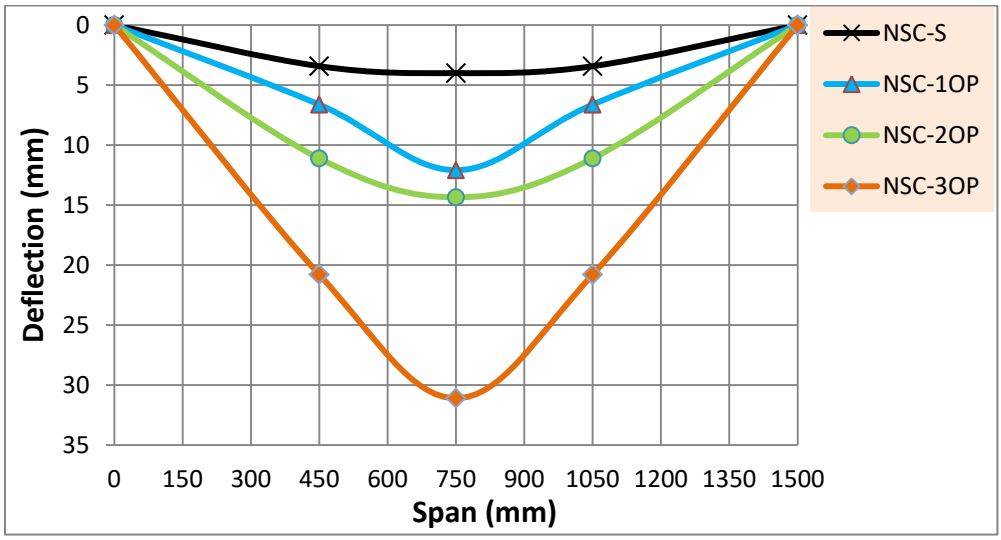

Figure (4-10): Effect of number and location of out of plane parts on the deflected shape along longitudinal-axis for beam models at load (176 kN).

The central deflection of NSC-1OP, NSC-2OP, and NSC-3OP beams were higher than the NSC-S beam by about 198.76%, 254.32%, and 732.09% respectively.

Therefore, the deflected shape responses gave indicate that the increasing number of out of plane parts increased the deflection, that means increasing the ductility and decreasing the flexural and torsional stiffness of the beams due to the increasing of loads combinations at the selected loading level.

Furthermore, it was observed that the NSC-3OP has the maximum deflection because its ultimate load was considered as reference load for measured deflection of all the other beams and its deflection was taken at its ultimate load.

Case Study No.2:- The effect of using high strength concrete (HSC) instead of normal strength concrete (NSC) on the deflection characteristics at the load (176 kN) for the beam models are shown in Figure (4-11).

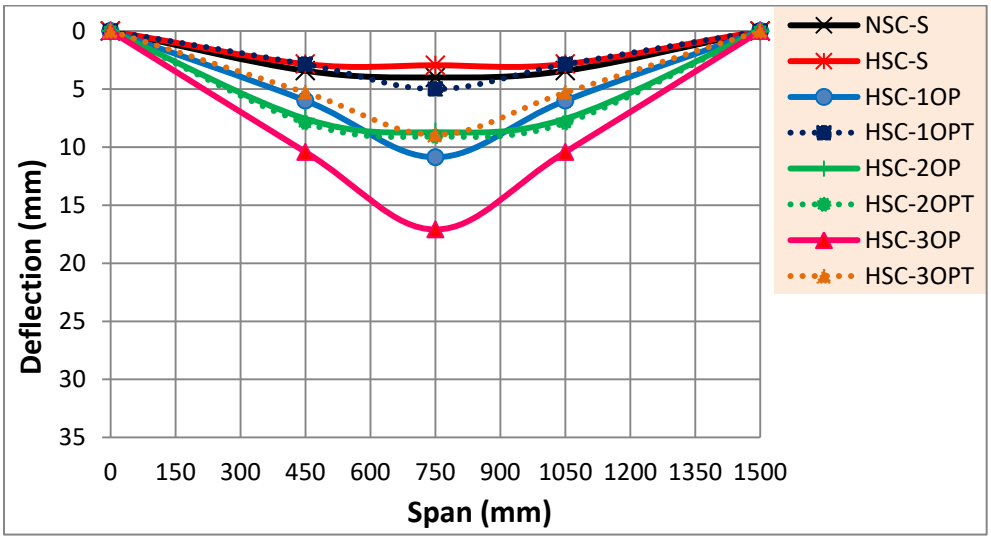

Figure (4-11): Effect of replacement of NSC by HSC on the deflected shape of beam models at load (176 kN).

The using of HSC in the beams with the out of plane parts decreased greatly the differences between their mid span deflection and the deflection of NSC-S control beam. In addition, the using of HSC made the deflected shape of HSC-2OP is closer to the deflected shape of the NSC-S and HSC-S beams.

Case Study No.3:- The effect of adding torsion reinforcement and using high strength concrete (HSC) instead of normal strength concrete (NSC) on the deflection characteristics for the beam models at the load level (176.14 kN) are shown in Figure (4-12).

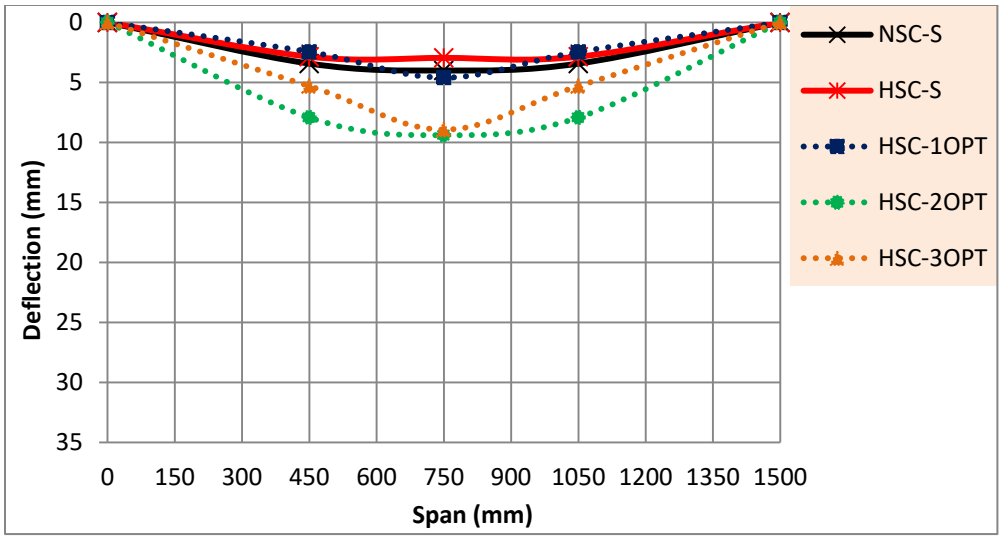

Figure (4-12): Effect of addition torsion reinforcement with replacement of NSC by HSC on the deflected shape of beam models at load (176 kN).

Figure (4-12) can summarize that using torsion reinforcement in addition to use HSC in the beams with the out of plane parts decrease the differences between the mid span deflection of the HSC beams with the out of plane parts and the deflection of NSC-S and HSC-S beams. This behavior gave an impression that the stiffness of the beams had been increased, and the beams with odd number of the out of plane parts became stiffer than the beam with even number of the out of plane parts. This behavior happened because the parts in the beams with odd number of the out of plane parts have torsion higher than the parts in the beams with even number of the out of plane parts, so, the torsion reinforcement became more effective in the beams with odd number of the out of plane parts.

Case Study No.4: The effect of increasing the length of the out of plane parts in conjunction with the number and location of out of plane parts of NSC beams on their deflected shape as compared with the NSC straight

beam at the load level (176.14 kN) are shown in Figure (4-13) to Figure (4-15).

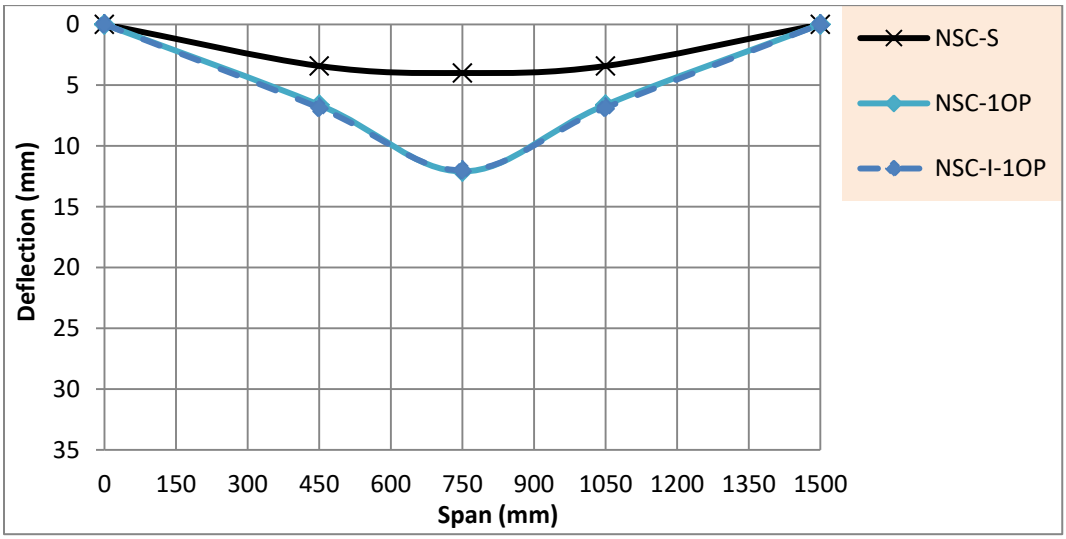

Figure (4-13): Effect of increasing length of out of plane part on deflected shape of NSC-I-1OP beam models as compared with NSC- 1OP and NSC-S beam at load (176 kN).

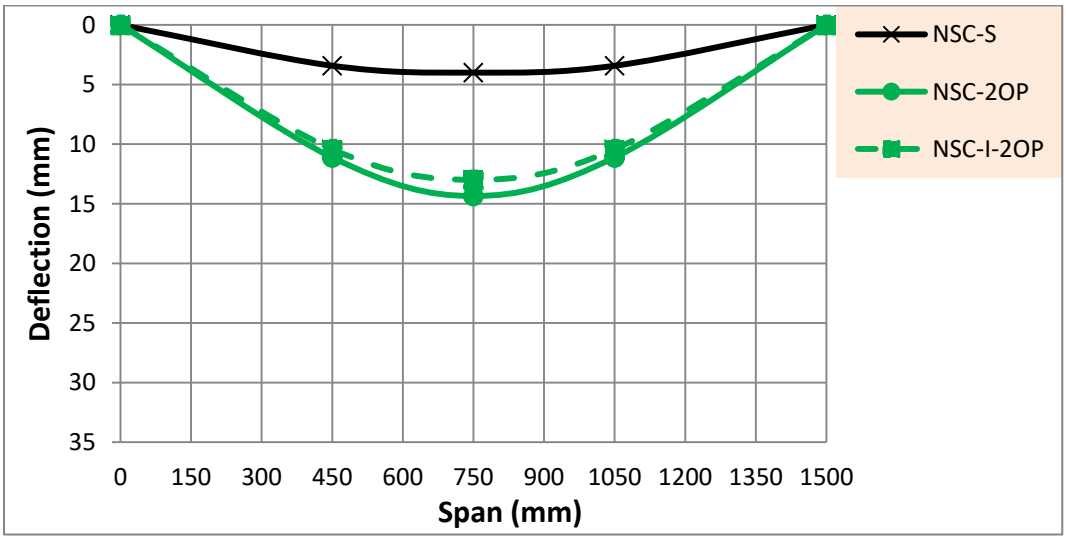

Figure (4-14): Effect of increasing length of out of plane part on the deflected shape of NSC-I-2OP beam models as compared with NSC-2OP and NSC-S beam at load (176 kN).

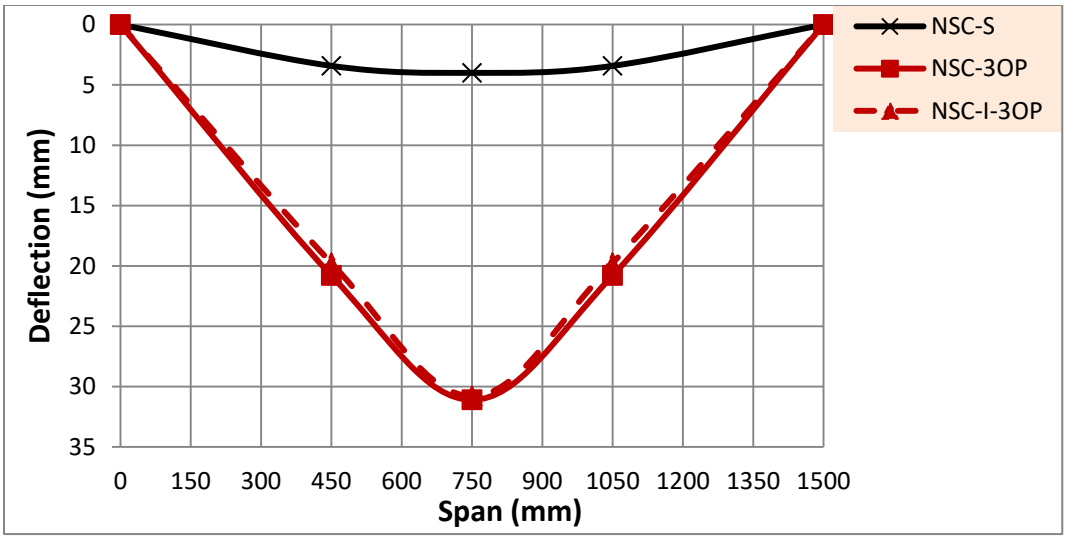

Figure (4-15): Effect of increasing length of out of plane part on deflected shape of NSC-I-3OP beam models as compared with NSC-3OP and NSC-S beam at load (176 kN).

This case could be concluded that the increase length of the out of plane parts led to almost the same mid span deflection for the corresponding beam with shorter out of plane part.

4.3.1.3 Serviceability Limit State

In order to satisfy the serviceability limit states, the reinforced concrete structural member must be serviceable and perform its intended function throughout its working life. One of the important behaviors in the serviceability limit states assessment is the excessive deflection at the service load. ACI-318-19 code was mentioned that the calculated deflections should not exceed the limits in Table (4-4).

Table (4-4):- Maximum permissible calculated deflections (ACI-318-19 code)

<table>
<tr><th>Member</th><th colspan="2">Condition</th><th>Deflection to be considered</th><th>Deflection limitation</th></tr>
<tr><td>Flat roofs</td><td colspan="2" rowspan="2">Not supporting or attached to nonstructural elements likely to be damaged by large deflections.
Immediate deflection due to L</td><td>Immediate deflection due to maximum of Lr, S, and R</td><td>ℓ/180</td></tr>
<tr><td>Floors</td><td>ℓ/360</td><td></td></tr>
<tr><td rowspan="2">Roof or floors</td><td rowspan="2">Supporting or attached to nonstructural elements</td><td>Likely to be damaged by
Large deflections</td><td rowspan="2">That part of the total deflection occurring after attachment
of nonstructural elements, which is the sum of the time dependent
deflection due to all sustained loads and the immediate deflection due to any additional live load</td><td>ℓ/480</td></tr>
<tr><td>Not likely to be damaged
by large deflections</td><td>ℓ/240</td></tr>
</table>

The comparison of the experimental results of beams deflections at the service load and the code limitation are listed in Table (4-5) and showed in Figure (4-16).

Table (4-5):- Comparison of experimental service load deflection and ACI Code deflection limit

Beam Models Symbol	**Experimental Central Deflection (mm) at Service Load (0.60 P_U)**	**ACI Code Deflection Limit (L/180)(mm)**	**EXP/ACI**
NSC-S	8.13	8.33	0.98
NSC-1OP	22.85		2.74
NSC-2OP	19.77		2.37
NSC-3OP	8.45		1.01
HSC-S	9.35		1.12
HSC-1OP	19.28		2.31
HSC-2OP	14.38		1.73
HSC-3OP	13.04		1.56
HSC-1OPT	17.64		2.12
HSC-2OPT	16.07		1.93
HSC-3OPT	9.91		1.19
NSC-I-1OP	23.82		2.86
NSC-I-2OP	16.60		1.99
NSC-I-3OP	5.12		0.61

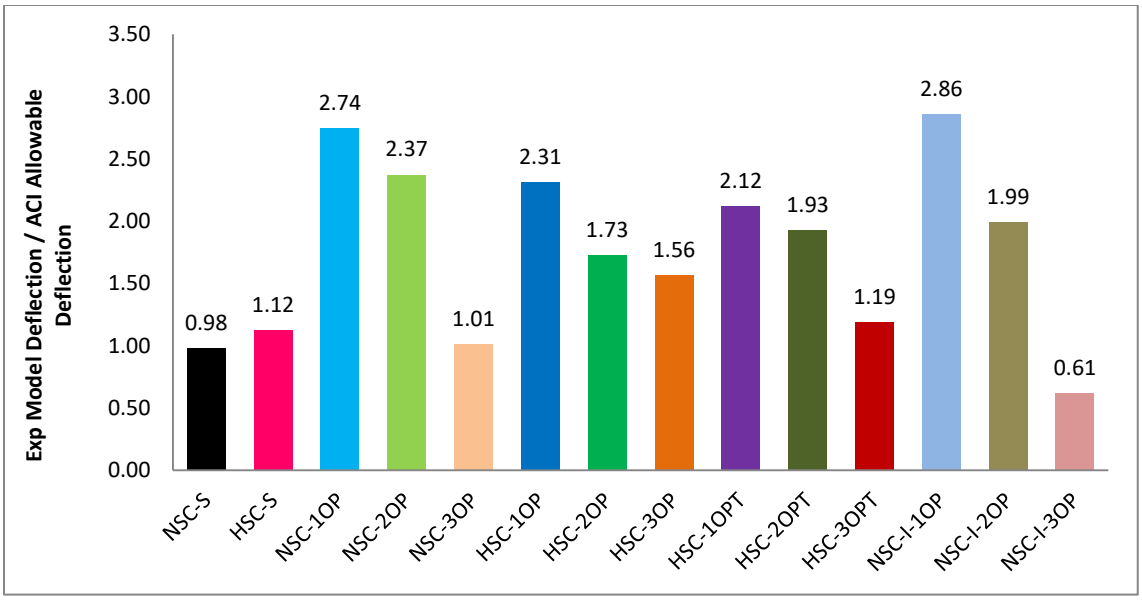

Figure (4-16): Service load deflection of each beam relative to the ACI Code service load deflection Limit.

From the Table (4-5) and Figure (4-16) it was observed that the deflection of the NSC-S control beam within the code limit, but the deflection of all the other beams unless NSC-I-3OP was passed the limit. Furthermore, the ratio between the experimental test results and code limitation was decreased with the increasing number of the out of plane parts for all the case studies.

Therefore, the deflection limits of the beams with out of plane parts at service load cannot be considered at 60% of their ultimate load as the straight beam, but it was noticed from the results that deflection limit should be taken at service load below 60% of their ultimate load and such percentage is computed from the following equation:

$$P_{S.Out}\% = \frac{P_{S.Out}}{P_{U.Out}} \qquad (4.2)$$

Where; $P_{S.Out}\%$ is the service load percentage from the ultimate load of the beams with out of plane part, $P_{S.Out}$ is the service load of the beam with out

of plane part that satisfy the deflection limit according to ACI 318M-19, $P_{U.Out}$ is the ultimate load of the beams with out of plane part.

The new proposed service load percentages from the ultimate load for the beams with out of plane part are shown in Table (4-6).

Table (4-6):- Proposed service load percentage limits of the beams with out of plane part

Beam Models Symbol	**NSC-1OP**	**NSC-2OP**	**NSC-3OP**	**HSC-1OP**	**HSC-2OP**	**HSC-3OP**
$P_{S.Out}$%	40	30	60	40	40	45
Beam Models Symbol	**HSC-1OPT**	**HSC-2OPT**	**HSC-3OPT**	**NSC-I-1OP**	**NSC-I-2OP**	**NSC-I-3OP**
$P_{S.Out}$%	45	35	60	30	30	75

Another way to evaluate serviceability limit state is the checking service load of the beams with out of plane parts at the allowable maximum crack width of straight beam which equal to 0.30 mm as stated in ACI-318-19 code by checkin it if can satisfy the service load of straight beam (0.60 P_U). Table (4-7) showed the service load for each beam at the maximum crack width of 0.30 mm and its percent from ultimate load.

Table (4-7):- Comparison of experimental service load at crack width limit (0.3 mm) according to ACI Code.

Beam Models Symbol	Experimental Service Load at (Crack width 0.30 mm) (kN)	Ultimate load (kN)	P_{cr}/P_U
NSC-S	360	576.76	0.63
NSC-1OP	115	369.36	0.31
NSC-2OP	60	392.3	0.15
NSC-3OP	50	176.14	0.28
HSC-S	350	757.57	0.46
HSC-1OP	115	384.51	0.30
HSC-2OP	110	404.88	0.27
HSC-3OP	60	241.57	0.25
HSC-1OPT	100	460.48	0.22
HSC-2OPT	65	467.96	0.14
HSC-3OPT	105	289.3	0.36
NSC-I-1OP	110	369.29	0.30
NSC-I-2OP	118	387.24	0.30
NSC-I-3OP	80	175	0.46

From the Table (4-7) it was observed that the service load of the NSC-S control beam was approximately within the limit of 60% of its ultimate load, while all the other beams service loads were below 60% of their

ultimate load at the allowable maximum crack width of straight beam which equal to 0.30 mm.

Therefore, the service load of the beams with out of plane parts cannot be considered at 60% of their ultimate load as the straight beam, but it was noticed from the results that deflection limit should be taken at service load below 60% of their ultimate load. This also proves what has been clarified regarding the behavior of deflection at the service load as it was shown in Table (4-6) by the consider equation 4.2 in calculating service load that achieves the maximum permissible deflection limit (L/180). In another way, the ratios mentioned in Table (4-7) can be adopted with regard to the service load that achieves the maximum crack width of 0.30 mm.

4.3.1.4 Ductility Index

Ductility represents one of the materials properties which could be defined as the ability of material or a member to undergo large deformations without significant resistance loss or rupture before the collapse. In concrete structural members, it could be obtained by the ratio of steel reinforcement within it, because mild steel is a ductile material that can be bent and twisted without rupture, **Punmia, 1992 and Khamees et al., 2021** [66, 67].

The ductility of the structural member in experimental work could be estimated in terms of ductility index. There were two common methods to estimate the ductility index, the first one was the displacement ductility index, and the second one was the energy ductility index.

Kim et al., 2010 [68] **and Maghsoudi et al., 2011** [69] defined the displacement ductility index μ as:

$$\mu = \frac{\Delta_U}{\Delta_y} \qquad (4.3)$$

Where; μ is the ductility index, Δ_U is the deflection of the beam at the ultimate load, and Δ_y is the defection of the beam at the yield load.

Park [70, 71] based on the equivalent elasto-plastic yield point that depends on the equivalent elasto-plastic energy absorption, otherwise used the ultimate load deflection at the first fracture of any element that occurs at the end of the elastic zone and causes a reduction in stiffness as shown in Figure (4-17). In this approach, the deflection at yield point (Δy) was taken at the intersection point of two lines; the first line is a horizontal tangent to the load-deflection curve at the ultimate load, whilst the second one is a line passing through the origin point to the point that represents 75% of the ultimate load.

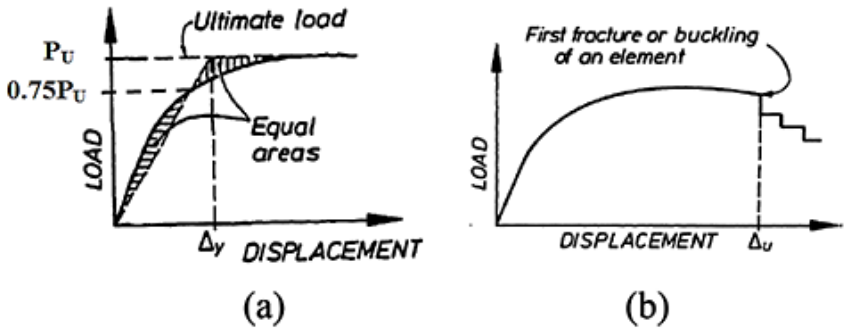

Figure (4-17): Park definition for displacements [70, 71]: (a) yield displacement by equivalent elasto-plastic energy absorption. (b) The ultimate deflection is based on the first fracture of an element.

The energy absorption capacity of the concrete beam could be approximated as the area under the load-deflection curve up to its ultimate load, which represents the energy absorption that could sustain before displaying a significant drop in load-carrying capacity [72, 73, 74]. Absorbed energy could be obtained by integrating the area at each loading step in a load-displacement relationship [75, 76, 77, 78]. Figure (4-18)

represented the load-deflection curve where; the total energy *E* was done by integrate the product the magnitude of the load *P* and of the small deflection *dx* and which is equal to the area under the load-deformation diagram between x = 0 and x = x_1 and could be written as:

$$E = \int_0^{x_1} P\, dx \qquad (4.4)$$

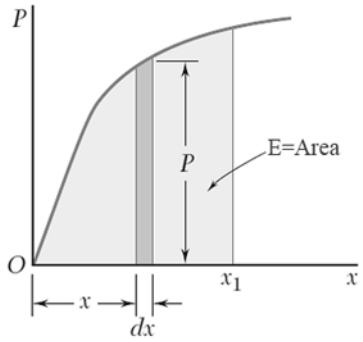

Figure (4-18): Determination of energy based ductility capacity.

Thomsen et al., 2004 [78] and Maghsoudi et al. , 2009 [79] defined the energy ductility index as (μ_E) which is the ratio between the energy of the system at failure (E_u) and the energy of the system at yielding load of tensile steel reinforcement at the central support (E_y):

$$\mu_E = \frac{E_u}{E_y} \qquad (4.5)$$

Where E_u is the failure energy of the beam at ultimate load, E_y is the elastic energy at first steel yield load as shown in Figure (4-19), and μ_E is the energy ductility index.

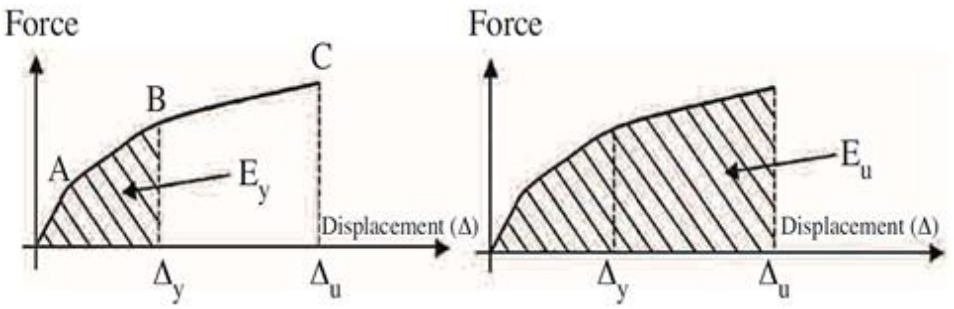

Figure (4-19): Determination of energy based ductility capacity.

Abdulraheem, 2018 [80] proposed a new approach to evaluating the ability of RC beams to absorb the energy in terms of energy ductility index μ_{en} by classifying the total energy absorption into two regions, first one is the elastic energy zone E_{el}, and the second one is the plastic energy zone E_{PL}. This index could be estimated as the ratio of the plastic energy to the elastic energy as shown in Figure 4.24, and calculated using the following equation:

$$\mu_{en} = \frac{E_{Pl}}{E_{el}} = \frac{E_{total} - E_{el}}{E_{el}} \qquad (4.6)$$

Where E_{pl} is the plastic energy that represents the area under the load-deflection curve from the yielding point up to the ultimate load, and E_{el} is the elastic energy that represents the area under the linear part of the load-deflection curve up to the yielding point as shown in Figure (4-20).

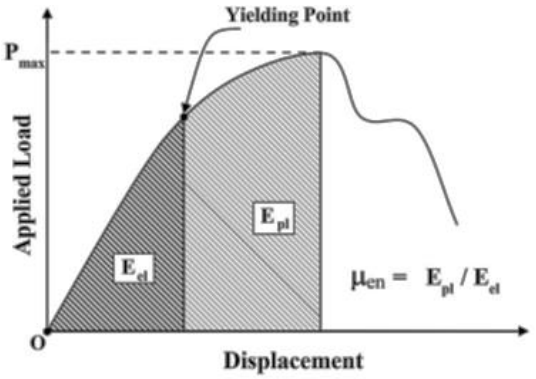

Figure (4-20): Procedure of energy absorption index Evaluation

In this study, equation (4.6) was used to estimate the energy absorption index for the tested beams, because it gave results more acceptable as compared with the displacement ductility index that was estimated by equation (4.3).

Case Study No.1: The effect of number and location of out of plane parts of NSC beams on their ductility indexes as compared with the NSC straight beam are shown in Figure (4-21).

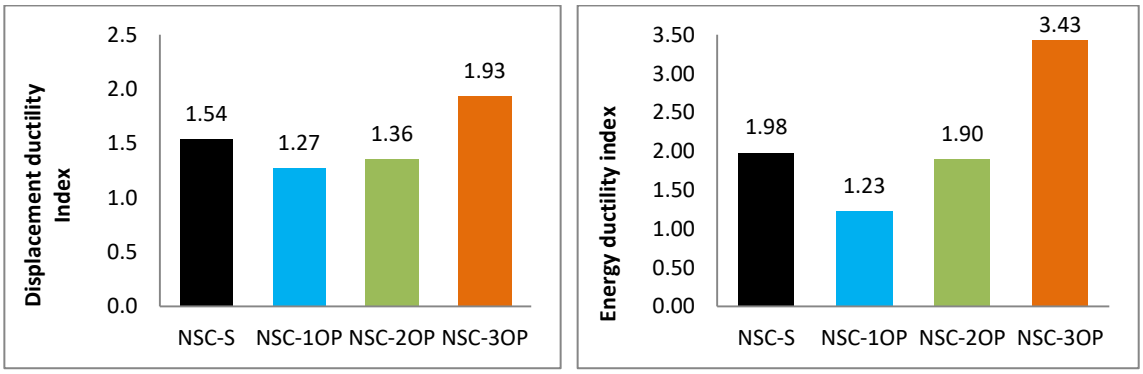

(a) Displacement ductility index *(b) Energy ductility index*

Figure (4-21): Effect of number and location of out of plane parts on the ductility index of NSC beam models.

Figure (4-21-a) showed that the displacement ductility of NSC-1OP and NSC-2OP was less than NSC-S by 17.53% and 11.68% respectively, while NSC-3OP is 20.20% higher than NSC-S. From the Figure (4-21-b), it could be seen that the energy ductility of NSC-1OP and NSC-2OP was less than NSC-S by 37.87% and 4.04% respectively, while NSC-3OP is 36.23% higher than NSC-S.

From these results, it could be concluded that increasing the number of out of plane parts improved the ductility and reduced the difference with NSC-S. The ductility improved with increasing number of the out of plane

parts because increasing total length of beams and increasing torsional effect as copared with flecutural effect that led to decreas bending to tosion ratios.

Case Study No.2: The effect of using high strength concrete (HSC) instead of normal strength concrete (NSC) on the ductility index for the beam models are shown in Figure (4-22).

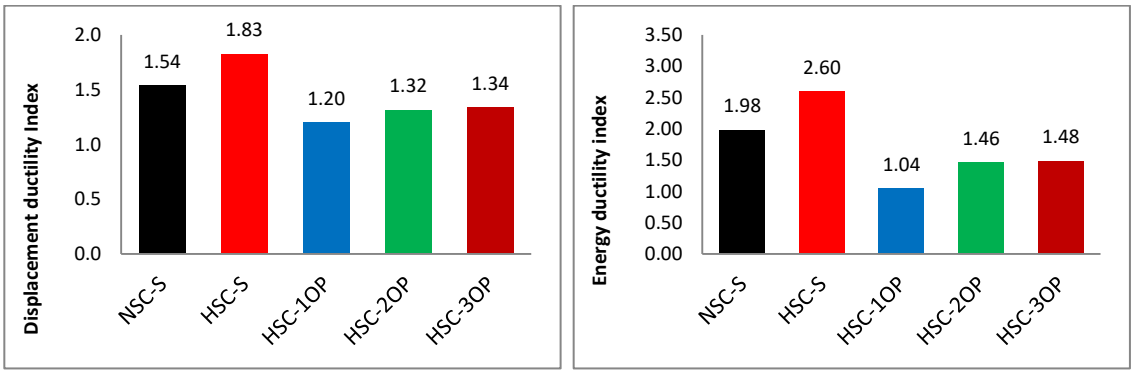

(a) Displacement ductility index *(b) Energy ductility index*

Figure (4-22): Effect of replacement of NSC by HSC on the ductility index of HSC beam models.

Figure (4-22-a) showed that the displacement ductility of HSC-1OP, HSC-2OP, and HSC-3OP was less than NSC-S by 22.18%, 14.65%, and 13.31% respectively, and less than HSC-S by 34.34%, 27.99%, and 26.86% respectively. From the Figure (4-22-b), it could be seen that the energy ductility of HSC-1OP, HSC-2OP, and HSC-3OP is less than NSC-S by 47.31%, 26.19%, and 25.00% respectively, and less than HSC-S by 59.90%, 43.83%, and 42.92% respectively.

These results gave indicate that the HSC beams with out of plane parts had less ductility than NSC-S and HSC-S beams, but increasing the number of out of plane parts improved the ductility and reduced the difference with NSC-S and HSC-S beams.

Furthermore, it was observed that the ductility of straight beam increased when using HSC and this behavior proved the fact the increasing concrete compressive strength led to improve ductility of the straight concrete beam as mentioned in the literature review, while the beams with out of plane parts was showed behavior opposite to that of the straight beam.

Case Study No.3: The effect of adding torsion reinforcement and using high strength concrete (HSC) instead of normal strength concrete (NSC) on the ductility index for the beam models are shown in Figure (4-23).

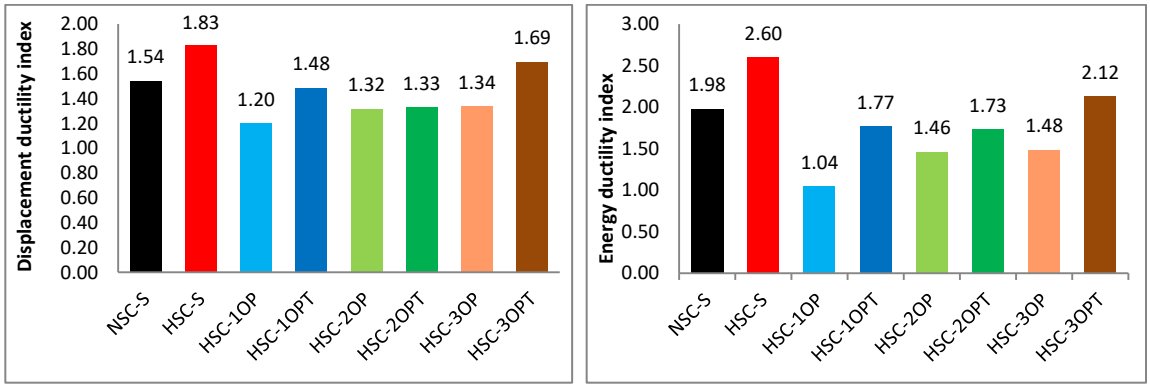

(a) Displacement ductility index *(b) Energy ductility index*

Figure (4-23): Effect of addition torsion reinforcement with replacement of NSC by HSC on the ductility index of HSC beam models.

Figure (4-23-a) showed that the displacement ductility of HSC-1OPT, and HSC-2OPT less than NSC-S by 3.89%, and 13.63%, while the ductility of HSC-3OPT higher than NSC-S by 9.74%, but when comparing with the HSC-S beam, it was observed that the ductility of HSC-1OPT, HSC-2OPT, and HSC-3OPT were less than HSC-S by 19.12%, 27.32%, and 7.65% respectively. From the Figure (4-23-b), it could be seen that the energy ductility of HSC-1OPT, and HSC-2OPT less than NSC-S by 10.60%, and

12.62% only, while the ductility of HSC-3OPT higher than NSC-S by 7.07%.

These results gave indication that the using torsion reinforcement in addition to use HSC in the beams with out of plane parts had improved the displacement ductility index by 23.33%, 0.75%, and 26.12% and energy ductility index by 70.19%, 18.49%, and 43.24% for the beams with one, two, and three out of plane parts respectively as compared with HSC beams.

Moreover, the ductility of the beams with one and two out of plane parts was somewhere less than NSC-S beam, but the beam with three out of plane parts has ductility higher than NSC-S beam.

The using torsion reinforcement improved the ductility of HSC beams with out of plane part, because these beams exposed to torsion effect especially when increasing number of the out of plane parts. The using HSC improved their stiffness, but using torsional reinforcement together with using HSC made torsional reinforcement more effective to contribute in the improvement each of stiffness and ductility. In adtion, the using HSC improved the bond strength between concrete and reinforcement, which improved stiffness and ductility.

Case Study No.4: The effect of increasing the length of the out of plane parts of NSC beams on their ductility index for the beam models are shown in Figure (4-24) to Figure (4-26).

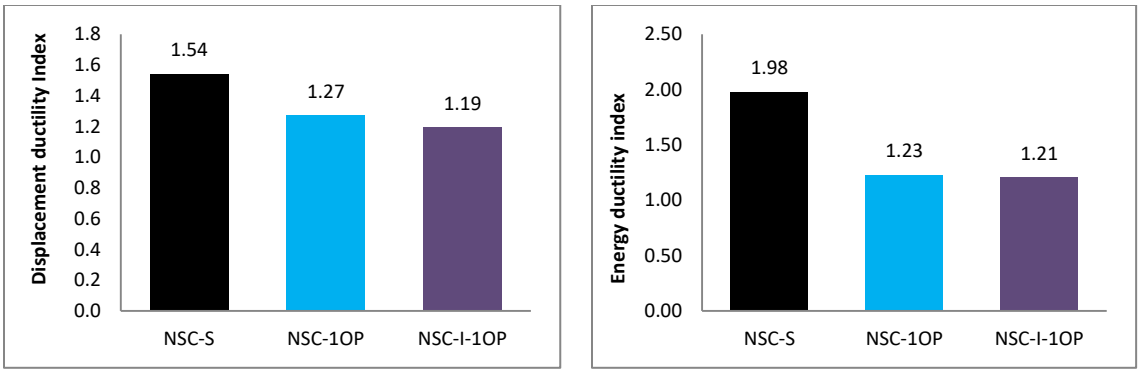

(a) Displacement ductility index *(b) Energy ductility index*

Figure (4-24): Effect of increasing length of out of plane part on the ductility index of NSC-I-1OP beam models as compared with NSC- 1OP and NSC-S beam.

Figure (4-24-a) showed that the displacement ductility of NSC-I-1OP less than NSC-1OP and NSC-S by 6.29%, and 22.72% respectively, and from the Figure (4-24-b) for energy ductility, it could be seen that these ratios were 1.62%, and 38.88% respectively.

These results gave indicate that the NSC-1OP and NSC-1-1OP had ductility less than NSC-S beam and increase length of out of plane part caused a little decrease in the ductility of the beam with one out of plane part.

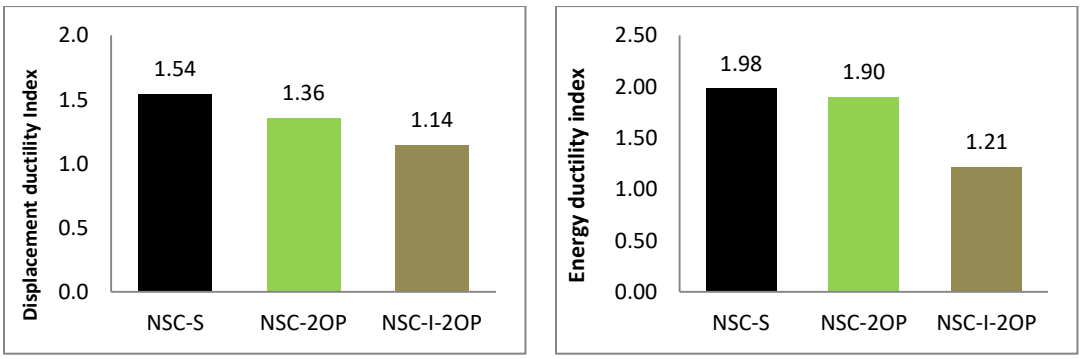

(a) Displacement ductility index *(b) Energy ductility index*

Figure (4-25): Effect of increasing length of out of plane part on the ductility index of NSC-I-2OP beam models as compared with NSC-2OP and NSC-S beam.

Figure (4-25-a) showed that the ductility of NSC-I-2OP was less than NSC-2OP and NSC-S by 16.17%, and 25.97% respectively, and from the Figure (4-25-b), it could be seen that these ratios were 36.31%, and 38.88% respectively.

The results of this case showed that the NSC-2OP and NSC-1-2OP beams had ductility less than NSC-S beam, and increasing length of out of plane part caused a decreasing in the ductility of the beam.

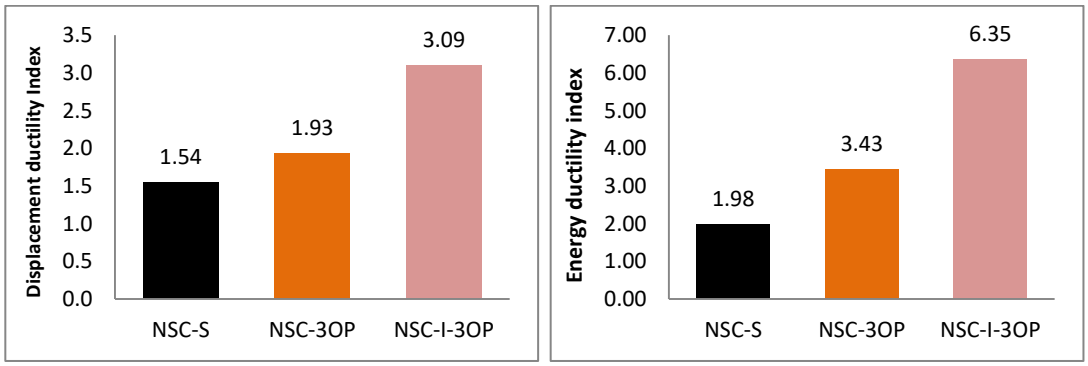

(a) Displacement ductility index *(b) Energy ductility index*

Figure (4-26): Effect of increasing length of out of plane part on the ductility index of NSC-I-3OP beam models as compared with NSC-3OP and NSC-S beam.

On the other hand, Figure (4-26-a) showed that the ductility of NSC-I-3OP was higher than NSC-3OP and NSC-S by 37.54%, and 50.16% respectively, and it can be shown from Figure (4-26-b) that these ratios are 45.98% and 68.81% respectively.

These results gave indication that the NSC-3OP and NSC-I-3OP had ductility higher than NSC-S beam and increasing the length of out of plane parts increased the ductility of the beam with three out of plane parts.

This behavior is due to the fact that the beam, which contains three out-of-plane parts, has a torque ratio in all of its parts higher than the ratio in

the other parts of the beams. In addition, increasing the length of the parts leads to an increase in deflection and as a result leads to an increase in plasticity.

Finally, according to the results, and when comparing the two methods for calculating ductility, the energy method is better because in its calculations the effect of load and precipitation is included, but in the displacement method, only precipitation values are adopted.

4.3.1.4 Load-Rotation Curve

The load versus angle of twist for the cross-sections at the mid span of the beams with out of plane parts was calculated at each loading stage in the experimental work up to the beams rupture. The angle of twist was measured by taking the maximum absolute different readings between the LVDTs that were installed at the at front and back points of mid span and the LVDT at centerline of the beam which was installed as explained in Figure (3-13), Figure (3-14), and Plate (3-18), then this vertical displacement was divided on the horizontal distance between them and took the average of front and back angles. The load and mid span twisting response are explained for each case of this study. Figure (4-27) and equations (4-7) to (4-9) shows an example of calculating twisting angle.

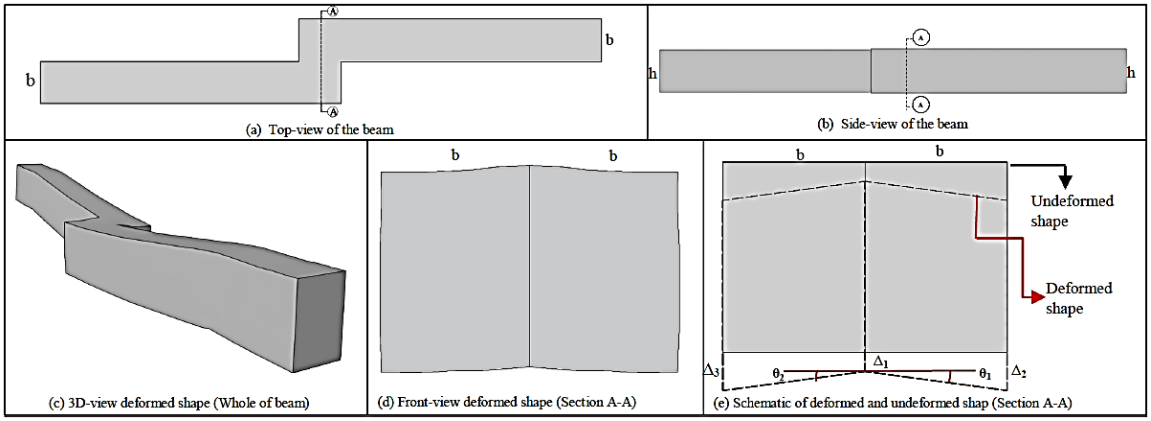

Figure (4-27): Twisting angle calculation of the beam with one out of plane part at mid span.

$$\theta_1 = \frac{\Delta_2 - \Delta_1}{b} \qquad (4.7)$$

$$\theta_2 = \frac{\Delta_3 - \Delta_1}{b} \qquad (4.8)$$

$$\theta = \frac{\theta_1 + \theta_2}{2} \qquad (4.9)$$

Case Study No.1

The effect of number and location of out of plane parts of NSC beams on load–rotation curve as compared with the NSC-1OP beam are shown in Figure (4-28).

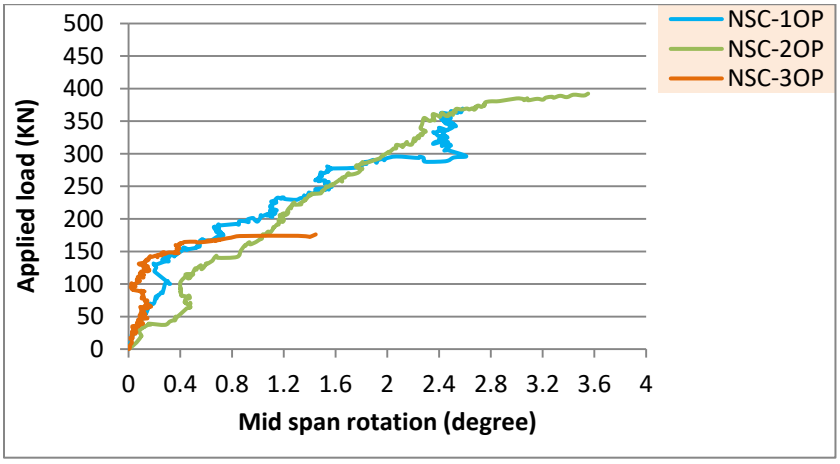

Figure (4-28): Effect of number and location of out of plane part on the load-mid span rotation response of beam models.

According to Figure (4-28) and Table 4.2, it can be observed that the NSC-2OP beam had the angle of twist at the ultimate load higher than NSC-1OP and NSC-3OP beams by 27.32% and 59.43%, and rotation of NSC-3OP was lower than NSC-1OP by 44.18%. These results gave the impression that the NSC-2OP beam had the highest mid-span rotation at the ultimate load, because its mid-span part direction was parallel to the beam axis, while the mid-span part of NSC-1OP and NSC-3OP beam was perpendicular to the beam axis and this decreasing the angle of twist, especially when increasing the number of out of plane parts.

Case Study No.2

The effect of replacement NSC by HSC on the load-rotation response of HSC beams with the out of plane parts beams is shown in Figure (4-29).

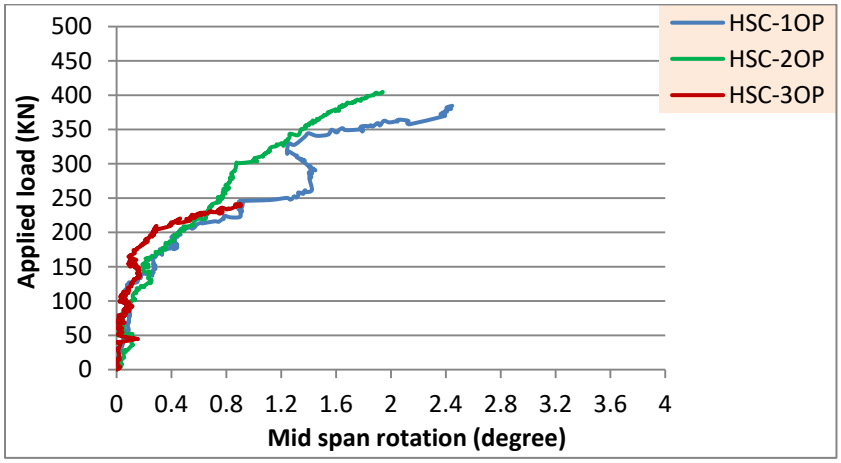

Figure (4-29): Effect of replacement NSC by HSC on the load- mid span rotation response of beam models.

Figure (4-29) and Table (4-2) showed that the angle of twist HSC-2OP and HSC-3OP beam at the ultimate load lesser than HSC-1OP by 20.08% and 42.21% respectively.

Case Study No.3

The effect of adding torsion reinforcement and using high strength concrete (HSC) instead of normal strength concrete (NSC) on the load-rotation characteristics for the beam models are shown in Figure (4-30).

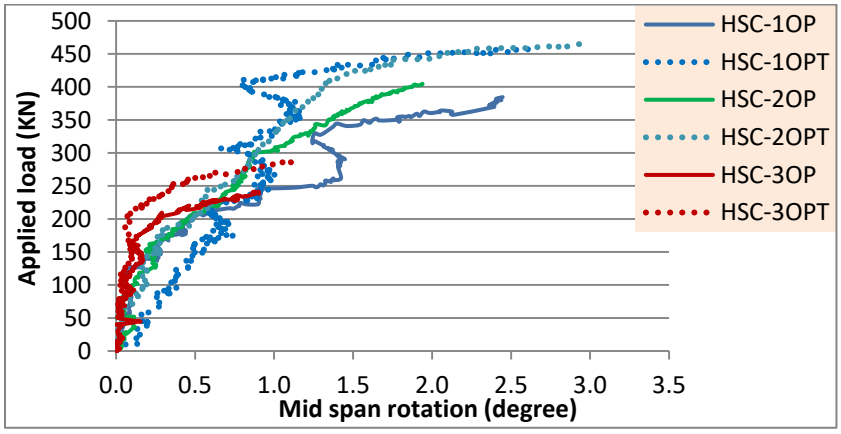

Figure (4-30): Effect of using torsion reinforcement on load- mid span rotation response of HSC beam models.

From Figure (4-30) and Table (4-2), it could be observed that the HSC-2OPT beam had the angle of twist at the ultimate load higher than HSC-1OPT and HSC-3OPT beams by 11.37% and 35.78% respectively, and rotation of HSC-3OPT was lower than HSC-1OPT by 27.54%. Furthermore, the addition torsion reinforcement increased mid span rotations of HSC-1OPT, HSC-2OPT, and HSC-3OPT by 10.81%, 55.44%, and 24.44% as compared with the HSC beams without using torsion reinforcement.

Case Study No.4

The effect of increasing the length of the out of plane parts on the load-rotation characteristics of the NSC beam models are shown in Figure (4-31) to Figure (4-33).

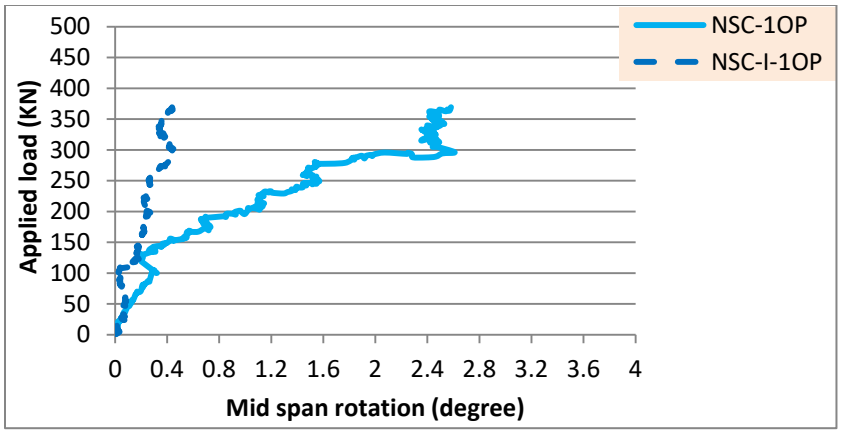

Figure (4-31): Effect of increasing length of the out of plane part on the load- mid span rotation response of beam with one out of plane part.

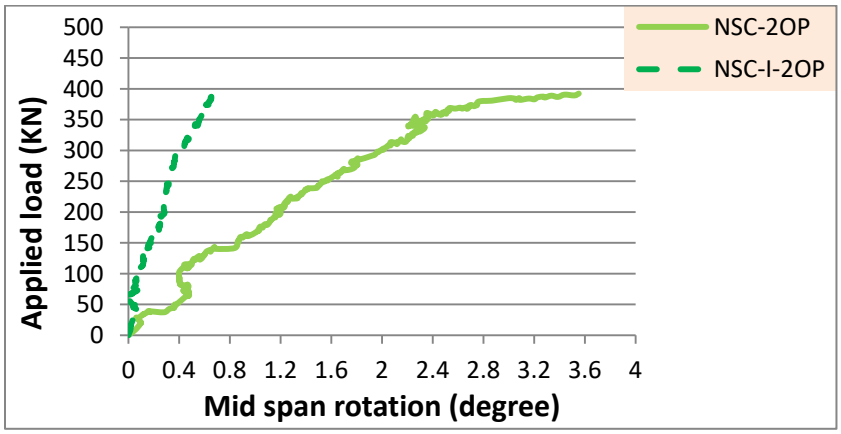

Figure (4-32): Effect of increasing length of the out of plane part on the load- mid span rotation response of beam with two out of plane parts.

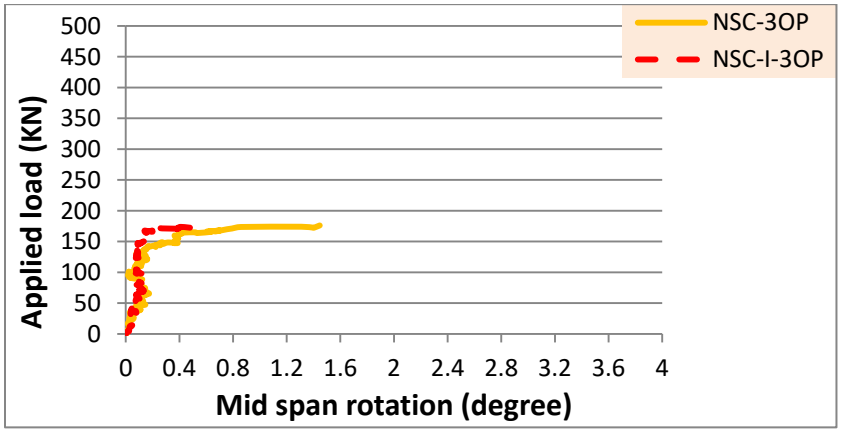

Figure (4-33): Effect of increasing length of the out of plane part on the load- mid span rotation response of beam with three out of plane parts.

From the figures and Table (4-2), The NSC-I-1OP model showed mid-span rotation 78.29% lower than NSC-1OP. The NSC-I-2OP model showed mid-span rotation lower than NSC-2OP beam by 81.69%. In same way, the rotation of NSC-I-3OP model was lower than NSC-3OP beam by 61.11% at ultimate load.

It could be seen that the increase length of out of plane parts led to a high decrease of the mid span rotation about the longitudinal beam axis at the ultimate load of all the NSC beam with the out of plane parts. This behavior occur due to increase torsional effect at the parts that is perpendicular to the beam axis and reduced its effect at the parts that is parallel to the beam axis which led to decrease the mid span rotation about the longitudinal axis of the beam.

The results of all the case studies at the load (176 kN) are summarized and explained in Figure (4-34).

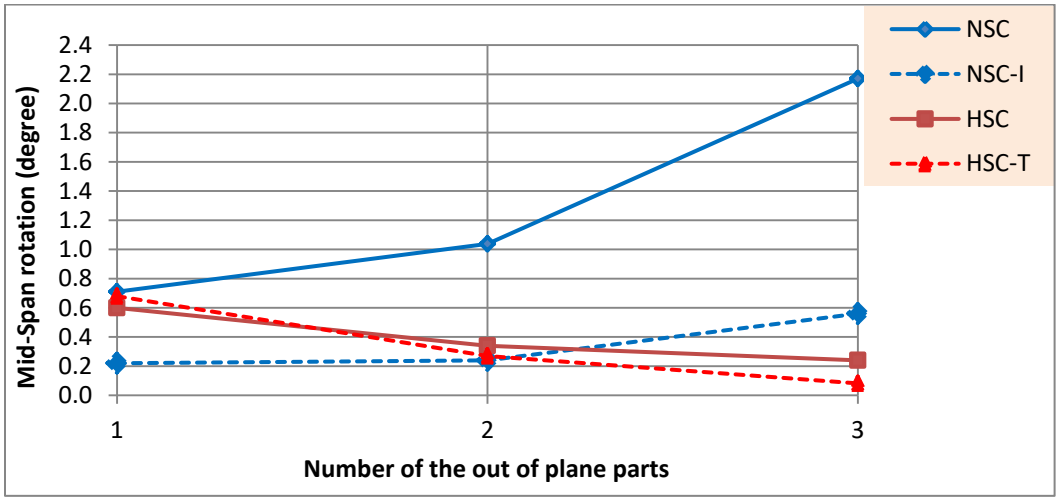

Figure (4-34): Effect of the number of the out of plane parts on the mid span rotation for all the beams at the load (176 kN).

Figure (4-34) showed that the mid span rotations of NSC beams were increased but they were decreased in HSC beams when the number of the out of plane parts increased.

4.3.2 Cracking Behavior and Failure Mode

The cracks propagation and the maximum crack width were monitored throughout tests in order to compare between the beams and identify the failure mode of each model. The first cracking load and its percentage of the ultimate load, the maximum crack width at the service load and ultimate load, and failure mode are shown Table (4-8). These results in addition to the cracking patterns for all the beam models are discussed in the following subtitles.

Table (4-8):- Results of cracks for all the tested beam models. (Continued).

Beam models symbol	Ultimate load Pu kN	Cracking load Pcr kN	Pcr/ Pu%	Crack width at 60% Pu (w_s) (mm)	Crack width at ultimate load Pu (w_u) (mm)	Failure mode
NSC-S	576.76	38	6.59	0.294	3.00	Flexure
NSC-1OP	369.36	26	7.04	0.969	9.89	Flexure plus torsion
NSC-2OP	392.30	26	6.63	7.64	8.72	Flexure plus torsion
NSC-3OP	176.14	14	7.95	1.6	11.60	Torsion
HSC-S	757.57	65	8.58	0.45	3.44	Flexure
HSC-1OP	384.51	43	11.18	5.30	13	Flexure plus torsion
HSC-2OP	404.88	44	10.86	4.50	7.45	Flexure plus torsion

Table (4-8):- (Continued).

Beam models symbol	Ultimate load Pu KN	Cracking load Pcr KN	Pcr/ Pu%	Crack width at 60% Pu (w_s) (mm)	Crack width at ultimate load Pu (w_u) (mm)	Failure mode
HSC-3OP	241.57	40	16.55	2.12	4.50	Torsion
HSC-1OPT	460.48	48	10.42	1.28	6.00	Flexure plus torsion
HSC-2OPT	467.96	45	9.61	4.75	10.00	Flexure plus torsion
HSC-3OPT	289.30	65	22.46	1.00	3.05	Torsion
NSC-I-1OP	369.29	26	7.04	1.15	2.40	Flexure plus torsion
NSC-I-2OP	387.24	41	10.59	1.40	2.20	Flexure plus torsion
NSC-I-3OP	176.45	20	11	0.40	2.5	Torsion

4.3.2.1 Cracking Behavior

The cracking behavior of the tested beam models was monitored during the loading stages in the case of elastic ranges (linear), then the applied load was increased up to the first crack became visible, finally the plastic range when the cracks number increased and propagated up to the models' failure.

Generally, the straight beams started to cracking at the supports by the negative moment flexural cracks then followed by the positive moment flexural cracks at the mid span. Then the combined flexural and shear cracks appeared below the loading points and at the shear spans and these cracks increased and propagated up to the beams failure by flexural

cracks at the supports and mid-span with the concrete crushing at compression zone. The beams with the out of plane parts were started to cracking by the torsional cracks at the interior corners of the out of plane parts and continued from bottom to the top then distributed at the top face of the beams and at the side faces of the out of plane parts, while the flexural and other torsional cracks observed bellow the point load and at the shear span (a), and then the torsional and flexural cracks at the supports. The beams' cracks patterns at the failure load after release load are shown in Plate (4-1).

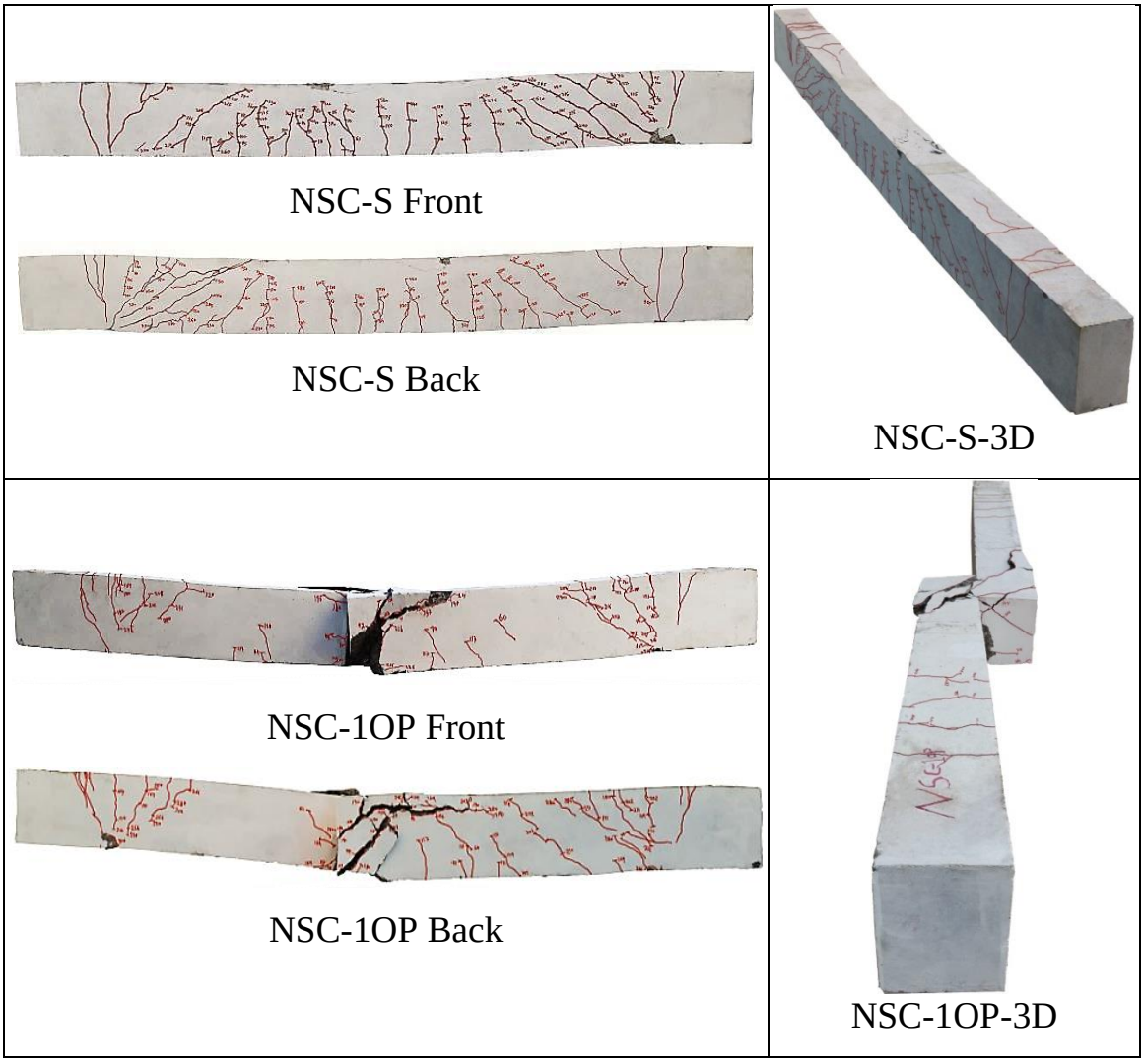

Plate (4-1): Cracks patterns at failure for the tested beam models.

NSC-2OP Front

NSC-2OP Back

NSC-2OP-3D

NSC-3OP Front

NSC-3OP Back

NSC-3OP-3D

HSC-S Front

HSC-S Back

HSC-S-3D

Plate (4-1): (Continued).

HSC-1OP Front

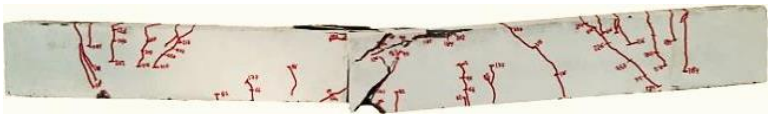

HSC-1OP Back

HSC-1OP-3D

HSC-2OP Front

HSC-2OP Back

HSC-2OP-3D

HSC-3OP Front

HSC-3OP Back

HSC-3OP-3D

Plate (4-1): (Continued).

HSC-1OPT Front

HSC-1OPT Back

HSC-1OPT-3D

HSC-2OPT Front

HSC-2OPT Back

HSC-2OPT-3D

HSC-3OPT Front

HSC-3OPT Back

HSC-3OPT-3D

Plate (4-1): (Continued).

NSC-I-1OP Front

NSC-I-1OP Back

NSC-I-1OP-3D

NSC-I-2OP Front

NSC-I-2OP Back

NSC-I-2OP-3D

NSC-I-3OP Front

NSC-I-3OP Back

NSC-I-3OP-3D

Plate (4-1): (Continued).

The cracking behavior of the beam models in each case study are described as follow:

Case Study No.1:- From Plate (4-1), could be concluded that the specimens with one and two out of plane parts were failed in the torsion at out of plane part then followed by flexure mode at the fixed supports. The specimen with three out of plane parts failed in the torsion at out of plane parts. The cracks of the NSC-1OP and NSC-3OP were flexural vertical and inclined torsional cracks at the flexural span (between points load), while in NSC-2OP it was only vertical flexural cracks. That is the behavior of the beam with two out of parts was similar to NSC-S at mid span because that the mid span part was parallel to the beam axis and which led to the preservation of the bending behavior at the mid span. The cracks of NSC-1OP and NSC-3OP beams were different from the NSC-S, because that the mid span part is perpendicular to the beam axis and which led to the appearance of torsional cracks in conjunction with the flexural cracks at the mid span.

Case Study No.2:- It could be observed from Plate (4-1) that the replacing the NSC by HSC led to increasing the number of cracks and the inclined torsional cracks at flexural span were changed to the vertical flexural cracks. The increase of concrete compressive strength did not change the location and mode of failure, but the cracks appeared rapidly with taller length and formed in an explosively shape.

Case Study No.3:- Experimental results showed that the using torsion reinforcement was also changed the cracks patterns from inclined into vertical cracks and the number of cracks at the shear spans was reduced. Furthermore it was noted during the lab test that the using HSC at first then using torsion reinforcement in conjunction with HSC led to decrease mid

span damage at the ultimate load and increase the damage at the supports gradually.

Case Study No.4:- It could be seen from Plate (4-1) that the increasing the length of the out of plane parts led to increased cracks number at the flexural span and change their slope from inclined to vertical cracks and also increased torsional cracks and damage at the out of plane parts that increased in their span.

4.3.2.2 First Crack Load

The first crack load for each beam model that was obtained from the experiments is listed in Table (4-8).

4.3.2.3 Crack Width

The formations of cracks were monitored during the test to record the width of these cracks with increasing load at each 10 kN until failure. When the concrete tensile stress in a beam models reached to the ultimate tensile strength, the cracking occurred. During the record of the first crack width, it was observed that other cracks increased in their width with increasing load more than first crack; therefore, it was necessary to record maximum crack width that occurred at each loading step until failure of beam models. The width of the first crack, the cracks width at service load (60% of ultimate load) and maximum crack width at failure are listed in Table (4-8).

Case Study No.1:- All the NSC beams with the out of plane parts gave higher maximum crack width at service and failure load than NSC-S. The maximum crack width of NSC-1OP, NSC-2OP, and NSC-3OP was higher than NSC-S by about 229.59%, 2498.64%, and 444.22% at service load, and

229.67%, 190.67%, and 286.67% at ultimate load. In addition, it was noted that the crack width of NSC-2OP at service load was higher than NSC-1OP and NSC-3OP by 87.30%, and 79.05%, but the crack width of NSC-2OP at the ultimate load was lower than NSC-1OP and NSC-3OP by 11.83%, and 24.82% respectively.

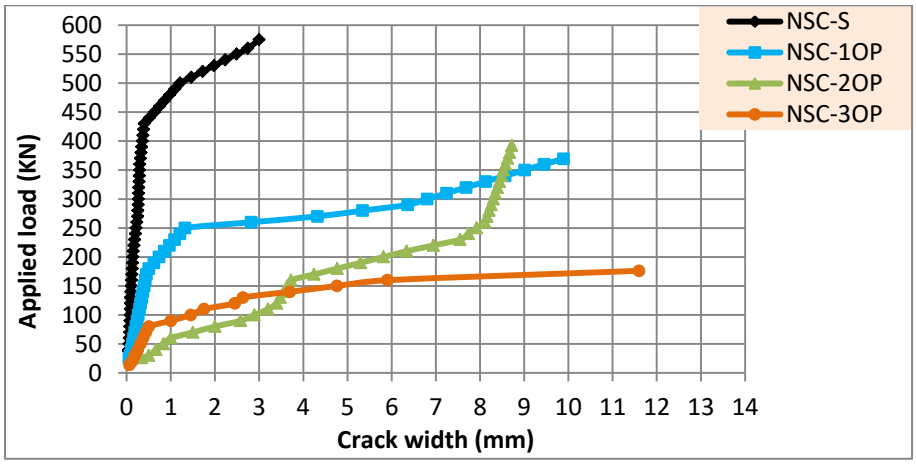

Figure (4-35): Effect of number and location of the out of plane parts on the load-maximum crack width for beam models.

Case Study No.2:- All the HSC beams with the out of plane parts gave higher maximum crack width at service and failure load than NSC-S and HSC-S. The maximum crack width of HSC-1OP, HSC-2OP, and HSC-3OP was higher than NSC-S by about 1702.72%, 1430.61%, and 621.09% at service load, and 333.33%, 148.33%, and 50.00% at ultimate load, while it was higher than HSC-S by 1077.78%, 900.00% and 371.11% at service load, and 73.53%, 53.82%, and 23.55% at ultimate load.

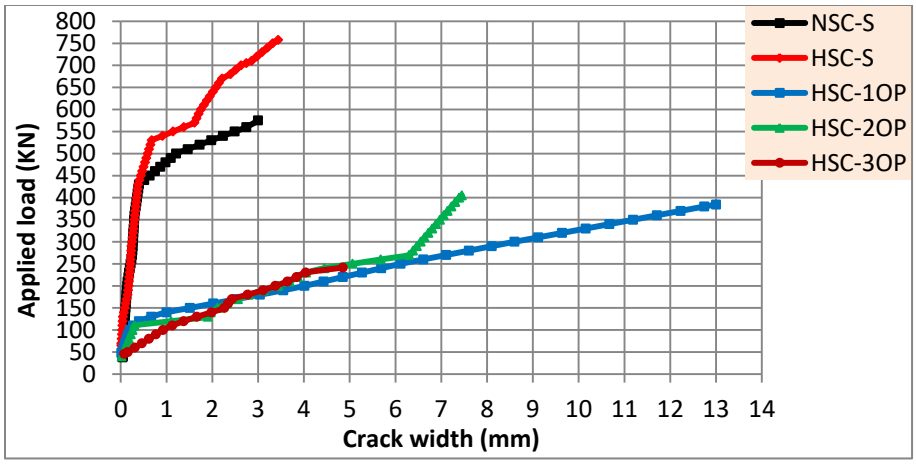

Figure (4-36): Effect of replacement NSC by HSC on the load-maximum crack width of beam models.

Case Study No.3:- The using of HSC with addition torsional reinforcement have kept the beams with the out of plane parts to give higher maximum crack width at service and ultimate load than NSC-S and HSC-S. The maximum crack width of HSC-1OPT, HSC-2OPT, and HSC-3OPT was higher than NSC-S by about 335.37%, 1515.65%, and 240.14% at service load, and 100.00%, 233.33%, and 1.67% at ultimate load, while it was higher than HSC-S by 184.44%, 955.56% and 122.22% at service load, but it was observed that the crack width of HSC-1OPT and HSC-2OPT at ultimate load was higher than HSC-S by 74.42% and 190.70% respectively, while the crack with of HSC-3OPT was 11.33% lower than HSC-S. Furthermore, it was noted that the crack width of HSC-3OPT was lower than HSC-1OPT and HSC-2OPT by 28% and 375% at service load, and 96.72% and 227.87% at ultimate load.

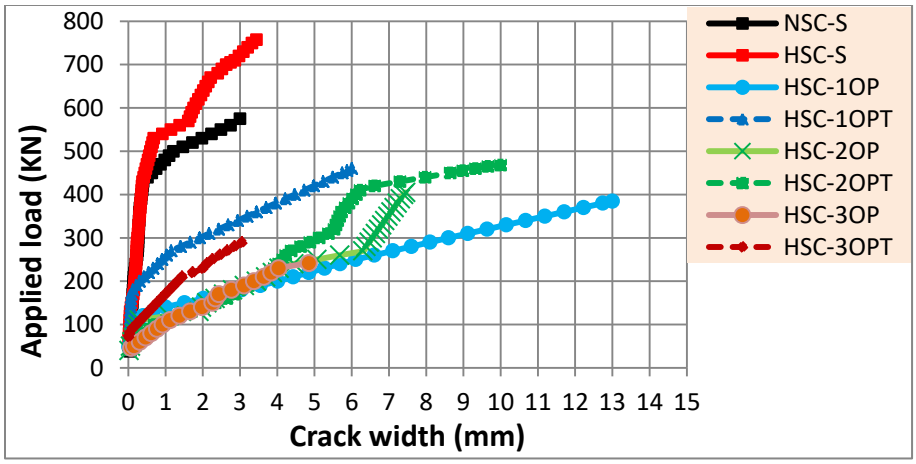

Figure (4-37): Effect of using torsion reinforcement on load-maximum crack width of HSC beam models.

Case Study No.4: the increasing length of the out of plane parts led to a decrease in the cracks width at services and ultimate load as compared with the NSC beams. From Figure (4-38) to Figure (4-40) it could be seen that the crack width of NSC-I-1OP is higher than NSC-1OP and by NSC-S by 26.50% and 74.43% at services load, but at ultimate load the crack width of NSC-I-1OP was smaller than NSC-1OP by 45.39% and higher than NSC-S by 44.44%. The crack width of NSC-I-2OP was smaller than NSC-2OP by 81.67% but higher than NSC-S by 79.00% at services load, while at ultimate load it was smaller than NSC-2OP and NSC-S by 74.77% and 26.67% respectively. In addition, the crack width of NSC-I-3OP was smaller than NSC-3OP by 75.00% and higher than NSC-S by 26.50% at services loads while it was smaller than NSC-3OP and NSC-S by 78.44% and 16.67% at ultimate load.

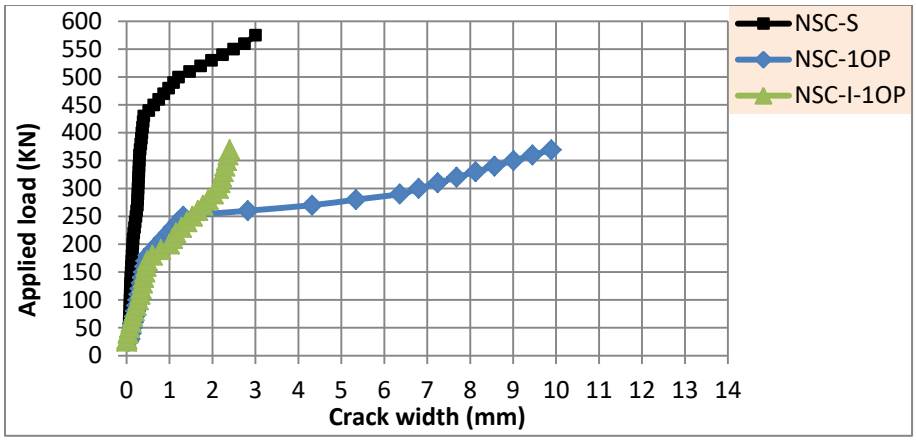

Figure (4-38): Effect of increasing length of the out of plane part on the load-maximum crack width of beam with one out of plane part.

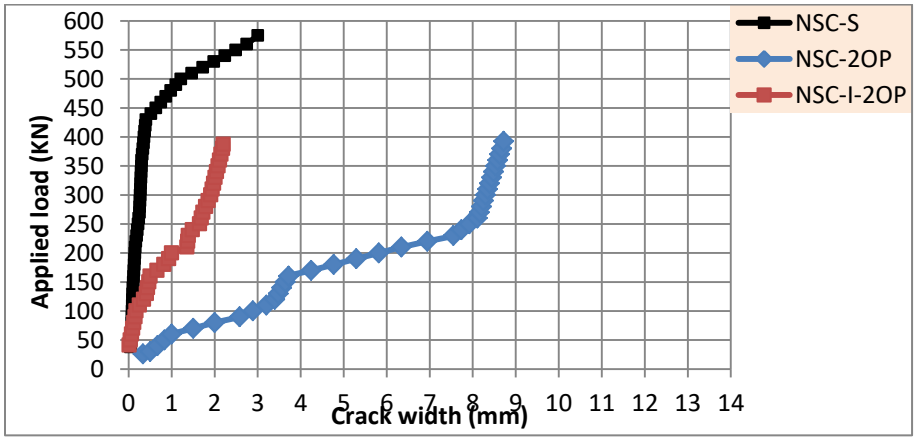

Figure (4-39): Effect of increasing length of the out of plane part on the load-maximum crack width of beam with two out of plane parts.

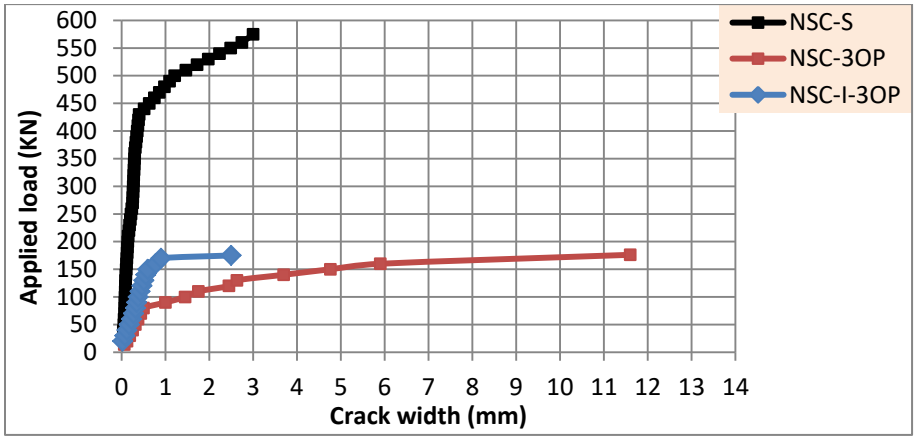

Figure (4-40): Effect of increasing length of the out of plane part on the load-maximum crack width of the beam with three out of plane parts.

This case could be concluded that the increasing length of the out of plane parts led to decrease the maximum crack with as compared with the beams that has not been increased in length of their out of plane parts. This behavior occur due to increase beams stiffness as it was clearly seen through the decrease both of deflection and rotation at mid span increasing length of the out of plane parts.

Chapter Five: Nonlinear Finite Element Analysis

5.1 Introduction

Finite element method was used to investigate the structural behavior of all the experimentally tested beam models. There are many software packages available now for solving engineering problems like solid and structural mechanics, heat and mass transfer, fluid mechanics, acoustics and multi-physics, which might be static, dynamic, linear or non-linear behavior. These softwares use the FEM as an independent methodology or combined with other numerical methods to solve physical problems, but they have different capabilities for more complex problems with the development of detailed and fine-tuned algorithms and numerical schemes. (**Liu, and Quek, 2003**) [(81)].

In this study the ABAQUS software packages (Version 2019) was used to perform this numerical analysis due to its high ability in dealing with non-linear FEM problems. The main items presented in this chapter are the outline of ABAQUS functional units called models analysis procedure which one listed below:

- Parts geometry
- Materials data
- Parts assembly
- Analysis steps
- Interaction between the parts also with boundary conditions
- Loads and boundary conditions
- Element types and mesh properties
- Analysis job performed
- Output results visualization

5.2 Modeling of R.C. Beams

5.2.1 Parts Geometry

There are five parts defined in the modeling of reinforced concrete beam under applied loads as a concrete beam, longitudinal reinforcement, transverse reinforcement, steel loading part, and steel supports part.

5.2.1.1 Concrete Beam Geometry

Straight control beam geometry defined as a 3D solid deformable type by extrusion drawing method, and non- straight beam was drawn by sweep method. 3D elements used, because it can be used for modeling all types of large structural parts which cannot be modeling by 1D or 2D element. Beams geometry and span length are shown in Figure (5-1).

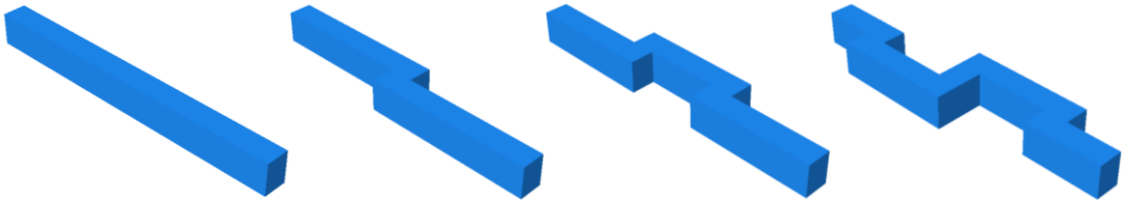

(a) Geometry of NSC and HSC beam models

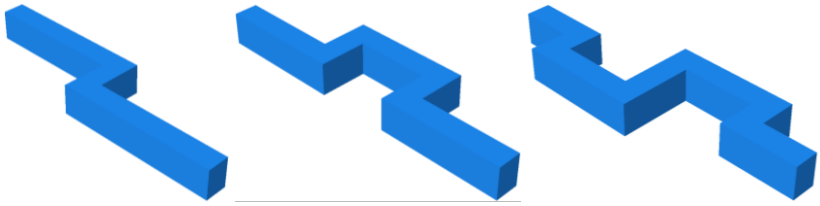

(b) Geometry of NSC beam models with longer span of the out of plane part

Figure (5-1): Beams Geometry.

5.2.1.2 Reinforcement Parts Geometry

Longitudinal and transverse reinforcement defined as a 3D wire deformable type by planar drawing method as shown in Figure (5-2).

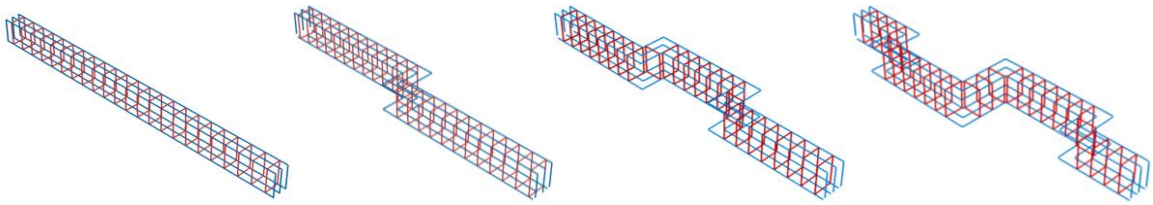

(a) Reinforcement of NSC and HSC beam models

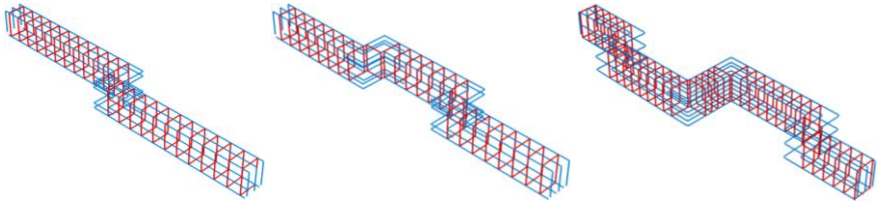

(a) Reinforcement of HSC beam models with torsion reinforcement

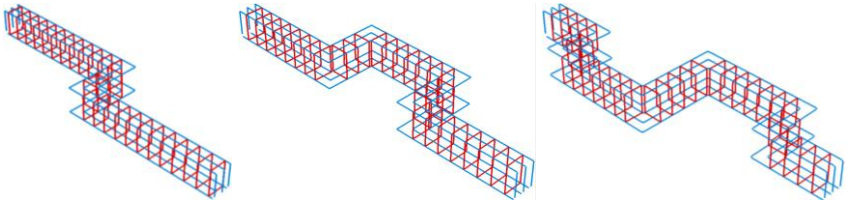

(b) Reinforcement of NSC beam models with longer span of the out of plane part

Figure (5-2): Reinforcement Geometry

5.2.1.3 Loading Steel Parts Geometry

Loading steel part geometry defined as a 3D solid deformable type by extrusion drawing method. It is dimension was 75 mm width, 150 mm length and 20 mm thickness as shown in Figure (5-3).

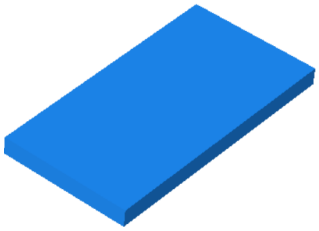

Figure (5-3): Loading Steel Part Geometry.

5.2.1.4 Support Steel Parts Geometry

The geometry of the steel support part defined as a 3D solid deformable type by extrusion drawing method. It was modeled as performed

in experimental work by using the same steel sections and provides the opening with dimension 150 mm width, 200 mm height, which can be fitted with the cross section of the beam as shown in Figure (5-4).

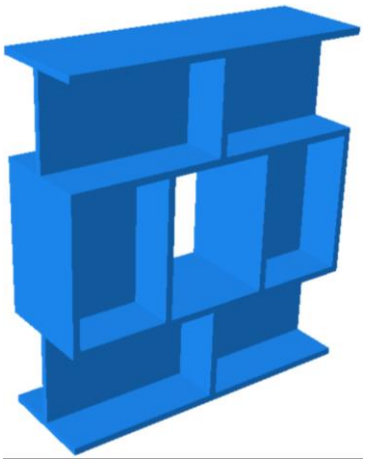

Figure (5-4): Steel Support Parts Geometry.

5.2.2 Material Models

The concrete and steel materials that used in concrete beam, steel reinforcement, and supports have been fully modeled for all behavior cases of elastic, elastic-plastic and plastic, as well as the definition of the damage that resulting from the plastic behavior was defined according to models prepared by researchers and as explained in detail in the **Appendix E**.

5.2.3 Parts Assembly

Each part that created was oriented in its own coordinate system and is independent of the other parts in the model. Although a model may consist of numerous parts, it contains only one assembly. The geometry of the assembly could be defined by creating instances of a part and then positioning the instances relative to each other in a global coordinate system. An instance may be independent or dependent. Independent part instances

are meshed individually, while the dependent part instance mesh is related to the mesh of the original part.

In this research five parts (concrete beam, longitudinal reinforcement, transverse reinforcement, loading plate, and support part) were assembled by using order of create instance as shown in Figure (5-5).

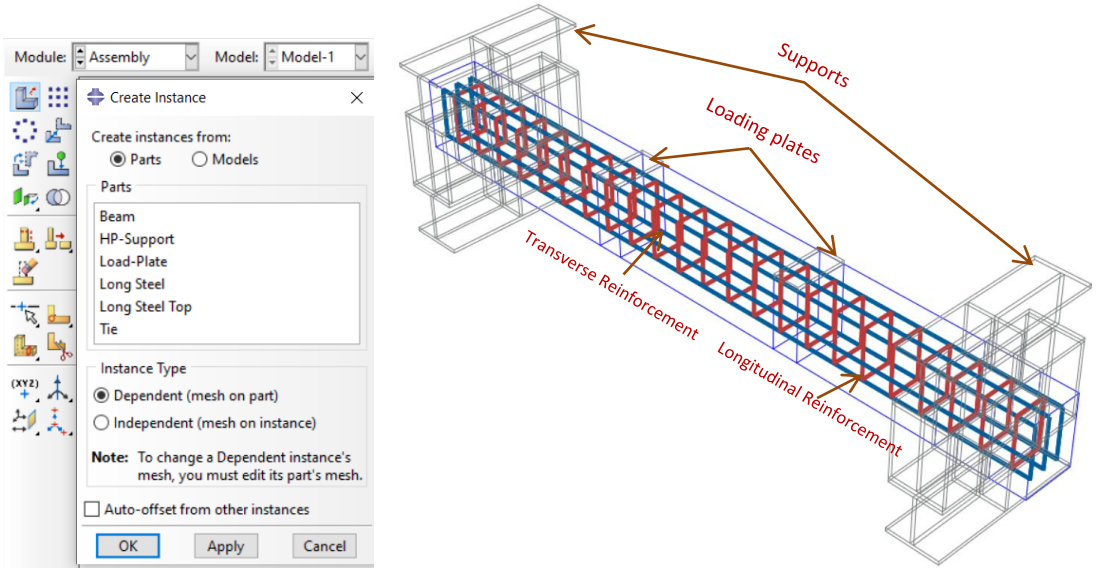

(a) **(b)**

Figure (5-5): (a) Abaqus Assembly window; (b) assembled parts

5.2.4 Step Module

Step module that was used in Abaqus modeling to perform the following tasks:

- Create analysis steps.
- Specify output requests.
- Specify adaptive meshing.
- Specify analysis controls.

A sequence of one or more steps could be defined within a model that generated. The steps sequence provides appropriate way to notes the variations in the loading and boundary conditions of the model, variations in the way parts of the model interact with each other, the removing or adding of parts, and any other variations that may occur in the model during the analysis processes.

An Abaqus/CAE model used the following two types of steps:

- An initial step, in which can define boundary conditions, predefined fields, and interactions that are applicable at the very beginning of the analysis.
- An analysis step, in which applied the loads on the model. Analysis steps can be classified into two types: general analysis steps, which can be used to analyze linear or nonlinear response, and linear perturbation steps, which can be used only to analyze linear problems.

  In this research, the initial step used to define boundary condition of beam to support connection and analysis steps defined as a general dynamic implicit quasi-static for monotonic loading on the beam. The magnitude load of loading step showed in chapter three. Figure (5-6) show the loading step define with the input data.

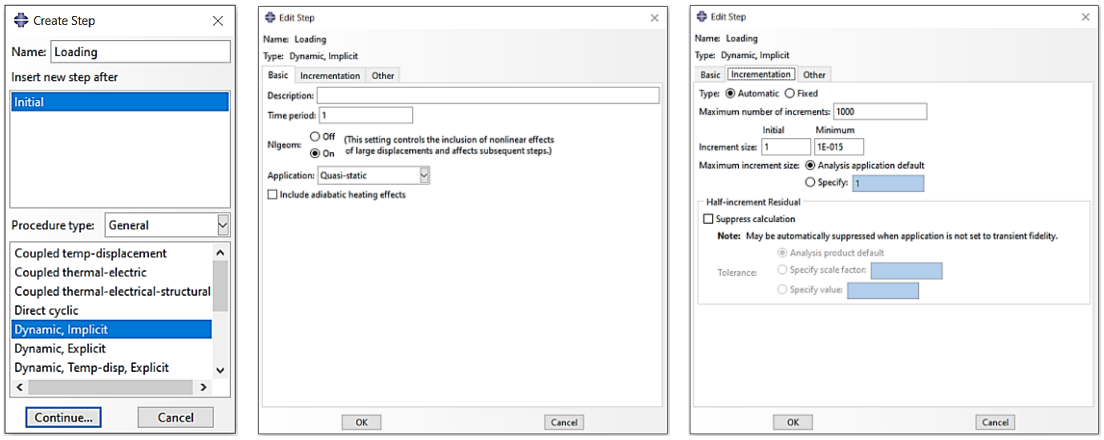

Figure (5-6): Steps definition in Abaqus.

Each loading step consists of smaller increments to represent the nonlinear solution path. The first increment size required to be assumed in the loading analysis step, which is typically taken as a small percent of the applied load through the step to ensure that the elastic limit has not been overstepped. In the loading step for instance, the initial increment size used as 5% of the ultimate applied load, then Abaqus/Standard automatically modify the increments size.

Abaqus uses Newton-Raphson equilibrium iterations to update the stiffness of model, when these iterations give a convergence at the end of each step load increment within the force and displacement tolerance limits.

5.2.5 The Interaction Module

Interaction module that was used to define the interaction between the parts also with boundary conditions. Interactions are step-dependent objects, which mean that the define them was required to identify the steps of the analysis for each one.

This model adopted to define many types of contact and constrains, but in this study it was required to define two types only; contact interaction and embedded region constraints.

5.2.5.1 Contact Interaction

The contact of the concrete surface with the steel loading plates and supports surfaces was defined by the surface to surface friction penalty type with a friction coefficient 0.4 between concrete and steel surfaces. This constraint allows two surfaces separate by relative motion between them at these regions even though the deferent meshes created on the surfaces of the regions. The definition and assign this interaction are shown in the Figure (5-7).

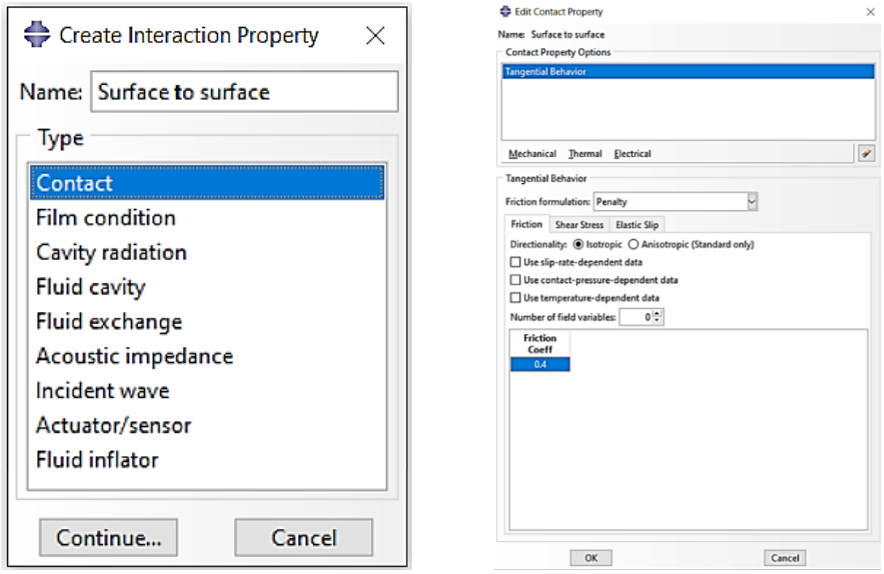

(a) Defining interaction.

Figure (5-7): Surfaces interaction definition.

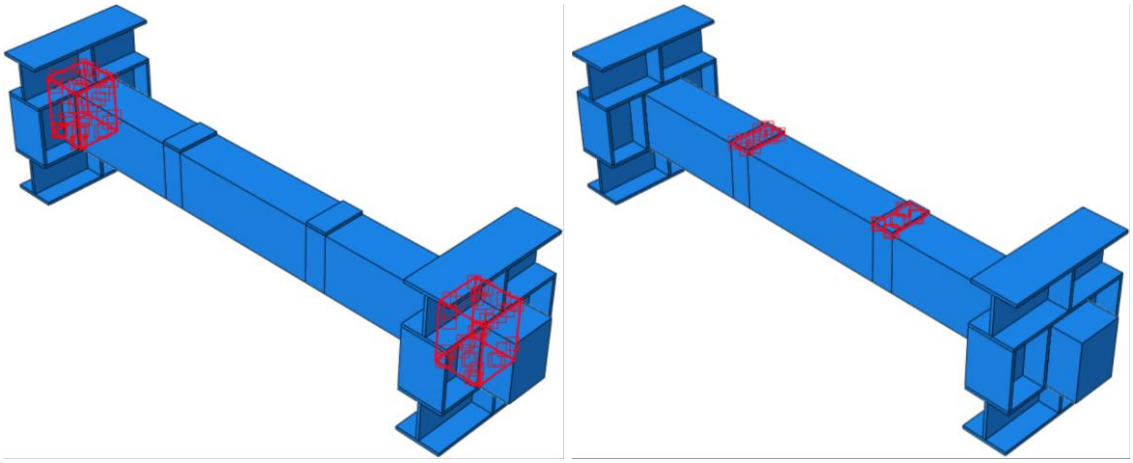

(b) Defined supports Interactions. (c) Defined loading plats interactions.

Figure (5-7): (Continued).

5.2.5.2 Embedded Region Constraints

The embedded region constraint technique allows to specifying an element or group of elements and embedded it in “host” elements. The nodes of embedded elements become embedded nodes in host elements and the number of translational degrees of freedom of these nodes must be identical to the number of translational degrees of freedom of nodes in the host element.

This technique was defined and used to model reinforcement bars embedded in concrete as shown in Figure (5-8).

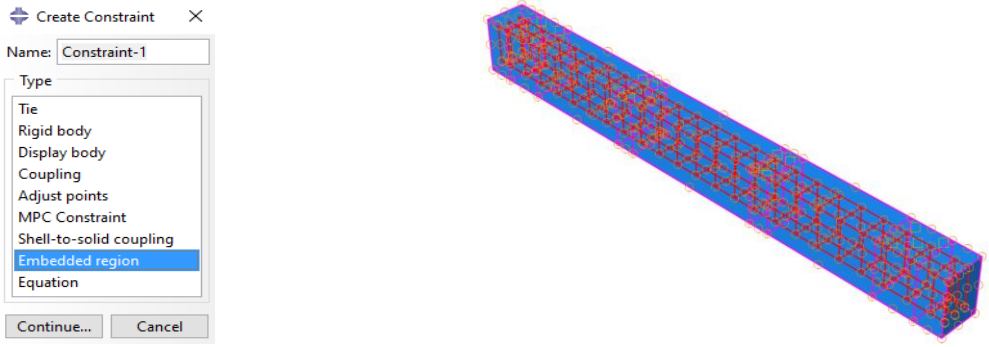

(a) Defining constraint. (b) Model with defined constraints.

Figure (5-8): Embedded region constraints definition

5.2.6 Loads and Boundary Conditions

Loads and boundary conditions are step-dependent, which means that the step must be specified and activate for each type of load and boundary condition. The boundary conditions were applied by using the initial step, while the loads were applied by using the general analysis step.

All the beams connections were fixed supports by using rectangular ring steel HP-sections at the ends of beam and applying the boundary conditions on the out flanges and webs surfaces of the steel sections, while the inner flange surfaces which in contact with the concrete beam surfaces defined as a friction penalty type as mentioned in section 5.6.1. Boundary conditions defined as a Symmetry/Antisymmetry/Encastre type with a restricted motions and rotations in X, Y, and Z-directions. Figure (5-9) shows the defining and assign boundary conditions.

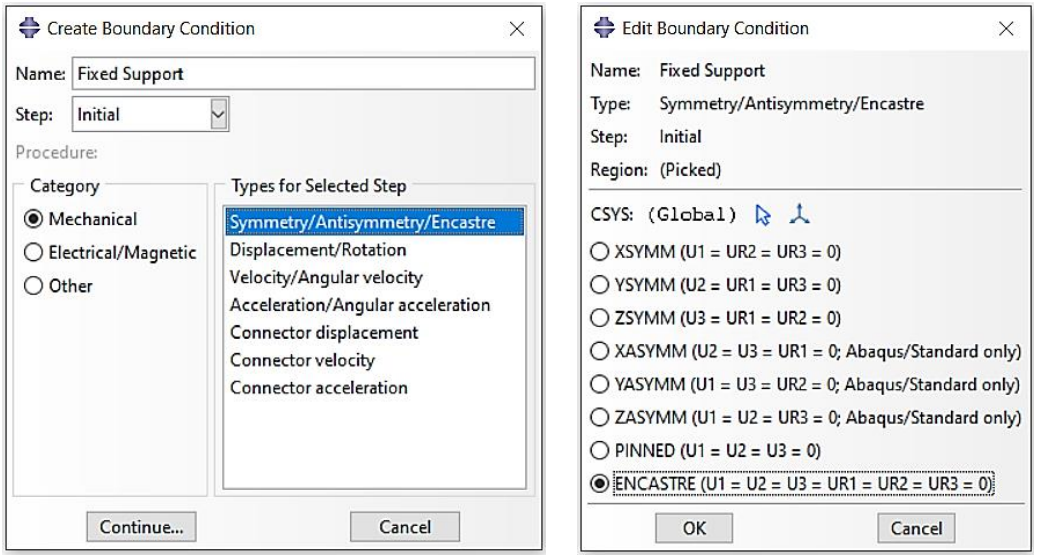

(a) Defining boundary conditions.

Figure (5-9): Defining and assign boundary conditions.

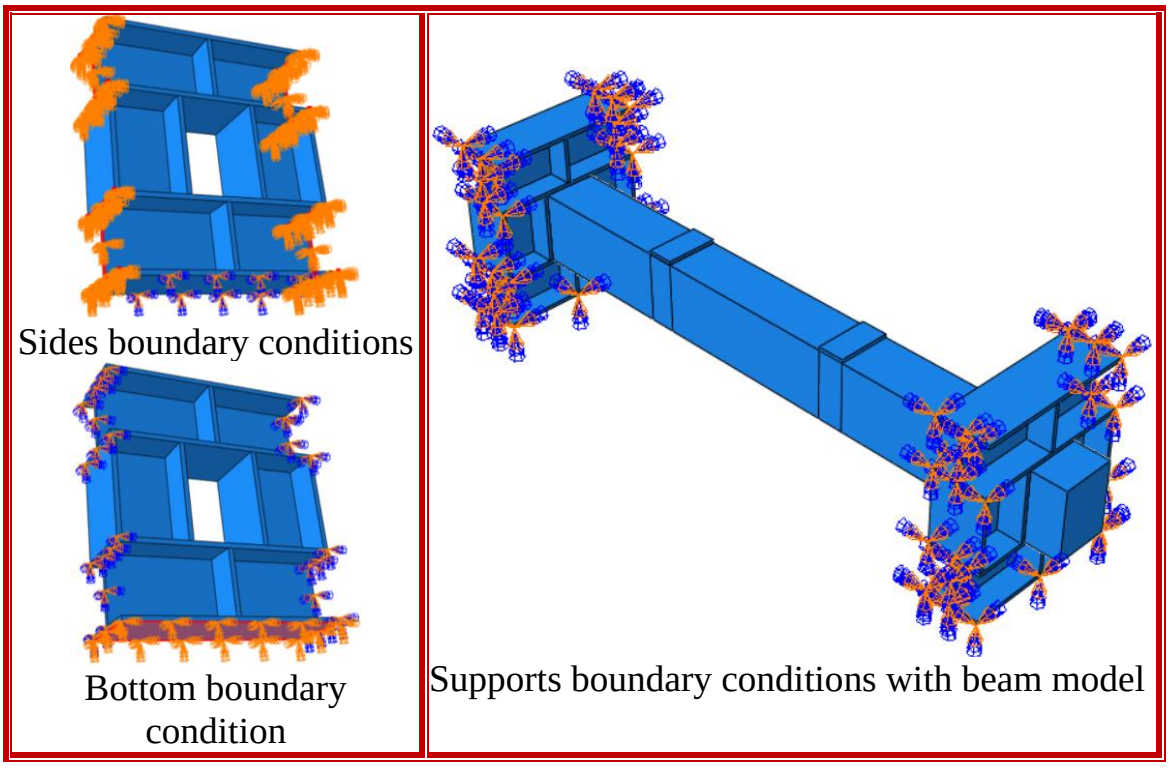

(b) Assign boundary conditions.

Figure (5-9): (Continued).

The load was applied in Abaqus as a pressure on the top surface of the loading plates by N/mm^2 unit. Figure (5-10) shows defining and assigning applied load loads on the loading plates.

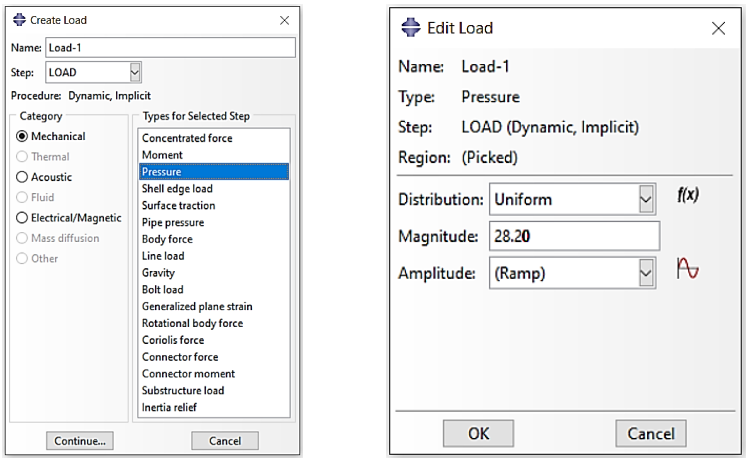

(a) Defining load.

Figure (5-10): Defining and assign loads

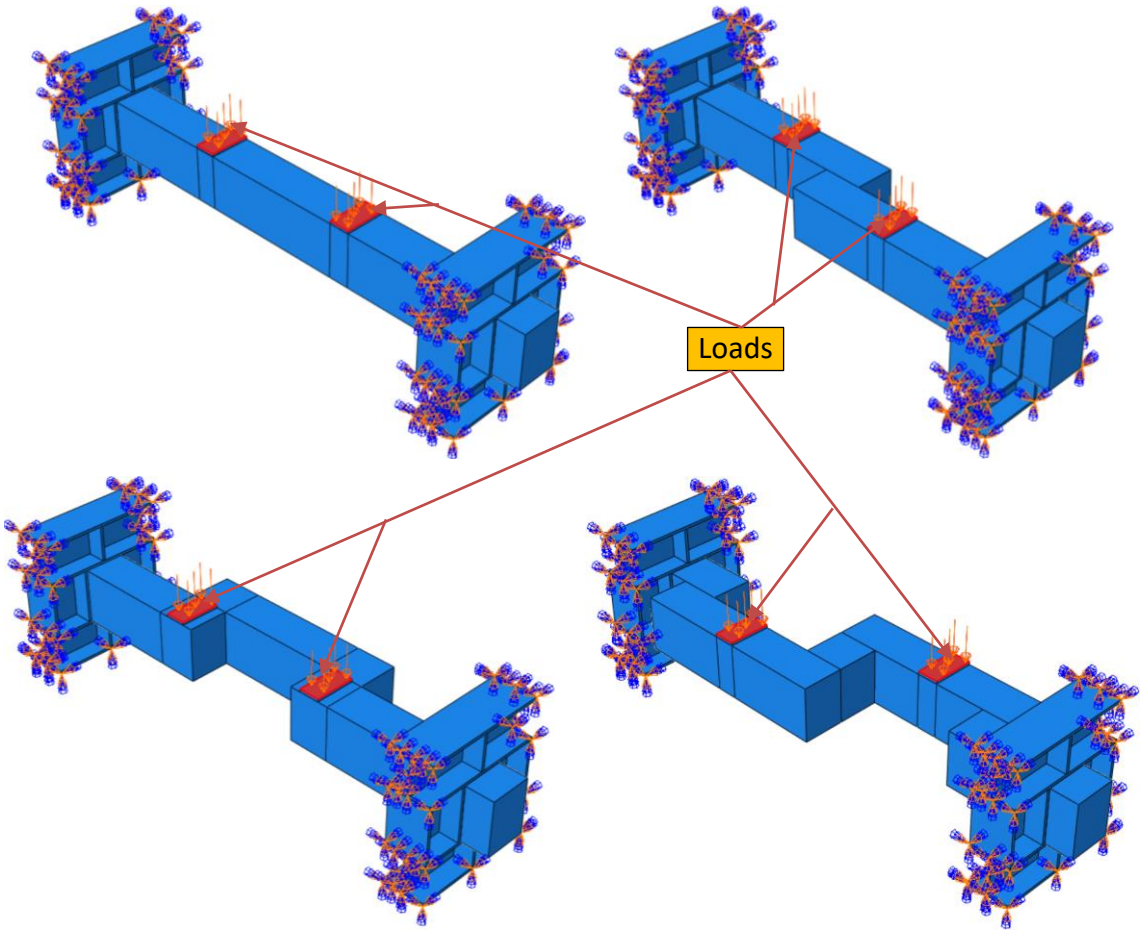

(b) Assign loads.

Figure (5-10): (Continued).

5.2.7 Meshing Elements

The models in this study were meshed by using two types of mesh element, the first one is the solid element and the second one is the truss element, which can be explained in detail as follows:

5.2.7.1 Solid Element

The ABAQUS standard library contains two types of solid element; these types are linear and quadratic interpolation elements in one, two or

three dimensions. They could be utilized in practically for both linear and nonlinear stress-displacement analysis and almost to model any shape.

Typically, the name of an element is clearly classified according to its dimension and nodes number. The eight-node isoperimetric brick element (C3D8R, 8-node linear brick) adopted here to model the concrete beams with reduced integration to prevent the shear locking effect. In this type, each node had three components of the displacement.

The quadratic elements provide better boundary compatibility and convergence issues. Furthermore, the quadrilateral shape with eight nodes contributes to mesh and follows nonlinear calculation. This interface element also has excellent connection effect, thus has higher convergence in iteration calculation.

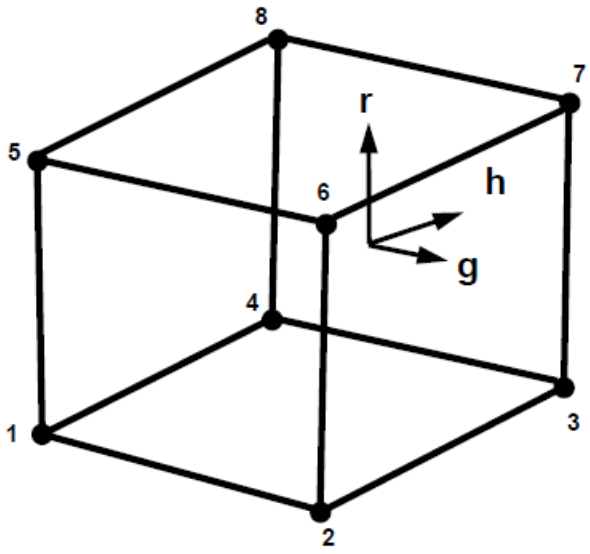

Figure (5-11): First-order brick element (ABAQUS Theory Manual, 2013).

5.2.7.2 Truss Element

Typical in ABAQUS, the longitudinal reinforcement and stirrups simulated with automatically embedded reinforcement type, which can be embedded into continuum all structural element types as shown in Figure (5-12). The embedding term meaning that the reinforcement elements can automatically enter and couple with any kind of surrounding host concrete elements without users manually setting up the bond interface elements between reinforcement and concrete, which additionally means that stiffness can only be contributed by embedded reinforcement as well as host concrete elements.

A two-node three dimensional linear displacement (T3D2) truss element adopted to idealize the internal steel reinforcements and stirrups. Each node has only one axial elongation translation displacement in uniaxial X, Y or Z directions.

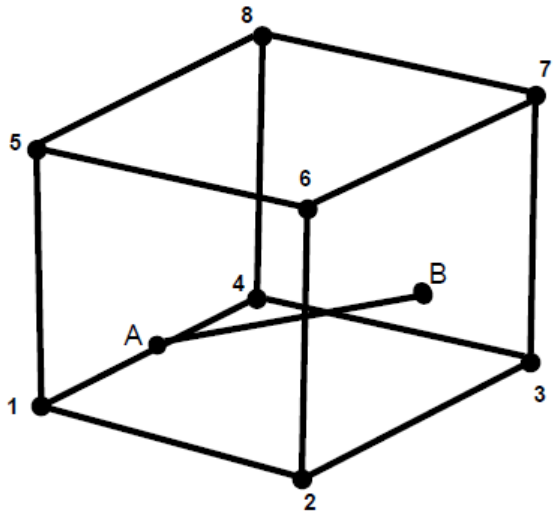

Figure (5-12): Truss element AB embedded in solid element; node A is constrained to edge 1-4 and node B is constrained to face 2-6-7-3 (ABAQUS Theory Manual, 2013).

5.3 Finite Element Analysis Results

The main objective of this chapter is to show the results of the numerical analysis and compare them with the experimental results in order to discover an appropriate representation for each of the element types, the material modeling, the convergence criteria, and the real constants to represent the high strength concrete (HSC) and normal strength concrete (NSC) beams reinforced by steel bars and subjected to static load.

In this chapter, the powerful nonlinear finite element method (FEM) package ABAQUS software (version 2019) was used to show the results of the numerical analysis of the beams whose experimental results were shown in chapter four.

5.3.1 Convergence Study

The selection of mesh density is very important to obtain convergence of results. The meshing of the model was done in the initial step of the FEM analysis. The mesh density has been increased to the point where the analysis results did not influence.

The study was conducted on the convergence of the results of the control straight beam model to find the suitable mesh density. The results converge when using a suitable number of elements in the model. This is be realized in practice when the increase in the number of elements has a slight effect on the results.

Four different numbers of elements 492, 1020, 2380, and 8160 were used to model the beams that have the same properties of the material as shown in Figure (5-13).

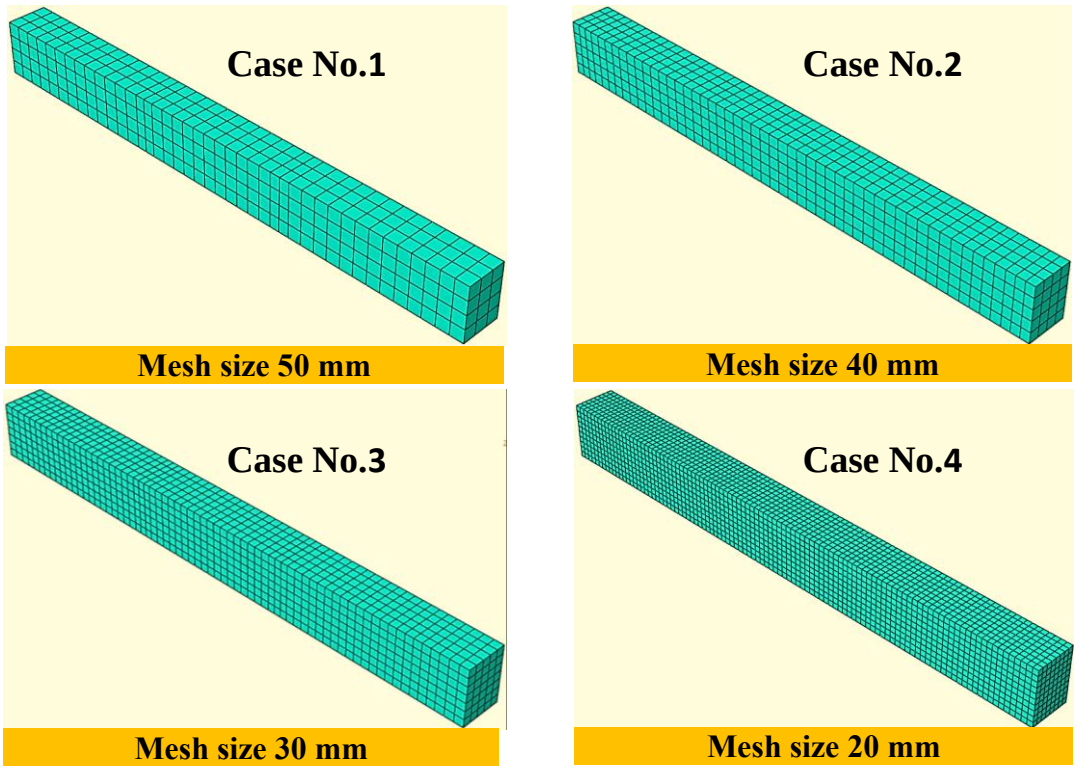

Figure (5-13): Mesh density.

The relation between the central deflection and the number of elements for the tested control HSC and NSC beams was the ruling in choosing the appropriate number of elements for the convergence purposes. Figure (5-14) shows results of the central deflection of the convergence study of NSC-S and HSC-S models.

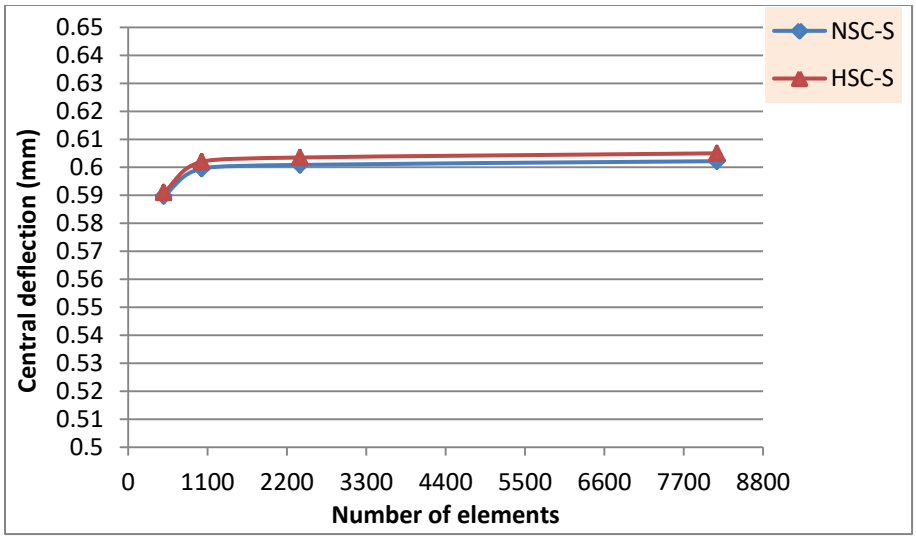

Figure (5-14): The convergence study of NSC-S and HSC-S models under applied load.

According to Figure (5-14), the number of elements 2380 with mesh size 30 mm (Case No.3 in Figure (5-13)) was used for the entire study which represent the results stability point. Figure (5-15) shows the mesh of steel reinforcement for all the analyzed models.

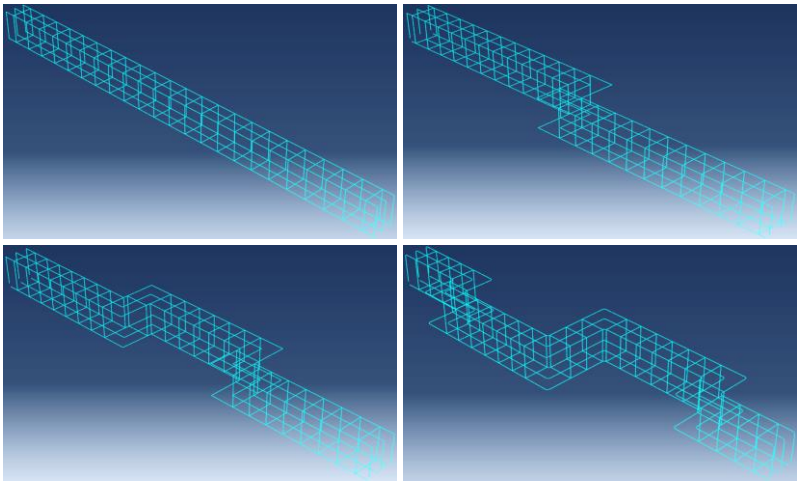

(a) Reinforcement mesh of NSC and HSC beam models.

Figure (5-15): Mesh of steel reinforcement.

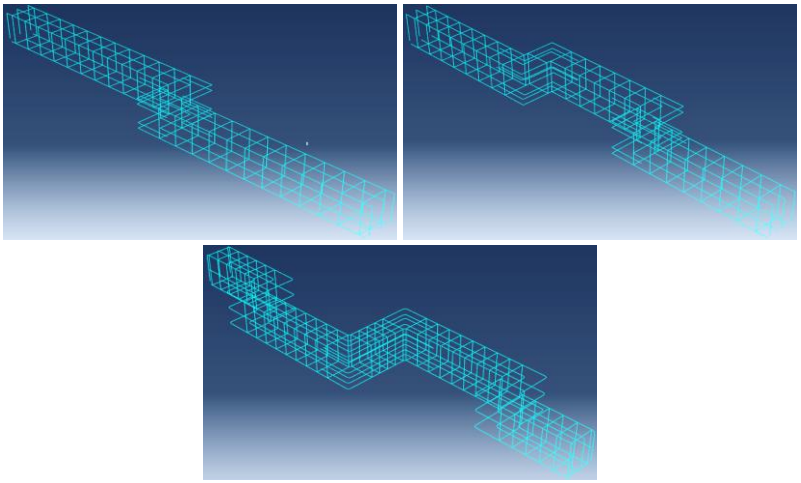

(a) Reinforcement mesh of HSC beam models with torsion reinforcement

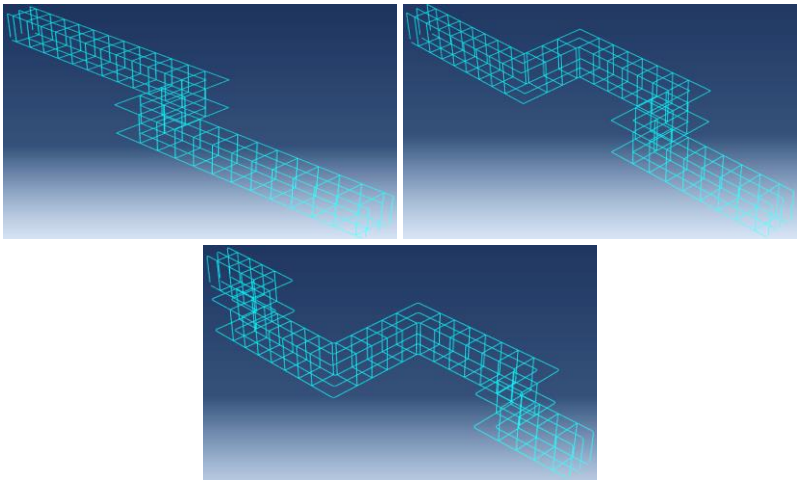

(b) Reinforcement mesh of NSC beam models with increase span of the out of plane part

Figure (5-15): (Continued).

5.4 Comparison between Numerical and Experimental Results

The comparison between numerical analysis and experimental results was conducted in terms of ultimate load, load-deflection curves, deflected shape, and first cracking loads in addition to cracks pattern propagations at failure.

5.4.1 Ultimate Load

The comparisons between the ultimate loads of FE models analysis and the ultimate loads of experimental models results of all the tested beams are shown in Table (5-1). It could be seen that the ultimate loads that obtained from numerical FEA agreed well when compared with the corresponding values of experimental test results of tested beams, where the average difference of the ultimate load was about 4.35 %.

Table (5-1):- Comparison between experimental and numerical ultimate loads for tested beam models.

Beam models symbol	Ultimate load P_U (kN)		Difference ratio %
	Experimental	FEM	
NSC-S	576.77	592.80	2.78
NSC-1OP	369.36	388.25	5.11
NSC-2OP	392.31	398.94	1.69
NSC-3OP	176.14	192.62	9.35
HSC-S	757.57	771.50	1.84
HSC-1OP	384.52	403.91	5.04
HSC-2OP	404.88	424.00	4.72
HSC-3OP	241.20	257.14	6.61
HSC-1OPT	460.49	485.95	5.53
HSC-2OPT	467.97	484.10	3.45
HSC-3OPT	289.30	295.16	2.02
NSC-I-1OP	384.55	390.77	1.62
NSC-I-2OP	387.24	394.39	1.85
NSC-I-3OP	176.45	192.80	9.27
average			4.35

5.4.2 Load-Deflection Curves

The mid span deflection of each tested beam was measured by the experimental work and numerical analysis. The load-deflection curves as found from numerical (ABAQUS) together with experimental results were drawn as shown in Figures (5-16) to (5-29). The finite element results for the high strength concrete as well as normal strength concrete beam models showed a stiffer response as compared with the experimentally recorded curve.

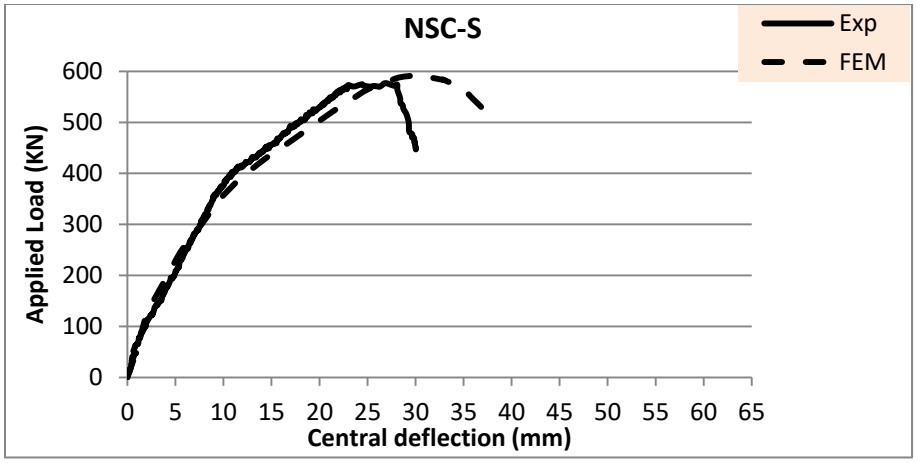

Figure (5-16): Load-deflection curves of beam NSC-S.

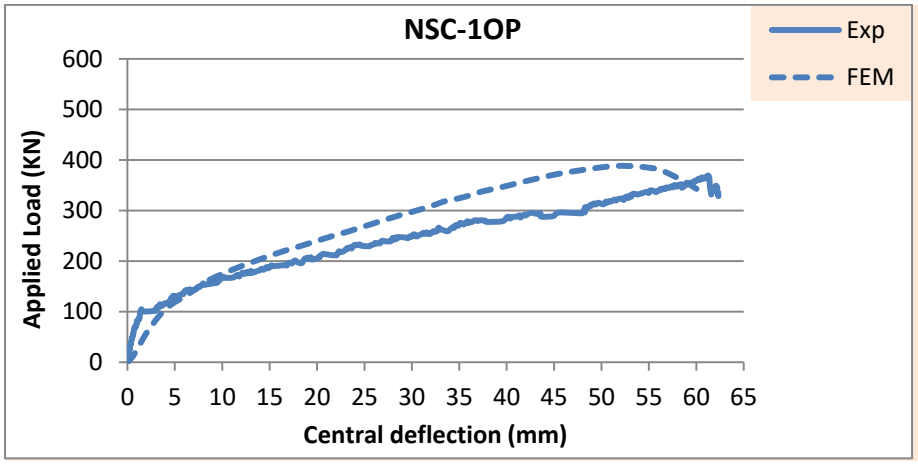

Figure (5-17): Load-deflection curves of beam NSC-1OP.

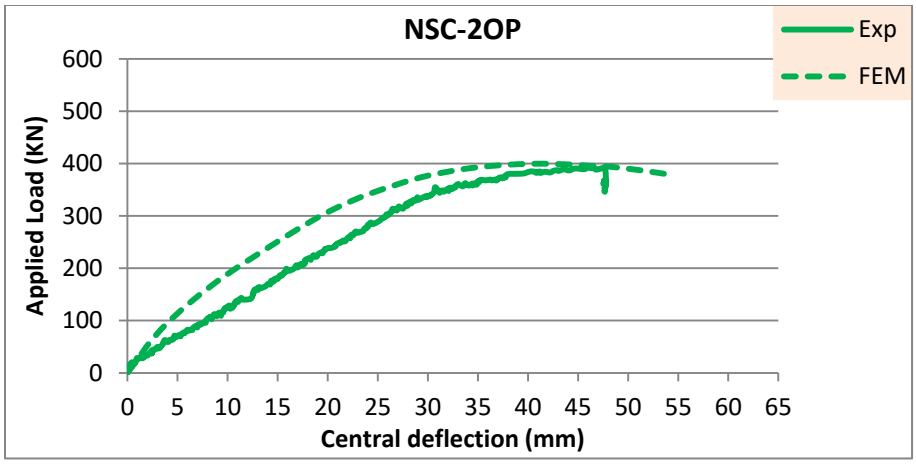

Figure (5-18): Load-deflection curves of beam NSC-2OP.

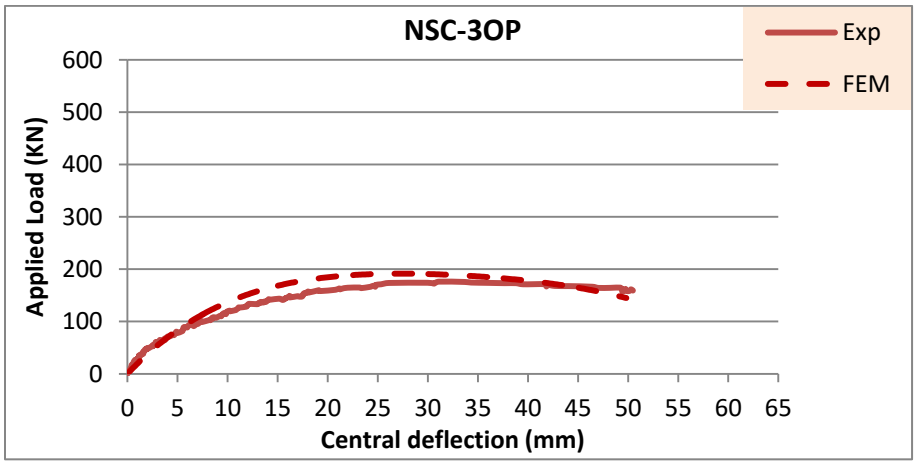

Figure (5-19): Load-deflection curves of beam NSC-3OP.

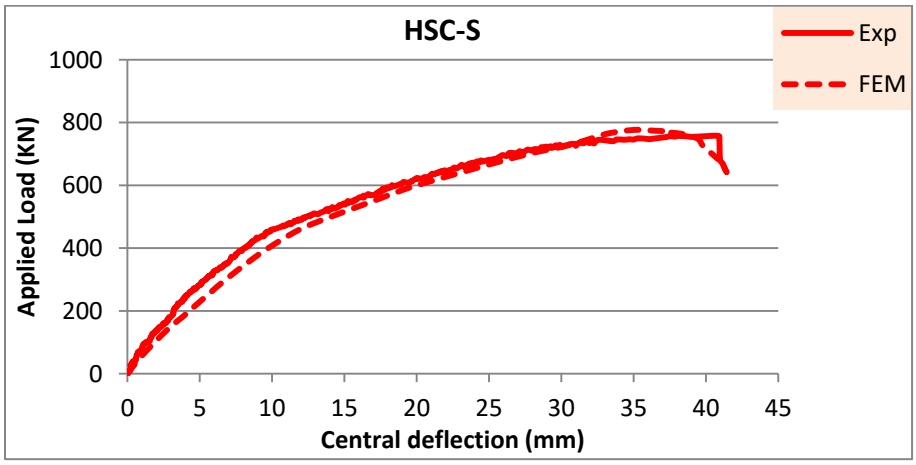

Figure (5-20): Load-deflection curves of beam HSC-S.

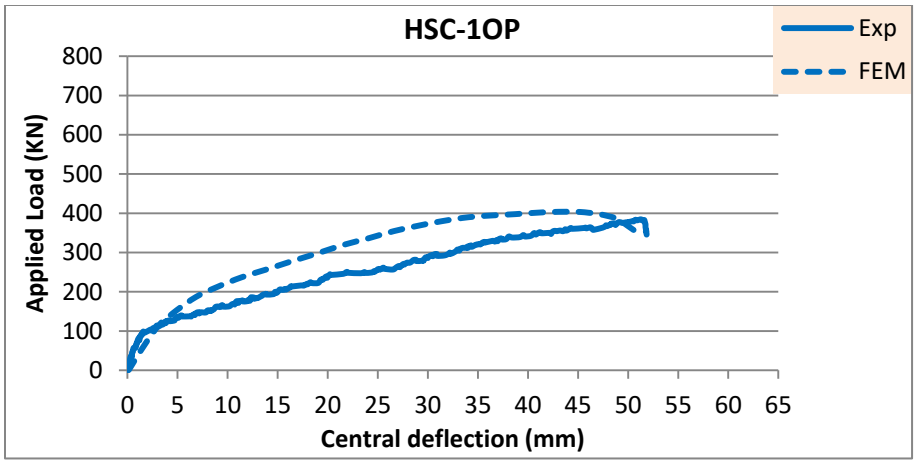

Figure (5-21): Load-deflection curves of beam HSC-1OP.

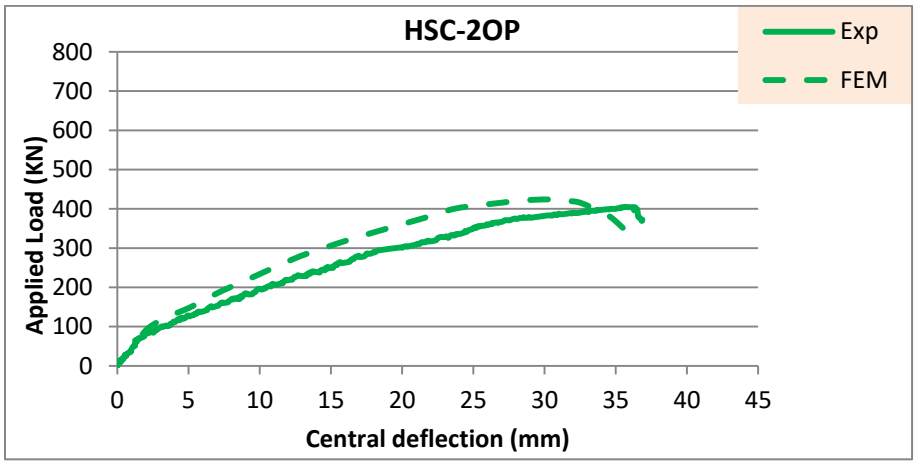

Figure (5-22): Load-deflection curves of beam HSC-2OP.

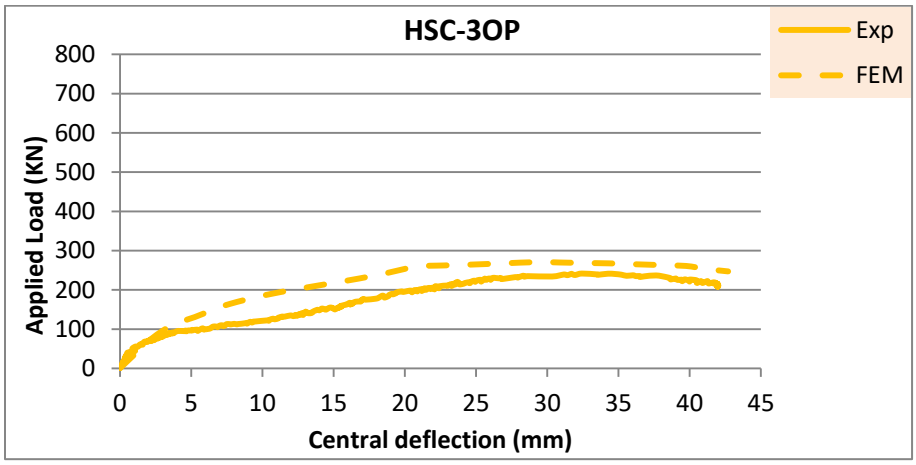

Figure (5-23): Load-deflection curves of beam HSC-3OP.

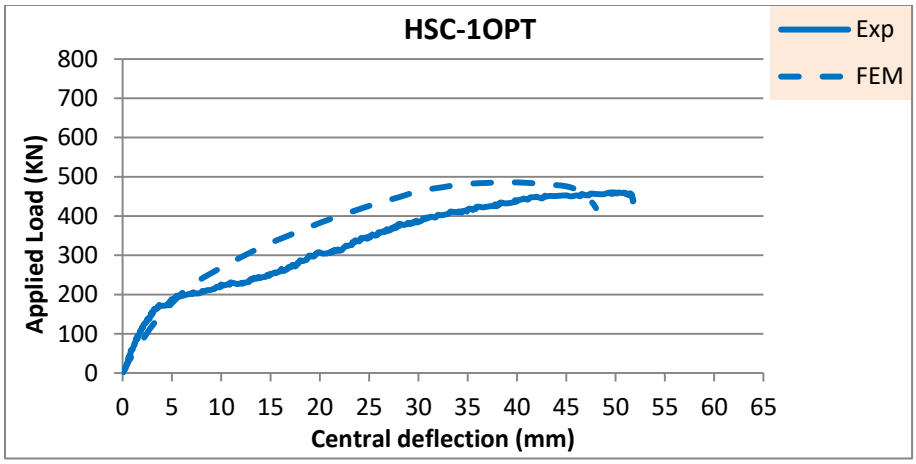

Figure (5-24): Load-deflection curves of beam HSC-1OPT.

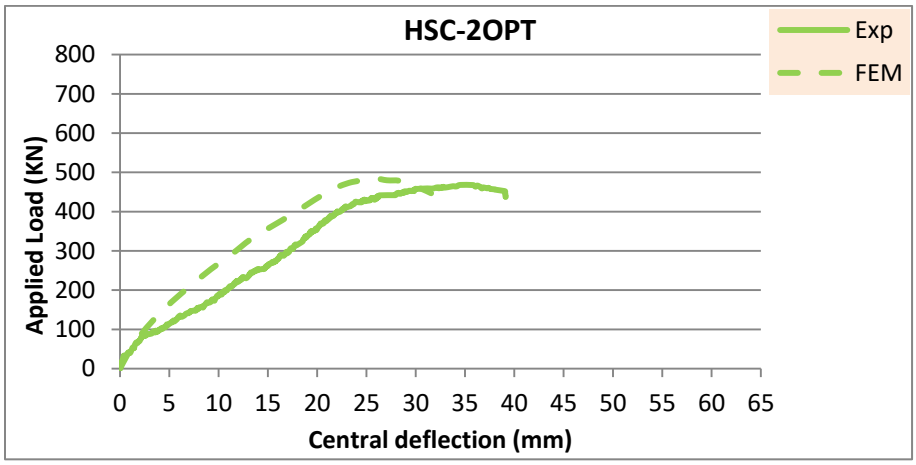

Figure (5-25): Load-deflection curves of beam HSC-2OPT.

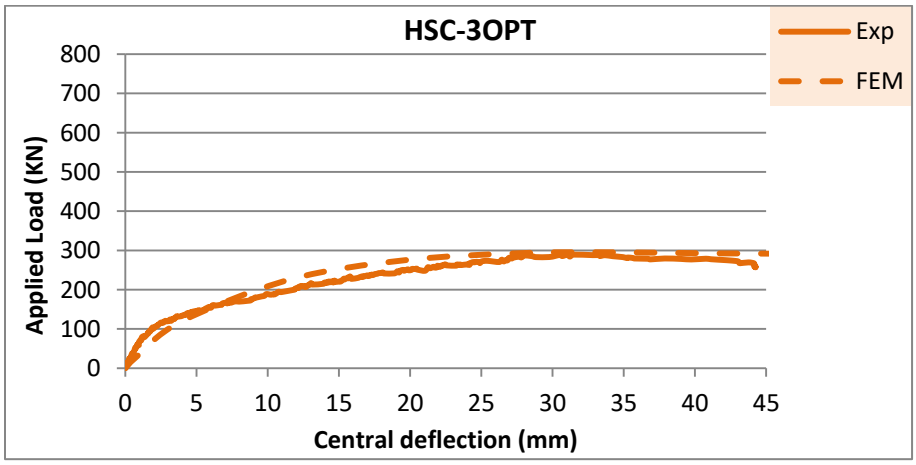

Figure (5-26): Load-deflection curves of beam HSC-3OPT.

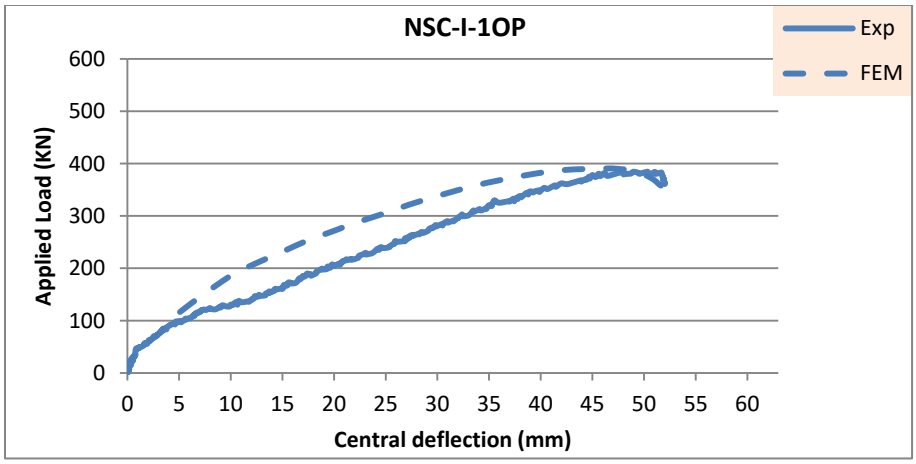

Figure (5-27): Load-deflection curves of beam NSC-I-1OP.

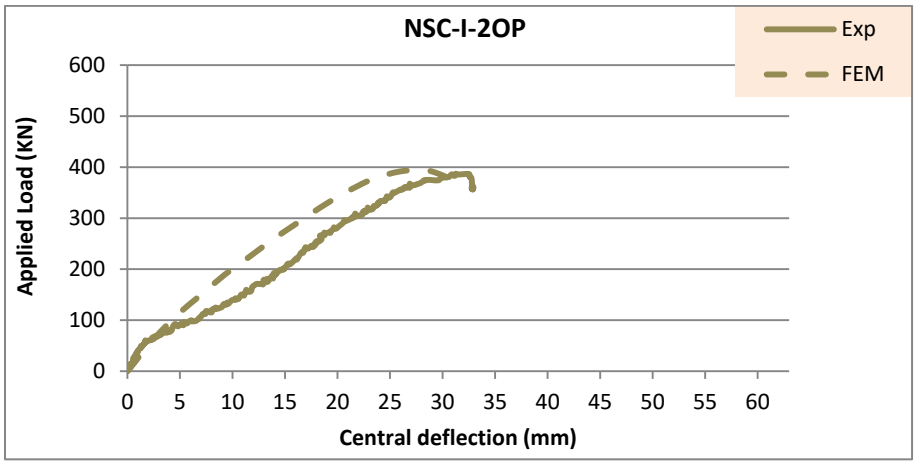

Figure (5-28): Load-deflection curves of beam NSC-I-2OP.

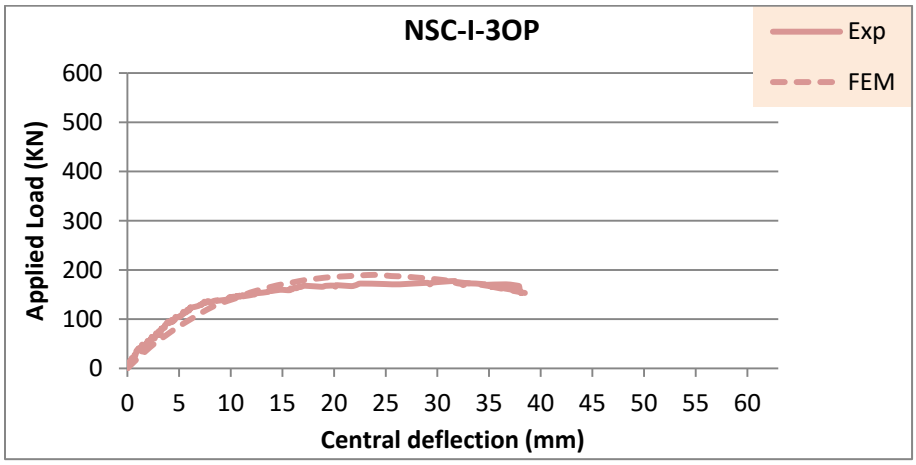

Figure (5-29): Load-deflection curves of beam NSC-I-3OP.

Generally, many factors made FE models had stiffness higher than experimental behavior and could be summarized as:

1- The finite element model was based on an assumed displacement field that means stiffer behavior than the actual one.

2- The finite element analysis deals with the concrete as a homogenous material, but really that it is a heterogeneous material.

3- The stiffness of the actual concrete beams was reduced by the generated micro cracks in the concrete due to the handling and drying shrinkage, but these effects are not taken in FEA.

4- The plastic behavior cracks of each element are only tested at gauss points, which give an overestimate of ultimate load and stiffer response.

5.4.3 Deflected Shape

The NSC-S, NSC-1OP, NSC-2OP, and NSC-3OP beam models were taken as an example to verify the application of the proposed numerical solutions by using ABAQUS computer software. The deflected shapes for these beam models due to applied loads at failure are shown in Figure (5-30).

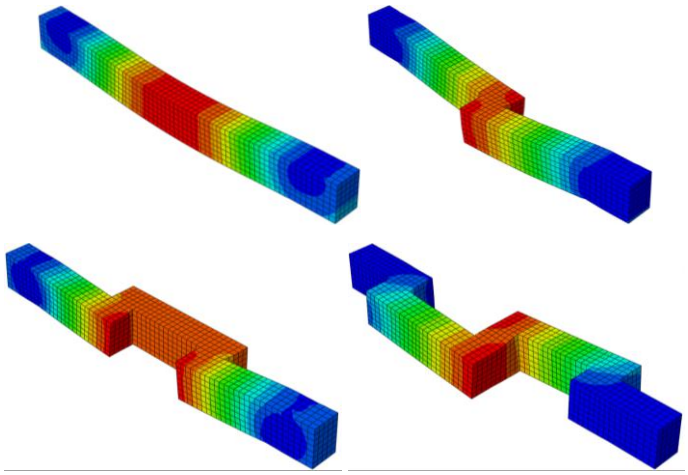

Figure (5-30):- Deflected shape for NSC-S, NSC-1OP, NSC-2OP, and NSC-3OP beam models.

The displacements in three dimensions of all the nodes in the model mesh were got in the results outputs of the analysis, but the displacement of the nodes at mid span and under load points was recorded for each load step up to the ultimate load. The ultimate load of the NSC-3OP beam was used as a references load value which was (192.62 kN) from the FEA and (176.14 kN) from the experimental results. The deflection profiles were plotted at these loads that being obtained from numerical analysis together with the plots of experimental results are compared and given in Table (5-2) and Figures (5-31) to (5-34) for all the tested beams for each case study.

Table (5-2):- Comparison between experimental and numerical deflections for tested beam models.

Beam models symbol	Central deflection (mm)		Difference ratio %
	Experimental	FEM	
NSC-S	4.00	3.93	1.75
NSC-1OP	12.10	11.79	2.56
NSC-2OP	14.35	10.23	28.71
NSC-3OP	31.09	26.88	13.54
HSC-S	2.85	3.98	-39.65
HSC-1OP	10.87	8.11	25.39
HSC-2OP	8.72	7.44	14.68
HSC-3OP	17.09	11.01	35.58
HSC-1OPT	5.00	5.55	-11.00
HSC-2OPT	9.10	7.00	23.08
HSC-3OPT	8.93	8.24	7.73
NSC-I-1OP	16.45	10.50	36.17
NSC-I-2OP	12.99	9.46	27.17
NSC-I-3OP	30.78	25.52	17.09
Average			13.06

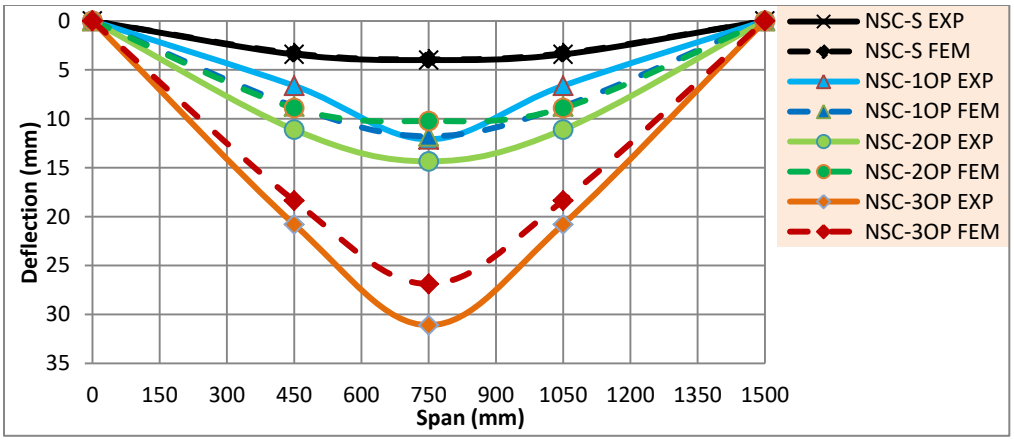

Figure (5-31):- Deflection profile for shape for NSC-S, NSC-1OP, NSC-2OP, and NSC-3OP beam models.

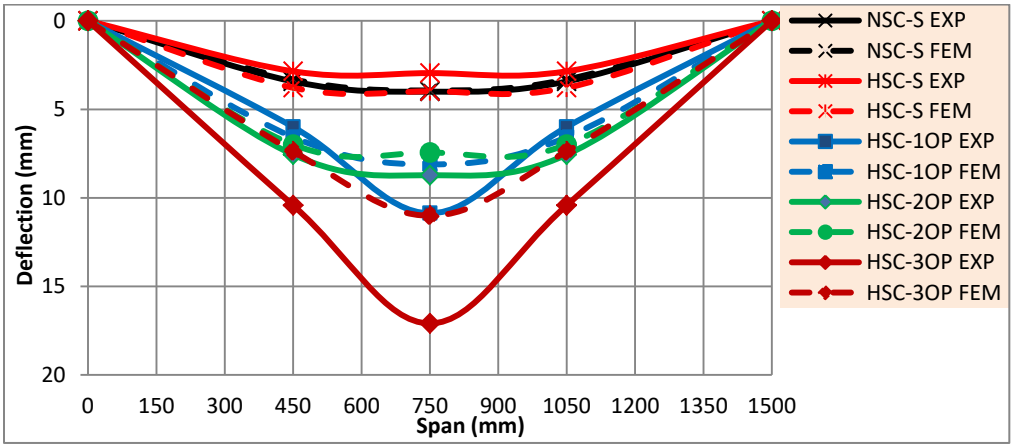

Figure (5-32):- Deflection profile for shape for NSC-S, HSC-S, HSC-1OP, HSC-2OP, and HSC-3OP beam models.

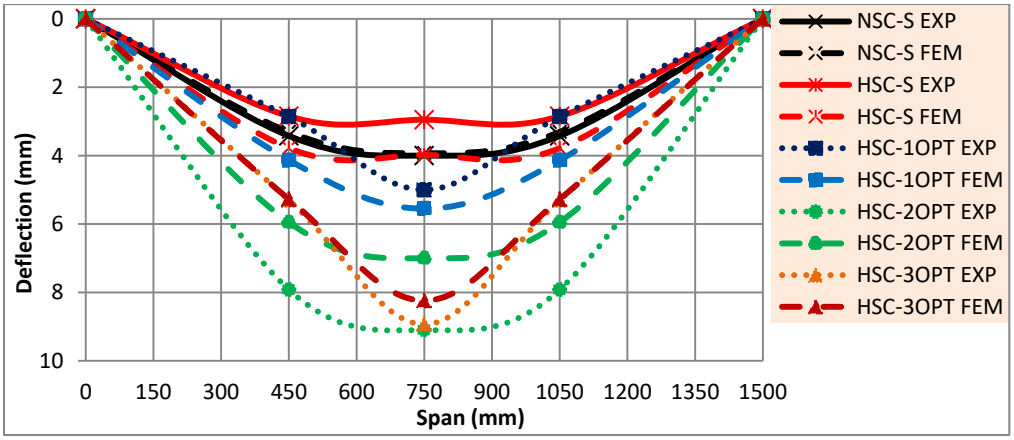

Figure (5-33):- Deflection profile for shape for NSC-S, HSC-S, HSC-1OPT, HSC-2OPT, and HSC-3OPT beam models.

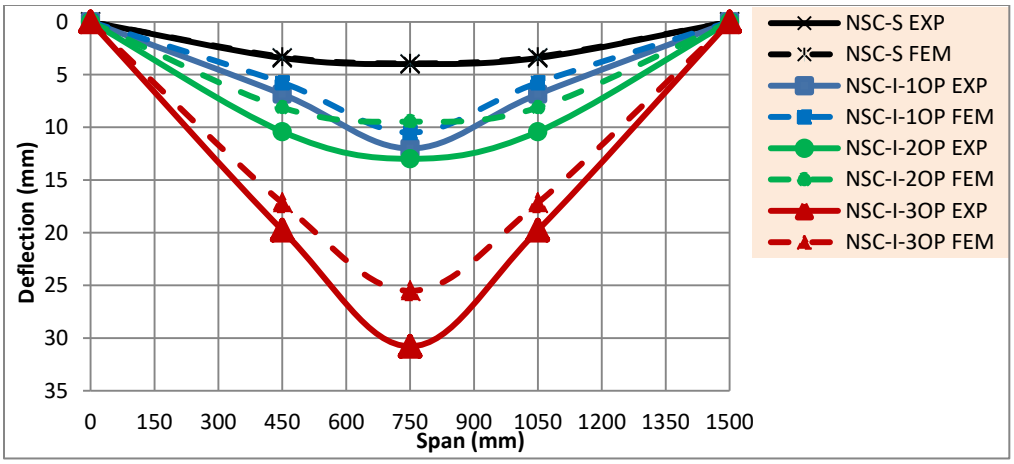

Figure (5-34):- Deflection profile for shape for NSC-S, NSC-I-1OP, NSC-I-2OP, and NSC-I-3OP beam models.

From the Table (5-2) and deflection profile figures, based on the mid span deflection it observed that the average absolute differences between the experimental and FEA deflections was 13.06%, so it can be said that the FEA could foresee the experimental behavior of the beams fairly well.

Furthermore, it was noted that the most of the FEM mid span deflections were lower than the experimental results, this behavior gave indicates that the FE models had stiffness higher than experimental models as mentioned in the load-deflection behavior.

5.4.4 First Cracking Loads

The comparison between numerical and experimental results of the first cracking load for the tested beam models is shown in Table (5-3); the first cracks have appeared in the tension face.

Table (5-3):- Comparison between experimental and numerical first crack loads for tested beam models.

Beam models symbol	First crack load P_{cr} (kN)		Difference ratio %
	Experimental	FEM	
NSC-S	38.00	52.89	39.19
NSC-1OP	26.00	33.53	28.97
NSC-2OP	26.00	35.00	34.62
NSC-3OP	14.00	19.89	42.07
HSC-S	65.00	72.95	12.23
HSC-1OP	43.00	50.68	17.86
HSC-2OP	44.00	52.43	19.16
HSC-3OP	40.00	34.76	-13.10
HSC-1OPT	48.00	54.43	13.40
HSC-2OPT	45.00	45.95	2.11
HSC-3OPT	65.00	68.69	5.68
NSC-I-1OP	26.00	28.69	10.33
NSC-I-2OP	41.00	51.89	26.56
NSC-I-3OP	20.00	24.36	21.80
Average			18.63

The first cracking load obtained from numerical analysis results for all the cases was mostly higher than the experimental results and recorded with an average difference of 18.63% for the tested beam models. This is probably owing to the homogenous FE models in comparison with the heterogeneous experimental beam models that had many micro cracks.

5.4.5 Cracking Pattern

At each increment of loading step, the ABAQUS program reported the cracks' pattern and their propagation. The plastic damage of the beam models in the FEA is classified into two types, first one is the tension stress damage cracks that represented by DAMAGET, and the second one is compression stress damage cracks that represented by DAMAGEC. The

original beam color is blue and the color of the cracks is red as shown on the analyzed beam models.

As an example, Figures (5-35) to (5-38) show the cracks pattern in the tension face and compression face at ultimate load for HSC beam models.

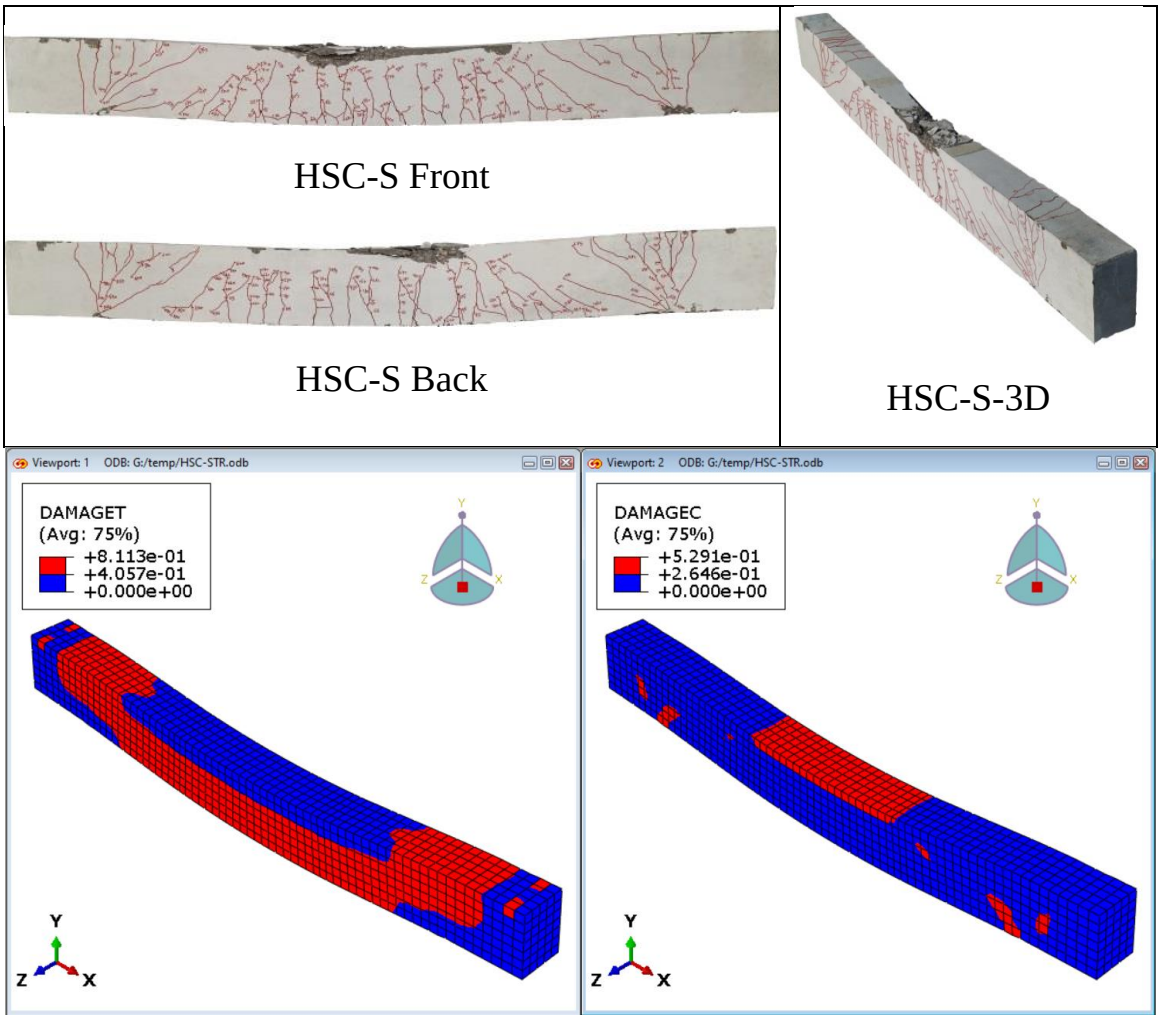

Figure (5-35): Cracks pattern of HSC-S model at the ultimate load.

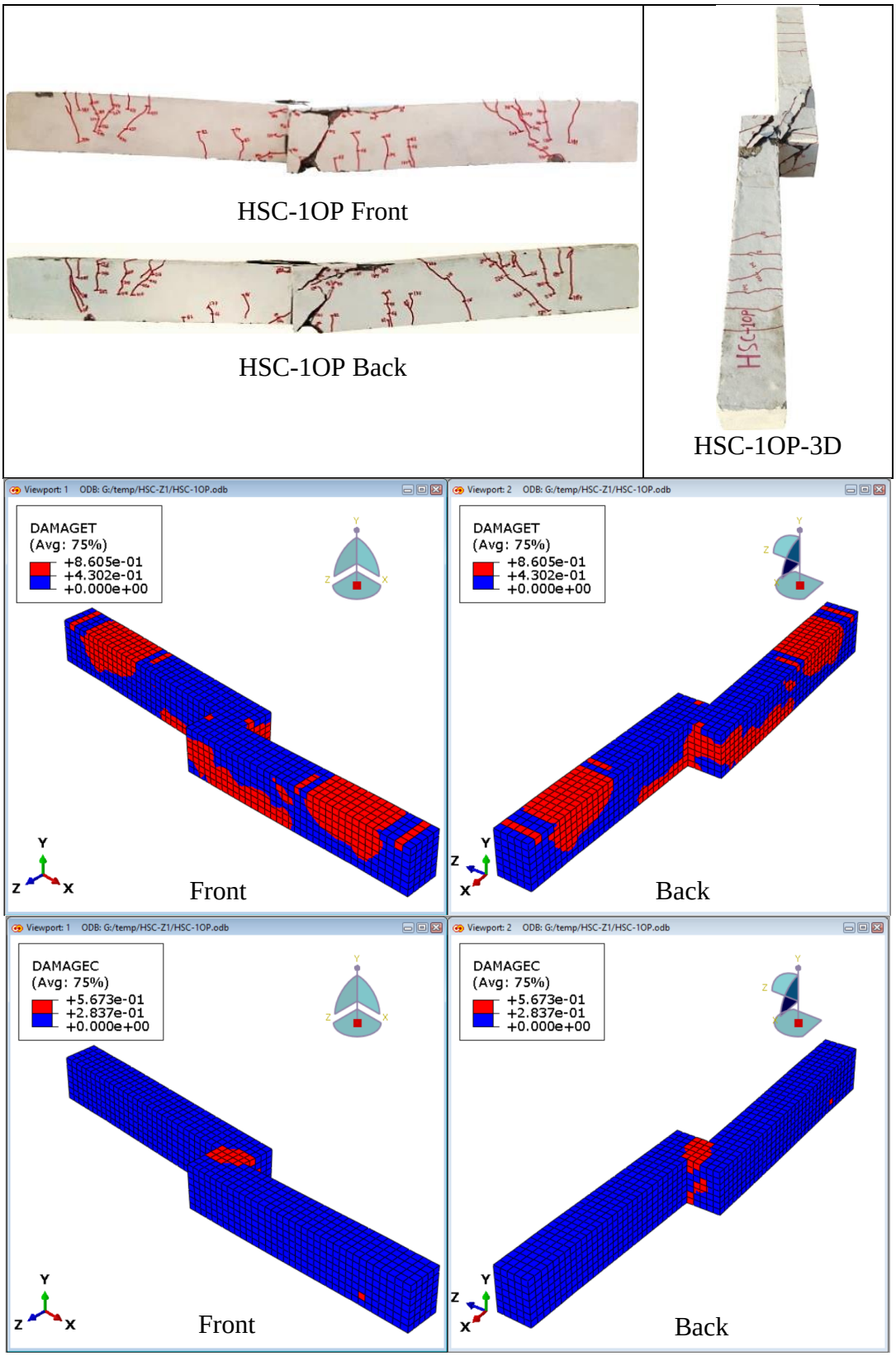

Figure (5-36): Cracks pattern of HSC-1OP model at the ultimate load.

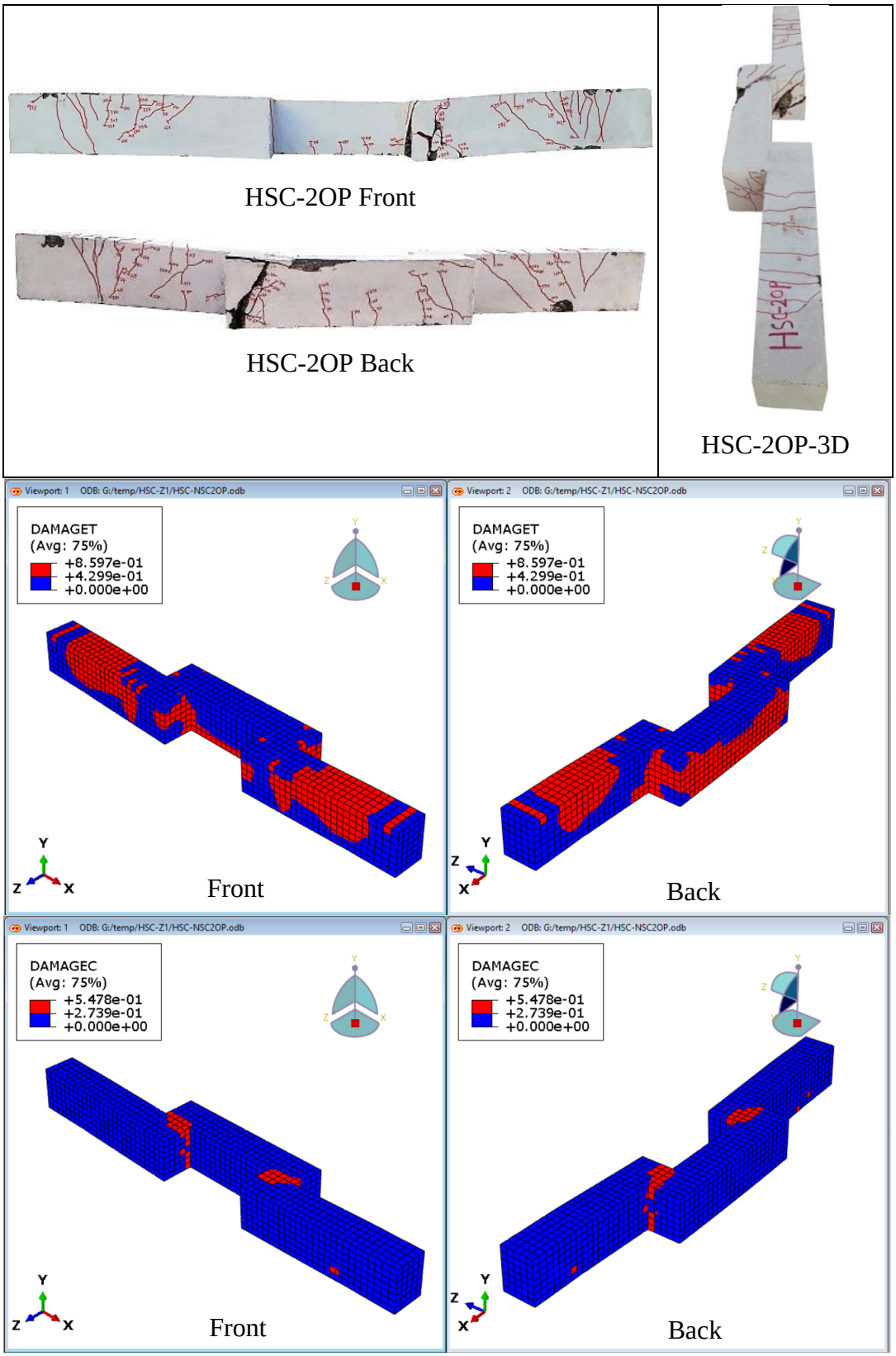

Figure (5-37): Cracks pattern of HSC-2OP model at the ultimate load.

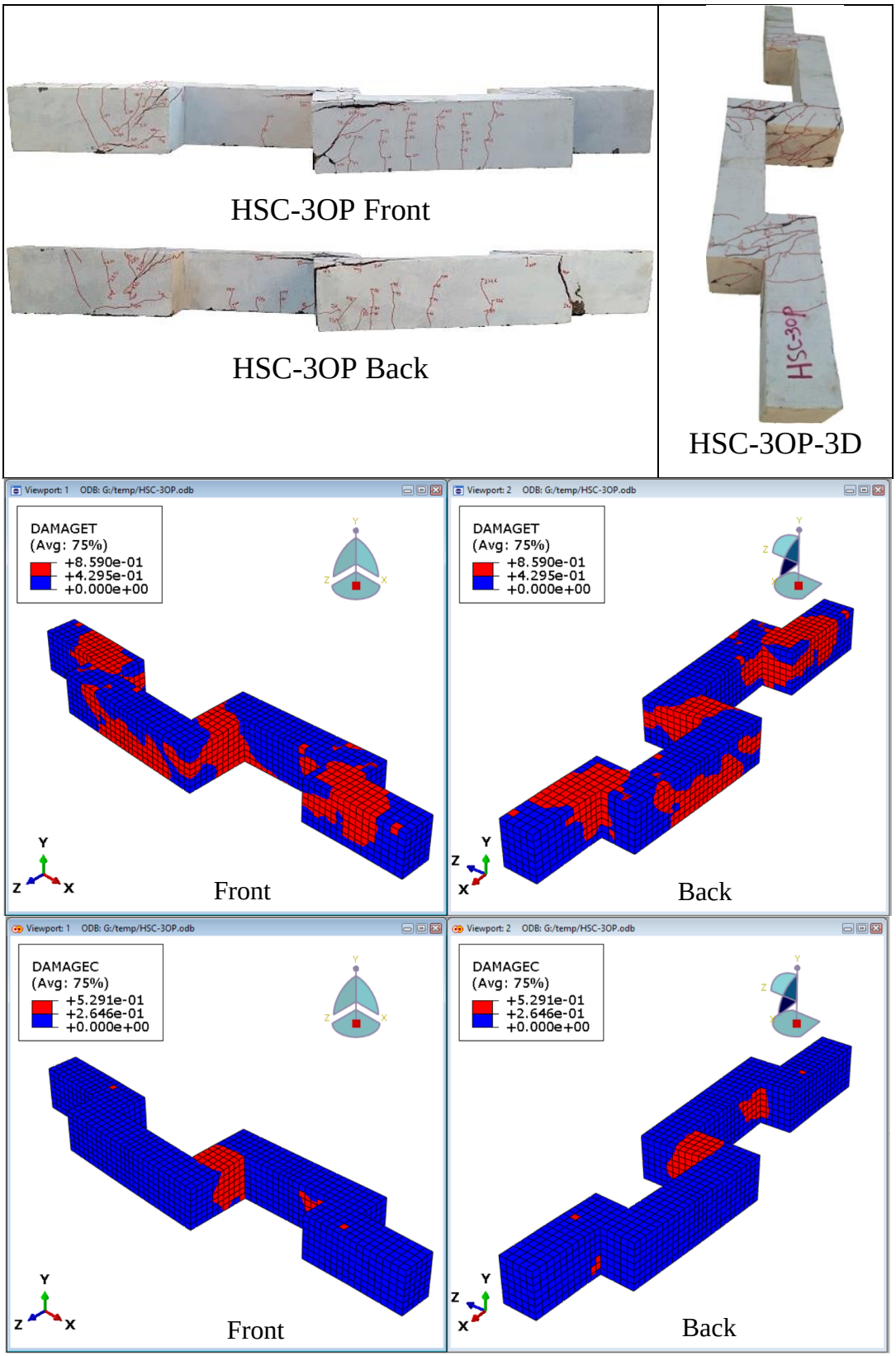

Figure (5-38): Cracks pattern of HSC-3OP model at the ultimate load.

By comparing the crack patterns and failure modes of FEA results with the experimental results it could be noticed that was acceptable agreement between them. Furthermore, from the monitoring numerical analysis at each loading step, it was observed that the places where cracks appeared were the same as those that appeared in experimental work and their propagation was the same behavior approximately.

5.5 Parametric Study

A parametric study was carried on the beam NSC-4OP as compared NSC-2OP, and NSC-5OP as compared with NSC-3OP to study the influence of increasing the number of the out of plane parts in conjunction with the direction of mid span part to the beam axis on the overall behavior of the beams. The geometry and mesh of the beam models are shown in Figure (5-39).

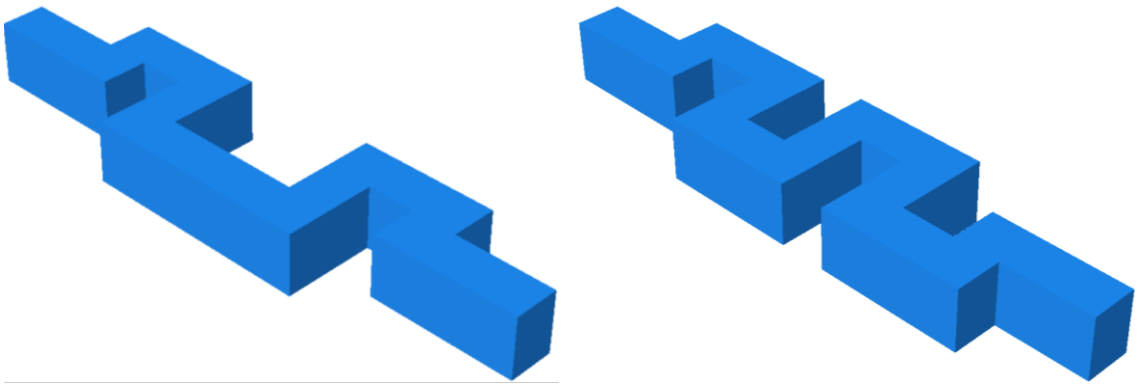

NSC-4OP NSC-5OP

(a) Concrete beams geometry

Figure (5-39): Geometry and mesh of the NSC-4OP and NSC-5OP beam models.

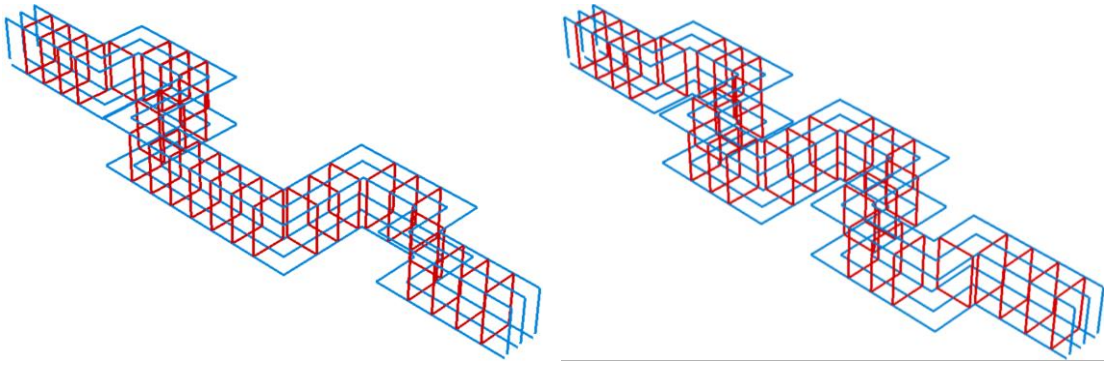

(b) Reinforcement geometry

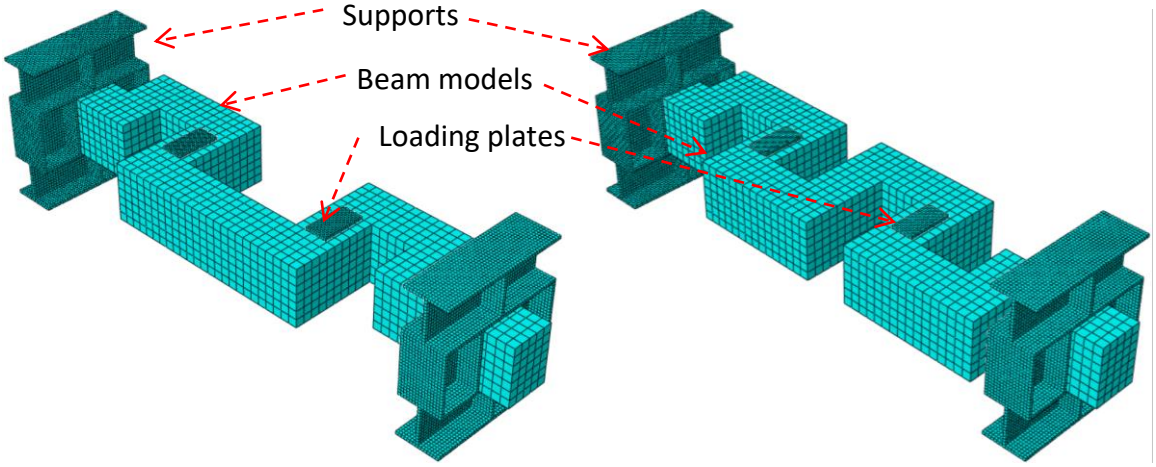

(c) Models element mesh

Figure (5-39): (Continued).

Figure (5-40) showed the load-deflection behavior and Figure (5-41) showed the cracks patterns at the ultimate load.

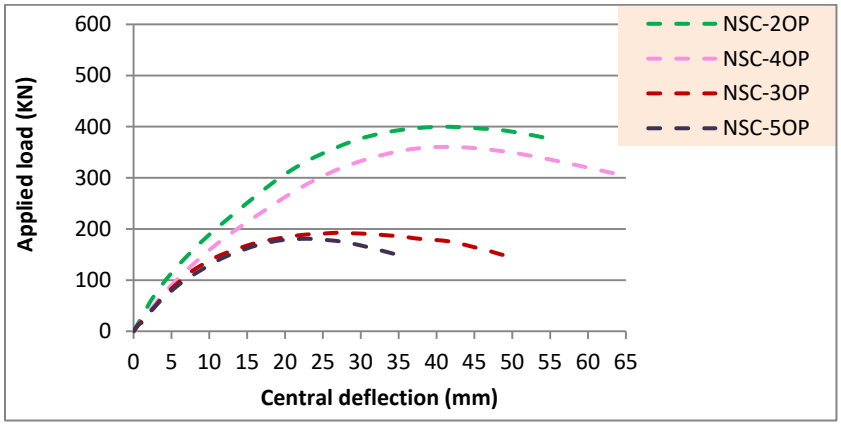

Figure (5-40):- FEA Load -mid span deflection response of beam models.

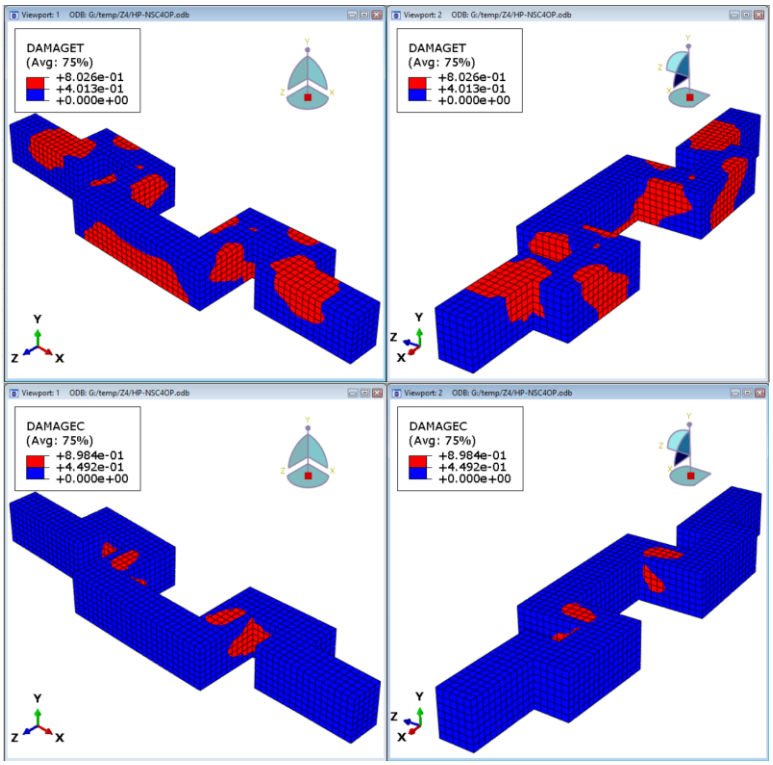

(a) Crack patterns of NSC-4OP

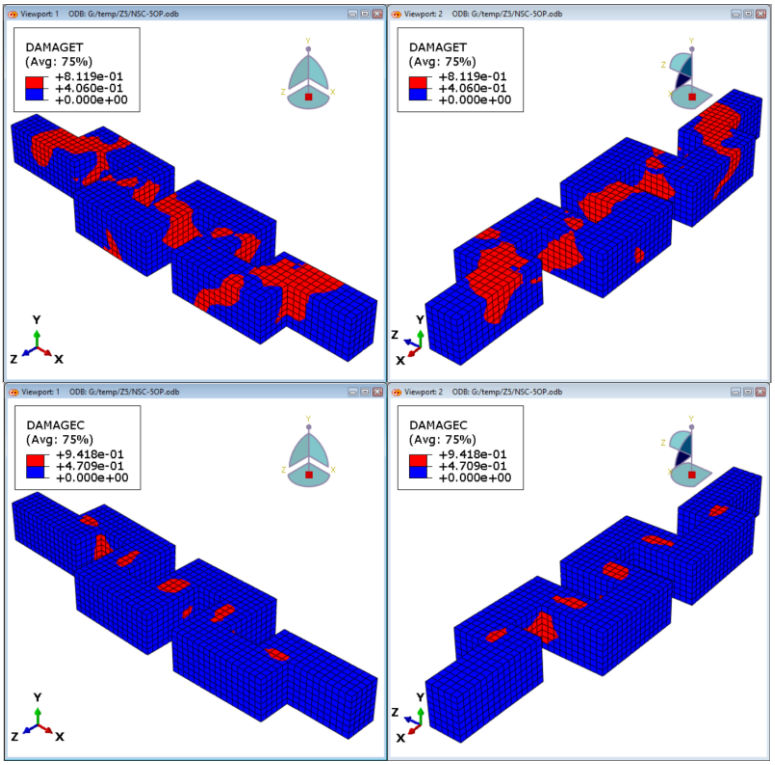

(b) Crack patterns of NSC-5OP

Figure (5-41): FEA Cracks pattern of NSC-4OP and NSC-5OP beam models at the ultimate load.

From Figure (5-40), it could be seen that the ultimate load and deflection of NSC-4OP was somewhat lower than NSC-2OP by 9.91% and 4.32% respectively, and ultimate load and deflection of NSC-5OP was rather lower than NSC-3OP by 6.13% and 14.50% respectively. However, the ultimate load and deflection of NSC-4OP was clearly higher than NSC-3OP by 43.91% and 19.64% respectively. These results proved that the increasing number of the out of plane parts for the beams that classified according to the odd and even number of the out of plane parts led to decreasing load bearing capacity and deflection for each class. However, beams with even number of the out of plane parts were much better than those with odd number of the out of plane parts.

From Figure (5-41), the cracks propagation was also affected by the increasing number of the out of plane parts, increasing number of the out of plane parts led to decreasing flexural tensile stress damage and increasing torsional compressive stress damage.

Another parameter was evaluated for convergence is one of the concrete material properties that is called dilation angle. Concrete is a brittle material and it is experience a great change in volume when it is in the inelastic strains. This criterion known as dilatancy is captured in CDPM by the dilation angle, ψ. The dilation angle in ABAQUS ranges between 0 to 56.30. In this study, four values of the ψ were inspected (30, 31, 35 and 42) for NSC and (20, 21, 25 and 30) for HSC. It was observed that the ψ of 35 for NSC and 25 were for HSC gave acceptance results as compared with the experimental results.

Chapter Seven: Conclusions and Recommendations

7.1 Conclusions

This research introduces the behavior of reinforced concrete beams with out of plane part that made with high and normal strength concrete with several of longitudinal and transverce reinforcement ratios and subjected to the monotonic load. From the results of the experimental work and numerical analysis the following conclusions are drown:

7.1.1 Experimental Work

1. The presence of the out of plane part reduced the ultimate load of all beams with different number of the out of plane parts by above 30% -70% and increasing deflection about 14%-56% as compared with the corresponding straight beam.
2. Beams with even number of the out of plane parts showed better load capacity than beams with odd number of the out of plane parts (e.g. beam with two out of plane parts is better than beam with one and three out of plane parts).
3. The existence of the out of plane parts affected on the caracks patterns and led to a change of their failure modes from flexure to combined flexure plus torsion.
4. Using HSC instead of NSC in producing the beams led to an increase in the load bearing capacity by more than 30% for the straight beam and more than 3% for the beams with out of plane parts.
5. Adding torsion reinforcement in conjunction with using HSC leads to an increase in the load bearing capacity by the range about 16% to 20% as

compared with the HSC beams with out of plane parts without using torsion reinforcement.

6. Using torsion reinforcement led to a decrease mid span deflection of HSC beams with one, two, and three out of plane parts by about 3%.
7. Increasing length of the out of plane parts had a limited effect on the ultimate load with different not more than 2%, while the deflections were decreased by the range about 5% to 32%.
8. Increasing length of the out of plane parts led to a decrease of mid span rotation by 78%, 82%, and 61% of the NSC beams with one, two, and three out of plane parts respectively.
9. The mid span rotations of HSC beams with out of plane parts were decreased by the range about 2% to 45%, as compared with NSC beams.
10. The beams with an even number of the out of plane parts had mid span rotation higher than the beams with odd number of the out of plane parts.
11. Using HSC reduced the mid span deflection of HSC beams with one and two out of plane parts by above 16% and 22% respectively, while the deflection of the beam with three out of plane parts was increased by above 4% as compared with NSC beams.
12. The mid span rotations of the HSC beams with out of plane parts with using torsion reinforcement were increased by the range about 6% to 53% as compared with the HSC beams without using torsion reinforcement.
13. The increasing number of the out of plane parts from one to three led to improve the displacement ductility index by about 1.27 to 1.93 and energy ductility index from 1.23 to 3.43 of the NSC beams, and also these indexes increased from 1.2 to 1.34 and from 1.04 to 1.48 of the HSC beams.

14. Using HSC led to a decrease in the displacement ductility index by the range about 3% to 31% and energy ductility index by the range about 15% to 57%, but the displacement ductility index of the straight beam increased by 18.83%, and energy ductility index by 31%.
15. Adding torsion reinforcement led to increased displacement ductility index by the range about 0.75%, to 26%, and energy ductility index by the range about 18% to 70% as compared with the HSC beams with out of plane parts without using torsion reinforcement.
16. When increasing the length of the out of plane parts, the displacement ductility index of the beams with one and two out of plane parts was decreased by 6% and 16%, and energy ductility index by 2%, and 36%, while the displacement ductility index of the beam with three out of plane parts was increased by 60% and energy ductility index by 85%.
17. The beams with the out of plane parts is not sufficient to be reinforced by the same reinforcement of the straight beam because each part has different values of shear force, bending moment, and torsion however it can be designed in the same way by using strength reduction factors lower than that used in the straight beam.
18. When using modified strength reduction factors (lower than those for straight beam), the service load deflections of the beams with the out of plane parts may become within the codes limits.

7.1.2 Finite Element Analysis

1. The three-dimensional finite element model by ABAQUS/Standard was capable to simulate the structural behavior of the beams with out of plane parts and straight beam with an average variation ratio not exceeding 4 % for the ultimate load capacity and 19% for the central deflection.

2. The numerical results showed that increasing the number of the out of plane parts from two to four and from three to five led to a reduction in the ultimate load capacity of 10% and 6% and decreasing in the deflection by about 4% and 20% respectively.
3. In general, the numerical and experimental results showed that beams with an even number of the out of plane parts had load bearing capacity higher than the beams with the odd number of the out of plane parts (e.g. beam with two out of plane parts is better than beam with one and three out of plane parts and beam with four out of plane parts was better than beam with three and five out of plane parts).

7.2 Recommendations for Future Studies

1. Investigating the structural behavior of the beams with out of plane parts that strengthened and repaired using externally bonded carbon fiber reinforced polymer sheets.
2. Investigating the structural behavior of continuous beams with out of plane parts with different loading and supporting conditions.
3. Investigating the structural behavior of the beams with out of plane parts as a part of reinforced concrete frames.
4. Studying the effects of introducing openings of various locations and shapes on the mechanical behavior of the beams with out of plane parts.
5. Investigating the structural behavior of the beams with out of plane parts subjected to fire.
6. Studying the structural behavior of the beams with out of plane parts that supported reinforced concrete slabs.

7. Investigating the structural behavior of the beams with out of plane parts by using different types of materials like ultra high strength concrete (UHSC), self compact concrete (SCC), light weight concrete (LWC).
8. Studying the structural behavior of the beams with out of plane parts under the action of dynamic loads.

References

[1] Arafah, A. M. (2000). Factors affecting the reliability of reinforced concrete beams. WIT Transactions on Ecology and the Environment, 45.

[2] Khalel, R. I. (2013). Torsional Behavior of High-Strength Reinforced Concrete Beams. Journal of Engineering and Sustainable Development, 17(1), 317-32.

[3] Jagana, R., Vinodh Kumar, C. (2017). High Strength Concrete. International Journal of Engineering Sciences & Research Technology, 394-407.

[4] Rashid, M. A., & Mansur, M. A. (2005). Reinforced high-strength concrete beams in flexure. ACI Structural Journal, 102(3), 462.

[5] Studio, M. P. A. (2015). from https://arquitecturaviva.com/works/museo-infantil-iztapalapa-ciudad-de-mexico.

[6] Herr, C. M., & Fischer, T. (2013, July). Generative column and beam layout for reinforced concrete structures in China. In International Conference on Computer-Aided Architectural Design Futures (pp. 84-95). Springer, Berlin, Heidelberg.

[7] Anon., 2005-2020. 123RF. [Online] Available at: https://www.123rf.com/photo_75688304_modern-concrete-building-structure-under-construction.html.

[8] Griffiths, A., 2014. dezeen. [Online] Available at: https://www.dezeen.com/2014/12/04/spora-architects-metro-stations-budapest-concrete-lattice-beams/[Accessed 4 12 2014].

[9] Ahsmann, M. (2011). Wikimedia. [Online] Available at: https://commons.wikimedia.org/wiki/File:Concrete_balconies_at_The_National_Theatre,_London.jpg

[10] Russell, H. G., Anderson, A. R., Banning, J. O., Cantor, I. G., Carrasquillo, R. L., Cook, J. E., & Anderson, F. D. (1977). State-of-the-Art Report on High-Strength Concrete. Chicago Committee on High-Rise Buildings.

[11] Elbasha, N. M. (2013). High strength reinforced concrete beam and helix confinement. In First International Conference on Concrete Sustainability. Tokyo, Japan.

[12] Kovačević, I., & Džidić, S. (2018). High-strength concrete (HSC) material for high-rise buildings. In 12th Scientific Research Symposium with International Participation «Metallic and Nonmetallic Materials: production-properties-application (No. 12, pp. 214-223).

[13] ACI Committee 363. (2010). Report on High-Strength Concrete (ACI 363R-10). ACI

[14] Ashour, S. A. (2000). Effect of compressive strength and tensile reinforcement ratio on flexural behavior of high-strength concrete beams. Engineering structures, 22(5), 413-423.

[15] Pam, H. J., Kwan, A. K. H., & Islam, M. S. (2001). Flexural strength and ductility of reinforced normal-and high-strength concrete beams. Proceedings of the Institution of Civil Engineers-Structures and Buildings, 146(4), 381-389.

[16] Ho, J. C. M., Kwan, A. K., & Pam, H. J. (2003). Theoretical analysis of post-peak flexural behaviour of normal-and high-strength concrete beams. The Structural Design of Tall and Special Buildings, 12(2), 109-125.

[17] Rashid, M. A., & Mansur, M. A. (2005). Reinforced high-strength concrete beams in flexure. ACI Structural Journal, 102(3), 462.Arslan, G. and Cihanli, E., 2010. Curvature ductility prediction of reinforced high-strength concrete beam sections. Journal of Civil Engineering and Management, 16(4), pp.462-470.

[18] Arslan, G., & Cihanli, E. (2010). Curvature ductility prediction of reinforced high-strength concrete beam sections. Journal of Civil Engineering and Management, 16(4), 462-470.

[19] Muhaisin, M. H. (2012). Long-Term Deflections for Normal and High Strength Reinforced Concrete Beams. Journal of University of Babylon, 20(1).

[20] Al-Kamal, M. K. (2019). Nominal flexural strength of high-strength concrete beams. Advances in concrete construction, 7(1), 001. Cladera, A., & Mari, A. R. (2005). Experimental study on high-strength concrete beams failing in shear. Engineering Structures, 27(10), 1519-1527.

[21] Cladera, A., & Mari, A. R. (2005). Experimental study on high-strength concrete beams failing in shear. Engineering Structures, 27(10), 1519-1527.

[22] Abd-Alla, S.M., Ibrahim, W.W., Hashem, M.M. and Eisa, A. (2007). Shear strength of normal, medium and high strength reinforced concrete beams. 46. 151-177. [Online] Available at:

https://www.researchgate.net/publication/293444093_Shear_strength_of_normal_medium_and_high_strength_reinforced_concrete_beams [Accessed 01 03 2007].

[23] Yi, W. J., & Lv, Y. M. (2009). Experimental Study on Shear Failure of High-Strength Concrete Beams with High-Strength Stirrups. In Key Engineering Materials (Vol. 400, pp. 857-863). Trans Tech Publications Ltd.

[24] Ahmad, S. H., Xie, Y., & Yu, T. (1995). Shear ductility of reinforced lightweight concrete beams of normal strength and high strength concrete. Cement and Concrete Composites, 17(2), 147-159.

[25] Hamrat, M., Boulekbache, B., Chemrouk, M., & Amziane, S. (2012). Effects of the transverse reinforcement on the shear behaviour of high strength concrete beams. Advances in Structural Engineering, 15(8), 1291-1306.

[26] Ismail, K.S. (2016). Shear behaviour of reinforced concrete deep beams (Doctoral dissertation, University of Sheffield).

[27] Tahenni, T., & Lecompte, T. (2019). Experimental and Theoretical Investigation on the Shear Behaviour of High Strength Reinforced Concrete Beams Using Digital Image Correlation. In Digital Imaging. IntechOpen.

[28] Hossain, T., Mendis, P.A., Aravinthan, T., and Baker, G. (2006). Torsional resistance of high-strength concrete beams. Progress in Mechanics of Structures and Materials, pp.673-680.

[29] Chiu, H. J., Fang, I. K., Young, W. T., & Shiau, J. K. (2007). Behavior of reinforced concrete beams with minimum torsional reinforcement. Engineering Structures, 29(9), 2193-2205.

[30] Rahal, K. N. (2013). Torsional strength of normal and high strength reinforced concrete beams. Engineering structures, 56, 2206-2216.

[31] Hafez, A. H., & Hassan, A. (2015). Investigation of Torsional Behaviour of High-Strength Reinforced Concrete Sections. World Applied Sciences Journal, 33(1), pp. 01-13.

[32] Prakash, M. R., Sadanand, P., Manjunath, H. R., Jagadeesh Kumar, B. G. and Prabhakarar. (2016). Cracking and Torsional Ductility Behavior of HSC Beams. International Journal of General, 5(1), pp. 25-34.

[33] Waryosh, W. A., Mohaisen, S. K., & Dkhel, R. H. (2018, November). Deformation responses of reinforced concrete beams under pure torsion. In IOP Conference Series: Materials Science and Engineering (Vol. 433, No. 1, p. 012037). IOP Publishing..

[34] Prabaghar. A., Kumaran. G. (2019). Experiment on Torsional Behaviour of Reinforced Concrete Beams. International Journal of Innovative Technology and Exploring Engineering, 8(6S4), pp. 1-5.

[35] Owainati, S. A. R. (1973). Behaviour of reinforced concrete beams under torsion, bending and shear.

[36] Ali, M. and Anis, A. (1983). Strength and behaviour of reinforced concrete spandrel beams.

[37] Rahal, K. N., & Collins, M. P. (2003). Experimental evaluation of ACI and AASHTO-LRFD design provisions for combined shear and torsion. Structural Journal, 100(3), 277-282.

[38] Kamiński, M., & Pawlak, W. (2011). Load capacity and stiffness of angular cross section reinforced concrete beams under torsion. Archives of civil and Mechanical Engineering, 11(4), 885-903.

[39] ACI Committee 363. (2013). Report on Torsion in Structural Concrete (ACI 445.1R-112). ACI

[40] Qian, K., & Li, B. (2013). Performance of three-dimensional reinforced concrete beam-column substructures under loss of a corner column scenario. Journal of Structural Engineering, 139(4), 584-594.

[41] Elsayed. A. A., Noaman. M., Abdallah. M. A. M., Abdelrahim. M. A. A. (2015). Behavior of R.C. Beams with Inclined Cantilever. IOSR Journal of Mechanical and Civil Engineering, 12(4 Ver. II), pp. 74-96.

[42] Karim, F.R., Abu Bakar, B.H., Kok Keong, C. and Aziz, O.Q. (2016). Influence of Double Idealized Shear Flow Zones on Torsional Resistance of High Strength Fibrous Concrete Beams. International Journal of Civil & Environmental Engineering IJCEE-IJENS, 16(4), pp.9-15.

[43] Nagendra, P. N., and Naresh, K. Y. (2017). Torsional behaviour of reinforced concrete 'L' beam. International journal of advanced research in basic engineering science and technology, ISSN: 2456 – 5717, Vol.3, Special issue 35: pp159-164.

[44] Buda-Ożóg, L. (2017). Assessment of stiffness beams subjected to combined shear and torsion designed using STM. Procedia engineering, 193, 152-159.

[45] Iraqi Specification Standards IQS No. 5, (1984) "Portland Cement", Central Agency for Standardization and Quality Control, Planning Council, Baghdad, IRAQ, (in Arabic).

[46] Iraqi Specification Standards IQS No.45, (1984) "Aggregate from Natural Sources for Concrete and Construction", Central Agency for Standardization and Quality Control, Planning Council, Baghdad, IRAQ, (in Arabic).

[47] ASTM C 1240-05, 2005 "Standard Specification for Silica Fume Used in Cementitious Mixtures", pp. 1-7.

[48] ASTM C 494/C 494M-05, 2005 "Standard Specification for Chemical Admixtures for Concrete", Annual Book of ASTM Standards, American Society for Testing and Materials, Vol. 04. 02.

[49] ASTM 496-02, 2002 "Standard Specification for Steel Wire, Deformed, for Concrete Reinforcement", ASTM Committee A-1 on Steel, Stainless Steel, and related Alloys, West Conshohocken, PA 19428-2959, United States, 5 pp.

[50] ACI Committee 211.1-91, 1991"Standard Practice for Selecting Proportions for Normal Heavyweight, and Mass Concrete (ACI 211.1-91) Reapproved 1997", Manual of Concrete Practices, American Concrete Institute, pp. 1-38.

[51] ACI Committee ACI 363.2R-11, 2011 “Guide to Quality Control and Assurance of High-Strength Concrete", American Concrete Institute of the ACI Materials.

[52] ASTM C 192/C 192M-05, 2005 "Standard Practice for Making and Curing Concrete Test Specimens in the Laboratory", Annual Book of ASTM Standards, American Society for Testing and Materials, pp. 1-8.

[53] ACI 363R-10, 2010 " Report on High-Strength Concrete", American Concrete Institute.

[54] ASTM C192/C192M − 15, 2015 "Standard Practice for Making and Curing Concrete Test Specimens in the Laboratory", Annual Book of ASTM Standards, American Society for Testing and Materials, pp. 1-8.

[55] ASTM C 143/C 143M-05a, 2005 "Standard Test Method for Slump of Hydraulic-Cement Concrete", Book of ASTM Standards, American Society for Testing and Materials, pp. 1-4.

[56] ASTM C138 / C138M - 17a, "Standard Test Method for Density (Unit Weight), Yield, and Air Content (Gravimetric) of Concrete," American Society for Testing and Materials, 2017.

[57] ASTM C642 - 13, " Standard Test Method for Density, Absorption, and Voids in Hardened Concrete" American Society for Testing and Materials, 2013.

[58] ASTM C 39/C 39M-05, 2005 "Standard Test Method for Compressive Strength of Cylindrical Concrete Specimens", Annual Book of ASTM Standards, Vol. 04.02 Concrete and Aggregates, West Conshohocken, PA, United States, 7 pp.

[59] BS 1881-Part 116:1983, 2000 "Method for Determination of Compressive Strength of Concrete Cubes", British Standards Institute BSI, London, 11 pp.

[60] ASTM C469 / C469M - 14, 2014 " Standard Test Method for Static Modulus of Elasticity and Poisson's Ratio of Concrete in Compression,", Annual Book of ASTM Standards, American Society for Testing and Materials.

[61] ASTM C496 / C496M - 17, 2017 "Standard Test Method for Splitting Tensile Strength of Cylindrical Concrete Specimens", Annual Book of ASTM Standards, Vol. 04.02 Concrete and Aggregates, West Conshohocken, PA, United States, 5 pp.

[62] ASTM C78 / C78M − 18, 2018 "Standard Test Method for Flexural Strength of Concrete (Using Simple Beam with Third-Point Loading)", Annual Book of ASTM Standards, American Society for Testing and Materials.

[63] AISC. (2017). Steel Construction Manual 15th Edition (15th ed.): AISC.

[64] ACI-ASCE Committee 445 ACI 445R-99, 1999 "Recent Approaches to Shear Design of Structural Concrete", American Concrete Institute of the ACI Materials.

[65] ACI Committee. (2019). Building code requirements for structural concrete (ACI 318-19) and commentary. American Concrete Institute.

[66] Punmia, B. C. (1992). Reinforced Concrete Structures Vol. I (Vol. 1). Firewall Media.

[67] Khamees, S. S., Kadhum, M. M., & Alwash, N. A. (2021). Effect of hollow ratio and cross-section shape on the behavior of hollow SIFCON columns. Journal of King Saud University-Engineering Sciences, 33(3), 166-175.

[68] Kim, S. B., Yi, N. H., Kim, H. Y., Kim, J. H. J., & Song, Y. C. (2010). Material and structural performance evaluation of recycled PET fiber reinforced concrete. Cement and concrete composites, 32(3), 232-240.

[69] Maghsoudi, A. A., & Bengar, H. A. (2011). Acceptable lower bound of the ductility index and serviceability state of RC continuous beams strengthened with CFRP sheets. Scientia Iranica, 18(1), 36-44.

[70] Park, R. (1988, August). Ductility evaluation from laboratory and analytical testing. In Proceedings of the 9th world conference on earthquake engineering, Tokyo-Kyoto, Japan (Vol. 8, pp. 605-616).

[71] Park, R. (1989). Evaluation of ductility of structures and structural assemblages from laboratory testing. Bulletin of the new Zealand society for earthquake engineering, 22(3), 155-166.

[72] Jaafer, A. A. (2015). Experimental investigation on the ferrocement slabs with a sifcon matrix. Wasit Journal of Engineering Sciences, 3(1), 40-54.

[73] Goldston, M., Remennikov, A., & Sheikh, M. N. (2016). Experimental investigation of the behaviour of concrete beams reinforced with GFRP bars under static and impact loading. Engineering Structures, 113, 220-232.

[74] Jomaah, M. M., & Diyaree, J. G. (2019). Energy Absorption Capacity Of Layered Lightweight Reinforced Concrete Beams With Openings In Web. Civil Engineering Journal, 5(3), 690-701.

[75] Ohno, T., & Nishioka, T. (1984). An experimental study on energy absorption capacity of columns in reinforced concrete structures. Doboku Gakkai Ronbunshu, 1984(350), 23-33.

[76] Beer, F. P., Johnston, E. R., DeWolf, J. T., & Mazurek, D. F. (2011). Mecânica dos materiais. Porto Alegre: Amgh.

[77] Yu, R., Spiesz, P., & Brouwers, H. J. H. (2016). Energy absorption capacity of a sustainable Ultra-High Performance Fibre Reinforced Concrete (UHPFRC) in quasi-static mode and under high velocity projectile impact. Cement and Concrete Composites, 68, 109-122.

[78] Thomsen, H., Spacone, E., Limkatanyu, S., & Camata, G. (2004). Failure mode analyses of reinforced concrete beams strengthened in flexure with externally bonded fiber-reinforced polymers. Journal of composites for construction, 8(2), 123-131.

[79] Maghsoudi, A. A., & Bengar, H. A. (2009). Moment redistribution and ductility of RHSC continuous beams strengthened with CFRP. Turkish Journal of Engineering and Environmental Sciences, 33(1), 45-59.

[80] Abdulraheem, M. S. (2018). Experimental investigation of fire effects on ductility and stiffness of reinforced reactive powder concrete columns under axial compression. Journal of Building Engineering, 20, 750-761.

[81] Liu, G.R. and Quek, S.S., The Finite Element Method: A Practical Course. 2003. Burlington MA: Butterworth-Heinemann.

[82] Simulia, D. S. (2013). Abaqus Analysis User's Guide, v. 6.13. Johnston, RI.

[83] Dere, Y., & Koroglu, M. A. (2017). Nonlinear FE modeling of reinforced concrete. International Journal of Structural and Civil Engineering Research, 6(1), 71-74.

[84] Malm, R. (2006). Shear cracks in concrete structures subjected to in-plane stresses (Doctoral dissertation, KTH).

[85] Hibbit, K. Sorensen, Inc.(2010) ABAQUS/Standard User's Manual, Version 6.10. Pawtucket, RI, USA.

[86] Lubliner, J., Oliver, J., Oller, S., & Onate, E. (1989). A plastic-damage model for concrete. International Journal of solids and structures, 25(3), 299-326.

[87] Lee, J., & Fenves, G. L. (1998). Plastic-damage model for cyclic loading of concrete structures. Journal of engineering mechanics, 124(8), 892-900.

[88] Hognestad, E. (1951). Study of combined bending and axial load in reinforced concrete members. University of Illinois at Urbana Champaign, College of Engineering. Engineering Experiment Station.

[89] Comité Euro-International du Béton. (1993). CEB-FIP model code 1990: Design code. Thomas Telford Publishing.

[90] Code, E. (2004). 2, Design of concrete structures-Part 1-1: General rules and rules for buildings, BS EN 1992-1-1: 2004. British Standards (BSi).

[91] Michael P. Collins and D. Mitchell (1997). Prestressed Concrete Structures, Response Publications.

[92] Wang, T., & Hsu, T. T. (2001). Nonlinear finite element analysis of concrete structures using new constitutive models. Computers & structures, 79(32), 2781-2791.

[93] Hafezolghorani, M., Hejazi, F., Vaghei, R., Jaafar, M. S. B., & Karimzade, K. (2017). Simplified damage plasticity model for concrete. Structural Engineering International, 27(1), 68-78.

[94] British Standards Institution (2005) BS EN 1992-1-2. Eurocode 2: Design of concrete structures. Part 1-2: General rules — Structural fire design. BSI.

[95] Hassoun, M. N., & Al-Manaseer, A. (2020). Structural concrete: theory and design. John wiley & sons.

Appendix A: Material Properties

A-1 Cement Properties

Table (A-1) Chemical Analysis of the Cement

Compound Composition	Chemical Composition	Perc. by Weight	Iraqi Specification No. 5/1984
Lime Oxide	CaO	61.61	-
Silica Dioxide	SiO_2	20.08	-
Alumina Oxide	Al_2O_3	4.62	-
Iron Oxide	Fe_2O_3	3.60	-
Magnesia Oxide	MgO	2.12	≤ 5.0%
Free Lime	Free CaO	1.40	-
Sulfate Trioxide	SO_3	2.71	≤ 2.5% if C3A ≤ 5% ≤ 2.8% if C3A >5%
Loss on ignition	L.O.I	2.39	≤ 4.0%
Total		98.53	
Insoluble Residue	I.R	0.73	≤ 1.5%
Lime Saturation Factor	L.S.F	0.93	0.66-1.02
Tricalcium Aluminates	C_3A	6.16	-

Table (A-2) Physical Properties of the Cement

Physical Characteristics	Results		Limits of IQS No.5/1984
Fineness by Blaine ($m^{2/}$ kg)	368		≥230
Setting time (Vicat) (min)	Initial Time	105	≥ 45
	Final Time	150	≤ 600
Compressive strength of cement paste 50 mm cube mold (MPa)	3 days	21.30	≥ 15
	7 days	28.25	≥ 23

A-2 Fine Aggregates Properties

Table (A-3) Sieve Analysis of Fine Aggregates

Sieve size	Cumulative Retained (%)	Passing (%)	IOS No.45/1984 (Zone2)
10 mm	0	100	100
4.75 mm	0.94	99.06	90-100
2.36 mm	20.93	79.07	75-100
1.18 mm	36.73	63.27	55-90
600 µm	49.10	50.90	35-59
300 µm	76.67	23.33	8-30
150 µm	97.60	2.40	0-10
Pan	100	0.0	-
Fineness modulus = 3.81			

Table (A-4) Physical and Chemical Properties of the Fine Aggregates

Physical Characteristics	Value	IOS No.45/1984
Specific gravity	2.61	-
Absorption	0.75 %	-
Sulfate content	0.34 %	≤ 0.50 %

A-3 Coarse Aggregates Properties

Table (A-5) Sieve Analysis of Coarse Aggregates

Sieve size	Cumulative Retained (%)	% Passing	IQS No. 45/1984 Limits
20	0	100.0	100
14	0.0	100	90-100
10	40.05	59.95	50-85
5	97.68	2.32	0-10
2.36	99.71	0.29	-
Pan	100.0	0	-

Table (A-6) Physical Properties and Sulfate Content of Coarse Aggregates

Physical Properties	Values	IQS No. 45/1984 Limits
Specific gravity	2.64	-
Sulfate content	0.08%	≤ 0.1 %
Absorption	0.71%	≤ 35%
Clay	0.13%	≤ 0.2%

A-4 Silica Fume

The Manufacture Company Catalogue of Sika® Fume S 92 D

Construction Chemicals

MegaAdd MS(D)

Densified Microsilica

DESCRIPTION

MegaAdd MS(D) is a very fine pozzolanic, ready to use high performance mineral additive for use in concrete. It acts physically to optimize particle packing of the concrete or mortar mixture and chemically as a highly reactive pozzolan.
MegaAdd MS(D) in contact with water, goes into solution within an hour. The silica in solution forms an amorphous silica rich, calcium poor gel on the surface of the silica fume particles and agglomerates. After time the silica rich calcium poor coating dissolves and the agglomerates of silica fume react with free lime ($CaOH_2$) to form calcium silicate hydrates (CSH). This is the pozzolanic reaction in cementitious system.

STANDARDS

ASTM C1240

USES

MegaAdd MS(D) can be used in a variety of applications such as concrete, grouts, mortars, fibre cement products, refractory, oil/gas well cements, ceramics, elastomer, polymer applications and all cement related products.

ADVANTAGES

- High to ultra high strength
- High resistance to chlorides and sulfates
- Protection against corrosion
- Increased durability, longer service life for structures
- Enhanced rheology, control of mixture segregation and bleed
- Greater resistance to chemicals

TYPICAL PROPERTIES at 25°C

PROPERTY	TEST METHOD	VALUE
State	Amorphous	Sub-micron powder
Colour	-	Grey to medium grey powder
Specific Gravity	-	2.10 to 2.40
Bulk Density	-	500 to 700 kg/m^3
Chemical Requirements		
Silicon Dioxide (SiO_2)	-	Minimum 85%
Moisture Content (H_2O)	-	Maximum 3%
Loss on Ignition (LOI)	-	Maximum 6%
Physical Requirements		
Specifi Surface Area	-	Minimum 15 m^2/g
Pozzolanic Activity Index, 7 days	-	Maximum 105% of control
Over size particles retained on 45 micron sieve	-	Maximum 10%

COMPATIBILITY

MegaAdd MS(D) is suitable for use with all types of cement and cementitious materials.
With Admixtures :
MegaAdd MS(D) is compatible to use with all types of water reducing plasticisers / superplasticisers and poly carboxylate based superplasticiser.

DOSAGE

The normal dosage of **MegaAdd MS(D)** is 5 - 8% by weight of cement, but it can be used up to 10%. Site trials should be carried out to establish the optimum dosage for the mix to be used as the dosage varies depending on application.

MegaAdd MS(D)

BATCHING	Batch **MegaAdd MS(D)** into the concrete mixer and mix thoroughly with the other mixture ingredients, adopting a procedure that ensures full dispersion of the product.	
PACK SIZE	600 Kgs and 1200 Kgs Jumbo bags	
GENERAL INFORMATION	**Shelf Life**	12 months from date of manufacture when stored under warehouse conditions in original unopened packing. Extreme temperature / humidity may reduce shelf life.
	Cleaning	Clean all equipments and tools with water immediately after use.
HEALTH and SAFETY	**PPE's**	Gloves, goggles and suitable mask must be worn.
	Precautions	Contact with skin, eyes, etc. must be avoided.
	Hazard	Regarded as non-hazardous for transportation.
	Disposal	Do not reuse bags. To be disposed off as per local rules and regulations.
	Additional Information	Refer MSDS. (Available on request.)
TECHNICAL SERVICE	**CONMIX Technical Services** are available on request for onsite support to assist in the correct use of its products.	

MSASA
Construction Solutions for Africa

CAPE TOWN
Tel: +27 (0)87 231 0253
Unit 5 | M5 Freeway Park
Upper Camp Rd | Maitland | 7405
Cape Town | South Africa

JOHANNESBURG
Tel: +27 (0)82 785 8529
64 Maple Street | Pomona
Kempton Park | Johannesburg | 1619
South Africa

Email: info@msasa.co.za | www.msasa.co.za

Manufacturer:
CONMIX LTD.
P.O. Box 5936, Sharjah
United Arab Emirates
Tel: +971 6 5314155
Fax: +971 6 5314332
Email: conmix@conmix.com

Sales Office:
Tel: +971 6 5682422
Fax: +971 6 5681442
www.conmix.com

Table (A-7) Chemical Analysis of the Silica Fume

Compound Composition	Chemical Composition	Oxid content%
Lime Oxide	CaO	1.323
Silica Dioxide	SiO_2	91.46
Alumina Oxide	Al_2O_3	0.794
Iron Oxide	Fe_2O_3	5.288
Magnesia Oxide	MgO	0.427
Sulfate Trioxide	SO_3	0.531
Loss on ignition	L.O.I	Less than 1%
Potassium Oxide	K_2O	1.032
Sodium Oxide	Na_2O	0.226

Table (A-8) physical Analysis of the Silica Fume

Physical Properties	Values
Specific gravity	2.2
Bulk density (kg/m^3)	570
Loss on ignition	Less than 1%
Color	Gray powder

A-5 Chemical Admixtures (Sika ViscoCrete® 5930-L)

The Manufacture Company Catalogue of Sika ViscoCrete® 5930-L

Construction

Product Data Sheet
Edition 2, 2015
Version no. 12.2014

Sika ViscoCrete® -5930L

High Performance Superplasticiser Concrete Admixture

Product Description	Sika ViscoCrete® -5930L is a third generation super plasticizer for concrete and mortar. It meets the requirements for super plasticizer according to ASTM-C- 494 Types G and F and BS EN 934 part 2: 2001.
Uses	Sika ViscoCrete® -5930L is suitable for the production of concrete. Sika ViscoCrete® -5930L facilitates extreme water reduction, excellent flowability at the same time optimal cohesion and highest self compacting behaviour. Sika ViscoCrete® -5930L is used for the following types of concrete: ■ Precast concrete. ■ Ready Mix Concretes. ■ Concrete with highest water reduction (up to 30%). ■ High strength concrete. ■ Hot weather Concrete. ■ Self compacting concretes. High water reduction, excellent flowability, coupled with high early strengths, have a positive influence on the above mentioned applications.
Advantages	Sika ViscoCrete® -5930L acts by different mechanisms. Through surfaces adsorption and sterical separation effect on the cement particles, In parallel to the hydration process, the following properties are obtained: ■ Strong self compacting behaviour. Therefore suitable for the production of self compacting concrete. ■ Extremely high water reduction (resulting in high density and strengths). ■ Excellent flowability (resulting in highly reduced placing - and compacting efforts) ■ Increase high early strengths development. ■ Improved shrinkage- and creep behaviour. ■ Reduced rate of carbonation of the concrete. ■ Improved Water Impermeability. Sika ViscoCrete® -5930L does not contain chloride or other, steel corrosion promoting ingredients, It may therefore be used without any restrictions for reinforced and prestressed concrete construction.
Technical Data	
Basis	Aqueous solution of modified Polycarboxylate
Appearance	Turbid liquid
Density	1.1 kg/lt. (ASTM C494)
Packaging	5 Kg, 20 Kg pails 200 kg drums Bulk Tanks are available upon request.
Storage/ Shelf Life	In unopened, undamaged original container, protected from direct sunlight and frost at temperatures between + 5 °C and + 35°C. Shelf life at least 12 months from date of production.

Construction

Application

Dosage

Recommended dosage:

- For soft plastic concrete: 0.2 - 0.8 % litre by weight of cement
- For flowing and self compacting concrete (S.C.C.) 0.8 - 2 % litre by weight of cement

Addition

Sika ViscoCrete® -5930L is added to the gauging water or simultaneously with it poured into the concrete mixer. For optimum utilisation of the high water reduction we recommend through mixing at a minimal wet mixing time of 60 seconds.

The addition of the remaining gauging water - to fine tune concrete consistency - may only be started after 2/3 of wet mixing time, to avoid surplus water in the concrete.

Concrete Placing

With the use of Sika ViscoCrete® -5930L concrete of highest quality is being produced. The standard rules of good concreting practice (production as well as placing) must also be observed with Sika ViscoCrete® -5930L concrete.

Fresh concrete must be cured properly.

Frozen Sika ViscoCrete® -5930

Frozen Sika ViscoCrete® -5930L may be used after it has been slowly thawed at room temperature and intensively mixed.

Combinations

Sika ViscoCrete® -5930L may be combined with the following Sika products:

- Sika Pump®.
- Sika Rapid®.
- Sika Ferrogard®-901.
- Sikafume®.
- Sika Fro® -V5A
- Sika Retarder®

Pre-trials are recommended if combinations with the above products are being made. Please consult our technical service.

Important Flowing Concrete S.C.C

Sika ViscoCrete® -5930L is also used to produce flowing and self compacting concrete (S.C.C.) For these, special mix designs are required, contact our Technical Service division.

Safety Instructions

Ecology

Do not dispose of into water or soil, but according to local regulations.

Transport

Non-hazardous.

Safety Precautions

In contact with skin, wash off with soap & water. In contact with eyes or mucous membrane, rinse immediately with clean warm water and seek medical attention without delay.

Toxicity

Non-Toxic under relevant health and safety codes.

Legal notes

Sika Egypt for Construction Chemicals
El Abour City
1st industrial zone (A)
Section # 10 Block 13035,
Egypt

Tel :+202- 4481 0580
Fax :+202- 4481 0459
Mob :+2012- 2390 8822/55
www.sika.com.eg

A-6 Deformed Steel Bars

Table (A-9) Properties of Deformed Steel Bars

Bar Diameter(mm)	**Area (mm^2)**	**Yield Strength f_y (MPa)**	**Ultimate Strength f_u (MPa)**
12 (11.99)	112.8	512.9	597.40
10 (9.93)	77.44	422	582
8 (8.18)	52.55	420	546.4

Appendix B: Design of NSC-S Beam Model

By using ACI code 318-19 (2019):-

❖ **Design of Flexural Reinforcement**:-

b=150 mm, h=200 mm, concrete cover = 16 mm, longitudinal bar diameter=12 mm, and transverse bar diameter=8 mm

$d = 200 - 16 - 8 - \frac{12}{2} = 170\text{mm}$

by using 3 bars for top and bottom longitudinal reinforcement

$As = 3(113) = 339\ \text{mm}^2 \quad \rightarrow \quad \rho = \frac{As}{bd} = \frac{339}{150 \times 170} = 0.013$

$A_s' = 3(113) = 339\ \text{mm}^2 \quad \rightarrow \quad \rho' = \frac{As'}{bd} = \frac{339}{150 \times 170} = 0.013$

Check if the beam acts as doubly reinforced

$\rho_{0.005} = 0.85\beta 1 \frac{fc'}{fy} \frac{0.003}{0.003+.005}$

$\beta_1 = 0.85 - 0.05 \frac{fc' - 28}{7} = 0.80$

$\rho_{0.005} = 0.85 \times 0.80 \times \frac{35}{512.9} \frac{0.003}{0.003+.005} = 0.017$

$\because \rho_{0.005} > \rho$ **$\therefore$ (Single Reinforcement and Ductile)**

$\rho_{\text{min}} = \frac{\sqrt{fc'}}{4fy} = 0.003 \geq \frac{1.4}{fy} = 0.0027$

$\rho_{\text{min}} = 0.003$

$As_{\text{min}} = \rho_{\text{min}}.bd = 0.003 \times 150 \times 170 = 73.53\ \text{mm}^2$

$\rho_b = 0.85\beta_1 \frac{fc'}{fy} \frac{600}{600+fy} = 0.024 > \rho$ $\therefore$ (Under Reinforcement)

Use: 3Ø12mm

Design Load

$a = \frac{As.fy}{0.85fc'b} = \frac{339\ X\ 512.9}{0.85\ X\ 35\ X150} = 38.96$

$Mn = As.fy\ (d - \frac{a}{2}) = 339 \times 512.9\ (170 - \frac{38.96}{2}) \times 10^{-6} = 26.17$ KN.m

Maximum Design Load at Support

$W_{self} = 24 \times 0.15 \times 0.2 = 0.72$ KN/m

$Mn = M_d + M_L = (\frac{W_{self} \times L^2}{12}) + \frac{Pa(L-a)}{1.5}$

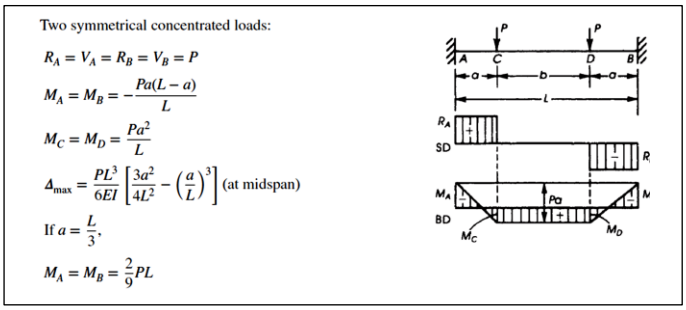

$26.17 = \frac{0.72 \times 1.5^2}{12} + \frac{2.25P}{1.5}$

P = 82.68 kN

So, the total load = 2P = 165.36 KN

Maximum Design Load at Mid-span

$Mn = Md + ML = (\frac{W_{self} \times L^2}{24}) + \frac{Pa^2}{1.5}$

$26.18 = \frac{0.72 \times 1.5^2}{24} + \frac{P.(0.45)^2}{1.5}$

P = 193.42 kN (Max Load)

So, the total load = 2P = 386.84 KN

❖ Shear Design

$Vc = \frac{\sqrt{fc'}}{6} b_w.d = \frac{\sqrt{35}}{6}$ x 150 x 170 x10^{-3} = 25.14 kN

$\emptyset Vc = 0.75 \times 25.14 = 18.86$ kN

$0.5\emptyset Vc = 0.5 \times 0.75 \times 25.14 = 9.43$ kN

$V_u = 82.68$ KN $> \emptyset Vc$ (Stirrups is required)

If use Ø8 mm (A stirrup = 52.55 mm^2)

Spacing Calculations

$Vu = \emptyset(Vc + Vs)$

$Vs = \frac{82.68}{0.75} - 25.14 = 85.10$ kN

$S = \frac{Av.fy.d}{Vs} = \frac{2\ X52.55X\ 420\ X\ 170}{85.10\ X10^3} = 88.18$ mm

Maximum spacing to provide ***Av***

$$S \leq \begin{cases} \frac{16Av.fy}{bw\sqrt{fc'}} = \frac{16\ X\ 2\ X\ 52.55X\ 420}{150\sqrt{35}} = 795.87\ mm \\ \frac{3Av.fy}{bw} = \frac{3\ X\ 2\ X\ 52.55X\ 420}{150} = 882.84\ mm \\ \frac{d}{2} = \frac{170}{2} = 85\ mm \\ 600\ mm \end{cases} \quad \therefore Smax = 85\ mm$$

$\therefore Use$ Ø8 mm @ 81 mm $center\ to\ center$

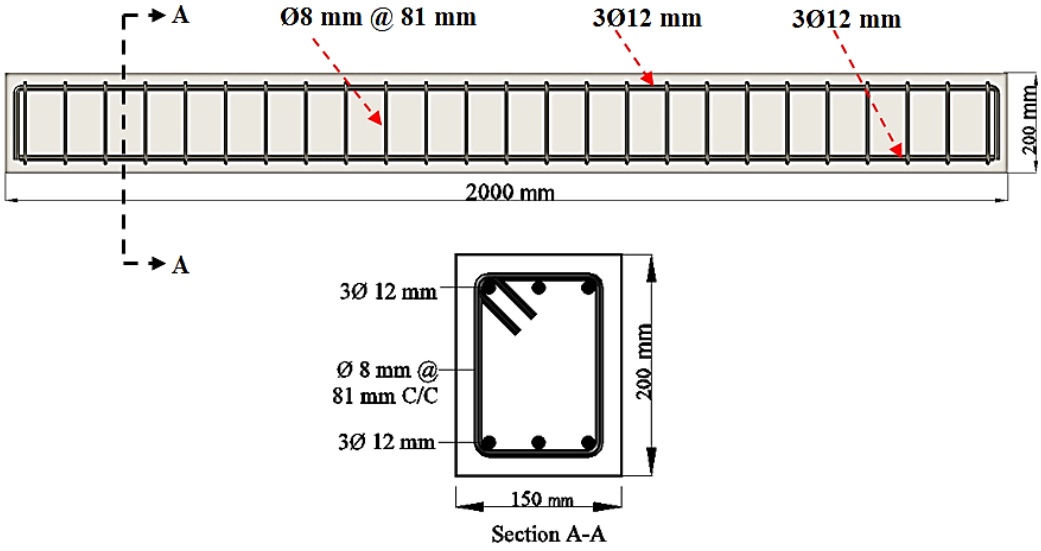

Appendix C: Shear force, Bending Moment, and Torsion Moment Diagrams of The Beam Models

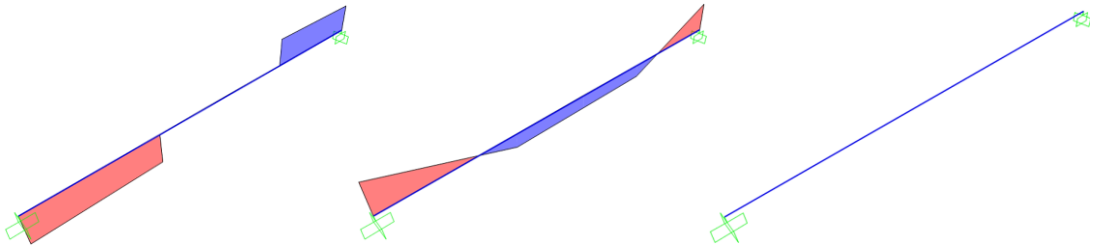

S.F.D B.M.D T.M.D

Diagrams of the straight beam

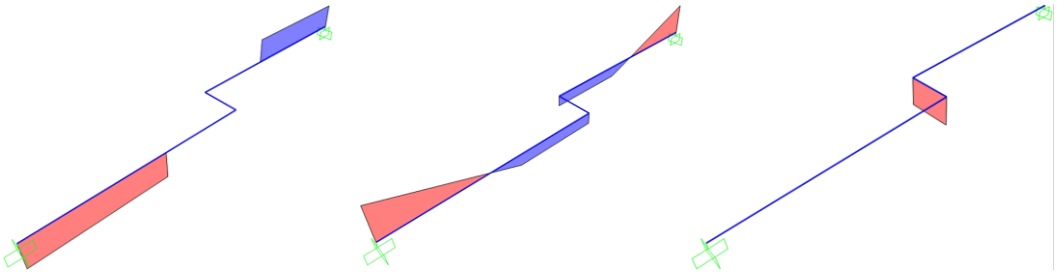

S.F.D B.M.D T.M.D

Diagrams of the beam with one out of plane part

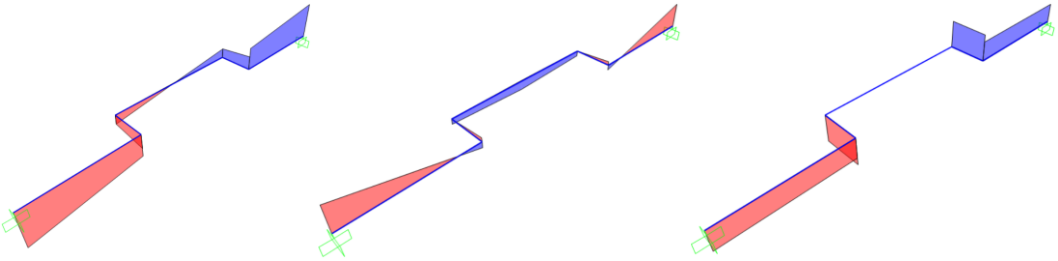

S.F.D B.M.D T.M.D

Diagrams of the beam with two out of plane parts

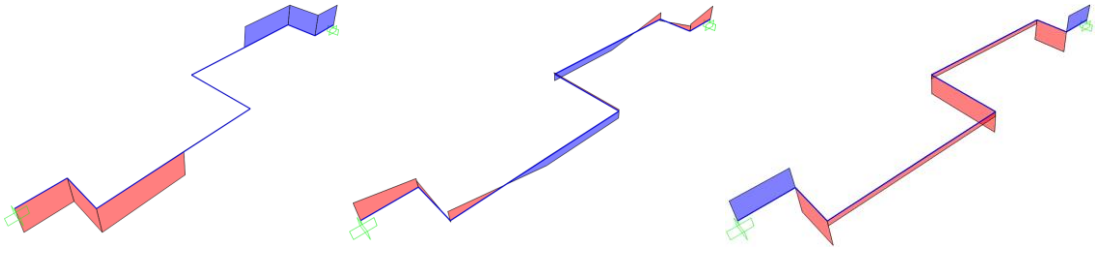

S.F.D B.M.D T.M.D

Diagrams of the beam with three out of plane parts.

Appendix D: Design Details of Steel Support

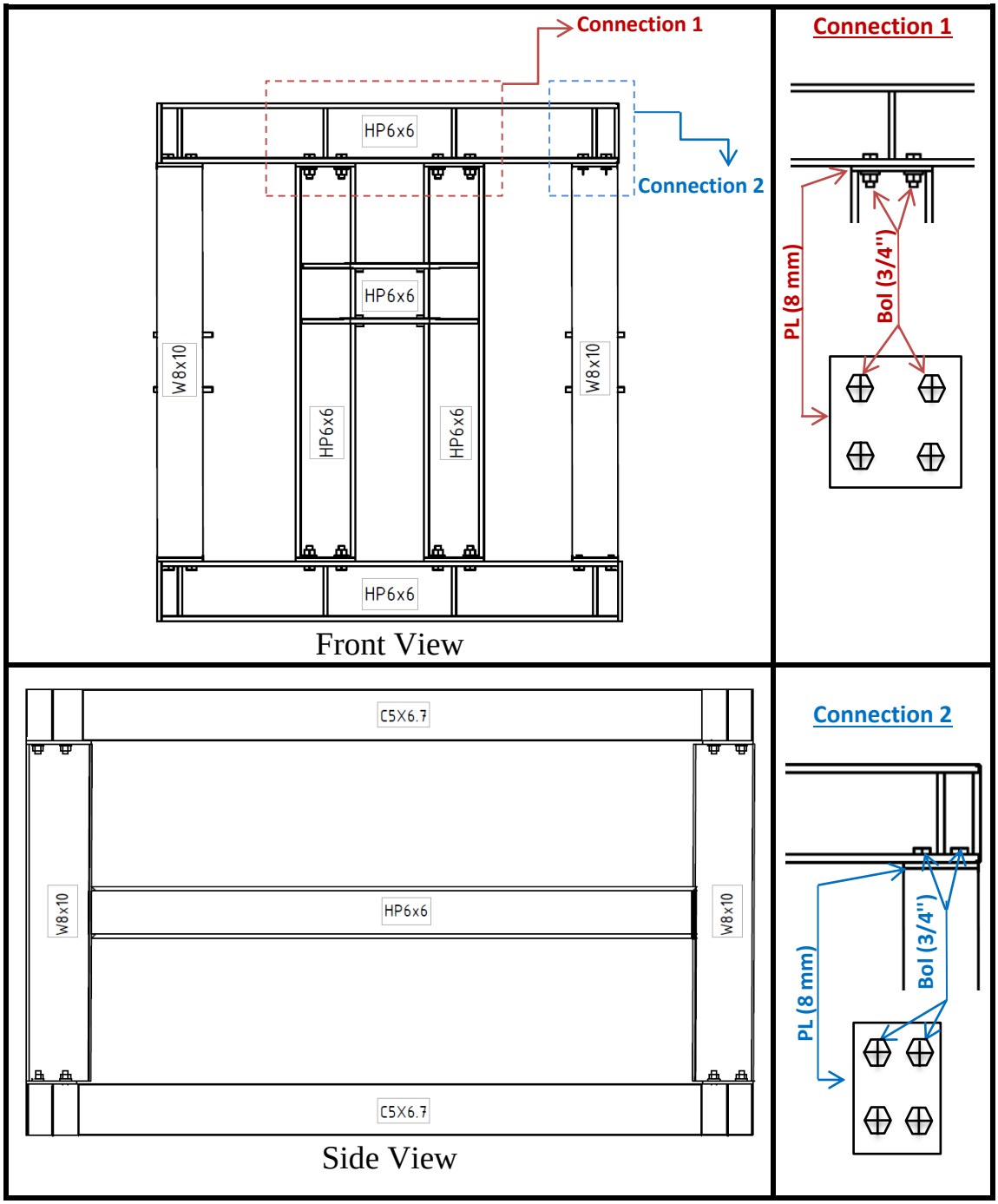

Appendix E: Finite Element Mdeling

E.1 Concrete

The concrete material can be defined in three different constituent models in ABAQUS; the smeared crack concrete standard model, the brittle cracking explicit model, and the concrete damaged plasticity model in both Abaqus/Standard and Abaqus/Explicit.

Smeared crack concrete model is preferred in the case of the concrete is basically subjected to monotonic straining and a material point exposed to tensile cracking or compressive crushing.

The brittle cracking model is prepared for the cases in which the concrete behavior in tensile cracking and compressive failure is not important. The model involves status of the anisotropy created by cracking and the model assumed elastic behavior in compression.

The concrete damaged plasticity model adopted for the cases in which the concrete exposed to arbitrary loading conditions, involving cyclic loading and considerations for stiffness recovery. This type of damage depended on the assumption of scalar (isotropic) damage. The model also deals with the decreasing of the elastic stiffness induced by plastic straining both in tension and compression (**ABAQUS Analysis User's Guide, 2013)[82].**

Concrete damaged plasticity model is chosen in the present study according to the ability to deal with the following issues:

1- Concrete material can be modeling for all types of structural members like beams, truss members, shells, and solid bodies.
2- It can define a combination of elastic isotropic damaged with plastic isotropic tensile and compressive to represent the inelastic behavior of concrete material.
3- The convergence of CDP model in the softening regime is higher than that of the smeared crack model.
4- It can define model have sensitivity to the rate of straining.
5- It can show the true post yielding (plastic behavior) like softening in tension while the initial hardening occur then followed by the softening in compression region.

E.1.1 Failure Criterion of Concrete

Concrete behavior can be evaluated by checking the load-deformation relation, tensile cracking and compressive stresses crushing. There are many factors affects on the behavior including the composition of concrete, the loading type, the loading fashion which can be uni-axial, bi-axial or multi-axial, confinement effect, loading rate, and temperature (**Dere, Y. and Koroglu, M.A., 2017**) [(83)].

In this study the loading fashion is assumed to be uniaxial loading in compression and tension because it can be easily obtained through laboratory experiments of cylinder standard sized specimens for the uniaxial compression strength test and tension strength which determined by splitting tests. The CDP properties can be defined by three parameters, plasticity, uniaxial compressive, and uniaxial tensile behavior.

E.1.2 Plastic Behavior

Plastic can be defined by four constitutive parameters. First one called the dilation angle (ψ) is measured in the p-q plane which represents the inclination of the plastic flow potential at high confining pressure as shown in Figure (5-5) and it is equal to the friction angle in low stresses. Its values range between $25^o \leq \psi \leq 40^o$ and it can be neglected in some cases, but for normal strength concrete $\psi = 30^o$ and for high strength concrete $\psi = 25^o$ **(Malm, 2006) [84].**

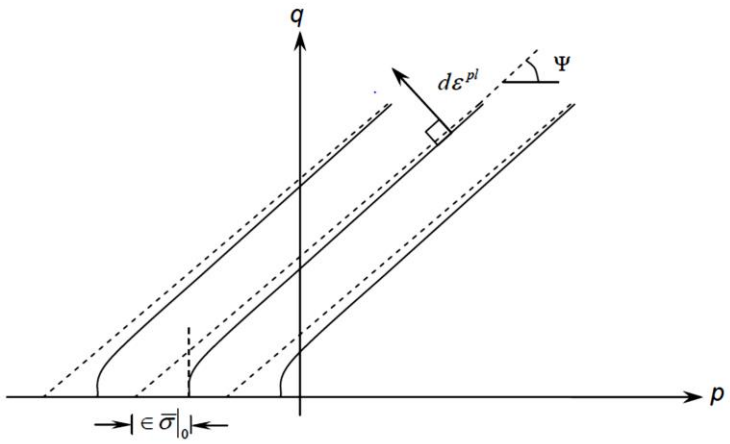

Figure (E-1): Flow potentials in p-q plane, (Hibbitt, 2010).

Second parameter is an eccentricity of the plastic potential surface (ϵ) which equal to 0.1 as default value. To account for the different evolution of strength under compression and tension, the CDP model uses the yield function of **Lubliner et al. (1989) [86]**, with the modifications suggested by **Lee** and **Fenves (1998) [87]**. The yield surfaces in the plane stress and deviatoric plane conditions are depicted in Figure (E-2 (a) and (b)), respectively. The yield function defined by **Lubliner et al. (1989) [86]** can be expressed in terms of the effective stress as follows:

$$F = \frac{1}{1-\alpha}\left[\bar{q} - 3\alpha\bar{p} + \beta\left(\tilde{\varepsilon}, \tilde{\varepsilon}_c^{pl}\right)\langle\hat{\bar{\sigma}}_{max}\rangle - \gamma\langle-\hat{\bar{\sigma}}_{max}\rangle\right] - \bar{\sigma_c}\left(\tilde{\varepsilon}_c^{pl}\right) \quad \text{(E.1)}$$

Where

$$\alpha = \frac{(\sigma b0/\sigma c0) - 1}{2(\sigma b0/\sigma c0) - 1};\ 0 \le \alpha \le 0.5$$

$$\beta = \frac{\bar{\sigma}c(\tilde{\varepsilon}_c^{pl})}{\bar{\sigma}t(\tilde{\varepsilon}_t^{pl})}(1-\alpha) - (1+\alpha);$$

$$\gamma = \frac{3(1-Kc)}{2Kc-1}$$

$\hat{\bar{\sigma}}_{max}$ is the maximum principal effective stress; $\sigma b0/\sigma c0$ is the ratio of initial equibiaxial compressive yield stress to initial uniaxial compressive yield stress. $\sigma b_0/\sigma c_0$ was set to the default value of 1.16 in the conducted simulations, which is the maximum of the range of experimentally found values reported by **Lubliner et al. (1989)** [(86)], the minimum being 1.10. $\bar{\sigma c}$ ($\tilde{\varepsilon}_c^{pl}$) and $\bar{\sigma}(\tilde{\varepsilon}_t^{pl})$ are compression and tension cohesion values, assumed to depend on the compressive and tensile equivalent plastic strains, $\tilde{\varepsilon}_c^{pl}$ and $\tilde{\varepsilon}_t^{pl}$, respectively.

Parameter Kc is the ratio of the second stress invariant on the tensile meridian, q(TM) , to that on the compressive meridian, q(CM), shown in Figure (E-2 (b)), at any value of the hydrostatic stress. In the simulations presented, Kc was set to the default value of 2/3, which is in same line with what is suggested by **Lubliner et al. (1989)** [(86)].

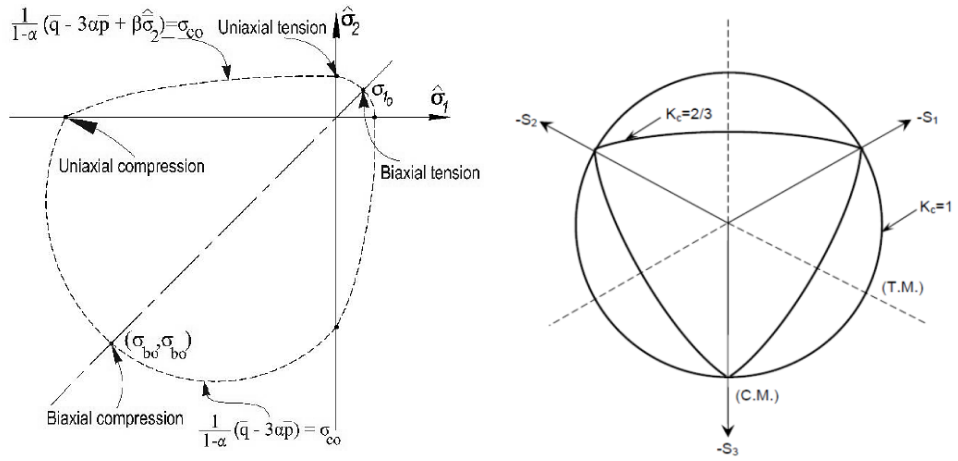

(a) **(b)**

Figure (E-2): Concrete yield surface in (a) plane stress and (b) deviatoric plane.

In this research the parameters ϵ, $\sigma b_0/\sigma c_0$, and Kc defined by the default values as 0.1, 1.16, and 2/3 respectively because tests that are going to be verified do not have such information.

E.1.3 Compressive Behavior of Concrete

The uniaxial compressive behavior of concrete is linear elastic behavior up to 40% of compressive strength then the behavior change to nonlinear behavior because tensile cracks began which lead to change the stiffness of material according to (**ASTM 496-17 and EC2**) [61, 94].

The stress-strain relation for a given concrete should be based on the uniaxial compression experimental tests data which can be modified to finite element analysis input data by using the relations for this purpose.

In this research for the normal and high strength concrete used, the uniaxial stress-strain behavior of concrete in compression was introduced in

the CDPM according to the procedure of **Wang and Hsu, 2001** [92] is shown in Figure (E-3) and expressed as below:

$$\sigma_c = \zeta f_c'[2(\frac{\varepsilon_c}{\varepsilon_{c0}})-(\frac{\varepsilon_c}{\varepsilon_{c0}})^2] \quad , \text{if } \frac{\varepsilon_c}{\zeta\varepsilon_{c0}} \leq 1 \text{.....(E.2)}$$

$$\sigma_c = \zeta f_c' [1-(\frac{\varepsilon_c/\zeta\varepsilon_{c0}-1}{\frac{4}{\zeta}-1})^2] \quad , \text{if } \frac{\varepsilon_c}{\zeta\varepsilon_{c0}} > 1 \text{.....(E.3)}$$

Where,

- σc is the compressive stress;
- f_c' is the mean value of concrete cylinder compressive strength;
- ε_{c0} is the concrete compressive strain at the maximum compressive stress ($\varepsilon_{c0}=2\, f_c'/E_c$)
- ε_c is the compressive strain in the concrete at the compressive stress σc ($\varepsilon_c = 0.4 f_c'/E_c + 2\ 2.25 \cdot 10^{-3}/7$)
- E_c is the modulus of elasticity of concrete

  For normal strength concrete

$$E_c = 4700\sqrt{fc'} \qquad \text{(E.4)}$$

  For high strength concrete

$$E_c = 3300\sqrt{fc'} + 6900 \qquad \text{(E.5)}$$

- ζ is the softened coefficient which can be taken as $0 \leq \zeta \leq 1$.

Figure (E-3) as explained the behavior of concrete under uniaxial compression.

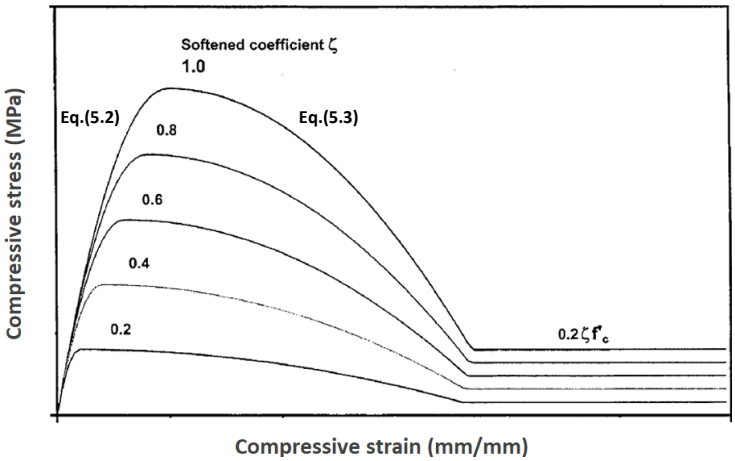

Figure (E-3): Schematic of the compressive stress-strain curve of concrete (Wang and Hsu, 2001).

According to ABAQUS analysis user's guide the model under uniaxial compression stress response linear until the value of initial yield σ_{co}, then the plastic response is typically characterized by stress hardening followed by strain softening beyond the ultimate stress σ_{cu} as shown in Figure (E-4).

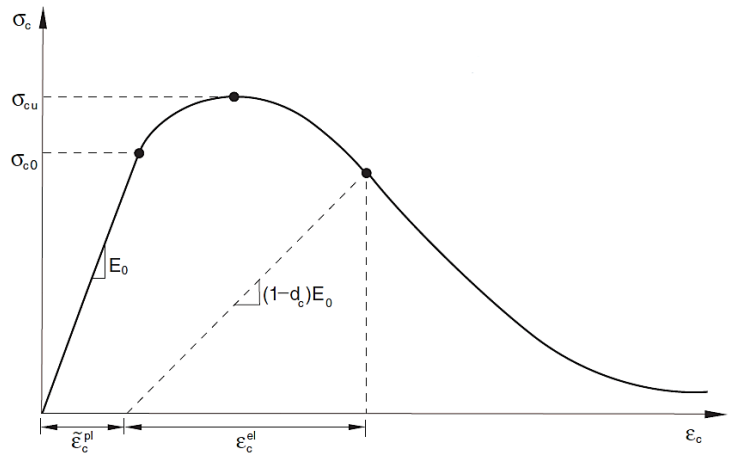

Figure (E-4): Response of concrete under uniaxial compression (ABAQUS Analysis User's Guide, 2013).

In ABAQUS required enter two input variables to define CDP in compression behavior are σc (start from yield value) and inelastic strain ($\tilde{\varepsilon}_c^{in}$). These inputs defined by equations below:

$$\tilde{\varepsilon}_c^{in} = \varepsilon_c - \varepsilon_c^{el} \qquad \text{(E.6)}$$

Where,

$$\varepsilon_c^{el} = \frac{\sigma_c}{E_c}$$

σ_c is the total stress at specific point or element that can be input as defined in equation E.2 and E.3; and E_c is the modulus of elasticity as defined in equations E.4 and E.5 .

The material required as input data for the program to define compressive damage parameter d_c in order to behave from undamaged when its value is zero to full-damaged material when its value is 1. Damage parameter can be defined in a tabular form by using equation E.7 and if it is not specified, the model behaves as a plasticity model (**Hafezolghorani, 2017**) [(92)].

$$d_c = 1 - \frac{\sigma_c}{f_c'} \qquad \text{(E.7)}$$

E.1.4 Uniaxial Tensile Behavior of Concrete

The uniaxial tension behavior of concrete could be experimentally estimated by indirect methods, such as sample splitting or beam bending test because the direct tension test is difficult in execution and the large scatter of the results. The stress-strain responses under uniaxial tension were characterized by plastic damage, as can be seen in Figure (E-5).

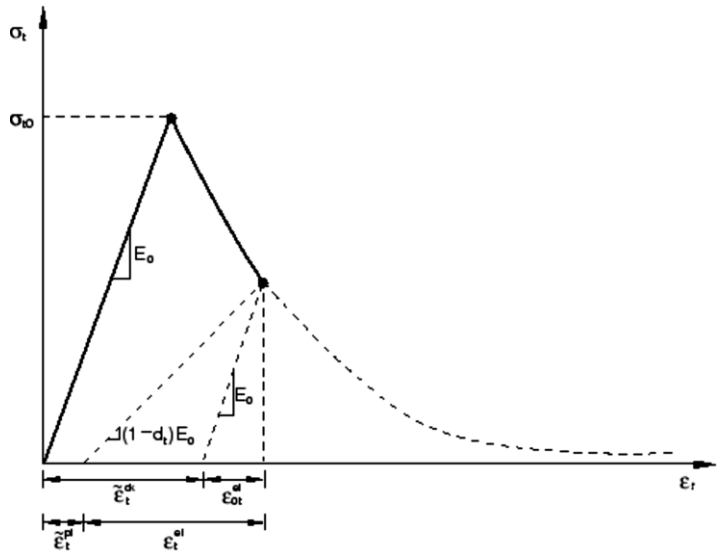

Figure (E-5): Response of concrete under uniaxial tension (ABAQUS Analysis User's Guide, 2013).

From the Figure (E-6) the effects of the tension stiffening could be defined in three ways:

- Stress-Strain diagram
- Stress-Displacement
- Fracture Energy, *Gf*

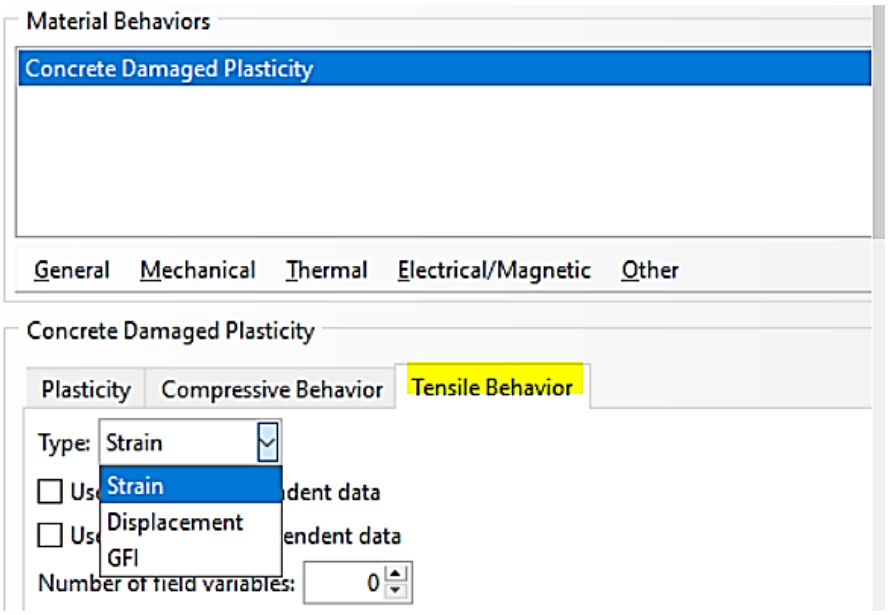

Figure (E-6): Tension damage definition.

The tensile Stress-Strain relation input data required to enter the cracking strain $\varepsilon_t{}^{ck}$ in tabular values as a function of, defined as:

$$\varepsilon_t{}^{ck} = \varepsilon_t - \varepsilon_{0t}{}^{el} = \varepsilon_t \frac{\sigma_t}{E} \qquad \text{(E.8)}$$

Where; $\varepsilon_t{}^{ck}$ is the cracking strain, ε_t is the total tensile strain, $\varepsilon_{0t}{}^{el}$ is the elastic tensile strain corresponding to the undamaged material, σ_t is the tensile stress, and E is the initial undamaged modulus of elasticity.

The tensile stress could be defined in tabular values by using proper relation was proposed by, among others, **Wang and Hsu**:

$$\sigma_t = E_c\, \varepsilon_t \quad , \varepsilon_t \leq \varepsilon_{cr} \qquad \text{(E.9)}$$

$$\sigma_t = f_{\text{cr}} \left(\frac{\varepsilon_{cr}}{\varepsilon_t} \right)^{\text{n}} \quad , \varepsilon_t > \varepsilon_{cr} \qquad \text{(E.10)}$$

Where; $f_{cr} = 0.31\sqrt{f_c{}'}$

$$\varepsilon_{cr} = \frac{f_{cr}}{E_c}$$

Wang and T.C Hsu proposed the rate of weakening n=0.4 and suggested defining a short plateau at the peak point of the curve with sharp change at cracking strain to avoid the problems during a finite element analysis as shown in Figure (E-7). This relation used in this research.

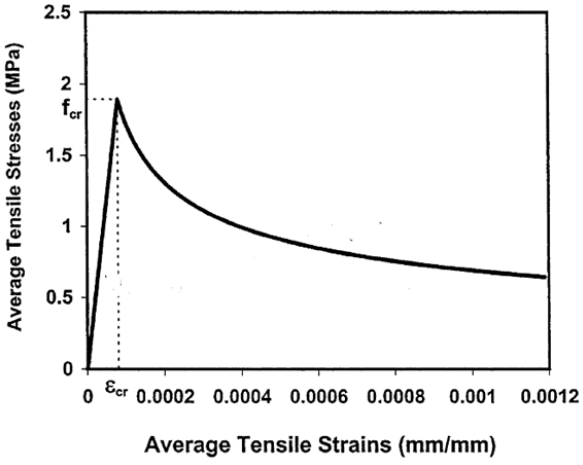

Figure (E-7): adopted tensile stress-strain curve of concrete (Wang and Hsu, 2001).

The tensile damage of concrete material defined in CDPM as a parameter d_t in the program input data. The tension damage defined according to **(Hafezolghorani, 2017)** [93], and this could be expressed as follows:

$$d_t = 1 - \frac{\sigma_t}{f_t} \qquad \text{(E.11)}$$

Where; d_t is the tension damage parameter, σ_t is the tension stress, and f_t is the tensile strength of concrete.

E.2 Steel Reinforcement and Steel Plate

There were three types of reinforcement (stirrups Ø8 mm, and longitudinal Ø12 mm and Ø10 mm) used and defined as a steel material based on the experimental stress-strain results of the uniaxial tensile tests as explained in Appendix-A. The behavior was defined as elastic linear strain hardening bilinear curve. The elastic behavior was defined by defining the longitudinal elasticity modulus of 200 GPa and Poisson's ratio of 0.3, while the plastic behavior was defined according to **British Standards Institution**[94] by true stress σ_s, and true plastic strain ε_s^{pl}, data pairs as follow:

$$\sigma_s = \sigma_n (1+\varepsilon_n) \qquad \text{(E.12).}$$

$$\varepsilon_s^{pl} = \varepsilon_s - \varepsilon_s^{el} \qquad \text{(E.13).}$$

Where

$\varepsilon_s = \ln(1+\varepsilon_n)$, and $\varepsilon_s^{el} = \frac{\sigma_s}{E_s}$

σ_s is the true stress, ε_s is the true strain, σ_n is the nominal stress, ε_n is the nominal strain, and E_s is the modulus of elasticity.

Figure (E-8 (a) and (b)) show the true stress and true strain relationships and steel plastic behavior according to the code and according to ABAQUS input data.

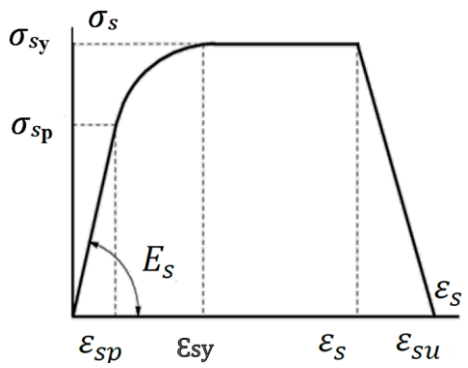

(a) Steel stress-strain relationship from Euro code EC2-2.

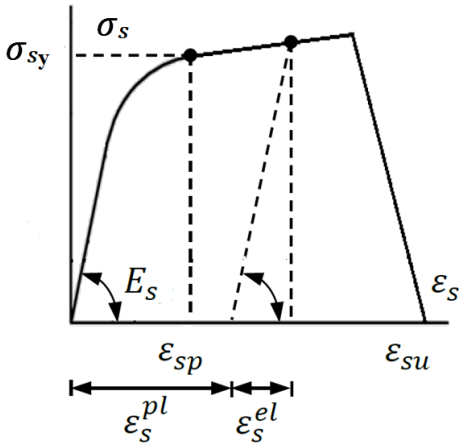

(b) Main parameters for ABAQUS input data.

Figure (E-8): Stress-plastic strain relationship of reinforcing steel and steel plate.

E.3 Support and Loading Steel Parts

Steel parts were used under loading points and at ring supports and its required parameters just elastic behavior because it required only for loading and support, so there was no need to define plastic behavior. Elastic behavior defined just by values of Poisson ratio (v) is 0.3 and the modulus of elasticity (E_s) has 200 GPa.

جمهورية العراق
وزارة التعليم العالي والبحث العلمي
جامعة بابل
كلية الهندسة
قسم الهندسة المدنية

السلوك الإنشائي للاعتاب الخرسانية المسلحة عالية المقاومة مع جزء خارج عن المستوي

أطروحة

مقدمة إلى كلية الهندسة في جامعة بابل

كجزء من متطلبات نيل درجة الدكتوراه فلسفة في الهندسة / الهندسة المدنية / الانشاءات

من قبل

مرتضى سادة محسن سالم

أشراف

أ.د. نمير عبد الامير علوش
أ.د. محمد منصور كاظم

أيار 2022م

الخلاصة

يتضمن هذا البحث فحوصات تجريبية وتحليل بطريقة العناصر المحددة (FEA) للسلوك الإنشائي للأعتاب الخرسانية المسلحة ذات المساند الثابتة مع أجزاء خارجة عن المستوي والمصنوعة من الخرسانة عالية المقاومة (HSC) والخرسانة ذات المقاومة العادية (NSC) المعرضة لحمل ثابت.

يتكون البرنامج التجريبي من اختبار أربعة عشر نموذج عتب. اثنان من هذه الاعتاب كانت مستقيمة احدهما مصنوع من الخرسانة العادية والأخر من الخرسانة عالية المقاومة وجميع الاعتاب الأخرى كانت غير مستقيمة ومصنوعة بأجزاء خارجة عن المستوي. جميع الاعتاب لها نفس أبعاد المقطع العرضي بعرض 150 ملم وعمق 200 ملم مع طول كلي 2000 ملم وفضاء صافي يبلغ 1500 ملم.

كانت المتغيرات الرئيسية التي تم أخذها في الاعتبار في الدراسة التجريبية هي: عدد الأجزاء الخارجة عن المستوي (واحد ، اثنان ، و ثلاثة من الأجزاء الخارجة عن المستوي) ، نوع الخرسانة (الخرسانة ذات المقاومة العادية (NSC) والخرسانة عالية المقاومة (HSC)) ، إضافة حديد تسليح عزم الالتوائي بالتزامن مع استخدام الخرسانة عالية المقاومة (HSC) ، وزيادة طول الأجزاء الخارجة عن المستوي في نماذج الاعتاب الخرسانية ذات المقاومة العادية (NSC). بالإضافة إلى ذلك ، تم تقييم معامل أخر باستخدام FEA يتضمن زيادة عدد الأجزاء الخارج عن المستوي بعدد أكثر من تلك التي تمت دراستها تجريبياً.

أظهرت النتائج أن زيادة عدد الأجزاء الخارجة عن المستوي يؤدي إلى تقليل سعة الحمولة. ومع ذلك ، فإن الاعتاب التي تحتوي على عدد زوجي من الأجزاء الخارجة من المستوي أفضل من الاعتاب التي تحتوي على عدد فردي من الأجزاء الخارجة عن المستوي (على سبيل المثال ، العتب الذي يحتوي على جزئين خارجين عن المستوي أفضل من العتب اللذي يحتوي على جزء واحد خارج عن المستوي). هذا الانخفاض في سعة التحميل القصوى يصل إلى حوالي 70 ٪ في بعض الحالات. أدى استخدام HSC إلى تحسين بسيط في سعة التحميل القصوى وتقلص الفارق في سعة التحميل القصوى إلى حوالي 60 ٪ مقارنةً بـالعتب المستقيم ذو الخرسانة NSC. أدى استخدام حديد تسليح عزم الالتواء بالتزامن مع استخدام الخرسانة عالية المقاومة إلى تحسن ملحوظ في قدرة تحمل الاعتاب ذات ألاجزاء الخارج عن المستوي ولكنها ظلت أقل من العتب المستقيم نوع NSC بحوالي

20٪ إلى 50٪. لقد وجد أن زيادة طول الأجزاء الخارجة عن المستوي لها تأثير ضئيل على سعة تحمل الاعتاب ولكنه أدى إلى تقليل هطولها.

بشكل عام ، كان هطول جميع الاعتاب ذات ألاجزاء الخارجة عن المستوي أعلى من هطول العتب المستقيم نوع NSC وتناقصت قيم هذا الهطول مع زيادة عدد وطول الأجزاء الخارجة عن المستوي. بالإضافة إلى ذلك ، كانت ليونة الاعتاب التي تحتوي على جزء واحد واثنين من الأجزاء الخارجة عن المستوي أقل من الحزمة المستقيمة ولكن العتب الذي يحتوي على ثلاثة أجزاء خارجة عن المستوي يتمتع بليونة أعلى ، وقد لوحظ أن الليونة زادت تدريجيًا مع زيادة عدد الأجزاء الخارجة عن المستوي.

علاوة على ذلك ، لا يمكن تصميم وتسليح الاعتاب ذات ألاجزاء الخارجة عن المستوي على اعتبارها عتبا" مستقيمًا لأن لها قيمًا مختلفة من قوة القص , عزم الانحناء, وعزم اللي. ومع ذلك ، من الممكن تطبيق خطوات تصميم العتب المستقيم ولكن مع معامل تقليل مقاومة اقل.

أخيرًا ، تم إجراء تحليل بطريقة العناصر المحددة غير الخطية ثلاثية الأبعاد لإجراء التحليل العددي للسلوك العام لنماذج الاعتاب باستخدام برنامج ABAQUS الحاسوبي في هذا العمل. أظهرت المقارنة بين التحليل العددي والنتائج التجريبية صحة معقولة للتحليل العددي حيث أن متوسط نسبة الاختلاف على أساس قدرة التحميل النهائية حوالي 4٪ و 19٪ للهطول الوسطي لجميع النماذج التي تم تحليلها.